UNIVERSITÀ DEGLI STUDI DI BRESCIA

DOTTORATO DI RICERCA IN

Ingegneria Civile, Ambientale della Cooperazione Internazionale e di Matematica

Curriculum: Analisi e gestione dei rischi naturali

XXXIV CICLO

Evaluation of the effect of climate variability on the hydro-glaciological regime in the Upper Indus Basin

Relatore e Tutor:

Prof. Roberto Ranzi

Correlatrice

Prof. Giovanna Grossi

Tesi di Dottorato di:

Muhammad Usman Liaqat

Coordinatore del Dottorato:

Prof. Paolo Secchi

Riassunto

Il ritiro dei ghiacciai osservato a scala planetaria e gli effetti del riscaldamento globale che accelererà la fusione dei ghiacciai e delle nevi stagionali andranno ad alterare alterare i regimi idrologici che interessano non solo i bacini montani, ma anche le aree a valle. Gran parte dell'approvvigionamento idrico del Pakistan è generato dalla fusione nivale e glaciale nelle regioni montuose del Karakoram. Tuttavia, il cambiamento climatico rappresenta un rischio elevato per questi bacini idrografici. Le caratteristiche geografiche e climatiche del Pakistan ne fanno un paese molto sensibile agli effetti negativi del riscaldamento globale. Pertanto, quantificare questi cambiamenti prevedibili è una sfida importante per la gestione e la pianificazione delle risorse idriche. L'obiettivo di questa tesi è valutare l'effetto della variabilità climatica sul regime idrologico e glaciologico nell'Alto Bacino dell'Indo (nel seguito Upper Indus Basin-UIB).

Il primo capitolo di questa tesi di dottorato presenta la climatologia delle precipitazioni ad alta risoluzione nell'UIB basata sul metodo delle anomalie (1995-2017) e sviluppato utilizzando quattro set di dati su griglia (APHRODITE, CHIRPS, PERSIANN-CDR e ERA5) su scala stagionale e annuale. Inoltre, il set di dati delle precipitazioni con le migliori prestazioni rispetto alle misure dei pluviometri e le serie temporali osservate sono state sottoposte all'analisi delle tendenze utilizzando le medie con finestra mobile insieme al test di Pettitt per il rilevamento degli annidi cambiamento. I risultati indicano le migliori prestazioni della precipitazione stimata con il dataset CHIRPS con correzione del bias seguito dalle rianalisi del modello ERA5; infatti il set di dati di precipitazione CHIRPS con correzione del bias ha ottenuto risultati migliori nella simulazione delle precipitazioni con RMSE, MAE, MAPE [%] e BIAS più piccoli seguiti da ERA5.

Le precipitazioni e le portate hanno rivelato una variabilità significativa, negli anni, su scala stagionale più che su scala annuale. Dai risultati delle analisi si raccomanda di correggere le precipitazioni su griglia prima del loro utilizzo in vari studi di modellazione idrologica, specialmente nei bacini glaciali. La relazione tra precipitazioni e deflussi e i coefficienti di deflusso annuale suggeriscono ulteriori indagini sul contributo dellanivo-glaciale deflusso.

Sulla base dei risultati del Capitolo 1, nel Capitolo 2 si utilizza il modello distribuito di bilancio energetico Physically Based Distributed Snow Land and Ice Model (PDSLIM), già testato nelle Alpi da Ranzi e Rosso (1991), Ranzi et al. (2010) e Grossi et al. (2013) per il bacino del Naltar situato nel bacino del fiume Hunza, in Pakistan, per simulare i regimi idro-glaciologici attuali e futuri. La calibrazione e la validazione di questo modello di bilancio energetico è condotta utilizzando un approccio multicriterio che considera la progressione stagionale della fusione nivo-glaciale e il deflusso idrico. I risultati hanno mostrato prestazioni molto soddisfacenti del modello verificato rispetto all'area di copertura nevosa (Snow Cover Area) stimata dalle immagini del sensore satellitare LANDSAT-TM e Terra/Aqua-MODIS per tutti gli anni simulati con coefficiente medio di determinazione R^2 = 0,96 e Nash-Sutcliffe Efficiency NSE= 0,95. Le simulazioni di deflusso hanno rivelato un buon accordo con la portata giornaliera osservata ottenuta con NSE e Kling-Gupta Efficiency (KGE) medi di 0,90 e 0,89. L'analisi della composizione del deflusso ha rivelato che la componente sotterranea, con risposta lenta, è la componente principale, seguita dal deflusso del ghiacciaio e dal deflusso superficiale.

Nel Capitolo 3 si illustra l'impiego del modello PDSLIM calibrato per esaminare le proiezioni future dei regimi glaciologico-idrologici per i due periodi temporali (2040-2059) e (2080-2099) negli scenari RCP 2.6, RCP 4.5 e RCP 8.5. I modelli climatici sono stati selezionati dal database CORDEX-WAS44 attraverso un approccio multiprospettico, prendendo in considerazione l'intero spettro del futuro cambiamento climatico. Le simulazioni previste del bilancio di massa ed energetico indicano che la progressione della fusione della neve e del ghiaccio aumenterà costantemente in entrambi i periodi di tempo futuri con un'anticipazione dei tempi della massima fusione nivale. Inoltre, si prevede che l'aumento della temperatura avrà un impatto sostanziale sui regimi idrologici con una anticipazione del massimo deflusso mensile da uno a due mesi entro il 2090 nel bacino di Naltar. Dalle stime del bilancio di massa attuale (-737 mm anno^{-1}) e previsto (-887 mm anno^{-1} per lo scenario 2050_4.5; -2018 mm anno^{-1} per il 2050_8.5 e -1154 mm anno^{-1} entro il 2090_4.5 ; -2597 mm anno^{-1} per 2090_8.5) e dalle immagini satellitari MODIS e LANDSAT sembra che anche nel bacino del Naltar i ghiacciai stiano per ritirarsi rapidamente indicando un'eccezione alla cosiddetta 'anomalia del Karakoram', una congettura di un rallentamento del ritiro dei ghiacciai nella regione a causa dell'accumulo nivale indotto dalle precipitazioni ad alta quota. Nel complesso il modello PDSLIM mostra prestazioni molto buonei nel simulare le dinamiche glacio-idrologiche attuali e, probabilmente, anche quelle future e pone una solida base per il potenziale utilizzo dell'approccio del bilancio energetico distribuito nei bacini glaciali del Karakorum e del'Hymalaia.

PAROLE CHIAVE: Running trend analysis, bacini glaciali, PDSLIM, modellazione glacio-idrologica, bilancio di massa, cambiamento climatico, disponibilità di risorse idriche.

Abstract

Projections of glaciers' retreat and earlier snowmelt driven by global warming could alter the hydro-glaciological regimes affecting not only the upstream watershed but also downstream areas. A large portion of Pakistan's water supply is generated by the melting of snow and ice in the mountainous regions of the Karakoram. However, climate change poses a high risk to these watersheds. The geographical and climate characteristics of Pakistan make it a country very sensitive to the adverse effects of global warming. Thus, quantifying these changes at the right time is an important challenge for water resources planners. The objective of this dissertation is to assess the effect of climate variability on the hydro-glaciological regime in the Upper Indus Basin (UIB) in the present and future projected climate.

Chapter 1 compiles the high resolution precipitation climatology (1995-2017) of the UIB developed using the anomaly method and four gridded datasets (APHRODITE, CHIRPS, PERSIANN-CDR and ERA5) which are bias corrected with interpolated observations at seasonal and annual scale. Further, the best performing gridded precipitation dataset and observed discharge timeseries were subjected to running trends analysis using moving window along with Pettitt test for change points detection. The results indicate the better performance of bias corrected CHIRPS precipitation followed by ERA5; bias corrected CHIRPS precipitation datasets performed better in simulating precipitation with smaller RMSE, MAE, MAPE [%] and BIAS followed by ERA5. Precipitation and discharge revealed significant variability at the seasonal scale more than at annual scale. The study results also indicate that gridded precipitation should be corrected before their usage in various hydrological modeling studies especially in glacierized catchments. The rainfall and runoff relationship and annual runoff coefficients suggest the need of further investigation and monitoring about snow-glacier melt contribution in streamflow.

Based on Chapter 1 outcomes, Chapter 2 employs the Physically Based Distributed Snow Land and Ice Model (PDSLIM), already tested in the Alps by Ranzi and Rosso (1991), Ranzi et al. (2010) and Grossi et al. (2013); Ranzi and Rosso (1991) for the Naltar catchment situated in the Hunza river basin (Pakistan) to simulate current and future hydro-glaciological regimes. The calibration and validation of this energy balance model is conducted using a multi-criteria approach considering snow and ice melt progression and streamflow. The results exhibited very satisfactory performances of the model verified against satellite-based snow cover area for all simulated years with average coefficient of determination $R^2 = 0.96$ and Nash-Sutcliffe

Efficiency *NSE= 0.95*. Runoff simulations revealed good agreement with observed daily discharge obtained with mean NSE and KGE of 0.90 and 0.89. Flow composition analysis revealed that subsurface runoff is the primary component of net streamflow, followed by glacier runoff and surface runoff.

Chapter 3 employs the calibrated PDSLIM to examine future projections of glaciological-hydrological regimes for the two-time periods 2040-2059 and 2080-2099 under RCP 2.6, RCP 4.5 and RCP 8.5 scenarios. Climate models were selected from the CORDEX-WAS44 database through a multi-perspective approach, taking into consideration the full spectrum of projected future climate change. The projected simulations of the energy and mass balance indicate that snow and ice melt progression will consistently increase in both future time periods with an anticipation in the timing of the maximum snowmelt. Additionally, the rise in temperature is expected to have a substantial impact on peak hydrological regimes from one to two months earlier by 2090s over Naltar catchment. From the actual (-737 mm a^{-1}) and projected mass balance estimates (-887 mm a^{-1} by 2050_4.5 scenario; -2018 mm a^{-1} for 2050_8.5 and -1154 mm a^{-1} by 2090_4.5; -2597 mm a^{-1} for 2090_8.5) and the MODIS and LANDSAT satellite images it appears that also in the Naltar catchment glaciers are going to retreat fast indicating an exception to the so-called 'Karakoram anomaly', a conjecture of a slower retreat of glaciers in the region because of accumulated precipitation at high altitudes . Overall, PDSLIM performs well for the current and, likely, future glacio-hydrological dynamics and sets a strong foundation for the potential usage of distributed energy balance approach in the glacierized catchments of High Mountain Asia (HMA) including Karakoram and Himalaya.

KEYWORDS: Running trend analysis, glacierized catchments, PDSLIM, glacio-hydrological modelling, mass balance, climate change, water resource availability, Karakoram, Indus basin

Acknowledgments

I would like to give tribute many people who helped me during my PhD journey.

First and foremost, I would like to express my gratitude to my supervisor Prof. Roberto Ranzi for providing me the opportunity to work under his supervision and for his endless support, encouragement, and mentorship throughout my Ph.D. I always feel honored to say that his guidance not only extended to my academic career, but also to my personal and professional interests. I also warmly thank my co-supervisor Prof. Giovanna Grossi for her excellent guidance, valuable comments, and continuous support which helped me in taking my research in right direction in climatological studies.

I am also grateful to Dr. Shahbeh ul Hasson for advising me with his knowledge and expertise to refine my chapter#1 work. My sincere thanks to Dr Ana Casanueva Vicente for welcoming me to her research team at Universidad De Cantabria, Spain. It has been an invaluable experience for me to gain new skills in the field of climatic modeling and the use of R language during the three-month visiting period. I would like to express my appreciation also to Talha Mehmood and Paolo Colosio for their contributions to my research.

I also pay my gratitude to my parents, my caring wife, and my beloved son for their unconditional support and love. They have always been an immense source of motivation and encouragement during my Ph.D. journey. Finally, I am grateful to Allah, the most merciful and beneficent.

Statement of Authorship

I **Muhammad Usman Liaqat** hereby confirm that my PhD thesis entitled "Evaluation of the effect of climate variability on the hydro-glaciological regime in the Upper Indus Basin" is my own work and has been completed by me under guidance of my supervisors. I also certify that

- Work has not been submitted to any other university for obtaining any degree or diploma.
- I have followed guidelines and norms instructed by University of Brescia in preparing the thesis.
- Whenever I have used materials (data, theoretical analysis, figures, and satellite data) from multiple sources, I have given due credit to them by citing them in the text of the thesis, giving their details in the references.
- All statistical analysis in the thesis and initial draft of published and under-review manuscripts was completed by me. Subsequently, it was circulated among co-authors and underwent peer review before publication, which led to the editing of the manuscript and inclusion of additional analysis.

Name of Student: **Muhammad Usman Liaqat**

Date: 20-12-2022

Contents

Riassunto 2
Abstract 4
Acknowledgments 6
Statement of Authorship 7
1. INTRODUCTION 11
1.1 Problem Statement 11
1.2 Aim and Objectives of the Study 13
1.3 Thesis Outline 14
Chapter I **15**
Characterization of Interannual and Seasonal Variability of Hydro-Climatic Trends in the Upper Indus Basin 15
Summary 16
1. Introduction 17
2. Material and Methods 19
2.1 Description of the study area 19
2.2 Hydroclimatology of the Upper Indus Basin 21
2.3 Meteorological data 23
2.4 Streamflow Data 23
2.5 Gridded observations 24
2.6 Anomaly Method: the interpolation scheme from rain-gauge network to regular grid 25
2.7 Evaluation Criteria 26
2.8 Precipitation and runoff trend analysis 26
2.9 Change Point Analysis 27
3. Results 28
3.1 Climatology, anomalies and precipitation records 28
3.2 Variability and trends of the precipitation in Upper Indus Basin 31
3.3 Long Term Temperature Trends 35
3.4 Variability and trends of the runoff in Upper Indus Basin 36
3.5 Rainfall-runoff relationship in the Upper Indus Basin 40
4. Discussion 41
5. Conclusions 42
Acknowledgements 43
Chapter II **44**
Energy balance modeling of snow and ice melt in the Naltar Catchment (UIB, Pakistan) .. 44
Summary 45
1. Introduction 46

2. Material and Methods 48
2.1 Description of the study area 48
2.1 Meteorological Data 49
2.2 Hydrological Data 50
2.3 Geo-topographic Data 50
2.3.1 Landcover and Lead Area Index 51
2.4 Satellite snow and glacier data 52
2.5 Modeling Strategy 53
2.5.1 Calibration with MODIS and LANDSAT Snow Cover Area 53
2.5.2 Calibration and Validation with Naltar Streamflow 54
2.6 Glacier Surface Mass Balance 54
2.6.1 Annual Mass Balance 54
2.6.2 Winter Mass Balance 55
2.6.3 Summer Mass Balance 55
2.7 Energy Balance of Snow and Ice 56
3 PDSLIM Model Structure 58
3.1 Hydrological Simulations 63
3.2 Sensitivity and Uncertainty Analysis 65
3.3 Net Summer Glacier Mass Balance 65
3.4 Visualizing Water Balance Change in Non-Dimensional Space 65
4. Results and Discussion 66
4.1 Snow Cover Simulation 66
4.2 Hydrological Simulations 71
4.3 Water Balance 76
4.3.1 Water Balance Analysis using Truc-Budyko 77
4.4 Net Glacier Mass Balance Simulations 78
4.5 Sensitivity Analysis. 79
5. Discussion and Conclusion 81
Chapter III **83**
Impact of climate change on Naltar Catchment Hydrology, Upper Indus Basin 83
Summary 84
1. Introduction 85
2. Material and Methods 87
2.1 Study Area 87
2.2 Hydro- meteorological, satellite and snow cover measurements for the Naltar catchment 88
2.3 Climate Projections 89

2.4 Energy and mass balance of snow and ice: the physical based hydrological model 91
3. Results and discussions 94
3.1 Future Climate Forcings 94
3.2 Projected changes in snow water equivalent 97
3.3 Projected change in snow and ice melt progression and mass balance 98
3.4 Glacier Mass Change Projections 101
3.5 Projected change in streamflow 102
3.6 Projected change in hydrological components to net streamflow 106
3.7 Projected change in water balance 108
4. Conclusions 111
Bibliography 113
Conclusion and perspectives of the PhD thesis 123
1 Conclusion 123
2 Outlook for further research 125
Supplementary Material Chapter # 1 126
Supplementary Material Chapter # 2 133
Supplementary Material for Chapter # 3 136
Details of scientific activities performed during Ph.D. 140
1. International mobility 140
2. Conference Publications 140
3. Journal Publications 140
4. Courses 141
5. Seminars and workshops 141

1. INTRODUCTION

1.1 Problem Statement

The work of thesis consists in the evaluation of the effect of climate variability on the hydro-glaciological regime in the Upper Indus Basin (UIB).

But why we are concerned about the UIB? And why is the attention mainly focused on highly glacierized catchments?

The Upper Indus Basin (UIB) is marked as the source region of Pakistan's breadbasket (Rieu-Clarke 2015), which encompass the largest cryosphere volumes outside poles. Being known as the water tower of Asia, UIB plays an important role in feeding the population of 220 million of Pakistan and millions of inhabitants in India as well. Pakistan is highly dependent on water resources generated from snow and ice melting in the mountainous regions of UIB. However, UIB is highly sensitive to climate change. Pakistan is ranked among the top ten countries most affected by climate change. A number of hydro-climatic trends studies reported the significant variations in temperature, precipitation, and streamflow that triggered the extreme events (i.e., droughts, floods, landsliding etc.). Thus, it is imperative to quantify these changes at historical, current, and future time scales in order to effectively manage water resources downstream. In previous assessments of hydro-climatic trends (Ahmad et al. 2018; Bolch et al. 2012; Fowler and Archer 2006); Janes and Bush (2012); (Krakauer et al. 2019; Latif et al. 2018; Masood et al. 2019; Rahman et al. 2018; Sharif et al. 2013), they did not incorporate variations within specific temporal sub-periods, nor did they describe non-linear dynamics of hydro-climatic variability.

Additionally, studies of climate impacts require precise and reliable hydrometeorological data at higher spatio-temporal resolution, both from retrospective (i.e., past) and prospective (i.e., future) climate perspectives. Ideally, long-term measurements from well-distributed rain gauges and/or radar networks are the most reliable. Nevertheless, in real-world conditions, these measurements are limited in time and space, particularly on the vast and complex terrains of the High Mountains of Asia (HMA), which restricts the ability to accurately identify spatiotemporal patterns. The same goes for UIB, which is a transboundary basin and observed hydro-meteorological data are mostly scattered, discontinuous and not easily accessible. Hence, it is difficult to assess the spatial and temporal variability in high altitude mountainous regions using a sparse ground-based observation network, as it cannot depict horizontal and vertical precipitation variability effectively (Lutz et al. 2014). Gridded datasets provide a better solution in terms of temporal and spatial coverage, even if they are affected by likely greater errors, in particular in high altitude areas where large bias and uncertainty may occur, especially in conditions of significant snowfall (Andermann et al. 2011) and in glacierized catchments (Wortmann et al. 2018). Therefore, it is necessary to reduce biases in grided datasets before using in hydrological modelling studies.

UIB is endowed with one of the world's largest reserves of natural snow and ice, which have a significant impact on maintaining the water balance in this region and its surrounding valleys

(Immerzeel and Bierkens 2010). Early nineteenth-century explorations suggested that the Karakoram glaciers behaved in a peculiar manner (Godwin-Austen 1864; Hayden 1907). Hewitt (2005) who coined the term 'Karakoram Anomaly', the stability or abnormal growth of glaciers in the central Karakoram, as opposed to glaciers retreating in nearby mountain ranges such as the Himalayan range and other mountain ranges around the world as in the alps (Paul et al. 2014) and the Italian alps in particular (Carturan et al. 2016). Comparing the evolution of Karakoram's glaciers to those of other regions on Earth, modern observations are more conclusive (Berthier and Brun 2019; Minora et al. 2013; Minora et al. 2016). However, in light of current climate projections, Farinotti et al. (2020), it appears unlikely that long-term Karakoram Anomaly persistence will occur. Thus, it is imperative to examine this phenome especially at sub-regional scale where glacier surging occurred two years ago.

Generally, hydrological and energy balance model is commonly used in glacierized catchments for analyzing melting of snow and ice while taking into account the effects of extremely dynamic climatic processes. Water availability in downstream areas of the UIB has been impacted by climate-mediated changes, such as glaciers retreating, early snowmelt, and variable precipitation. It has been found that previous studies use simple conceptual models and lumped approaches in order to examine snow and ice melt and hydrological dynamics in current and future climate scenarios with less data requirement, computational time, and ease of calibration in UIB compared to spatially distributed models (Atif et al. 2019; Ayub et al. 2020; Immerzeel and Bierkens 2010; Naeem et al. 2016; Pellicciotti et al. 2012; Saleem et al. 2020; Shah et al. 2020). Further, snow and ice melt progression and resulting hydrological consequences have been carried out at regional and basin level (Ali et al. 2018; Dolk et al. 2020; Faiz et al. 2020; Hayat et al. 2019; Shrestha and Nepal 2019). However, water resources management decision mostly take place at catchment or sub-basins level. Additionally, data availability is also one major reason for site selection of Naltar catchment especially for energy mass balance simulation. There is a need for further investigation into these gaps in knowledge. Moreover, it is also imperative to examine future water availability at catchment scale which is not only important to computer water demand for people living in downstream areas but also helpful to fulfill energy demand for the area of interest.

In this context, a comprehensive study on historical hydro-climatic trends, investigation of all available hydrological, glaciological and snow data to monitor snow and ice melt progression and runoff regimes at current and future climate change is needed to examine Karakoram anomaly and to serve communal and scientific interests.

1.2 Aim and Objectives of the Study

The study is divided into two major sections: in the first part, a comprehensive evaluation of hydro-climatic trends was investigated. In the second part, performance of fully distributed energy balance model is evaluated under present and future climate change scenarios. The specific objectives of this study are given below:

1) Characterization of interannual and seasonal variability of hydro-climatic trends in the Upper Indus Basin

a) Comparison and bias correction of gridded precipitation datasets (CHIRPS, ERA5, PERSIANN-CDR and APHRODITE) against WAPDA-DCPs stations over the Upper Indus Basin.

b) Assessment of hydro-climatic variability from decadal to interdecadal time scale using novel running trends analysis in the UIB at sub-basin scale.

2) Energy balance modeling of snow and ice melt in the Naltar Catchment UIB, Pakistan.

a) Examine the performance of PDSLIM tested in Alps can transfer to Karakoram to compute accurate flow composition and snow cover extent.

b) Quantify the contribution of snow and glacier melt to net river runoff and explore the ability of PDSLIM for prospective applications in forthcoming studies.

3) Impact of climate change on Naltar Catchment Hydrology, Upper Indus Basin.

a) Project glacio-hydrological regimes generated by snow-glacier melt, future flow and precipitation by near future (2040-2059) and far future (2080-2099) under RCP 2.6, RCP 4.5 and RCP 8.5.

b) How will change mass balance of glaciers in the future and does Karakoram anomaly apply in Naltar catchment.

1.3 Thesis Outline

The introductory chapter describes the importance of the research topic, its objectives and methods. Chapter #1 provides a comprehensive description of interannual and seasonal variability of hydro-climatic trends in seven subbasins of the Upper Indus Basin. High resolution seasonal and annual precipitation climatology were developed for the Upper Indus Basin for period 1995-2017 using four gridded datasets (APHRODITE, CHIRPS, PERSIANN-CDR, and ERA5) and quality-controlled observations of high- and mid-elevation stations. The variability of precipitation and discharge on a finer time scale was calculated using running-trend analysis or moving average window approach. Chapter#2 explores the feasibility of an energy balance modelling system known as Physical Based Distributed Snow Land and Ice Model to simulate hydro-glaciological regimes for the first time in Karakoram for the Naltar catchment located in the Hunza river basin (Pakistan). In order to verify the accuracy of the model in simulating snow and glacier retreat, improved MODIS snow cover product (M100A1GL06) and Landsat based snow cover area were employed both at temporal and spatial scale. Downstream runoff measurement at the outlet of Naltar catchment at Naltar Bala station was used as a reference for the verification of simulated summer melt. Chapter 3 addresses future climatic and glacio-hydrological projections. In this study, sixteen (16) CORDEX-SA RCMs at 0.44^{o} (~50 km) spatial resolution were employed for the period 1991-2099. In particular, the study considered daily data from six meteorological variables (precipitation, temperature, solar radiation, wind speed, relative humidity and air pressure). Three representative concentration pathways (RCP 2.6, RCP 4.5 and RCP 8.5) were analyzed in this study in order to assess future snow and ice melt progression, mass balance change and runoff regimes. Finally, the overall conclusion of this research and an outlook for the future work are given.

Chapter I

Characterization of Interannual and Seasonal Variability of Hydro-Climatic Trends in the Upper Indus Basin

This chapter consist in the paper published in the Theoretical and Applied Climatology

Liaqat, M.U., Grossi, G., Hasson, S.u. et al. Characterization of interannual and seasonal variability of hydro-climatic trends in the Upper Indus Basin. Theor Appl Climatol 147, 1163–1184 (2022). https://doi.org/10.1007/s00704-021-03850-3

[1]Department of Civil, Environmental, Architectural Engineering and Mathematics,Università degli Studi di Brescia-DICATAM, Via Branze, 43, 25123 Brescia BS, Italy [2]CEN, Centre for Earth System Research and Sustainability, University of Hamburg, Hamburg, Germany

Summary

High resolution seasonal and annual precipitation climatologies for the Upper Indus Basin were developed on the basis of 1995-2017 precipitation normals obtained from four gridded datasets (APHRODITE, CHIRPS, PERSIANN-CDR and ERA5) and the quality-controlled high- and mid-elevation station observations. Monthly precipitation is estimated through the anomaly method at the catchment scale and then it is compared with the observed runoff over the 1975-2017 period for verification and detection of changes in the hydrological cycle. Running trends and spectral analysis on the precipitation gridded dataset were performed. The Mann–Kendall test was employed to detect the significance of trends whereas the Pettitt test was used to identify change points in precipitation and runoff time series.

The results indicate that the bias corrected CHIRPS precipitation, followed by the ERA5, performed better in terms of RMSE, MAE, MAPE and BIAS against the rain gauge observations. The running trend analysis exhibits a slight increase in annual precipitation but significant increase in winter precipitation. A runoff coefficient greater than one, especially in the glacierized sub-catchments of Shigar, Shyok, Astore and Gilgit indicate that precipitation is likely to be underestimated and glacial melt provides excess runoff volumes in a warming climate.

Streamflow variability is found to be pronounced at the seasonal rather than at the annual scale. The annual runoff at Shyok, Gilgit, and Indus at Kachura gauges are slightly significantly increasing. Seasonal runoff analysis reveals more complex regimes, varying in different catchments, and its comparison with precipitation variability favors a deeper understanding of precipitation, snow-, and ice-melt runoff dynamics, addressing the hydroclimatic behavior of the Karakoram region and some weaknesses in the monitoring network at high altitude.

Keywords: precipitation, runoff, high-resolution climatology, running trend, Indus basin

1. Introduction

Changes in the hydrological cycle at both global and regional scales is a major concern as these changes occurring either due to climatic or anthropogenic factors can have adverse impacts on society in general. This emphasizes on monitoring these changes on all relevant scales. Precipitation is a key component of the hydrological cycle and perhaps the most difficult one to be monitored, particularly in the glacierized and snow-fed catchments such as the Upper Indus Basin (UIB), where complex Himalayan terrain and harsh environment makes the high-altitude precipitation monitoring further difficult. As a result, the observations are sparse, short, and discontinuous with large gaps, all making it difficult to understand the variability and changes and its subsequent impact on the basin hydrology and water yield (Archer and Fowler 2004).Hence, a combined study of both precipitation and runoff provides a better insight into the variability of the water cycle in the high mountain areas and the cryosphere in general (Poloczanska et al. 2018) and in the UIB in particular.

The UIB span over confluence of the Hindukush, Karakoram and Himalayan (HKH) mountain ranges that constitute one of the largest cryosphere reserves outside the poles (Soncini et al. 2015). The UIB fulfills water demands of rapidly increasing population and feeds one of the world's largest irrigation systems within the Indus Basin. Pakistan's economy to a large extent depends upon the agriculture, and in turn, on the water resources of the UIB, which feeds around 16.5 x 10^6 hectares of irrigated land. The UIB up to the Besham Qila inflow gauging station drains an area of 163,528 km^2 and receives 26% of its annual flow from the snowmelt and 44% from the glacial melt (Mukhopadhyay and Khan 2015). The primary usage of the UIB waters is for irrigation and hydropower production as the climate of lower Indus basin is mainly arid and hyper-arid unlike other South Asian basins, which are characterized by wet regimes of summer monsoon. Immerzeel et al. (2015) marked the UIB as a climatic hotspot region, due to the wide variation in the climate anomalies, as well as due to the significant rising water demand downstream.

The UIB is characterized by diverse hydro-climatic regimes with contrasting patterns across sub-basins and over time. Archer and Fowler (2004) found rising rates in summer, winter and annual precipitation. Khattak et al. (2011) found summer cooling and winter warming and no confirmed changes in precipitation over the 1967-2005. Immerzeel and Bierkens (2012) noted the highest vulnerability of water scarcity conditions for the Indus River Basin among ten basins in Asia. They recognized that significant population increase, groundwater depletion, climate change, snowmelt and ice melt are key factors that affect the hydrological regimes of the Indus basin. Bocchiola and Diolaiuti (2013) found a slight increase in annual precipitation over northwest Karakoram and Chitral-Hindukush, its decrease on the greater Himalayan side. They also observed summer cooling and winter warming, which are prominent than earlier particularly at Bunji and Gilgit stations. Ali et al. (2015) examined current and future climatic and hydrological changes over the UIB. They showed that northern parts of the UIB experienced a larger increase in temperature and precipitation than southern parts. Projections of future changes show a consistent increase in temperature and precipitation. The rate of increase of river flow is greater in winter compared to summer season. They considered higher river flow possibly due to a larger increase in the air temperature and the consequent enhancement of the melting of the snow and ice cover. Latif et al. (2018) explored both seasonal

and annual precipitation trends in the UIB using low and mid altitude stations. The results exhibited significant falling rate of annual precipitation in six stations, while three stations showed a rising rate of precipitation. Overall, the UIB experienced a downward trend in precipitation both spatially and temporally.

The studies mentioned above mainly used valley-based sparse and fragmented low and mid altitude stations being operated by the Pakistan Meteorological Department (PMD). The estimates from these stations neither represent the climatology of high altitude areas, nor provide any quantifiable mechanism that draws logical inferences between low and high altitude precipitation(Khan and Koch 2018). As a great amount of the UIB streamflow originates from the active hydrological zone in the 2500-5500 m altitude range, data from low altitude stations (even if making up long time series of observations) are not representing reliable hydro-meteorological conditions over the frozen UIB water resources (Hussain et al. 2017).

Moreover, the Indus is a transboundary basin (see Fig. 1.1) and observed hydro-meteorological data are mostly scattered, discontinuous and not easily accessible. Hence, it is difficult to assess the spatial and temporal variability in high altitude mountainous regions using a sparse ground-based observation network, as it cannot depict horizontal and vertical precipitation variability effectively (Lutz et al. 2014a). Various gridded datasets have been developed based on satellite-based data (Huffman and Bolvin 2013), interpolated observation (Yatagai et al. 2012) and reanalysis data (Baudouin et al. 2020; Li et al. 2020) to handle this issue. Most of past studies concerning the UIB depend upon regional or global gridded datasets for mass balance and hydro-climatic studies (Baudouin et al. 2020; Dahri et al. 2016; Hasson et al. 2017; Immerzeel et al. 2009; Iqbal et al. 2019; Krakauer et al. 2019; Lutz et al. 2014a; Masood et al. 2019; Minallah and Ivanov 2019; Rizwan et al. 2019; Ullah et al. 2018).

Gridded datasets provide a better solution in terms of temporal and spatial coverage, even if they are affected by likely greater errors, in particular in high altitude areas where large bias and uncertainty may occur, especially in conditions of significant snowfall (Andermann et al. 2011) and in glacierized catchments (Wortmann et al. 2018). Uncertainties and biases in the gridded datasets are usually due to shortcomings of data sources and generation algorithms of these products (Sun et al. 2018). It is also noted that gridded datasets such as CHIRPS and APHRODITE mainly used the World Meteorological Organization's Global Telecommunication System (GTS) gauge data in their production mechanism (Yatagai et al. 2012). The WMO GTS collaborates with PMD for sharing observed meteorological data. In 1995, Water and Power Development Authority (WAPDA) in Pakistan collaborated with the International Development Research Centre, Canada to install automated weather stations within Pakistan side of the UIB known as the data collection platforms (DCPs). However, the data of these stations are neither publicly available, nor they are shared with the WMO. Keeping in mind above issues, the primary objective of this study is to discuss biases and uncertainties in each available gridded dataset (CHIRPS, ERA5, PERSIANN-CDR and APHRODITE), before and after their corrections performed using mid-altitude PMD and high-altitude WAPDA-DCPs stations. The second objective is to compare catchment scale precipitation to discharges to identify possible sources of errors and climatic anomalies, as well as their changes over time and space.

Previous assessments on hydro-climatic trends at the annual or seasonal scale considered

specific periods (Ahmad et al. 2018; Bolch et al. 2012; Fowler and Archer 2006; Hasson et al. 2017; Janes and Bush 2012; Krakauer et al. 2019; Latif et al. 2018; Masood et al. 2019; Rahman et al. 2018; Sharif et al. 2013; Zaman et al. 2020), but they neither incorporated variations within specific temporal sub-periods, nor they described non-linear dynamics of hydro-climatic variability. In an agriculture-based country, with substantial climatic variation, it is difficult to understand the hydro-climatic phenomenology using conventional linear trend schemes. Building on the need of generating future scenarios of water sustainability, this study shows the results of a running trend analysis that covers the entire dataset period to assess hydroclimatic variability from decadal to interdecadal trends in the UIB at the sub-basin scale. More specifically, this study provides a comprehensive investigation of the detectable links of short-term (sub-decadal and decadal) and long-term (multidecadal) precipitation and runoff variability at the seasonal and the annual scale. In this way, it supports a more detailed overview of precipitation and runoff regimes at the basin and the sub-basin level and improves the past analysis for examining hydro-climatic behavior. Within this context, a precipitation climatology (1995-2017) for the UIB at the seasonal and the annual scale was built using the anomaly-method applied in (Crespi et al. 2018; Crespi et al. 2021). This method is briefly recalled in the second section of the paper after the description of the study area, of the collected precipitation and runoff data and of the implemented statistical analyses. In the third section, the hydro-climatic trends in each sub-basin of the UIB are examined, together with biases and uncertainties of the gridded precipitation data compared with the ground observations. A discussion of the results, also in comparison with those coming from the analysis of runoff data, follows in the fourth section.

2. Material and Methods

2.1 Description of the study area

The UIB, including part of the western Himalayas, Karakoram, and northern Hindu Kush mountains, lies in the geographic domain within 31–37^{o} latitude and 72–82^{o} longitude. The basin hosts 14085 small and large glaciers, covering an area of 19338 km^{2} (RGI Version 6.0). The drainage area of the Indus Basin is around 163528 km^{2} at the Besham Qila (BQ) gauging site. The basin is shared between Pakistan, India and China with around 46% of its area lying within Pakistan's administrative boundaries (Hasson et al. 2017). The Indus River originates from Mount Kailash in the western Tibet at an elevation of 5486 m and has an overall length of 3180 km measured at the outlet into the Arabian Sea (Jain et al. 2007). The main stem flows initially through the Ladakh district in Jammu and Kashmir and afterwards it enters northern Pakistan (Gilgit-Baltistan), between Himalayas and the Karakoram range. The catchment area and, consequently, the discharge of the Indus River become larger in Gilgit-Baltistan (GB) when tributaries, such as Shyok, Shigar, Hunza and Gilgit Rivers in the Karakoram Mountains and Astore River in the western Himalayas merge with the main river stem. Afterwards, it turns towards south from Nanga Parbat (8126 m asl) and flows through three provinces of Pakistan, i.e. Khyber Pakhtunkhwa (KPK), Punjab, and Sindh, before its confluence to the Arabian sea. Additionally, Chitral, Swat and Kabul rivers that are originating from the Hindu Kush Mountains also join the mainstream of the Indus river in the KPK province, whereas western Himalayan rivers of Jehlum, Chenab, Ravi and Sutlej join main the Indus river stem at Punjnad

in the Punjab province.

The basin highest elevation is set by the K2 (Karkoram-2) peak, also known as "Godwin-Austen", the second highest mountain in the world (8611 m asl), whereas the lowest altitude at BQ is 542 m a.s.l. The mean altitude is around 3750 m asl whereas 35% of the area lies above 5000 m asl. The hypsometric curve of UIB is shown in Fig.S1. The UIB has seven subcatchments, i.e. Gilgit, Hunza, Astore, Shigar, Shyok, Shingo-Zanskar and Indus Downstream (Mukhopadhyay and Khan 2015). The Shyok and Shigar basins feed the eastern and the central part of the Karakoram. Almost one-third of the Shigar basin is covered with glaciers, including world's largest glaciers and ice masses after polar regions. The hydro-climatic characteristics of each sub-basin are quite different. Summer monsoon and westerlies are dominant sources of annual precipitation in UIB, however, the effect and contribution of both sources vary spatially, as well as temporally (Hasson 2016).

The average annual precipitation measured at different stations within the basin ranges from 156 mm at Gilgit station to around 1514 mm in Pir Chanasi valley. The mean annual discharge at Besham Qila is 2405 m^3s^{-1}(Hasson et al. 2017). The Indus Basin receives 70% of its annual flow during June to September with a maximum value in July. October to March are distinguished as low flow months. UIB climate falls into the "cold desert" category (BWK) according to the Köppen-Geiger climate classification, i.e. an area with a little precipitation and large daily temperature range. The relationship between station elevation and measured precipitation is represented in Fig.1.2, which shows that no significant altitudinal trend can be observed, although doubts arise about the reliability of precipitation data when snowfall occurs.

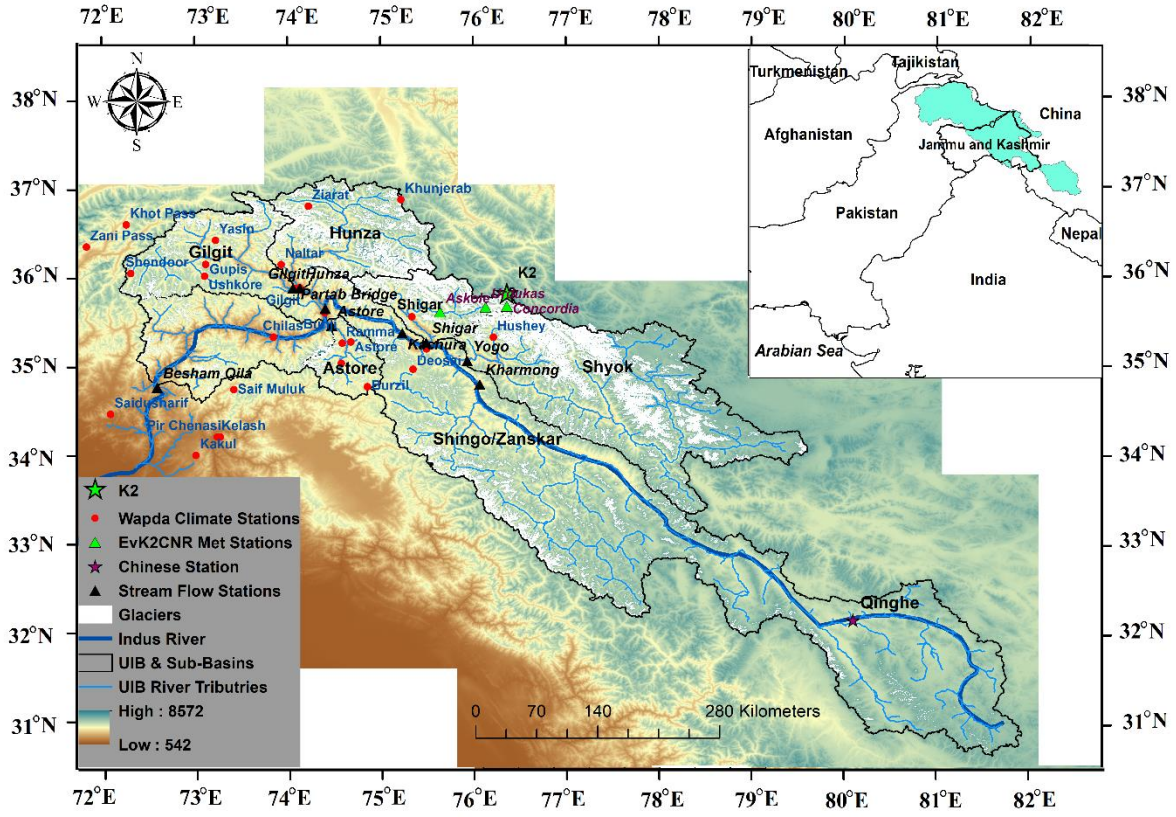

Figure.1.1 The location of the Upper Indus River Basin (UIB - light blue in the inset) and of the Hydro-Meteorological Stations used for the analysis.

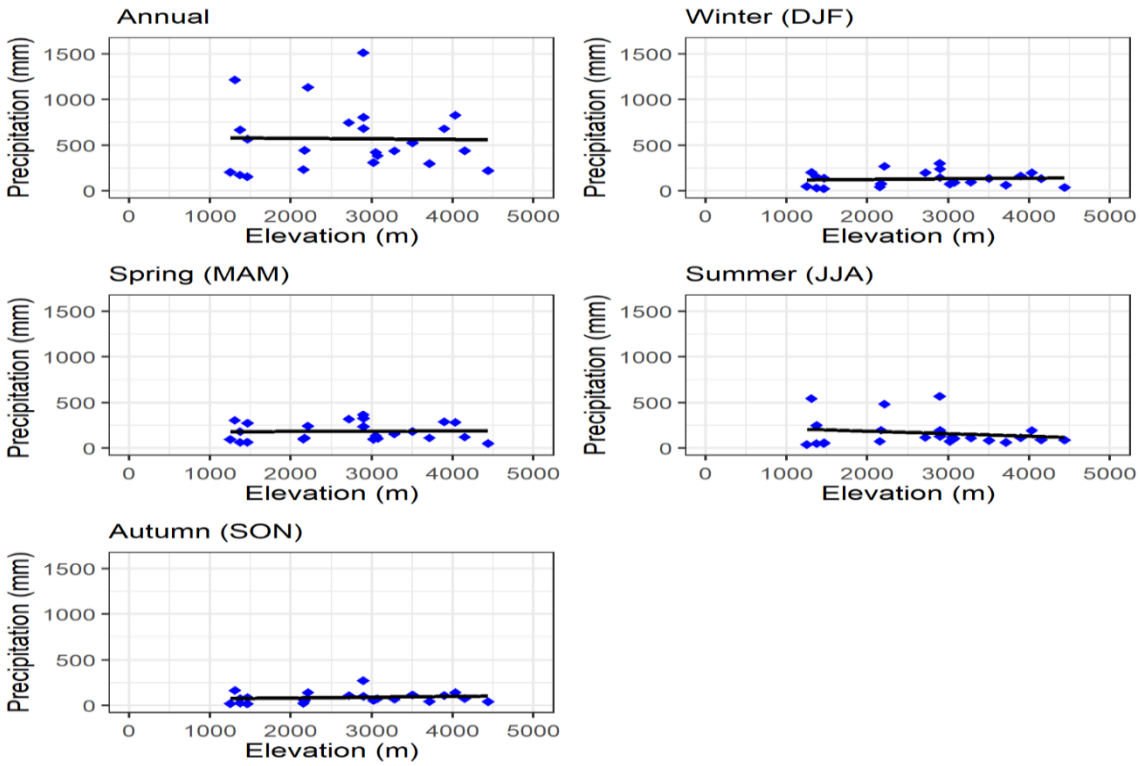

Figure.1.2 Relationship between gauge precipitation and elevation observed at the annual and seasonal scale in the UIB.

2.2 Hydroclimatology of the Upper Indus Basin

In the Upper Indus Basin hydrology, the precipitation regime features annual-round midlatitude western disturbances. Such disturbances sometimes carry solid form of moisture, mainly during winter and spring (Hewitt 2011).The rate of such unusual solid form of moisture is higher during the positive phase of the North Atlantic oscillation (NAO), when western disturbances affect Afghanistan and Iran due to low heat over the area, resulting in extra moisture input from the Arabian sea (Hasson 2016; Hasson et al. 2014; Syed et al. 2006);
Initially, water supply is generated by melting of snow starting from the mid of March to late June. The extent of water availability mainly depends upon the concurrent temperature and accumulated snow amount (Hasson et al. 2014; Hasson et al. 2013). Afterwards, snowmelt runoff is merged with glacier melt runoff from late June to late August as a consequence of high air temperatures. The climate of the UIB is classified by winter extra-tropical cyclonic/ anticyclonic circulations (westerlies) and South Asia summer monsoon atmosphere circulations. Both winter and summer have significant impact on the climatic patterns of the UIB (Hewitt 2011). The westerlies enter the UIB through northwest by the end of November or early in December. Initially, these westerlies are presented in distorted and diffuse state. Afterwards, they interact with already existing orographic trough with low pressure that allow them to recover their potency and frontal structure. The topographic blocking separates these westerlies into southern and northern sections around the western Tibetan Plateau and Karakorum (Pang et al. 2014).

The relationship between topography, local climate and circulation system determines the net precipitation and distribution pattern in the UIB. The differential heating between land and sea is the main reason for summer precipitation (Dahri et al. 2016). The summer monsoon carries moisture from the Arabian sea that move along the Indus valley towards western Himalayas. It also brings moisture from Bay of Bengal and moves northward to the eastern Himalayas, and from Indian ocean to the western Himalayas following the path along the Indus river valley (Ahmad et al. 2012; Hasson 2016; Pang et al. 2014)

It is generally believed that the precipitation rate is increasing with elevation up to a certain elevation where a maximum is reached. For the UIB some studies (Immerzeel and Bierkens 2012; Immerzeel et al. 2015; Winiger et al. 2005) found that precipitation is increasing up to a specific elevation, i.e. 5000 m, and shows downward trend above this elevation. Most of annual precipitation falls in the winter and spring and originates from the westerlies. Although summer carries occasional rain to trans-Himalayan areas, it accounts for only one third of total annual precipitation (Madhura et al. 2015). Some glaciological studies mentioned significant increase of precipitation rates of 1500-2000 mm at 5500 m (Soncini et al. 2015). At the high elevation zones, ice is the primary source of hydrological regimes, followed by snow melt, while the contribution of summer monsoon precipitation is small.

Table 1.1 Meteorological stations and their attributes

Basin	Stations	Period from	Period to	Agency	Latitude (^{0})	Longitude (^{0})	Elevation (m asl)	Precipitation (mm/year)
Gligat	Gilgit	1981	2017	PMD	35.92	74.33	1460	158
	Gupis	1981	2017	PMD	36.17	73.4	2156	234
	Ushkoor	1995	2017	WAPDA	36.05	73.39	3051	423
	Yasin	1995	2017	WAPDA	36.4	73.5	3280	439
	Shnedoor	1995	2017	WAPDA	36.09	72.55	3712	300
Hunza	Khunjerab	1995	2017	WAPDA	36.84	75.42	4440	224
	Ziarat	1995	2017	WAPDA	36.77	74.46	3020	310
	Naltar	1995	2017	WAPDA	36.17	74.18	2898	685
Astore	Astore	1981	2017	PMD	35.37	74.9	2168	444
	Ramma	1995	2017	WAPDA	35.36	74.81	3179	806
	Rattu	1995	2017	WAPDA	35.15	74.8	2718	750
	Burzil	1995	2017	WAPDA	34.91	75.09	4100	829
Shigar	Shigar	1996	2012	WAPDA	35.63	75.53	2367	348
	Askole	2005	2017	EVK2CNR	35.68	76.82	3051	535
	Urdukas	2011	2017	EVK2CNR	35.74	76.51	3926	283
	Concordia	2011	2017	EVK2CNR	35.73	76.29	4690	260
Shyok	Hushey	1995	2017	WAPDA	35.42	76.37	3075	386
	Skardu	1981	2017	PMD	35.3	75.68	2210	237
Shingo	Deosai	1995	2017	WAPDA	35.09	75.54	4149	440
	Qinghe	1995	2010	CMDC	32.5	80.08	4279	239
	Bunji	1981	2017	PMD	35.67	74.63	1372	174
Indus Down Stream	Chilas	1981	2017	PMD	35.42	74.1	1251	207
	Kakul	1981	2017	PMD	34.1	73.2	1308	1215
	Pir Chanasi	1995	2017	WAPDA	34.38	73.55	2872	1514
	Saif Muluk	1995	2017	WAPDA	34.9	73.65	2362	830
	Saidu Sharif	1981	2017	PMD	34.7	72.4	949	1070

2.3 Meteorological data

Data availability is a big issue in the HKH especially in the UIB where stations are neither densely nor uniformly distributed. There are primarily two organization: WAPDA and PMD who are responsible for collection and managing hydro- meteorological data across northern areas of Pakistan. Approximately, hundreds of gauging stations are installed in various places across UIB (Zaman et al., 2020) In this study, meteorological data from 26 stations were selected from PMD, WAPDA and China Meteorological Data Sharing Network (CMDSN) based on completeness, temporal duration and homogeneity. Out of these 26 stations, seven are operated and maintained by PMD. These are valley-based stations, which are located within the altitude range of 1200–2200 m asl. The data from these stations were collected for the period 1981-2017.

The second meteorological network is maintained by the Snow and Ice Hydrology Project (SIHP) of the WAPDA, which is operating 12 automated weather stations known as data collection platforms (DCPs), located in the elevation range of 1479-4440 m asl and providing observations since 1995. As Karakoram range hosts the largest snow ice reserves of the UIB, DCPs stations operated by the WAPDA are particularly relevant for examining the hydro-meteorological conditions prevailing over the UIB cryosphere (Hasson et al. 2017).

In addition there are also three high altitudes stations operated and maintained by EvK2-CNR (Italian based organization). Two stations of Askole (3015 m asl.) and Urdukas (3926 m asl) provide observations since 2005, and one located at Concordia (4690 m asl.) provide observations since 2011. All three stations are used to calculate standard meteorological parameters. However, data time series from these three stations feature large data gaps and are affected by uncertainties especially during the winter season due to sensor inefficiency in extreme weather conditions. The detailed information about climatic stations, their elevation, time period and mean precipitation are given in Table 1.1.

2.4 Streamflow Data

Upper Indus Basin is fed by three sources of streamflow i.e. glacier melt, especially in Shyok, Hunza and Shigar subbasins, followed by snow melt mainly in the Gilgit and Astore subbasins and rainfall runoff. The daily streamflow of nine hydrometric stations within the UIB have been taken from the Surface Water Hydrology Project (SWHP) of WAPDA, Pakistan from 1973-2017, except for Indus at Kharmong and Bunji stations where
data is available from 1983-2017 and 1973-2013, respectively. Discharge data of Astore at Doyian and Gilgit river at Gilgit are used in this study. Similarly, discharge of Hunza basin is collected at Dainyor station. Table 1.2 provides specfic information about these streamflow stations and their outflow points.

Table 1.2 SWHP WAPDA stream flow gauges given in the downstream order along with their characteristics and the analyzed periods of record.

Serial. No	Gauge River	Discharge Gauging Point	Period from	Period to	Latitude (^{0})	Longitude (^{0})	Elevation (m asl)
1	Indus	Kharmong	1983	2017	34.93	76.21	2542
2	Shyok	Yogo	1973	2017	35.18	76.1	2469
3	Indus	Kachura	1973	2017	35.45	75.41	2341
4	Hunza	Dainyor	1973	2017	35.92	74.37	1370
5	Gilgit	Gilgit	1973	2017	35.92	74.3	1430
6	Indus	Bunji	1973	2013	35.73	74.62	1792
7	Astore	Doyian	1973	2017	35.54	74.7	1583
8	UIB	Besham Qila	1973	2017	34.92	72.88	542
9	Shigar	3-2-1	1983	2017	35.33	75.75	2438
10	UIB Pakistan	8-1					
11	UIB Pakistan	8-2-1					

2.5 Gridded observations

In the last decades, a great progress was made in developing analysed fields of precipitation over regional and global scale providing different gridded climatic products. These products are avaialble at regional and global scale and are used in hydro-climatic assesment studies. Precipitation products can be devided into four major different cathegories: (1) climatic model reanalysis (2) satellite estimates (3) merged satellite and station observations (4) raingauge-based observations (Sun et al. 2018). In this study we used at least one product from each of these cathegories in order to check their accuracy for hydro-climatological studies based on precipitation estimates thourgh these datasets. The APHRODITE is based on station observations, CHIRPS is a combination of satellite and station observations, ERA5 is a reanalysis dataset and PERSIANN-CDR is based on remote sensing using Artifical Nureal Network. The detail information about these products are given in Table 1.3.

Table 1.3 Gridded datasets used in this study for performance evaluation of climatology in Upper Indus Basin

Dataset	**Resolution/frequency**	**Data Sources**	**Algorithm/Assimilation schemes**	**References**
APHRODITE **(Observed Values)**	0.25°/daily	Data Integration and Analysis System (DIAS)	Interpolation with rain gauge grided precipitation	(Yatagai et al. 2012)
CHIRPS **(Observed+ Satellite)**	0.05°/daily	USGS, CHG	Smart Interpolation Tech	(Funk et al. 2015)
PERSIANN-CDR **(Satellite)**	0.25°/3,6 h and /daily	TRMM, NOAA, GridSat-B1 IR, Metsat-6, GOES 8, DMSP F13	Artificial Neural Networks	(Ashouri et al. 2015)
ERA5 **(Reanalysis)**	0.25°/monthly/daily/ hourly	ECMWF	4D-Var	(Saha et al. 2010; Tarek et al. 2019)

For instance, APHRODITE (V1101 and V1101EX_R1) is specfically developed for summer in the Asian region with spatial resolution 0.25°× 0.25°; the products are provided by the Data Integration and Analysis System (DIAS, Japan) that is based on an interpolation of 3500 to 8000 gauge observation (Dile and Srinivasan 2014).

The second dataset is CHIRPS which was developed by the Climate Hazards Group (CHG) and the United States Geological Survey (USGS). It is avaible from 1981 to present with spatial resolution of 0.05º and temporal resolution at daily and monthly scale. It was developed by combination of ground based gauge information and cold cloud duration measurement by the synergistic use of satellite infrared radiometers. Passive microwave and GridSat-B1 satellite data were employed to update the PERSIANN algorithim to estimate daily precipitation. It is based on remotely sensed information combination with artifical neural network (Ashouri et al. 2015).The European Center for Medium-Range Weather Forecasts (ECMWF) launched the new renalysis product ERA5 data. The analysis is developed using advanced 4Dvar assimilation scheme at temporal and spatial scale. It is available at 0.25 x 0.25 degrees and computes various atmoshphetic variables at 139 pressure levels for 1979-present time period at different temporal scale (Baudouin et al. 2020).

2.6 Anomaly Method: the interpolation scheme from rain-gauge network to regular grid

The precipitation station observations in the UIB are sparse and do not provide complete temporal and spatial coverage. Therefore, it is inappropriate to develop basin wide annual and seasonal precipitation climatology based on available observations directly. For this purpose, monthly precipitation records for four gridded datasets (CHIRPS, PERSIANN-CDR and ERA5 from 1995 to 2017 and for APHRODITE from 1995-2015) were selected, according to data availability. The gridded data were reconstructed over the study area by means of the anomaly method as described by Crespi et al. (2021). To develop the precipitation climatology on the seasonal and annual scale, monthly gridded and observed data were aggregated at the seasonal scale, i.e. winter (DJF), spring (MAM), summer (JJA), autumn (SON), and annual scale. In this scheme, the precipitation signal is reconstructed by superimposing the spatial fields of seasonal climatology to the spatio-temporal fields of relative anomaly i.e. deviations from the reference for a certain season. The ratio or multiplicative correction factor between referenced and gridded precipitation at each i-th specific station is computed as below:

$$P_{test\ m,i} = \frac{p_{test_m}}{p_{refrence,i}} \quad (1)$$

Here p_{test_m} and $p_{refrence,i}$ are gridded and observed precipitation series at the specified time scale over the period of common data availability. It has to be pointed out that the rain gauge observations are here assumed to be 'true' reference precipitation values and the other precipitation products are adapted to them. $P_{test\ m,I}$ is the seasonal ratio anomaly or correction factor which is then interpolated as described in Crespi et al. (2018).

Similarly, the interpolation method is also applied on gridded datasets on the same scale. These two fields are calculated individually and the season estimates are finally obtained by their product. The same procedure is applied on the annual scale. The anomaly-based climatology

helps to develop fine-scale information provided by gridded datasets and incorporates the available records on a large area when the station distribution over the study domain does not provide complete coverage (Brunetti et al. 2012).

2.7 Evaluation Criteria

To evaluate the data quality of precipitation anomaly against observed precipitation for an overlapped period of 1995-2017 and 1995-2015 at seasonal and annual scale, four statistics i.e., bias (BIAS), mean absolute error (MAE), root mean square error (RMSE) and mean absolute percentage error (MAPE) were assessed in this study.

BIAS $$\frac{\sum_{i=1}^{N}(Ps_i - Po_i)}{N} \quad (2)$$

MAE $$\frac{1}{N}\sum_{i=1}^{N}(P_{S_i} - P_{O_i}) \quad (3)$$

RMSE $$\sqrt{\frac{\sum_{i=1}^{N}(Ps_i - Po_i)^2}{N}} \quad (4)$$

MAPE $$\frac{1}{N}\cdot\sum_{t=1}^{N}\frac{\left|P_{S_i} - P_{O_i}\right|}{P_{O_i}}\cdot 100 \quad (5)$$

where PS_i is the value of gridded precipitation estimate for the i_{th} event, PO_i is the value of rain gauge observation for the i^{th} event, N is the number of precipitation events. Bias represents the average difference between the gridded precipitation, after the anomaly method correction, and gauge precipitation, as reference. A negative value of bias implies underestimation, while a positive value indicates overestimation of observed precipitation. The gridded precipitation datasets were also compared with observed streamflow and the runoff coefficients was computed as shown in Table 1.6 in order to assess the ability of runoff data to close the water balance in each sub-basin of UIB and also to verify the reliability of raingaue-based precipitation assessed at the catchment scale as pointed out, for instance, by (Ranzi et al. 2021).

2.8 Precipitation and runoff trend analysis

The anomaly-derived precipitation and streamflow runoff were used for the trend analysis in sub-basins of UIB at seasonal and annual timescales. Runoff period from 1973 to 2017 was selected for four rivers (Astore, Indus at Besham Qila, Indus at Shyok, Indus at Kachura), 1973-2013 and 1983 to 2017 were selected, respectively, for Indus at Bunji and Kharmong and Shigar due to the available data. There are two basic tests which are mainly used to detect trend significance i.e., parametric, and nonparametric approach (Zaman et al. 2015; Zaman et al. 2016). The trend for this hydro-climatic time series were estimated using robust nonparametric regression techniques i.e. Mann–Kendall (MK) test (Kendall 1948; Mann 1945) in conjunction with Theil–Sen (Sen 1968; Theil 1950) slope method to determine the trend's slope. Mann–Kendall is a ranked based method that determines the presence of any trend irrespective of the type of sample data distribution and whether such trend is linear or nonlinear (Tabari and Talaee 2011). There are two reasons for using MK test for trend analysis. Firstly, it is not necessary for time series data to be normally distributed. Secondly, it is insensitive to missing

values and data outliers and less sensitive to breaks caused by inhomogeneous time series (Bocchiola and Diolaiuti 2013). A running trend with a moving time window approach, a type of exploratory data analysis similar to that adopted by Brunetti et al. (2012) is used to calculate and visualise trends for precipitation and runoff over different time windows and access their significance using consecutive years of the datasets as starting point (x axis in Fig.1.4 and 1.5) and ending points (y axis in Fig.1.4 and 1.5). As trends in climate change studies are expected to be analysed after 20 years of monitoring, at least, a minimum duration of 15 years was considered for precipitation trend analysis, due to limited availability of data time series, and 20 years for runoff. However, generally, running trend analysis does not require a fix threshold on the length of time series and the threshold value can be altered according to study objectives, climatic parameters, data availability and local issues. Such analysis is not only helpful to detect non-linear hydro-climatic trends in UIB over the different temporal scales, but it also facilitates a comparison of these results with other studies which did not show overall climatic fluctuations in the study period.

2.9 Change Point Analysis

The nonparametric Pettitt test is also employed in this study to observe change point in hydro-climatic time series (Palaniswami and Muthiah 2018; Zhang et al. 2015). It supposes a time series X_t with t = 1,2….N has a change point at time step T. The values of X_t for t=1,2,…,T have CDF $F_1(x)$ and t=T+1,T+2,…,N have CDF $F_2(x)$ and $F_1(x) \neq F_2(x)$. Like other statistical measures, the null hypothesis (H_o) depicts the absence of change point against the alternative hypothesis (H_1: change point present). Given the random variable k(T) defined as:

$$k(T) = \sum_i^T \sum_j^N sgn(X_i - X_j) \quad , \tag{6}$$

the Pettitt statistics *K* is written as,

$$K = \max_{0 \leq T \leq N} |k(T)| \tag{7}$$

And time at which change occurs in time series is determined by

$$T = arg(\max_{0 \leq T \leq N} |k(T)|) \tag{8}$$

p-values of the two-tailed Pettitt test is computed by as,

$$p \approx 2 \exp\left(-\frac{6K^2}{N^3+N^2}\right) \tag{9}$$

The null hypothesis (H_0) would be rejected for $p<\alpha$, where α is the significance level. In our study, we keep significance level at 5%.

3.Results

3.1 Climatology, anomalies and precipitation records

The annual and seasonal precipitation climatology for the study basin is shown in Fig.1.3. The mean annual bias corrected CHIRPS precipitation for the study domain was estimated as 536 mm a^{-1} which is closer to the results obtained by (Cheema and Bastiaanssen 2012; Reggiani and Rientjes 2015; Rizwan et al. 2019; Shafeeque et al. 2019) who suggested corrected precipitation 523, 675$\pm$100, 550 and 593 mm a^{-1} respectively in UIB using various methods. The driest area is located over the South-Western part of the study domain along the Shingo and Zanskar basins followed by the upper part of Hunza, Shigar and the central part of Gilgit, while the highest precipitation values occur over the central part of Indus downstream, Astore, Shingo, and the upper part of Shyok. Other wet conditions are also observed over the border of Gilgit/ Indus downstream Besham Qila and Astore/Shingo basin.

On a seasonal scale, the driest conditions occur during the autumn season with less than 100 mm $season^{-1}$ over wider portion of the basin. In summer slightly wetter conditions occur, followed by the monsoon season which receives the major portion of precipitation. Considering the mean seasonal precipitation over the whole study basin, the precipitation rate is 96 mm in winter (DJF), 150 mm in spring (MAM), 220 mm in summer (JJA) and 70 mm in autumn (SON). It is generally believed that the precipitation rate is getting higher with elevation until an orographic optimum. However, the observation of this phenomenon is quite uncertain in UIB where higher precipitation values are measured at lower altitudes or no significant increase with altitude is observed (see Fig. 1.2). There can be two main possible reasons: the first one is related to the fact that the majority of meteorological stations are located in low lying areas and so there are significant chances of under catch snow precipitation, a common problem in windy and snow dominated areas like UIB (Petäjä et al. 2016). The second is related to the representation of precipitation with gridded datasets which are often lacking sufficient as well as reliable gauge observations. The values of error statistics (2) to (5) computed with the leave-one-out method over the grid points with gauge observations are presented in Table.1.5. The bias corrected CHIRPS precipitation had the best performance at annual and seasonal scale followed by ERA5 whereas PERSIAN-CDR had the worst performance at both scales.

The summary performance of selected gridded datasets is as follows: CHIRPS datasets is slightly underestimated before correction while ERA5 is highly overestimated before correction. However, after correction the statistical results of ERA5 are closer to CHIRPS gridded datasets. The higher values of MAE, BIAS and RMSE for ERA5 before correction due to incorporating liquid and frozen water, consisting rain and snow that falls on the earth surface. Secondly, reanalysis datasets mostly rely on coupled numerical models, ocean and atmospheric data and do not dependent upon the ground-based observations (Copernicus Climate Change Service, 2017).

Table 1.4 Comparison of LWLR Interpolated Precipitation with previous studies

Sub-Basins	PPT mm/a^{-1}	Dataset used	Reference period
Indus-Behsam Qila	536	This Study (CHIRPS)	1995-2017
	594	This Study (ERA5)	1995-2017
	671	APHRODITE * 1.17	1998-2007 (Lutz et al. 2014a)
	482	Station data + KED interpolation	1998-2012 (Dahri et al. 2016)
	675	ERA-Interim, NCEP/NCAR	1998-2009 (Reggiani and Rientjes 2015)
Gilgit	289	This Study (CHIRPS)	1995-2017
	402	This Study (ERA5)	1995-2017
	326	APHRODITE * 1.17	1998-2007 (Lutz et al., 2014)
	162	Station Observations	1998-2007 (Akhtar et al. 2008)
	575	Station data + KED interpolation	1998-2012 (Dahri et al. 2016)
Hunza	574	This Study (CHIRPS)	1995-2017
	372	This Study (ERA5)	1995-2017
	205	APHRODITE * 1.17	1998-2007 (Lutz et al. 2014a)
	582	India-WRIS	1971-2004 CWC and NRSC, 2014
	455	Observed + SRM	2000-2013 (Hayat et al. 2019)
Shyok	245	This Study (ERA5)	1995-2017
	395	This Study (CHIRPS)	1995-2017
	175	APHRODITE * 1.17	1998-2007 (Lutz et al. 2014a)
	342	Station data + KED interpolation	1998-2012 (Dahri et al. 2016)
Shigar	654	This Study (ERA5)	1995-2017
	576	This Study (CHIRPS)	1995-2017
	917	Station data + KED interpolation	1998-2012 (Dahri et al., 2016)
	550	Model	1980-2009 (Bocchiola et al. 2011b)
Astore	649	This Study (ERA5)	1995-2017
	868	This Study (CHIRPS)	1995-2017
	904	Station data + KED interpolation	1998-2012 (Dahri et al. 2016)
	431	APHRODITE * 1.17	1998-2007 (Lutz et al. 2014a)
	541	Observed+ SRM	2000-2013(Hayat et al. 2019)
Shingo/ Zanskar	383	This Study (ERA5)	1995-2017
	302	This Study (CHIRPS)	1995-2017
	277	Station data + KED interpolation	1998-2012 (Dahri et al. 2016)
	161	APHRODITE * 1.17	1998-2007(Lutz et al. 2014a)

The performance of Aphrodite dataset is found to be inferior to ERA5 especially at annual scale. A great variation of PERSIAN-CDR with observed values might be associated to bias-adjustment, which is based on GPCC dataset with coarse resolution of 2.5^{o} resolution (Fallah et al. 2019). The reliability of CHIRPS and ERA5 were also cross checked by comparing with some previous studies as shown in Table.1.4. The results show reliable agreement for developing precipitation climatology using observed and gridded data series extended in space and time in UIB. The discrepancies with other studies are due to varied coverage of study area, time period and number of meteorological stations applied in the analysis.

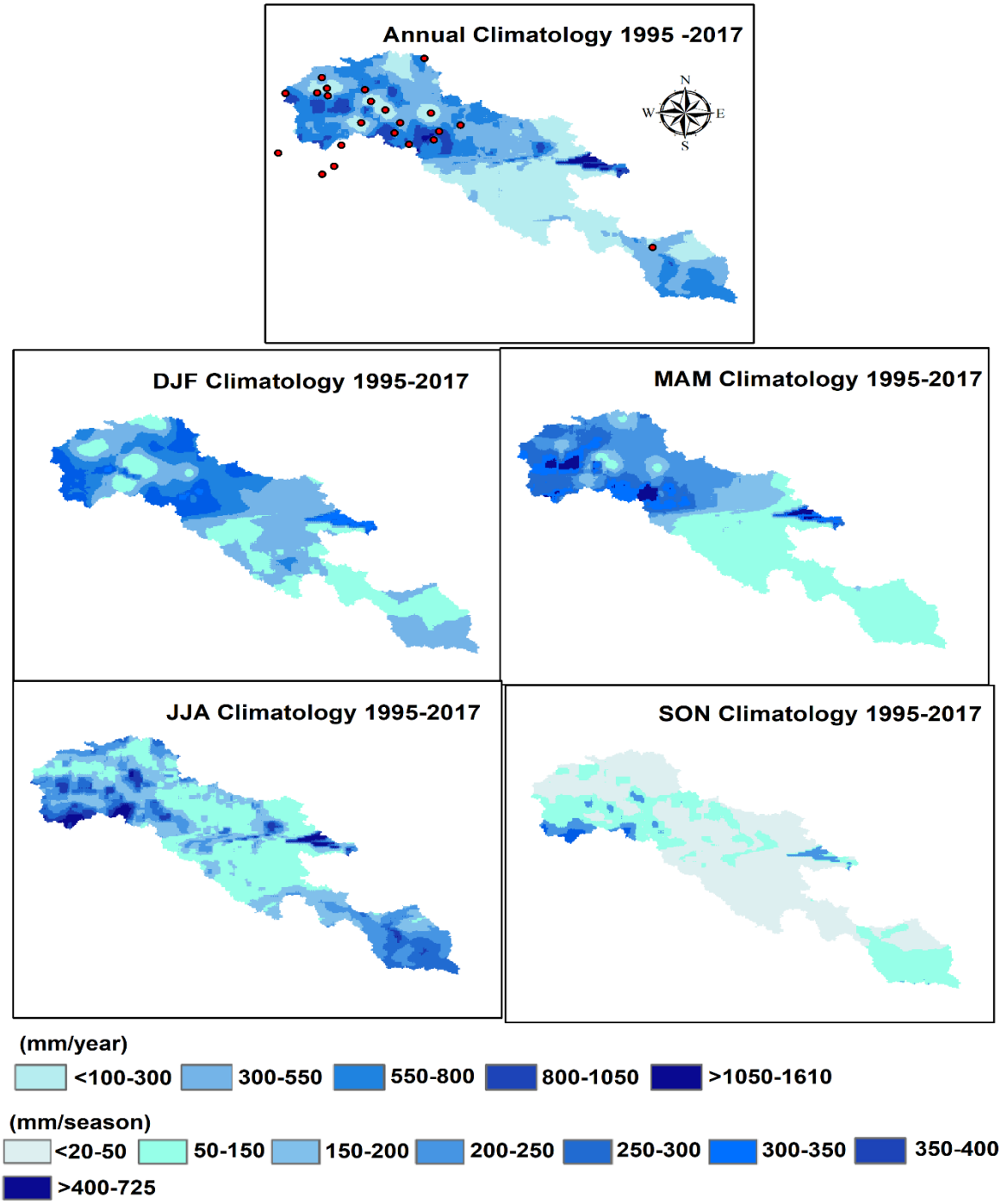

Figure.1.3 Annual and seasonal precipitation climatology based on CHIRPS gridded datasets corrected using observed data.

Table 1.5 Annual and seasonal leave-one-out reconstruction errors of the 1995–2017 normal for the 5 testing stations (Astore, Chilas, Deosai, Gilgit and Ziarat) included in the study domain.

Datasets	Seasons	MAE (mm)	MAPE [%]	BIAS (mm)	RMSE (mm)
CHIRPS	Uncorrected Annual	69.7	20.5	-2.6	93.4
	Annual	50.0	14.0	21.1	56.9
	DJF	19.7	27.0	13.9	23
	MAM	27.1	26.3	15.2	28.4
	JJA	23.0	25.7	10.6	34.4
	SON	17.3	36.2	-10.2	20.9
ERA5	Uncorrected Annual	516.6	64.8	516.6	563.8
	Annual	53.7	15.4	27.7	61.6
	DJF	36.7	35.4	32.6	41.4
	MAM	20.5	15.7	14.5	23.3
	JJA	25.6	33.2	14.3	40.3
	SON	17.4	33.1	5.0	22.1
APHRODITE	Uncorrected Annual	111.4	30.7	36.1	118.4
	Annual	68.4	19.1	28.2	75.3
	DJF	30.1	31.3	26.9	34.9
	MAM	36.4	30.8	12.5	40.1
	JJA	36.1	39.9	-5.0	42.1
	SON	15.9	26.2	-6.2	18.3
PERSIANN-CDR	Uncorrected Annual	155.6	28.9	155.7	195.5
	Annual	78.5	23.5	36.1	85.3
	DJF	40.4	38.1	28.1	43.2
	MAM	38.5	29.4	31.8	36.5
	JJA	49.4	33.7	-15.7	53.7
	SON	26.6	53.9	-9.6	30.8
Mean (mm)					
Observed Rain gauge	Annual	358.9			
	DJF	86.6			
	MAM	131.6			
	JJA	86.8			
	SON	53.9			

3.2 Variability and trends of the precipitation in Upper Indus Basin

The 1995-2017 annual and seasonal precipitation records for the study domain were evaluated for short and long term trends by using the Theil-Sen slope test (Theil 1950) while the trend significance was evaluated by MK test (Mann 1945). By assuming a confidence interval (C.I) 0.05 (95%), the variability of precipitation on a finer time scale was calculated using running-trend analysis or moving average window approach on the 1995-2017 records.

Moreover, change point analysis of precipitation at annual and seasonal time series was also investigated using the Pettitt test as shown in Fig.1.4, Table.S1.2 and Fig S1.2. The trend rate for initial three years were excluded both for precipitation and runoff from because it is very difficult to examine upward/downward trend with small moving window. The value of MK-Test significance is estimated on window of increasing width from 15 years up to the entire period spanned by series and running from the start to the end of the record. The long-term annual precipitation series exhibited varying interdecadal rising and falling trends. For annual scale, the trend analysis revealed significant increase of precipitation for Shyok, Shigar, UIB Kharmong basins and slightly significant for Indus Downstream and Gilgit basins. Although, Hunza and overall flow at Besham Qila also depicts increasing rate of precipitation but nonsignificant whereas Astore exhibited non-significance falling rate in precipitation. The Pettitt test marked 2004 as a change point year i.e., shift from drying to wetting phase for Indus Downstream, UIB Kharmong-Shyok and Shingo basins, 2005 was noted for UIB Kharmong.. In case of Hunza Gilgit and Shyok basins, change point has been observed during 2009 and 2012, respectively.

In nutshell, precipitation is increasing but non significantly and nonuniformly. It is also noted that Hunza and Shyok basins only exhibited significant change point year by Pettitt Test while, all other basins depicted nonsignificant change point year. UIB is characterized by various climatic regimes like westerly disturbances and monsoonal effect orographic disturbance from Tibetan Plateu that make climatology of this region complex, nonuniform distribution and result in inconsistency in precipitation anomaly (Anjum et al. 2018).

On seasonal scale, trend analysis indicated significant increasing trend for Hunza, Shyok, UIB Kharmong, UIB Kharmong-Shyok and slightly significant rising trend of precipitation for (Gilgit, Shigar) during winter season. Astore and Indus at Besham Qila expressed non-significance increasing trend until 2008-09 followed by declining rate of precipitation. The 2003 years marked as a change point (drying to wetting phase) for Astore, Hunza (significant), Shingo, UIB Kharmong basins. Years 2009 and 2011 are noted as 5%-significant change points for Gilgit and Shyok basins. Although, Indus BQ exhibited change point for 2013 year but followed inverse phenomena i.e., wetting to drying phase. For spring season, UIB Kharmong, Astore, Shyok, Shigar and Indus BQ exhibited non-significant upward trend while, Shingo, Hunza and UIB Kharmong depicted nonsignificant decreasing trend. The change point line mainly found around the year 2003 for Gilgit, Hunza, Shingo, UIB Kharmong-Shyok and Shyok basins, 2009 for Shigar and Shyok basins.

The increasing rate of precipitation during winter and falling rate during spring is possibly align with alteration in westerly precipitation regimes under climate change. The results of winter wetting also consistent with some previous studies (Cannon et al. 2015; Hasson et al. 2017; Ridley et al. 2013) who also supported rising rate in winter precipitation and drying days during spring season under climate change is mostly linked with incursion of westerly precipitation regimes and northward transfer of rainstorm trajectories in UIB.

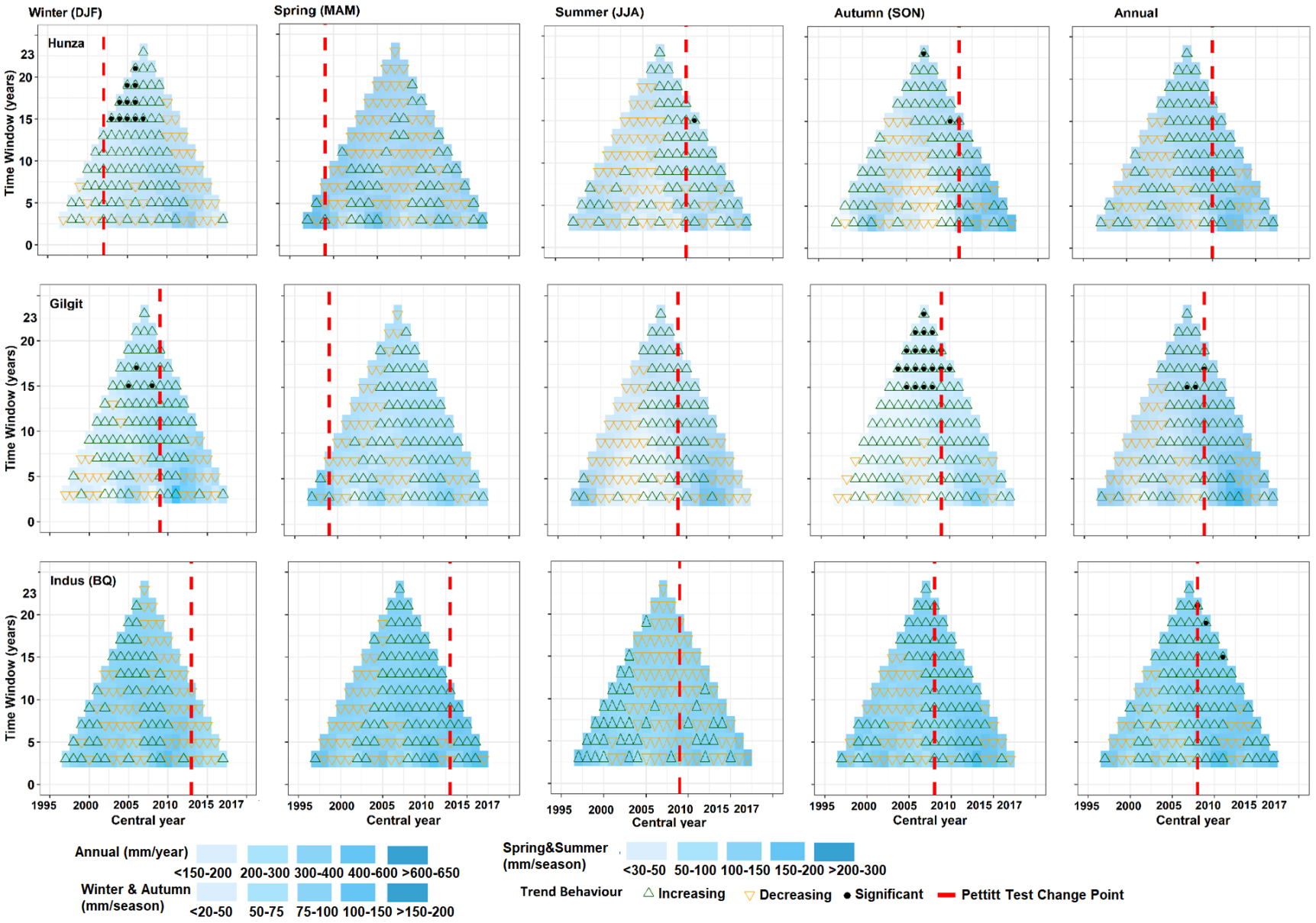
Winter (DJF)
Spring (MAM)
Summer (JJA)
Autumn (SON)
Annual
Hunza
Gilgit
Indus (BQ)
Time Window (years)
Central year
1995 2000 2005 2010 2015 2017
Annual (mm/year)
<150-200 200-300 300-400 400-600 >600-650
Winter & Autumn (mm/season)
<20-50 50-75 75-100 100-150 >150-200
Spring&Summer (mm/season)
<30-50 50-100 100-150 150-200 >200-300
Trend Behaviour
Increasing
Decreasing
Significant
Pettitt Test Change Point

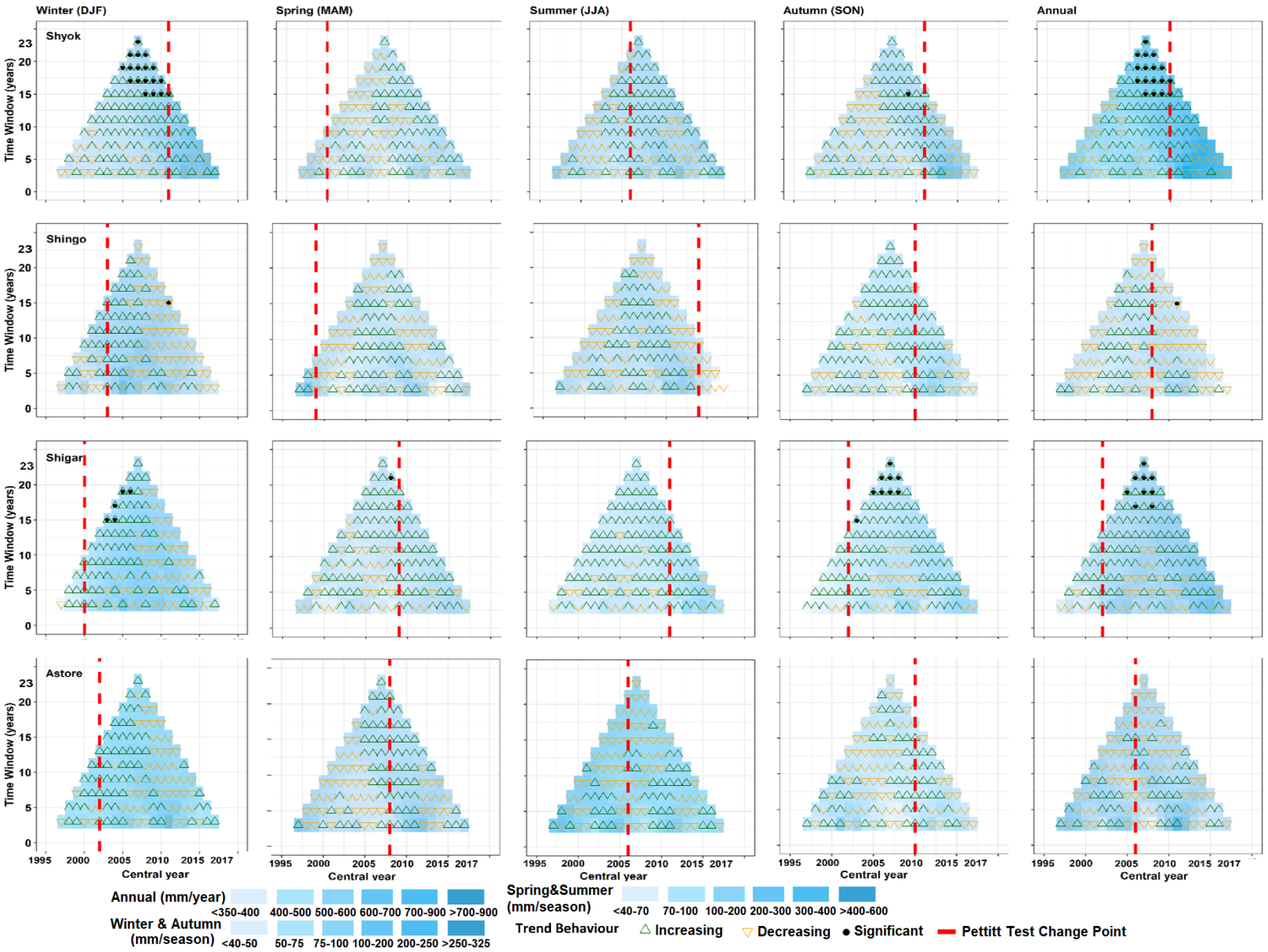
Winter (DJF)
Spring (MAM)
Summer (JJA)
Autumn (SON)
Annual
Shyok
Shingo
Shigar
Astore
Time Window (years)
Central year
Annual (mm/year)
<350-400 400-500 500-600 600-700 700-900 >700-900
Winter & Autumn (mm/season)
<40-50 50-75 75-100 100-200 200-250 >250-325
Spring&Summer (mm/season)
<40-70 70-100 100-200 200-300 300-400 >400-600
Trend Behaviour
Increasing
Decreasing
Significant
Pettitt Test Change Point

Figure.1.4 Running trend of annual and seasonal precipitation series. Average Precipitation values are divided into various classes (white to dark blue). Trend values are showed by upward (green) and downward triangles (yellow) while trend significance is described by filled circles (significant with at least 15 data) with Mann-Kendall p-values < 0.05). Red vertical line expresses 'change point' year (Pettitt Test) in the entire time series. The x axis is the starting year (central year), while the y axis is the moving window.

For summer season, nonsignificant declining trend in precipitation is observed in Shingo/Zanksar, Indus Besham Qila Astore and UIB Kharmong-Shyok basins. Such fragile monsoon impacts in lower side of basins is possible cause of dryness in summer season. Although, precipitation trends are increasing gradually in remaining basins, they were non-significant. Gilgit and Hunza, also experienced dryness from 1995-2010 that support the findings (Hasson et al. 2017) regarding precipitation decreased between 1995-2012. The change point (drying to wetting phase) varies from 2005 to 2014 for all basins except Shingo that follows in inverse direction. For autumn season, Shigar and Gilgit basins revealed significant upward trend in precipitation. Similarly, Hunza, Shyok and UIB-Kharmong also shows slightly significant rising trend. Although, Indus BQ and Shingo also reveal rising trend in precipitation, they were nonsignificant. Pettit Test found significant change point year for Shyok, Shigar, Gilgit and Hunza basins while rest of basins behaved nonsignificant.

3.3 Long Term Temperature Trends

The trends of long term annual and seasonal minimum, maximum, average temperature and diurnal temperature range (DTR) (T_{min}, T_{max}, T_{avg} and T_{max}- T_{min}) were observed in order to understand precipitation and streamflow behavior. The MK test and Theil–Sen slope were used to check the significance of trends and their slope. Table.1.6 shows the annual and seasonal slope values at different stations with bold values indicating trend's significance. The overall main features of minimum temperature consisted of warming during winter and spring while significant cooling was observed during summer season. The autumn and annual periods experienced a mixed response.

In case of maximum temperature, an overall significant increasing rate of temperature was noted for winter, spring and annual season while a significant cooling was noted for the summer season. Maximum and minimum winter temperature presented more warming trends than annual time series. Similarly, average temperature also followed a significant warming during winter, spring and annual season while a significant cooling is observed in the summer season. The high agreement of an upward trend for maximum and average temperature is also associated with the increasing streamflow for all stations during winter and spring season as shown in Fig.1.5. DTR also generally displays a significant increasing rate of temperature both for seasonal and annual scale except for the Chilas station.

Table 1.6 Long-term temperature trends (°C century^{-1}) at seasonal to annual scale

Variable	Stations	DJF	MAM	JJA	SON	ANN
T_{min}	Astore	1.2	**3.7**	-1.0	0.2	0.9
	Bunji	0.5	0.9	**-2.8**	-2.6	-1.1
	Chilas	**3.7**	1.0	**-1.8**	0.6	0.9
	Gilgit	1.3	1.0	**-1.9**	**-1.8**	-0.4
	Gupis	-1.3	-1.5	**-4.9**	**-3.4**	**-2.7**
	Skardu	0.4	-0.8	**-3.4**	**-3.1**	**-1.5**
	Naltar	**5.4**	4.2	2.3	1.9	**3.2**
	Shigar	**5.0**	3.6	1.8	-0.1	**2.7**
T_{max}	Astore	**3.2**	**5.0**	0.0	1.5	**1.7**
	Bunji	**3.4**	**2.7**	**-2.9**	-1.2	0.4
	Chilas	0.4	1.4	**-3.2**	1.1	0.6
	Gilgit	**4.2**	**4.2**	-2.0	1.2	**1.9**
	Gupis	**5.2**	**4.6**	-2.6	**1.7**	**2.6**
	Skardu	**4.8**	**4.8**	-0.2	**2.2**	**3.9**
	Naltar	3.2	1.9	-2.0	-3.7	0.3
	Shigar	2.7	2.1	-0.6	-2.0	0.7
T_{avg}	Astore	**2.4**	**4.8**	-0.6	0.9	**1.6**
	Bunji	**2.1**	1.7	**-2.6**	**-1.8**	-0.4
	Chilas	**2.0**	0.6	**-2.7**	-0.4	0.1
	Gilgit	**2.8**	**3.2**	**-2.7**	0.2	**1.1**
	Gupis	**1.8**	1.7	**-3.7**	-1.0	0.0
	Skardu	**2.6**	**1.7**	**-1.8**	-0.5	0.5
	Naltar	**4.3**	3.6	0.3	-0.2	1.4
	Shigar	3.8	1.7	0.08	-0.6	1.7
T_{DTR}	Astore	1.4	1.2	**0.9**	**1.5**	**1.3**
	Bunji	**2.7**	2.5	-0.2	1.6	**1.5**
	Chilas	**-2.9**	0.9	-0.8	**-1.8**	**-1.4**
	Gilgit	3.2	**3.3**	1.2	**3.8**	**2.9**
	Gupis	**6.9**	**5.6**	**2.6**	**5.3**	**5.5**
	Skardu	**4.5**	**4.9**	**3.6**	**5.9**	**5.0**
	Naltar	**-2.2**	-2.0	-2.8	-4.5	**-3.6**
	Shigar	-2.3	-0.4	**-1.9**	**-1.5**	**-1.5**

3.4 Variability and trends of the runoff in Upper Indus Basin

The variability and trends of the river runoff were evaluated in different sub-basins as shown in Fig.1.5, Table S1.1 and Fig.S1.3. The trend magnitude is represented with upward and downward triangles only starting with 20 years time window just for reasons of clarity of the figure. The annual streamflow trends expressed strong significant increasing trend at Indus Kachura and slightly significant at Shyok and Astore stations. Although streamflow is also rising for Indus (Besham Qila), Bunji and UIB-Kharmong stations, the rates of increase were not statistically significant. In contrast, streamflow followed non-significant downward trends for Indus at Kharmong, BQ and Yogo stations. Change point analysis with Pettitt test was also studied for respective streamflow stations. The results marked year 2004 for Indus at Besham Qila, UIB at Kharmong, UIB at Kharmong and Shyok, and year 1988 and 1994, respectively, as change point (drying to wetting phase) for Kachura and Shyok stations. The Pettitt test also

depicted a 5%-significant change point in streamflow for Indus (Kachura and Bunji), Astore and Shyok stations.

In winter season, most of subbasins showed a significant increase in streamflow. Although Shyok and Kharmong stations also followed positive trends in streamflow they were not statistically significant. The increasing streamflow trends in winter season is consistent with the increase of winter precipitation observed in most catchments, being significant in Shyok, Hunza and Shigar and also with earlier studies (Khattak et al. 2011; You et al. 2017) that reported climate warming causing early snow melt. Our analysis of temperature also reported similar results as shown in Table 1.6. Similarly, the change point analysis also confirms a 5%-significance change at Besham Qila, Kachura, Shyok, Bunji and Astore in Table S1.1.

In case of the spring season (MAM) streamflow overall shows an increasing trend in line with the winter season and this can be explained with temperature warming and resulting earlier and more intense snow- and ice-melt. Indus at Bunji and Astore revealed statistically significant increase in streamflow. The slightly rising trend in streamflow were also observed in Indus Downstream at Besham Qila, Kachura, Shyok, UIB-Kharmong and UIB-Kharmong and Yogo. Moreover, change point analysis exhibited significant changes in streamflow for Besham Qila, Astore and Bunji shown in Fig 1.5 and Fig S1.3.

For the summer season (JJA), the trend analysis shows a 5%-significance increase in streamflow for Indus at Kachura. The change point analysis also confirms significant variability in streamflow at Kachura. Similarly, slightly significant upward trends were also seen at Astore station. In contrast a significant decrease of streamflow were observed at Kharmong station. Although Indus at Behsam Qila and Bunji and Shyok also uncovered declining trend in streamflow, these were not significant. Such long term decrease in runoff behaviors are consistent with some previous studies for Indus at Besham Qila and Kharmong by (Arfan et al. 2019; Yaseen et al. 2020) and Indus at Kachura by (Farhan et al. 2015). Similarly trend behavior for Hunza and Shyok sub basins are also in agreement with (Mukhopadhyay and Khan 2015). The decrease of flow during the summer season can also be associated with declining temperature.

These finding demands a serious attention from policy makers and other stake holder agencies because variability of summer runoff significantly affects water availability in downstream areas in Indus Basin. In fact, about 70-75% of the Indus flow is generated during the summer season. Such changes in flow trends result in a significant reduction in water availability expected in the coming years. As a major share of this water is being used in the agricultural sector during the summer and winter season in Pakistan, if this trend of flow continues gradually in the long term, the reservoirs, farming and other water resources management operations must also be implemented and need to adapt accordingly.

In the autumn season (SON), streamflow exhibited a slightly significant rising trend for Indus at Kachura, Shyok, Astore, Bunji and Besham Qila stations. Similarly, Kharmong station showed non-significant rising trend in streamflow whereas BQ-Kharmong and BQ-Kharmong-Yogo depicted a slightly significant declining trend in streamflow. The change point analysis marked significant variation in streamflow for Bunji and Astore river. The finding of this study is also consistent with a recent study (Yaseen et al. 2020).

Table.1.7 Comprehensive Explanation of Basin Characteristics of UIB-Sub-Bains

Sub Basins	Gauge Location	Area	Elevation Range	Glacier area	Glacier Area	Q runoff	P CHIRPS	P ERA5	Annual_RF_C CHIRPS	Annual_RF_C ERA5
		(km^2)	m	(km^2)	%	($mm\ a^{-1}$)	($mm\ a^{-1}$)	($mm\ a^{-1}$)	(-)	(-)
UIB Down Stream	**Besham Qila**	163528	542–8572	19338	11.83	470	536	594	0.87	0.79
Gilgit	**Gilgit**	12761	1415-7104	1169	9.16	693	289	402	2.39	1.7
Hunza	**Dainyor**	13734	1420–7809	4285	31.20	369	574	372	0.642	0.98
Shyok	**Yogo**	33041	2389–7673	7388	22.36	368	395	302	0.931	1.22
Shigar	**Kachura-Yogo-Kharmong**	10639	2189–8448	2991	28.11	927	576	654	1.633	1.42
Astore	**Shital Bridge/Doyian**	3903	1504–8069	258	6.61	1146	876	1089	1.30	1.05
Shingo-Zanskar	**Kharmong**	69355	2250–7027	2763	3.98	205	302	383	0.68	0.53
UIB_Pakistan	**QUIB-QKhar-QShyok**	61132	569-8572	9187	15.03	824	664	877	1.24	0.93
UIB_Pakistan	**QUIB-QKhar**	94173	569-8572	16575	17.60	664	570	656	1.16	1.01

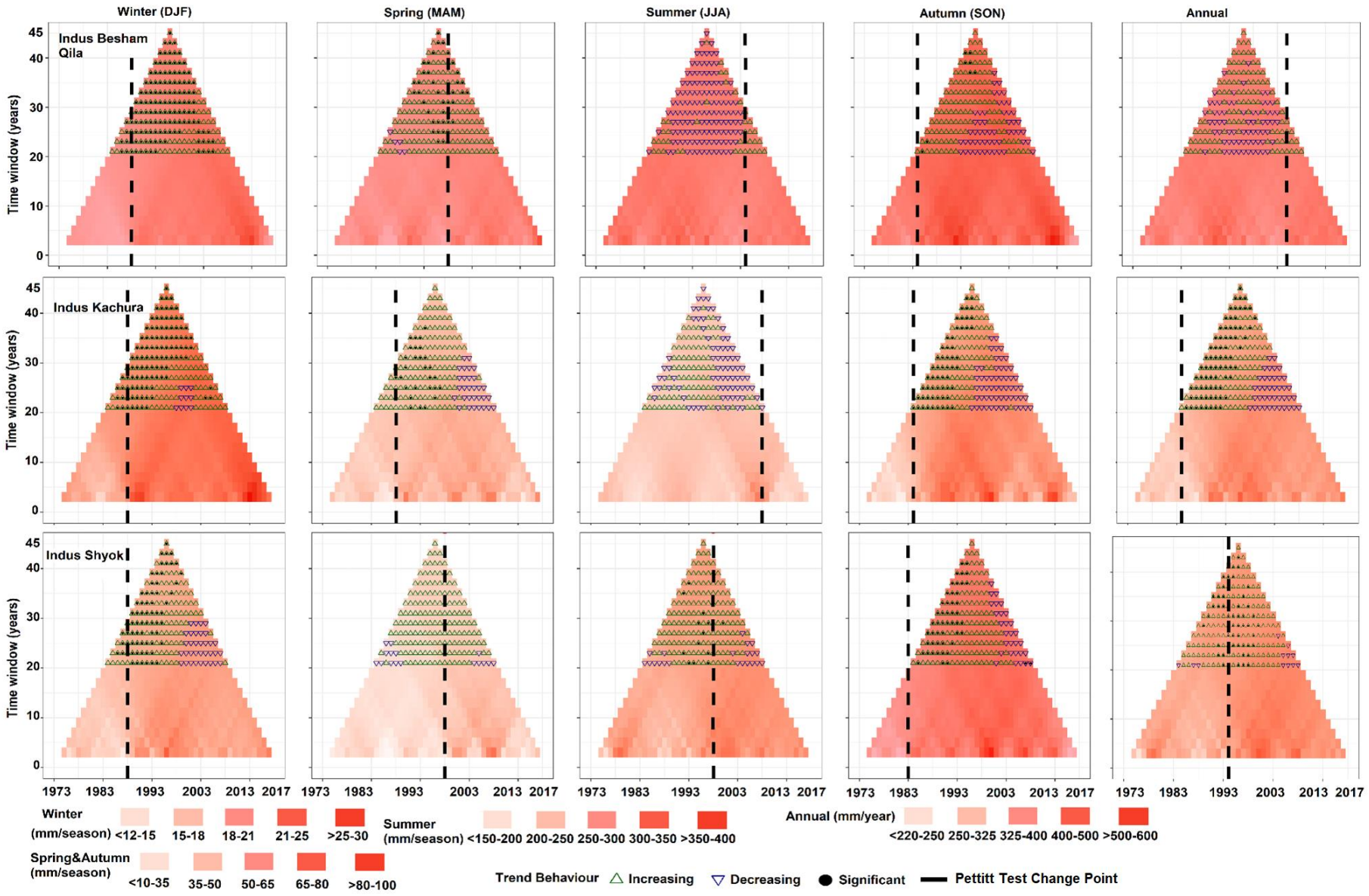
Winter (DJF)
Spring (MAM)
Summer (JJA)
Autumn (SON)
Annual
Indus Besham Qila
Indus Kachura
Indus Shyok
Time window (years)
0
10
20
30
40
45
1973
1983
1993
2003
2013
2017
Winter (mm/season) <12-15 15-18 18-21 21-25 >25-30
Spring&Autumn (mm/season) <10-35 35-50 50-65 65-80 >80-100
Summer (mm/season) <150-200 200-250 250-300 300-350 >350-400
Annual (mm/year) <220-250 250-325 325-400 400-500 >500-600
Trend Behaviour △ Increasing ▽ Decreasing ● Significant ━ Pettitt Test Change Point

Figure.1.5 Running trend of annual and seasonal runoff series. Average runoff values are divided into various classes (white to red). Trend values are showed by upward (green) and downward triangles (blue) while trend significance is described by filled circles (significant with at least 20 data and Mann-Kendall p-values < 0.05). Black vertical line expresses 'change point' year (Pettitt Test) in the entire time series. The x axis is the starting year (central year), while the y axis is the moving window (a minimum assessment duration of 10 year is selected).

3.5 Rainfall-runoff relationship in the Upper Indus Basin

The rainfall-runoff relationship and runoff coefficients are first order representation of under- or overestimation of precipitation in the watershed. The annual and monthly runoff coefficients at sub-basins scale were developed as shown in Table.1.7 and Fig.S1.4. The results show that both precipitation datasets (CHIRPS and ERA5) including observed values are not able to close the water balance because runoff coefficients (Q/P) higher than one have been calculated in the majority of sub-basins. Higher values of runoff coefficient for Gilgit, Shigar, and Shyok basins depict negative mass balance in these basins. Similarly, Astore, Hunza and Besham Qila exhibited higher precipitation values than river runoff except in summer season, because of snow and glacial melt and have natural to negative balance at monthly scale. The Indus Downstream with outlet point at Besham Qila which merges drainage of all upstream sub basins experiences positive to slight negative mass balance during summer season. These results need to search for possible explanations.

Overall, ERA5 performed better compared to CHIRPS precipitation dataset for closing the water balance. Although, CHIRPS dataset have good agreement with observed precipitation values, it is still unable to close the water balance in the majority of basins. Immerzeel et al. (2015) suggested that reanalysis products based on ECMWF IFS forecast model such as ERA5 can be used to validate atmospheric convergence. ERA5 incorporated fully coupled components of atmosphere, land surface and ocean waves that are useful for closing atmospheric water balance. Gao and Liu (2013) argued that mountain regions exhibited higher values of runoff coefficient due to greater magnitude of surface runoff, shallow soils, steep slope, permafrost and glaciers. In case of UIB, previous studies in this region and neighborhood glacierized catchments also indicated runoff coefficient values greater than one (Adnan et al. 2017; Dahri et al. 2016; Immerzeel et al. 2015; Wortmann et al. 2018). Siddique and Hashmi (2012) found 10%, 25% and 65% contribution of rainfall, snowmelt and glacier in the annual flows of Indus River at Tarbela outlet. The results of these studies about higher values of runoff coefficient also support our results. However, values are slightly changed from current study due to use of different gridded datasets, size and location of study area and in any case values higher than one are hardly acceptable.

Generally, it is believed that higher values of runoff coefficient indicate glaciers retreat and alteration of catchment hydrology. However, it is not only the single possible reason for negative mass balance. There are some other factors such as under catch observed precipitation as well as production mechanism of various gridded precipitation as reported in UIB (Immerzeel et al. 2015; Kääb et al. 2012) and it is also evident in our results as shown in Table.1.4 and Fig.S1.3. The runoff values greater than precipitation in Shigar, Shyok and Gilgit

basins might also be associated with under catch precipitation due to non-availability of observed gauge stations at high elevation in UIB, where the orographic effect on enhancing precipitation could be relevant and because of possible systematic errors in measuring solid precipitation (Eccel et al. 2012). Similarly, some other mass balance studies (Brun et al. 2017; Gao and Liu 2013) also reinforce our conclusion that glacier retreat is only a partial reason for the missing water volumes in UIB for closing the water balance.

4. Discussion

The diverse climatic signals and contrasting hydrological regimes observed in the UIB are the main sources of the uncertainties affecting the assessment of the key components of the hydrological balance, as precipitation, snow and ice accumulation and melt and runoff. A clear example of such an inconsistent behavior is the difference between accumulation patterns based on various remote sensing data acquisition techniques and the geodetic mass balance as reported in multiple studies (Immerzeel et al. 2015; Krakauer et al. 2019; Lutz et al. 2016).

Based on the results of the analysis, it is concluded that CHIRPS dataset performs well with respect to observed gauge precipitation with lowest BIAS, MAPE and RMSE at annual and seasonal scale, followed by ERA5.The basin wide corrected monthly precipitation values from CHIRPS and ERA5 and their corresponding runoff coefficient values from each sub basin are illustrated in Fig.S1.4. The results of rainfall runoff, based on novel combination of gridded datasets and comprehensive ground observations, are in good agreement with some previous studies (Dahri et al. 2016; Kääb et al. 2015).The higher values of runoff in Gilgit, Shigar, Shyok imply a significant contribution of glacier retreat and snow melt, as well as under catch precipitation. It is also concluded that ERA5 precipitation proved to be a better dataset in-terms of closure of the water balance.

In the second part of this study, varying positive and negative trends for both precipitation and runoff at seasonal and annual scale in all sub-basins are reported. Previous knowledge about hydro-climatic trend is mainly confined up to linear trend analysis or with specific time interval, not explaining non-stationary precipitation and runoff variability within decadal to interdecadal time scale. The reliable knowledge about hydro-climatic variability over the UIB is very challenging for effective management and precise usage of available water resources in downstream areas (Hasson et al., 2017). In summary, precipitation exhibited greater seasonal than annual variations. Although precipitation is increased annually, but its behavior non-significant except Shyok and Shigar basins. Pettitt test indicates that change points (drying to wetting phase) mostly lie annually from 2005 to 2010 in the majority of the basins.

An overall increasing trend of winter precipitation are found in all sub-basins. Such a rising rate of precipitation can be due to a significant contribution of winter westerlies regimes and a transfer of rainstorm trajectories in UIB. The results of higher rates in winter precipitation also consensuses with previous studies (Krakauer et al. 2019; Latif et al. 2018; Yaseen et al. 2020). In spring the majority of glacierized catchments show a downward trend in precipitation. On the other hand, Indus Besham Qila, Astore, UIB Kharmong indicate increasing rate of precipitation, but they are statically not significant. Change point analysis also did not record well any transition phase (drying to wetting) in all sub-basins. In summary, spring is drying, as it is also reported in some recent studies (Yaseen et al. 2020).

In summer the basin is not showing any significant trend in the precipitation amount. On the other hand, some basins (Shyok, Gilgit, Hunza and Shigar) show a rising rate of precipitation, but none of them is statistically significant. The results showing a decreasing rate of summer precipitation align with previous studies (Cannon et al. 2015; Latif et al. 2018; Rizwan et al. 2019). Lutz et al. (2016) found a clear shift of the summer long-term rising precipitation trends to drying, revealing a transition towards weaker monsoonal influence at lower levels. In order to crosscheck this hypothesis, it would be to better to analyse seasonality in precipitation and streamflow by modeling melt water runoff in the selected area under different climatic conditions. It will be discussed in future perspective of this study. The Indus Downstream with outlet point at Besham Qila usually receives 70% of the annual precipitation in the summer season. This water is stored in two major reservoirs, Tarbela and Mangla, for next cropping season, known as Kharif and Rabi season, when rice and wheat is cultivated in major downstream areas of the UIB. If the same downfall trend of precipitation continues in the future, it will reduce the water availability, ultimately putting further stress on already dwindling water reserves of Pakistan.

Concerning streamflow, variabilities are more pronounced seasonally than annually. Results indicate that winter and spring streamflow discharge significantly or slightly significantly increased in all sub-basins, whereas it decreased in summer. Yaseen et al. (2020) suggested that a rising trend of winter discharge is mainly linked with westerly precipitation regimes, because a major portion of UIB hydrology is dominated by westerly disturbances rather than monsoon offshoots. There are also different significant interpretations about these flow dynamics. One reason could be found in the significant warming in winter and spring, as shown in Table 1.6, whereas summer cooling caused early snow melt during spring and less flow available during summer (i.e., decreasing trends in summer discharge show lower melting rates in summer, resulting in potential stability of glaciers and consequently positive basin storage).

5. Conclusions

The study presents a comprehensive hydro-climatic trend and precipitation anomaly analysis for the UIB at the sub-basin scale. The primary objective of this study is to evaluate the performance of four gridded precipitation datasets for developing a precipitation climatology and check its reliability for the UIB. The datasets were examined for an overlapping period spanning from 1995 to 2017 at the seasonal and at the annual scale. Based on results, it is found that the performance of CHIRPS dataset is good to describe the distribution of observed precipitation with lowest BIAS, MAE, RMSE and MAPE, followed by ERA5. The mean annual corrected precipitation was calculated as 536 mm a^{-1} in the UIB gauged at Besham Qila. The precipitation climatology exhibited a higher rate of precipitation in the lower part of the basin for both the annual and the seasonal scale. The runoff coefficient for CHIRPS and ERA5 is though greater than one in some basins, making the water balance unrealistic. There can be two main reasons: 1) underestimate of precipitation, as most of the monitoring stations in the UIB are valley-based and do not represent the true basin hydrology in the high elevation bands 2) glacier retreat and early snow melt due to global warming and elevation-dependent warming. However, there are small chances for glacier retreat because most glaciers, especially in Karakorum, have been advancing or in stable conditions in the last decade (2008-2016)

(Berthier and Brun 2019). Meanwhile, precipitation rate declines with elevation annually, rises during winter and spring season but decreases during summer season. These issues demand further investigation, as they are affecting the contribution of glacier and snow melt in total flow from each sub-basin. The findings of this study would be helpful to understand the discrepancies between the observed and the gridded precipitation datasets referring to the UIB and may have substantial impact on studies related to the designing, planning, modeling and management of the water resources under climate change. The results of the study also recommend that gridded precipitation is corrected before its usage in hydrological modeling studies, especially in those involving glacierized catchments. The anomaly method proved to be worthwhile for assessing precipitation climatology, especially in data scarce regions with a sparse monitoring network.

In the second part of this study, annual and seasonal precipitation revealed significant variability seasonally rather than annually. Summer is drying while winter is wetting. The increasing rate of precipitation was also seen during spring in some basins, but they were not statistically significant. Similarly, trend analysis of observed streamflow at various gauge stations in the UIB facilitates understanding about comprehensive water balance for the region. Like precipitation variability, streamflow one is more pronounced seasonally rather than annually. At the annual scale, trend analysis of discharge shows slightly significant increasing trend at the Indus River Kachura, Shyok and Gilgat stations, while nonsignificant decreasing trends at Kharmong stations, BQ-Kharmong and BQ-Kharmong-Shyok stations are found. Seasonal flow analysis reveals more complex regime: winter (December-February) and spring (March-May) exhibit a rising trend in streamflow, while summer (June- August) shows a declining trend. The seasonal analysis also shows an increasing rate of warming in spring and early seasonal melt discharge from most of the sub-basins, whereas field significant low flow/drying was observed during summer.

The findings of this hydro-climatic analysis are expected to support future sustainable development projects in the study area. For instance, it would be helpful to assist engineers, the government and its organizations, as well as other stakeholder agencies to set up structural and non-structural measures to handle extreme flood and other natural hazard events, such as building dams and other control structures, lining canals and water course and adopt precision agricultural techniques (drip and sprinkler irrigation). It would also be viable to bridge the gap in terms of water availability and supplies especially in the lower area of the basin, where a major share of this water is being used for growing crops. These results would facilitate farmers and other stakeholder agencies to set cropping pattern according to water availability under prevailing climatic conditions.

Acknowledgements

The study covers one part of PhD research work funded by University of Brescia, Italy. The authors highly appreciate the Pakistan Meteorological Department (PMD), Water and Power Development Authority (WAPDA) and China Meteorological Data Sharing Network (CMDSN) for providing reliable data for this study and helping to publish valuable information.

Chapter II

Energy balance modeling of snow and ice melt in the Naltar Catchment (UIB, Pakistan)

Muhammad Usman Liaqat[*1], Roberto Ranzi[1]

This chapter consists of a paper in preparation for Advances in Water Resources:

Liaqat, M.U., Ranzi, R. 2022. Energy balance modeling of snow and ice melt in the Naltar Catchment (UIB, Pakistan). Advances in Water Resources (In preparation)

[1]Department of Civil, Environmental, Architectural Engineering and Mathematics, Università degli Studi di Brescia-DICATAM, Via Branze, 43, 25123 Brescia BS, Italy

Summary

Energy budget-based distributed modelling at High Mountain Asia (HMA) is important to examine glaciological-hydrological processes and quantify flow rates. Trends in ablation of snow and glaciers retreat depend upon initial ice reserves, meteorological parameters and geographical features which vary across sub-basin in HMA. In this study, the Physical Based Distributed Snow Land and Ice Model (Grossi et al. 2013; Ranzi et al. 2010; Ranzi and Rosso 1991) is employed in the Karakorum for the Naltar catchment located in Hunza river basin (Pakistan) to simulate snow and glacier retreat as well as daily runoff. The overall objective is to explore the feasibility of this modelling system in the Karakoram environment. The accuracy of the model in simulating snow and glacier retreat is crosschecked using improved MODIS snow cover product (M*D10A1GL06) and Landsat based snow cover area for both spatial and temporal scale. The results exhibited overall satisfactory performance in terms of coefficient of determination (R^2) = 0.96 and Nash-Sutcliffe Efficiency (*NSE) = 0.95* of model against satellite-based snow cover area for all simulated years. Downstream daily runoff measurement at the outlet of Naltar catchment at Naltar Bala station was used as a reference of comparison for simulated streamflow. The results of runoff simulations compared with observed daily discharge obtained NSE and KGE of 0.90 and 0.89 for calibration and validation period respectively. Simulated runoff volume computed by PDSLIM coupled with runoff model was in reasonable agreement and only 1.03% higher than mean observed runoff volume with mean absolute percentage error of 8%. Flow composition analysis revealed that runoff regime of Naltar catchment is composed 39% glacier runoff, 42% sub-surface runoff and 18% surface runoff. The eight years mean value of net mass balance exhibited slightly negative mass balance (-810 ± 311 mm w.e. a^{-1}) less pronounced than in the Alps. Overall, PDSLIM, so far tested in the Alps, is thus suitable to estimate energy and mass balance in the glacierized catchments of Karakorum and Himalayan and to understand snow-glacier melt runoff dynamics and floods in highly complex terrain with glacier rich mountains. This study provides a basis for potential application of such an integrated model to the entire Hindu-Kush-Karakoram-Himalaya region toward simulating snow and glacier hydrologic processes within a water and energy balance-based, distributed hydrological modeling framework.

Keywords: PDSLIM, energy balance, snow and ice melt, Naltar catchment, Karakoram

1. Introduction

Mountain glaciers are key freshwater resource and vital components of the hydrological cycle. Water resources are directly influenced by the dynamics of snow and glaciers melt runoff. However, there is still a lack of understating about hydrological processes linked with glacial dynamics and runoff. Blöschl et al. (2019) analyzed the impact of climate on glacial runoff and marked it as one of twenty third unsolved problems in hydrology. The significance of glacial runoff dynamics is worthwhile for million of people living in downstream areas worldwide. These questions are especially challenging for Indus Basin which is considered as a climatic hotspot region (Immerzeel et al. 2015).
The Upper Indus Basin (UIB) is enriched with world largest natural reserves of snow and ice that retain water balance in this region and surrounding valleys (Immerzeel and Bierkens 2010; Smiraglia et al. 2007). Snow and glacier melt runoff comprises the major share of Indus River flow (Tahir et al. 2011).

The economy of Pakistan is largely dependent upon the Indus River system which is providing indispensable water supply for irrigation, hydropower generation, municipal and industrial use (Kult et al. 2012). Additionally, the economy of the Pakistan is agriculture based and it is entirely dependent upon the flow of Indus river for irrigating its cash crop and 90% of country's food grains (Ringler and Anwar 2013). Indus River receives its major share of water from UIB- around 90% of overall flow. Out of 60% come from snow and glacial melt (Biemans et al. 2019). It makes UIB glaciers utmost important for providing fresh water supply to millions of people living downstream. Hence, any changes in UIB flow would have serious consequences on country water-food and energy nexuses.
Climate mediated changes, such as glaciers retreat, variability in snow cover area, melting and precipitation have altered seasonal and annual water availability in downstream areas of UIB. Rasul et al. (2011) found rising rate in temperature trends at annual and seasonal scale which accelerated flood events and lake formation in northern parts of Pakistan. Such catastrophic disasters brought uncertain and abrupt flow variation in mountainous area claiming massive loss of lives and property damages.

The northern part of Pakistan is enriched with 5218 glaciers and 2420 glacial lakes located in 10 sub-basins (Saifullah et al. 2020). However, a substantial number of uncertainties have been examined in previous hydrological studies in this region. These uncertainties are primarily associated with lack of reliable input data, diverse modeling tools and poor feedback mechanism. Some studies found rising rate of glacier retreat in the Himalaya and Hindu Kush region (Benn et al. 2012; Muhammad et al. 2019) while, others exhibited advancing in central Karakoram (Berthier and Brun 2019; Bolch et al. 2017; Muhammad et al. 2019). Hewitt (2005) who coined the term 'Karakoram Anomaly', the stability or abnormal growth of glaciers in the central Karakoram, as opposed to glaciers retreating in nearby mountain ranges such as the Himalayan range and other mountain ranges around the world as in the alps (Paul et al. 2014) and the Italian alps in particular (Carturan et al. 2016). Recently, (Javed et al. 2022) found ~10% increase in precipitation intensity and higher percentage of snow fall (65%) in Karakoram relative to total seasonal snow fall linked western disturbances behind the

emergence and continual presence of Karakoram anomaly in recent years. Thus, it is crucial to estimate the accurately of snow and glacier melt runoff to cope with the issues of Karakoram Anomaly in these catchments. It is also substantial to incorporate reliable tools and methods for modeling snow-glacier melt and runoff dynamics to handle the climate change impacts.

Over the past years, various hydrological, energy balance and temperature index models have been used to evaluate melt rates in Himalaya and Karakorum including Hydrologiska Byråns Vattenbalansavdelning (HBV) (Akhtar et al. 2008; Bergström 1976; Fowler and Archer 2006), the soil water assessment tool (Garee et al. 2017), the snowmelt runoff model (Adnan et al. 2017; Tahir et al. 2011) and the University of British Columbia watershed model (Hasson, 2016) . Although, fully distributed models are also used in High Mountain Asia (HMA) (Lutz et al. 2016; Shrestha et al. 2015), it demands extensive amount of data, time and efforts to correctly extrapolate snow glacier melt rate in high altitude terrains where surface atmosphere and meteorological process are widely varied.
Additionally, researchers preferred to use simple conceptual models and adopt lumped approach as compared to spatial distributed due to less data demand, smaller computational time and easy to calibrate in UIB in order examine melt and hydrological dynamics in current and future climatic scenarios (Ayub et al. 2020; Immerzeel et al. 2010; Naeem et al. 2016; Pellicciotti et al. 2012; Saleem et al. 2020). But considering climate change, temperature index models are disputable as they are not fairly capture the spatial variability of melt rates over glacier surfaces (Farinotti et al. 2010). Similarly, hydrological models used in UIB catchments exhibited considerable variation in results consequently set off uncertainties. These ambiguities are generally associated with inter-annual variation in temperature and precipitation due to climatic anomaly, modeling tools and calibrated parameters (Dolk et al. 2020; Ragettli et al. 2013).

In this study, high altitude automatic weather station data were used to assess the melt rate using fully distributed energy balance model. This technique works by the concept that simulated melt rates with a physically based energy balance model are reliable at the location of Automatic Weather Stations due to the use of available high-quality meteorological measurements. The present research employed the energy balance model Physical based Distributed Snow Land and Ice Model (PDSLIM) for first time in Pakistan at Naltar catchment located in Hunza river basin. Hunza river basin is the second largest glacierized basin in UIB. Glaciers are important part of the water balance for Hunza basin and any changes in glacial storage consequently influence the streamflow. Earlier studies on snow glacier melt runoff in Hunza basin were carried out at basin level (Ali et al. 2018; Dolk et al. 2020; Faiz et al. 2020; Farhan et al. 2020; Hayat et al. 2019; Ragettli et al. 2013; Shrestha and Nepal 2019) however, water resources management decisions take place at a smaller sub-basin /catchment scale except few one (Shakoor and Ejaz 2019). Furthermore, the availability of data is another important factor in selecting the Naltar catchment as a suitable location for energy mass balance simulations. UIB is a region with limited data sources, and most of the stations are not distributed uniformly. In Naltar catchment both hydro-metrological stations are providing complete attributes which are main requisite of PDSLIM model. Bearing all these considerations in mind, the study has two main objectives: (1) to examine the performance of

PDSLIM model to compute accurate flow composition and snow cover extent, (2) to quantify the contribution of snow and glacier melt to net river runoff and explore the ability of PDSLIM for prospective applications in forthcoming studies. This model exhibited good performance in snow and ice covered Italian Central Alps by (Grossi et al. 2013; Ranzi et al. 2010). It considers physical processes in a distributed hydrological modeling framework at a catchment scale to explore melting and would therefore lessen different sources of uncertainties. This study would also provide path for application of such modeling tool in future energy and mass balance studies in this region and will encourage accurate prediction of hydrological processes under climate change scenarios.

2. Material and Methods

In this section, both statics and dynamic type of input data are presented which were used by PDSLIM. Statistics data comprised of spatial data such as digital elevation model (DEM), landcover, leaf area index (LAI), snow albedo, SWE and catchments details while, dynamic data include hydro- meteorological data. The detailed information about stations locations, elevation, time period and available meteorological attributes are given in Table.2.1 as well as presented in Fig.2.1.

2.1 Description of the study area

The Naltar catchment was selected as a case study to conduct energy balance modeling test by examining melt and runoff. It is geographically located (36.10-36.37 N and -74.01-74.25 E), a climatically temperate region of Hunza river basin. The region is characterized by pine forests, snow peak trekking routes, glaciers, small lakes, and most important one of famous spot for winter skiing for national and international visitors (Gardezi et al. 2022). The elevation of Naltar catchment varies from 2270 m to 5886 m with mean elevation 3980 m. It is situated in Hunza basin about 42 km away from Gilgit city and 208 km from K2 (the second largest mountain range in world) in the Gilgit-Baltistan region of Pakistan. The total area of Naltar catchment is 242.62 km^2 with glacierized area of 42 km^2. The largest glacier within Naltar catchment is Shani glacier with an area of 19 km^2. The average annual precipitation and temperature recorded at Naltar station are 685 mm/yr and 6.5^oC (Liaqat et al. 2022). The streamflow was measured at Naltar Bala stations with mean flow 11.79 m^3/sec over period (2006-2016). The water further moves through Naltar stream into Hunza river which is one of the main tributaries of the Indus River. Fig.2.1 shows the location of Naltar catchment and, the location of 5 meteorological and streamflow gauge stations used in this study.

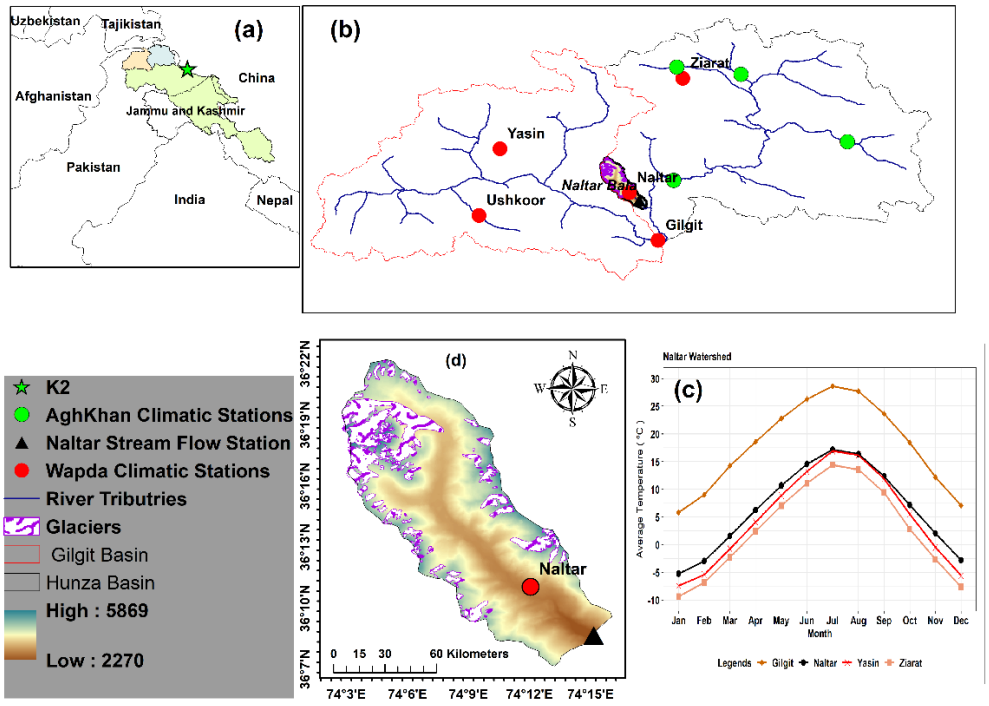

Figure.2.1 (a) The administrative and political boundary of the Upper Indus Basin (green), (b) Location of the Naltar catchment within the Hunza Basin (black border) and hydro-meteorological stations (circles), (c) Annual cycle of mean monthly temperature of several meteorological stations (d) a clear picture of Naltar catchment with glacier coverage.

2.1 Meteorological Data

Physical based distributed snow land and ice model (PDSLIM) requires six meteorological parameters to effectively simulate snow melt runoff and snow development. The input data consisted of precipitation, temperature, relative humidity (RH), wind speed (WS) solar radiation (SR) and pressure. All parameters except pressure were obtained from Water and Power development Authority (WAPDA), Pakistan based automated weather stations known as data collection platforms (DCPs), located in Gilgit and Hunza basin. The detail description about these stations is given in Table.1 as well as shown in Fig.2.1. The above stations are selected due to their location and data from these stations have converted into PDSLIM specific text format. A consistency check revealed that this dataset had some missing values for some variables at different dates and times. Initially, we selected 8 out of 11 years for which missing values amounted to less than 20%. The final set of years was 2006, 2008, 2009, 2010, 2011, 2012, 2014 and 2016 and simulations with PDSLIM cover from 1st April to 30th September each year. The remaining missing values were imputed through multiple linear regression as used by (Prabnakorn et al. 2019). The method involves developing a relationship between different sets of neighboring stations and choosing one (Naltar station) with the best coefficient of determination (R^2), but not less than 0.6 for precipitation, relative humidity, windspeed and solar radiation and 0.75 for temperature, respectively. Reconstructed hourly pressure values were obtained from (Bair et al. 2020).

Table.2.1 Details of meteorological data used in the study and their sources.

Basin	Stations	Period from	Period to	Agency	Latitude (^{0})	Longitude (^{0})	Elevation (m asl)
Gligat	Gilgit	2006	2016	WAPDA	35.92	74.33	1460
	Yasin	2006	2016	WAPDA	36.40	73.5	3280
Hunza	Ziarat	2006	2016	WAPDA	36.77	74.46	3629
	Naltar	2006	2016	WAPDA	36.17	74.18	2898

2.2 Hydrological Data

The hydrological station was installed at Naltar Bala since 2006. This streamflow measurement equipment was installed by WAPDA when Government of Pakistan decided to construct Naltar Hydro-power plant at Naltar river. Currently, Naltar-IV hydro-power plant is operational in Naltar. It has a small reservoir which holds enough water to produce electricity at full capacity of 18 MW. To a limited extent, the plant can shape hourly water releases during the day such that production is highest during peak load hours. The mean Explanatory Data Analysis (EDA) curve (2006-2016) for Naltar streamflow is shown in Fig.2.2.

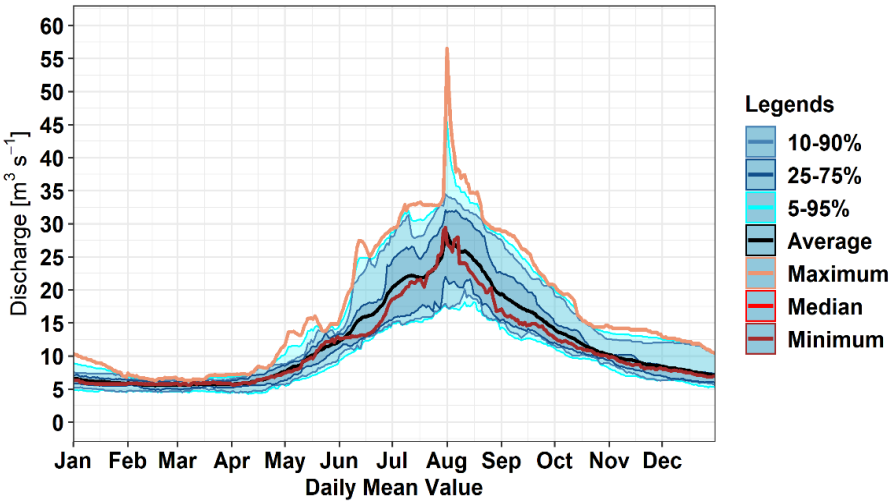

Figure 2.2. Explanatory data analysis of streamflow in naltar catchment (2006-2016)

2.3 Geo-topographic Data

The meteorological variables used by the PDSLIM for the evaluation of energy and hydrological balance components constitute only one part of input data by the model itself. In order to make a effective spatial distribution of the variables and to estimate energy balance, it is imperative to incorporate the topographic characteristics of the territory since they have different behavior in terms of energy exchange. These topographic variables include: the digital elevation model of the study area, albedo, land use/ land cover, the leaf cover index and the terrain view factor.

2.3.1 Landcover and Lead Area Index

Land use/land cover (LULC) and leaf area index (LAI) are two important parameters of PDSLIM model, as variation in land use/ land cover (LULC) and LAI cause significantly change on evapotranspiration, runoff and some other parameters of the hydrological cycle (Shah et al. 2020). The landcover data based on ENVISAT's MERIS Level 1B with spatial resolution of 300 m were obtained from GlobCover landcover product developed by European Space Agency (ESA)-GlobCover. The data were clipped according to the area of interest and divided into 15 major classes. For each land cover class, the model provides a unique code. The major LULC classes are snow/glacier, grassland, rocks, and mixed forest. A glacier layer derived from the Randolph Glacier Inventory (RGI) Version (V) 6.0 released on July 2017 was overlaid on landcover data. The LULC and LAI map of Naltar catchment are shown in Fig 2.3.

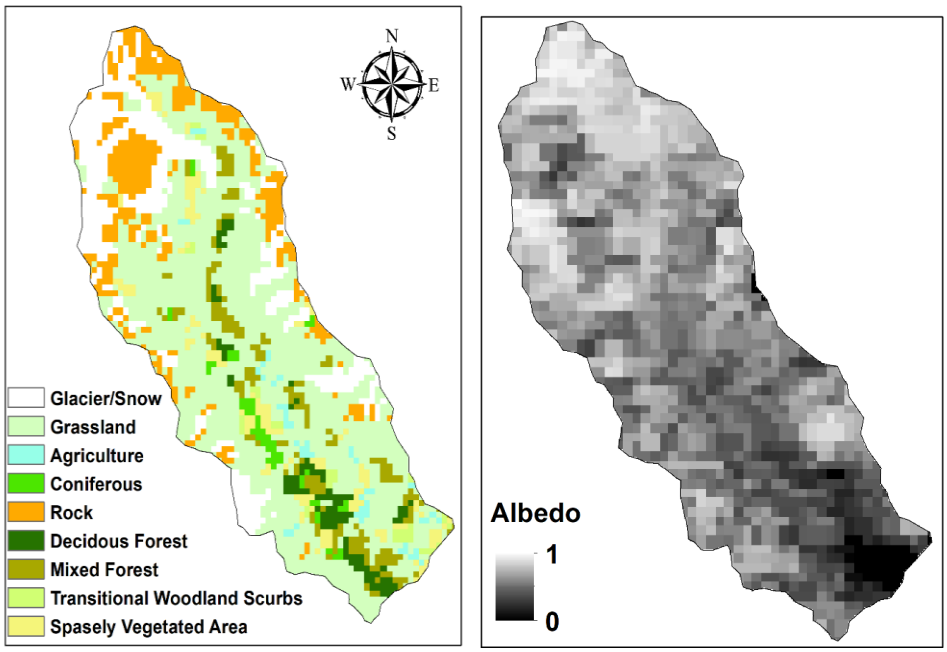

Figure.2.3 LULC classes and albedo observed in Naltar catchment.

MODIS 8DAY composite LAI product MYD15A2H.006 was acquired from Land Processes Distributed Active Archive Centre (LPDAAC) (https://lpdaacsvc.cr.usgs.gov/appeears/task/area) from the start of each melt period. The quality assessment (QA) flags in the databased were utilized to make sure the quality of the MODIS LAI data at given period. Both LULC and LAI were reclassified and resample according to PDSLIM requirement. The initial value of Snow Water equivalent (SWE) used in PDLSIM was derived from high resolution reconstructed SWE products using MODSCAG and SPIRES approaches developed by (Bair et al. 2019).

In this study, we used both products to put some uncertainty bounds on simulated results. The SWE was reconstructed from the snow melt-out date to the date of maximum SWE at the beginning of melting season using satellite-based retrievals of MODIS fractional snow cover

area in combination with energy balance equations and land surface metrological variables (Bair et al. 2016; Rittger et al. 2016). Further validation of reconstructed SWE product in High Mountain Asia (HMA) was carried out by employing full distributed energy balance model (SNOWPACK and ALPINE 3D) and in-situ values of snow depth collected and maintained by the Aga Khan Agency for Habitat (AKAH) (Bair et al. 2020). Further information about these products and its developing mechanism can be found in following studies (Bair et al. 2018; Bair et al. 2019; Rittger et al. 2016).

Table. 2.2 Sources, description and type of data used in this study.

Data Type	**Data Source**	**Scale**	**Description**
Digital Elevation Model	NASA-SRTM (90m)	grid cell (90 x 90 m)	NASA Shuttle Radar Topographic Mission (SRTM)
Landuse / Land Cover	GlobCover land cover	300 m	European Space Agency (ESA) GlobCover land cover product
LAI	MODIS	500 m	MODIS 8-day composite LAI product MYD15A2H.006
ALBEDO	MODIS	500 m	MOD10A.006 Daily Snow Albedo
Meteorological Data	WAPDA (Bair et al. 2020)	Hourly	Temperature, Wind Speed Relative Humidity, Solar Radiation, Rainfall Pressure
Discharge Data	WAPDA	Daily	Mean Daily Discharge at Naltar Bala Station (m^3/sec)
Snow Water equivalent (SWE)	(Bair et al. 2020)	Daily	Reconstructed SWE product using MODSCAG and SPIRES approaches

2.4 Satellite snow and glacier data

Accurate snow monitoring is indispensable for glacio-hydrological modelling studies, cryosphere monitoring and associated changes. Naltar catchment has wide spatial variability of ice, snow and seasonal snow cover. MODIS daily satellite images are reliable source to monitor spatial and temporal variability of snow cover areas. Although, MODIS daily snow cover product provide more reliable results than other remote sensing products, still significant proportion of cloud covers in images especially in winter and monsoon season may cause underestimation of snow and ice cover extent. The present study used improved MODIS snow cover product (M*D10A1GL06) developed by Muhammad and Thapa (2021) derived from original MOD10A1 (Terra) and MYD10A1 (Aqua) from same sensor using multi-step approach in order to access the accuracy of PDSLIM model to accurately simulate the snow cover areas during the melting season. Muhammad and Thapa (2021) improved the product by applying spatial, seasonal and temporal filters to reduce snow cover estimation caused by cloud cover and by swath and lower spatial resolution. They divided product into 13 classes (25: No Snow classes, 50: Cloud, 198: Snow only in Terra, 199: Snow only in Aqua, 200: Snow in both Terra and Aqua, 238: Debris-covered ice with Terra Snow, 239: Debris-covered ice with Aqua Snow, 240: Exposed debris-covered ice, 242: Debris-covered ice with Snow in both Terra and Aqua, 248: Debris-free ice with Terra Snow, 249: Debris-free ice with Aqua Snow, 250: Exposed debris-free ice, 252: Debris-free ice with snow in both Terra and Aqua). In this study, we used pixels of class (200+240+242+250+252) in order to compare with simulated snow and ice cover. The detail description about this product can be seen in Muhammad and Thapa (2021). Historical glacier boundaries in Naltar watershed were masked out from RGI V6.0.

Additionally, the Shuttle Radar Topographic Mission (SRTM) digital elevation model (DEM) at spatial resolution of 90 m for Naltar catchment was downloaded from CGIAR Consortium for Spatial Information (STRM,2013). The DEM data was used to define catchment boundary and topography. The boundary of Naltar catchment defined by filling the unnecessary cells with no-data in order to save from extra model computational time. Afterwards, the DEM map clipped to keep area of interest using QGIS. A temperature lapse rate of 0.0065 $^{o}C\ m^{-1}$ is applied at pixel at grid resolution to represents grid resolution. The sub-grid temperature correction is mandatory for presenting elevation gradients. The mean monthly temperature data and lapse rate were also used to compute freezing line altitude (FLA) $0^{o}C$ Isotherm is shown in Fig.2.4.

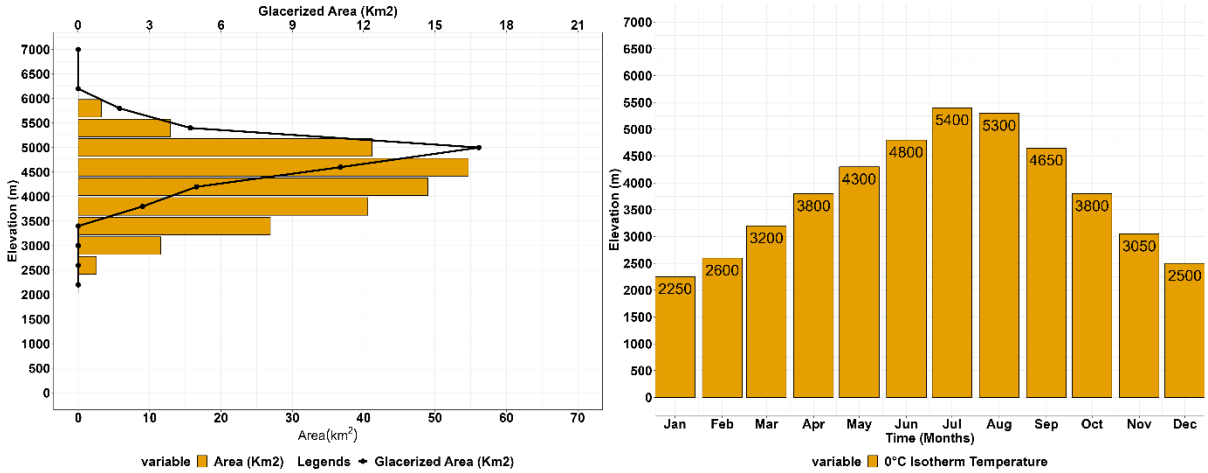

Figure 2.4 (a) The hypsometric curve of Naltar catchment and distribution of glacierized area under 500-meter elevation band layer b) Mean monthly freezing line altitude or $0^{o}c$ isotherm within Naltar catchment.

2.5 Modeling Strategy

Although, PDSLIM is a physical based model, it encompasses few parameters that can be optimized to attain better simulation results with respect to reference data. The most important parameters for snow cover extent include precipitation and temperature lapse rate, value of fresh snow albedo at start of melting season and debris cover. In case of hydrological simulations, the training parameters are runoff coefficient, saturated hydraulic conductivity of snow, ice, and soil and lag time. The PDSLIM simulated at the hourly time step with 90 m spatial resolution scale and PDSLIM need all meteorological inputs at the same scale. However, modeling outcomes can be ascertained at daily and monthly scales according to user's demand. The modeling outcomes have been examined at the site and catchment scale.

2.5.1 Calibration with MODIS and LANDSAT Snow Cover Area

The PDSLIM derived snow cover area was compared with MODIS snow cover product (M*D10A1GL06) and LANDSAT, and the comparison used to calibrate the snow and glacier related parameters. The snow + ice melt progression was carried from April 1st to September 30th for each of eight simulation year. Both the statistical evaluation and visual inspection were

employed to develop comparison between model and MODIS/LANDSAT based snow cover extent.

2.5.2 Calibration and Validation with Naltar Streamflow

The rainfall runoff and snow-ice melt from linear reservoir model were calibrated by comparing the observed runoff with model runoff at Naltar bala station. Simulated runoff data for (2006, 2008, 2010 and 2016) marked as low, medium and high flows were used for calibration while remaining (2009, 2011, 2012 and 2014) were used for validation respectively. The missing years (2007, 2013 and 2015) were excluded from simulation due to missing values and substantial inconsistencies present in the observed data. The model performance was investigated using both efficiency criteria and visual inspection associated with systematic (over or underestimation) and dynamic (rising/falling limbs, timing) and baseflow behavior of model. A combination of multiple efficiency criteria such as Nash-Sutcliffe efficiency (NSE), Percent bias (PBIAS), Mean Absolute Percentage Error (MAPE), Root-Mean-Square Error (RMSE), Coefficient of Determination (R^2), Kling Gupta efficiency (KGE) were used in this study as single criteria is not optimum to examine model performance. The KGE is goodness of-fit method developed by Gupta et al. (2009) to overcome drawbacks present in NSE.

2.6 Glacier Surface Mass Balance

The mass balance of glacier is considered as one of primary indicator of climate variation. The mass balance is basically divided into two parts:
rts: accumulation (c) and ablation (a). The accumulation on glacier is calculated by deposition of solid precipitation on the glacier surface and ablation is determined by melting of snow and ice.
At a given point (x,y) and at any time (t) on a glacier surface, the accumulation rate $\dot{c} = \dot{c}(x,y,t)$ is the rate of mass gain and ablation rate $\dot{a} = \dot{a}(x,y,t)$ is the rate of mass loss. The mass balance is usually expressed in kgm^{-2} or meters water equivalent (m.w.e). The integral b can be measured at any time in field.

$$b = b(x,y) = a+c = \int_{t1}^{t2} (\dot{c} + \dot{a})\, dt$$

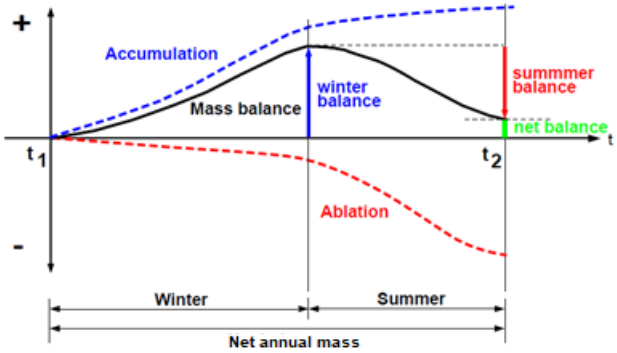

Figure.2.5 Basic representation of annual mass balance for a specific point (x, y) on the glacier surface

2.6.1 Annual Mass Balance

The computation of mass balance anomaly is very substantial to understand incoming and

outgoing water volume in glacierized catchments over a given period. Primarily, glaciological method is preferred to assess annual and seasonal mass balance. However, its applicability in large and high altitude glaciers in remote areas as Naltar is challenging due to complex terrain and poor accessibility. In this case, hydrological can be a valid alternative. It indicates the estimation of incoming and outgoing water volumes typically over one year or over the accumulation and the ablation seasons. For a given period, the annual mass balance of Naltar catchment is equal to winter and summer mass balance. It is usually expressed in terms of equivalent water volume B [L^3]. It is assumed that winter starts on 1st of October indicated as t_{ow} of the previous year and ends on the 31st of March denoted as t_{fw} of the current year. The ablation season start on the 1st of April $t_{os} = t_{fw}$ of the given year, when first snow melt event detected and ends on the 30th of September t_{fs} of the balance year.

2.6.2 Winter Mass Balance

The winter glacier's mass balance is computed as the sum of the snow mass balance and the firn and ice mass balance. The ice and firn mass balance $B_{w,ice}$ is equivalent to total volume of the snow water equivalent left at the beginning of the balance year $S_{weq}(t_{ow})$ which start its metamorphosis into firn and late ice. Ice melt is assumed to be negligible in winter. The snow winter balance Bw, snow is given by the difference S_{weq} (t_{fw})- $S_{weq}(t_{0w})$, between the snow water equivalent observed at the end S_{weq} (t_{fw}), S_{weq} (t_{0w}) at beginning, the last often being small or negligible. Hence, the glacier's winter mass balance is:

$$B_w = B_{w,ice} + B_{w,snow} = S_{weq}(t_{0w}) + S_{weq}(t_{fw}) - S_{weq}(t_{0w}) = S_{weq}(t_{fw}) \quad (1)$$

In this study winter balance i.e. SWE for each simulated years was derived from (Bair et al., 2019)

2.6.3 Summer Mass Balance

The summer mass balance on snow/glacier surface is computed as total of the point mass balance over each pixel of the study domain, measuring dA = 90 m x 90 m = 8100 m^2. Snow mass balance B_s is computed as

$B_s = B_{s,\,snow} + B_{s,\,ice}$

$B_{s,\,snow} = S_{weq}\,(t_{fs}) - S_{weq}\,(t_{0s}) =$

$$\int_{t_{0s}}^{t_{fs}} \int_{A_{snow}(t)} [r(A(t),t) + s(A(t),t) - m_{snow}(A(t),t) - e_{snow}(A(t),t)]\,dA\,dt \quad (2)$$

Here, s shows snowfall, m_{snow} (comprising drainage of the snow liquid water content), r depicts the rainfall rate and e_{snow} characterize the net snow sublimation and evaporation losses. All above mentioned terms have dimensions [LT^{-1}]. The rainfall over firn and ice areas is assumed to flow as runoff on the surface and on subsurface channels of the glacier. Therefore, summer balance $B_{s,ice}$ of this part of glacier with area $A_{ice}(t)$ is always negative being the sum of the sublimation rate e_{ice} and melt rate m_{ice} calculated as:

$$B_{s,\,ice} = \int_{t_{0s}}^{t_{fs}} \int_{A_{ice}(t)} [-m_{ice}(A(t),t) - e_{ice}(A(t),t)]\,dA\,dt \quad (3)$$

The summer mass balance of ice and snow over the glacier's area A_g is

$$B_{s,\,snow} = \int_{t_{0s}}^{t_{fs}} \int_{A_g(t)} [p_{snow}(A(t),t) - m(A(t),t) - e(A(t),t)]\,dA\,dt \quad (4)$$

Here p_{snow} shows total precipitation rate, either snow *(s)*, over snow or rain *(r)*, $m = m_{snow} + m_{ice}$ imply the total melt as well as drainage from the snowpack, and $e = e_{ice} + es_{now}$ evaporation and sublimation from snow and ice. Negative sign represents condensation of air water vapour occurs. All these terms have dimension [LT^{-1}]. Total precipitation over the glacier is the sum of the total precipitation on snow p_{snow}, rain on ice, r_{ice} that does not contribute to the glacier mass balance because it runs off the glacier's surface. The annual mass balance is represented by the sum of the winter and summer mass balance:

$$B_{s,\,snow} = S_{weq}(t_{fw}) + \int_{t_{0s}}^{t_{fs}} \int_{A_g(t)} [p_{snow}(A(t),t) - m(A(t),t) - e(A(t),t)]\,dA\,dt \quad (5)$$

The annual specific mass balance over a unit surface of the glacier with dimension [L] can be obtained as:

$$b = \frac{B}{A_g} = \frac{B_{snow} + B_{ice}}{A_{ice} + A_{snow}} \quad (6)$$

It is noted that areal changes are neglected in current mass balance computation as their estimation would require a continuous monitoring of the glacier's areal extent.

2.7 Energy Balance of Snow and Ice

In this section, energy balance modelling framework, known as PDSLIM (Physically based Distributed Snow Land and Ice Model) are described. The PDSLIM model is modified form of the PDSM model, applied at catchment scale to simulate snowmelt and evapotranspiration fluxes Cordevole Ranzi and Rosso (1991) and Toce Grossi and Falappi (2003) and then applied to Adamello glacier (Grossi et al. 2013; Ranzi et al. 2010).

For a unit area, melt rate for finite depth of layer of ice or snow superimposed over ice is computed using the energy balance equation:

$$H_m + H_c = S_{io} + L_{io} + H_l + H_s + H_p + H_g \quad , \quad (7)$$

Here unit of all terms are W/m^2

H_m: energy available for melt,

H_c: Internal Energy of the snow or ice layer,

S_{io}: net shortwave radiation,

L_{io}: net longwave radiation,

H_l: latent heat,

H_s: sensible heat,

H_p: advective heat from precipitation,

H_g: Conductive heat at the bottom side of the snow or ice layer

For an snow or ice layer with finite depth Δz, mean Temperature T, specific heat C and density p changes over time

$$H_c = C\,p\,\Delta z\,dT/dt \quad (8)$$

Here specific heat of ice is equal to $C = C_i = 2093.4$ J kg^{-1} K^{-1} and its density is assumed $p = p_i$ 830 kg m^{-3}. In case of snow, density changes over time according to snow pack simulation

depicted by (Ranzi and Rosso 1991). The detailed description of the shortwave and longwave radiation terms of the energy balance equation, S_{io} and L_{io}, followed by global shortwave radiation measurements, R_m can be seen in (Ranzi and Rosso 1991; Ranzi and Rosso 1995). For glacierized areas, the fraction of the measured incoming global radiation R_m reflected by terrain surrounding each point and the the diffused shortwave radiation from the sky calculated as R_d with mean albedo $\alpha_t(x,y)$ provide the flux of diffuse radiation at each point $R_d(x,y)$. The sky view factor V_s i.e. the fraction if sky hemisphere surrounding each point and the terrain view factor V_t which is its complementary value $V_t=1-V_s$ the diffuse radiation results:

$$R_d(x,y)=R_d\, V_s(x,y)+ \alpha_t(x,y)\, R_m\, V_t(x,y) \quad (9)$$

The sensible (H_s) and latent heat (H_l) fluxes of energy balance equation is computed based on mixing length theory, assuming stable conditions at the snow and ice surfaces (Hock and Holmgren 2005). It is considered as reliable supposition during melting period especially when detailed measurements of the wind field and turbulent structure are of scare quality. Accordingly, H_s and H_l are computed as:

$$H_s = C_p\, p_a\, D_h\, (T_a - T_s) \quad (10)$$

$$H_l = L_v\, p_a D_w \frac{0.622}{p} (e_a - e_s) \quad (11)$$

$$D_h = D_w = k^2 u_z/[ln(z/z_o)]^2 \quad (12)$$

Here D_h and D_w are turbulent and momentum exchange coefficients while, the other parameters are characterized as:

p_a (kg/m^3): air density,

C_p (J kg-1, K-1): specific heat of air

p(Pa) atmosphere pressure,

T_a *(K)* air temperature at height z,

T_s *(K)*: ice or snow surface temperature

e_a *(Pa)*: air vapor pressure,

e_s *(Pa)*: vapor pressure at snow or ice surface,

L_v (J kg^{-1}): latent heat of sublimation

u_z (m s^{-1}) wind velocity at measurement height z, assuming the same reference height for temperature and humidity,

z_o (m): surface aerodynamics roughness,

The value of surface roughness is assumed 0.007 m for ice (Hock 1998) and 0.003 for snow (Plüss and Mazzoni 1994). The value of Karman constant (k) is 0.4. The term conductive heat (H_g) is computed at the bottom of a surface firn or ice layer 0.1 m deep using Fourier law:

$$H_g = K_t\, dT/dz \quad (13)$$

Where value of thermal conductivity (K_t) of ice (Wm^{-1}K^{-1}) determined after Paterson (1994) as a function of mean temperature of the ice layer T_i

$$K_t = 9.828exp(-0.0057T_i) \quad (14)$$

The surface of ice or firn layer is considered to interchange conductive heat with an underlaying isothermal, T_g, a reasonable assumption for a temperate glacier in the melt season, semi-infinite and ice layer at constant 0^{o}C temperature a reasonable assumption for a temperate glacier in the melt season. By using this assumption, the conductive heat flux obtained from the glacier

during the time step $[t_k, t_k+1 = t_k+\Delta t]$ by the surface ice layer with mean temperature $T_{i,k}$ at the beginning of time step,

$$H_g = 2\sqrt{\frac{Cp_i K_t}{\pi \Delta t}}(T_g - T_{i,k}) \quad (15)$$

Where a and c depict the constant terms

$$\alpha = C_{P_i}\frac{\Delta z}{\Delta t} \quad (16)$$

$$c = 2\sqrt{\frac{C_{p_i}\rho_i K_t}{\pi \Delta t}}(T_g - T_{i,k}) \quad (17)$$

H_k the heat flux

$$H_k = S_{io} + L_{io} + H_l + H_s + H_p + H_g \quad (18)$$

H_k computed at the start of each computational time step $[t_k, t_{k+1}]$ in a finite difference implicit scheme to solve in time the energy balance equation (7) for the finite volume of surface layer assumed 0.1 m deep. Afterwards, merging equations (10), (11) ,(13), (15), (18) by assuming first that $H_m = 0$ we can solve equation (8)

$$H_c = H_k + H_g \quad (19)$$

With regard to the unknow average ice temperature $T_{i,k+1}$ at the end of the computational time step

$$(T_{i,k+1} - T_{i,k}) = H_k - c(T_{i,k+1} + T_{i,k})/2 \quad (20)$$

acquiring

$$T_{i,k+1} = [H_k + T_{i,k}(a - c/2)]/(a + c/2) \quad (21)$$

If temperature $T_{i,k+1}$ results greater than 0°C the ice temperature is equal to 0°C and excessive heat available for ice melt is

$$H_m = max\ (a\ T_{i,k+1}, 0) \quad (22)$$

The surface ice temperature T_0 which is required to determine the convective and radiative part of equation (6) at each computational time step, assuming a linear temperature profile within the ice layer is set twice the mean ice layer temperature $T_{0,k+1} = 2\ T_{i,k+1}$. A similar numerical approach is also adopted to estimate convective heat fluxes in the upper snow layer 0.1 m deep and at the bottom of the snowpack. The melt begins as soon as temperature of snow/ice layer reaches 0°C at a rate of m (m s^{-1}) processed by dividing the energy flux H_m by the latent heat of fusion of ice L_f = 334944 J/ kg and the water density, ρ_w, being ρ_w=1002.28 kg/m^3 at 0°C:

$$m_{ice/snow} = H_m / L_f / \rho_w \quad (23)$$

The relative low ice density (kg/m^3), close to literature value for firn was selected because ice crusts and sublimation crystals were observed on glacier surface that cause higher porosity.

3 PDSLIM Model Structure

The PDSLIM model consist of two main cycles: time and spatial cycle. In time cycle, model executed each hour of the day within a spatial cycle that calculates the individual components

of the energy balance on each cell of the area of interest considered. The spatial cycle follows various calculation processes depending upon cell position which it is executing is on a snowy, ice or ground. If the position of cell is on a glacierized surface, the model may take into account the possible presence of debris cover layer. The PDSLIM provides a abundant of output variables that can be chosen upon user demand. It also allows the users to turn on/ turn off segments (processes) that are relevant/ non-relevant with study region.

The energy available for glacierized surface is calculated by

$$H_m + H_c = S_{io} + L_{io} + H_l + H_s + H_p + H_g \quad (1)$$

Here unit of all terms are W/m^2

H_m: energy available for melt,

H_c: Internal Energy of the snow or ice layer,

S_{io}: net shortwave radiation,

L_{io}: net longwave radiation,

H_l: latent heat,

H_s: sensible heat,

H_p: advective heat from precipitation,

H_g: Conductive heat at the bottom side of the snow or ice layer

In the case of an ice surface, the contribution of the heat exchange with the H_g soil shall be 0. The short wave radiation balance is performed by the *G_{min}S0 function and* depends on the value of the albedo:

$$Swabva = (1\text{-}albedo)\ Radnet(x,y) \quad (2)$$

Albedo is determined with the following relationships:

$$Albedo = min[(albedi \cdot (1+VAR/100),1)] \quad (3)$$

Here: *VAR* increases the value of the albedo taking into account the possible presence of diffuse radiation:

$$VAR = 0.499+0.0097 \cdot (10 \cdot Difrad)^3 \quad (4)$$

- *Albedi* is the value of the ice albedo estimated by MODIS image from start from melting season for simulated years

In the literature, several values are attributed to the glacier ice albedo. This value is influenced by the degree of debris cover, the dust content, as well as the surface characteristics of the ice itself, such as roughness and crystal orientation. Table.2.3 shows some ice albedo values considered in some studies:

Table 2.3: Ice albedo values used and obtained from certain energy balance models. (a) simulated; (b) simulated albedo values $0.35<\alpha<0.39$; (c) simulated albedo values $0.33<\alpha<0.38$

	α Ice
Munro & Young, 1982	$0.25<\alpha<0.3$ (a)
Lang, 1987	0.27 (a)
Hock, 1998	0.37 (b)

Arnold, Willis & altri, 1996	0.24
Hock & Holmgren, 2005	0.355(c)

In the case of snow cover, the value of the albedo is different from that found on ice: a semi-empiric relationship is used, based on experimental cases, in which it is mainly a function of the season, expressed in days from December 21:

$$Alb_{cls}(t2112) = ASPRIN - \frac{A_0}{90} \cdot arc\ tan\ tan\ [\ A_1(t2112 - TSPRIN)] \quad (5)$$

Here the value of Spring Albedo in the Dolomites (Ranzi and Rosso 1991), Asprin assumed to be equal to approximately 0.735, A_0 seasonal albedo variability equal to 0.08 and the value of A1 and TSPRIN equal to 0.16 [g^{-1}] and106 [g]. The value of albedo is associated with fresh snow which is decreased by passage of time.
An exponential law of variation is assumed with snow metamorphism resulting from melt in which the variable T_{al} is represented by the sum of the maximum daily temperatures greater than 10°C.

An albedo value of the snow will tend asymptotically to AM_0:

$$Alb_{mel} = (Alb_{cls} - AM_0) \cdot exp\ (-CAM \cdot T_{al}) + AM_0 \quad (6)$$

Here CAM *and* AM_0 are *calibration* parameters of the model which took in the case under consideration based on albedo measurements in the Dolomites

$$CAM = 0.044 \text{ and } AM_0 = 0.4. \quad (7)$$

For a glacierized surface, the value of albedo is also a function of the radiation type. It grows well if it is widespread, i.e. for low angles of solar height; it is then evaluated taking into account the index of diffused radiation *Difrad:*

$$Alb_{dif} = MIN[1; Alb_{mel}(1 + 0{,}00449 + 0{,}097Difrad^3)] \quad (8)$$

The next step after albedo determination, the net net shortwave radiation can be evaluated:

$$Swabva\ (1\text{-}albedo)\ Radnet(x,y) \quad (9)$$

The long wave radiation balance is computed by the *RLio function:*

$$L_{io} = (1 - FOR) \cdot EMISS \cdot Stefaa + FOR \cdot (EMISS - 1) \cdot Stefaa - (1 - FOR) \cdot 0.99 \cdot Stefan(T_S + 273.14) \quad (10)$$

Here
FOR: shows the percentage of area covered by vegetation;
Stefaa: calculates Stefan-Boltzmann's law for a body at T= T_a;
*Stefan(Ts+273.14):*Stefan-Boltzmann's law for a body at T= T_s;
EMISS: represents the atmospheric emissivity which indicate presence of clouds. It is determined by following equation:

$$EMISS = (1 - Cloudi) \cdot EPsa(T_a, EA) + Cloudi \cdot 1 \quad (11)$$

Here

EPsa: characterizes atmospheric emissivity which is determined according to the *Satterlund* report (1979) dependent on *air temperature* T_a and steam pressure *EA.*

Cloudi: it is the percentage of cloud cover, it is taken equal to the percentage of diffuse radiation Difrad. The turbulent flow of sensitive and latent heat are also continuity to the energy balance. Both parameters are computed by H_C and H_L functions respectively.

In the literature there are many studies aimed at determining the roughness coefficients for wind speed, temperature and vapor pressure; in analogy with many experimental cases, the model assumes following $z_{0w} = z_{0e} = z_{0T} = z_0$ equality for the roughness coefficient. The roughness coefficient chosen in the present case as well as used different studies are shown in Table 2.4 depending on the type of area concerned.

Table 2.4 Equivalent roughness coefficient used in the model as a function of surface type

Surface type	z_0
snow	0.003
ice	0.007
Debris	0.01

Table 2.5 Surface Roughness values in literature

	Surface type	z_0
Plush & Mazzini, 1994	Snow before the melting season	0.0019
	Snow in the melting season	0.0044
Hock, 1998	snow	0.007
	ice	0.007
Hock & Holmgren, 2005	snow	0.01
	ice	0.01

As far as the snow core is concerned, the accumulation, expressed in terms of snow cover height h_s [m]:

$$h_s(t) = h_s(t-1) + PSNOW - DMELT - REDUCT \quad (12)$$

In the above equation, h_s (t-1) depicts the height of previous snow event followed by newly contribution of precipitation as snow (PSNOW). The term REDUCT revealed a reduction in snow cover. There are two primary reasons for snow reduction: 1) compaction from fresh snow layer 2) melting. As snow melt begins to increase, water content becomes higher that occupies the pore of snow which ultimately increase snow and reduce its height. The mathematical expression of these factors are given as follows:

$$PSNOW = \frac{SNOW}{R_{sf}}$$

$$REDUCT = \frac{SNOW}{R_s} \cdot \left[\frac{h_s(t-1)}{0{,}25}\right]^{0.35}$$

$$DMELT = \frac{SNMELT}{R_s}$$

Here R_{sf} ratio of specific weight of fresh snow to water and *Rs* ratio of specific weight of snow and water. The snowpack density varies over time and is determined by the equation of mass continuity in each layer of the snowpack. The nivale cover is also variable, so it is considered that, when the height of the snow cover of a cell is less than a fixed minimum value, that cell is excluded in the next time step, since the thin layer is supposed to have melted for soil heating, except that precipitation occurs to replenish it. For the evaluation of the initial coverage it would be very important to have a satellite-detected image available at the start date of the simulation, from which to deduce the snowy cells. In the present study, the map of the height of the snow cover has been reconstructed from MODIS SWE product (Bair et al. 2020). The SWE product is further divided by snow density (300 kg/m^3) in order to computer height of the snow cover.

Evaporation losses from snow and ice free areas are estimated using a Penman-Monteith approach:(Monteith 1981) adopted in (Grossi and Falappi 2003):

$$TP_d = \frac{1}{\lambda}\frac{\Delta R_n + \rho c_p\,(e_s - e_d)\,/\,r_a}{\Delta + \gamma(1 + {}^{r_s}/_{r_a})} \qquad (13)$$

Where TP_d represents potential transpiration from a dry vegetative surface, r_s is surface resistance, Δ is the gradient of saturated vapour pressure e_s, against temperature T, λ is the latent heat of vaporization, R_n is energy available for melting for processing, ρ is density of air, c_p is specific heat of air at a constant pressure, $e_s - e_d$ Water vapour pressure deficit, r_a and r_s are aerodynamic and surface resistances, γ describe about psychrometric constant**.** Monteith formula also used to compute potential evaporation (EP) of the intercepted water surface (assuming surface resistance $r_s = 0$). The aerodynamic resistance to the water vapour diffusion is computed using the formulation:

$$r_a = \frac{ln^2[\frac{(z-d)}{z_0}]}{k^2.u_z} \qquad (14)$$

Here, the height of wind speed measurement is indicated by the letter z, d is the zero plane displacement, k is the von Karman constant (= 0.41), u_z is windspeed at height z. Accrding to (Wigmosta et al. 1994), Dividing the two formulas results in the ratio of potential transpiration from a dry canopy and potential transpiration from a wet canopy

$$TP_d / EP = \frac{\Delta + \gamma}{\Delta + \gamma(1 + {}^{r_s}/_{r_a})} \qquad (15)$$

As with the calculation of TP, the same ratio is applicable to calculating the potential

transpiration rate of partially wet vegetation. It is proportional to the potential evaporation rate from wet surfaces, EP, diminished by the effective evaporation of intecepted water, EI:

$$TP = (EP\text{-}EI)\ \frac{\Delta+\gamma}{\Delta+\gamma(1+{}^{r_s}/_{r_a})} \quad (16)$$

3.1 Hydrological Simulations

A hydrological simulation consists of equations that helps in determination of runoff, thus making possible a correlation between melt the input and rainfall runoff output data. A hydrological model is function of multiple parameters which are used to portrait watershed characteristics. The primary function of fully distributed PDSLIM model to validate dynamics of snow and glacier cover in area of interest. It provides various forms of output such as SWE, snow cover area, precipitation, shortwave and longwave radiation, sensible and latent heat flux, rain on snow cover, rain no snow area, snow and ice melt, evaporation from snow and no snow cover area. In this study, the output of PDSLIM model: (snow melt on ice, runoff from ice melt, rainfall – evaporation on ice, melt from snow + ice free areas, net rainfall over terrain i.e., snow and ice-free areas) is used to compute glacier runoff, sub-surface runoff, surface runoff. The linear reservoir model (LRM) is based on theory of linear tank over run on which the entire project is based. This linear method integrates the behavior of basin into three separate tanks in which a *flow rate p(t) enters and* from which the flow rate q comes out.The general equation describing the function of a flow rate in a linear reservoir model:

$$q\ (t) = q\ (t-1)e^{-\frac{t}{k}} + p(t)\ \varphi\ \ (1-e^{-\frac{t}{k}}) \quad (1)$$

where: *p dt:* volume of water entered in time *dt*; *q dt:* volume of water released over time *dt*

For simplification, the equation is further divided into sub-component of net runoff i.e.

- For Glacier Runoff

$$q\ (t)glacier = q_{ice}\ (t-1)e^{-\frac{1}{k_{ice}}} + p_{glacier}(t)\ \ (1-e^{-\frac{1}{k_{ice}}}) \quad (2)$$

- For Surface Runoff

$$q\ (t)surface = q_{surface}\ (t-1)e^{-\frac{1}{k_{surface}}} + p_{surface}(t)\ \varphi_{surface}\ \ (1-e^{-\frac{1}{k_{surface}}}) \quad (3)$$

- For the Sub-Surface Runoff

$$q\ (t)sub = q_{sub}\ (t-1)e^{-\frac{1}{k_{sub}}} + p_{sub}(t)\ (1-\varphi_{sub})\ \ (1-e^{-\frac{1}{k_{sub}}}) \quad (4)$$

Here: $p_{glacier}(t)$ is composed of snow melt on ice, runoff from ice melt, rainfall – evaporation on ice. $p_{surface}(t)$ and $p_{sub-surface}(t)$ is composed of melt from snow + ice free areas, net rainfall over terrain or snow on ice-free areas

q(t)glacier, q(t) surface, q(t) sub-surface: (mm/h) is the melting flow flowing at the glacier's outlet, surface and sub-surface layers at time t respectively.

q(t-1): (mm/h) the flow rate recorded at time t-1 i.e. at the previous hour;

k_{ice}, $k_{surface}$, $k_{sub:}$ (h) Time constant of reservoirs; φ_{ice}, $\varphi_{surface}$, φ_{sub}: runoff coefficient.

in (mm/h): infiltration rate, which gives rise to a sub-surface outflow.

τ (h): delay for the linear channel.

The calibration parameters used by the hydrological LRM model is shown in Table.S2.2. The values of these calibrated parameters are optimized by examining the statistical indices that were used to check difference between simulated and observed runoff. The schematization of the hydrological model considered is shown in Fig.2.6 (a). Similarly, layout of this study is give in Fig.2.6 (b).

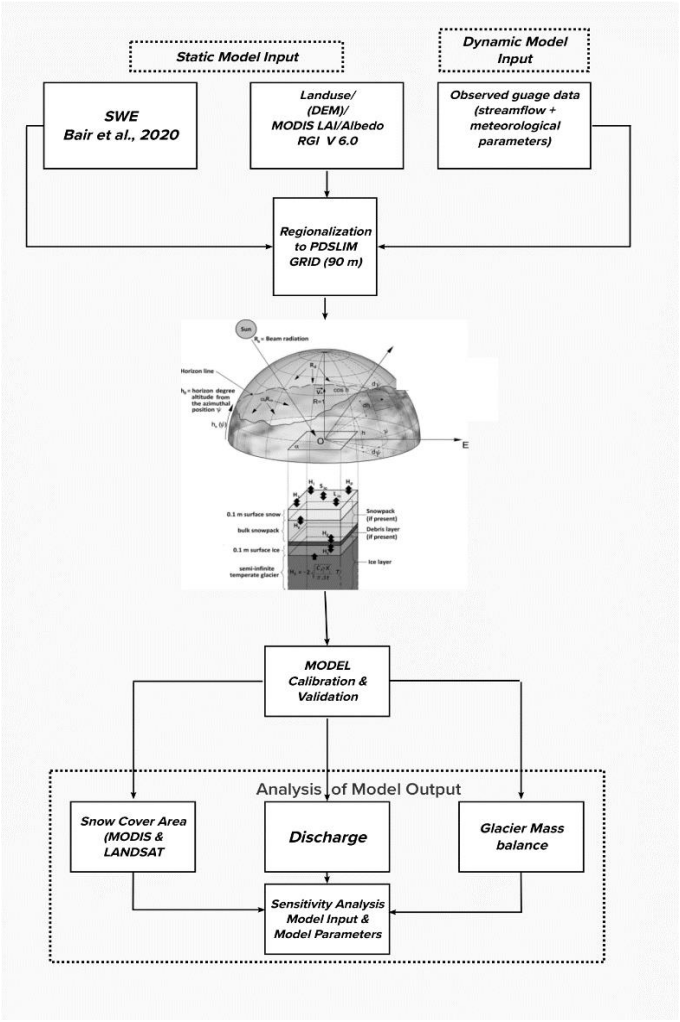

Figure.2.6 (a) PDLSIM and LRM modelling scheme

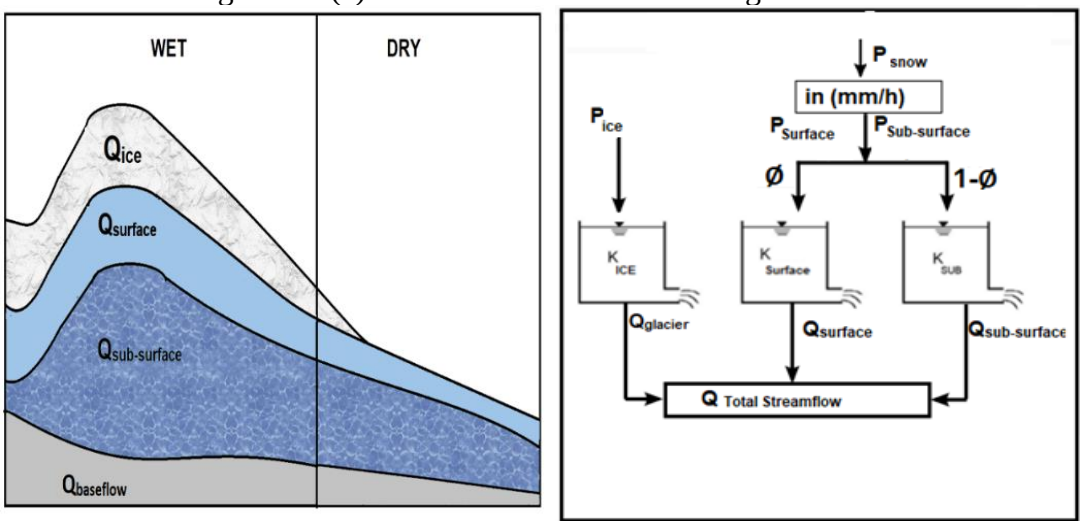

Figure.2.6 (b) Scheme of LRM model for inflow and outflow transformation.

Here P_{ice} indicate melt ice and effective precipitation over ice, P_{snow} refers to snowmelt and effective precipitation over ice-free areas, $P_{surface}$ denotes net precipitation, $P_{sub\text{-}surface}$ infiltration, $Q_{surface}$ surface runoff from ice-free areas, $Q_{sub\text{-}surface}$ sub-surface runoff from ice free areas and $Q_{glacier}$ is runoff from glacierized areas.

3.2 Sensitivity and Uncertainty Analysis

The performance of any model largely depends on availability and quality of observed datasets. In this study, primary meteorological parameters were acquired from station-based values. However, all these stations are valley based and the altitudinal difference among weather stations is not appropriate for estimation of temperature lapse rate (TLR), which may cause uncertainties in the distribution of model input to each of altitudinal belt and grid. Therefore, sensitivity of model performance was tested for the change in TLR ±0.065-0.0085°C 100 m^{-1} for clear sky and ±0.051-0.045°C 100 m^{-1} for cloud cover). Moreover, observed weather stations are unable to estimate SWE which substitutionally are used in PDSLIM as snow depth. In this study, initial SWE values were derived from derived from high resolution reconstructed SWE products using MODSCAG and SPIRES approaches developed by (Bair et al. 2019). In this study, we used both products to put some uncertainty bounds on simulated results. The simulated snow and ice progression, glacier mass balance and catchment runoff were examined using multiple statistical indicators for sensitivity analysis of model parameters.

3.3 Net Summer Glacier Mass Balance

The simulated glacier wide summer mass balance (April-September) is processed by analyzing the hydrological balance of Naltar catchment using following equation:

$$SMBhydro_{(Apr\text{-}Sep)} = -Q_{in\text{-}situ\ (Apr\text{-}Sep)} + P_{tot\ (Apr\text{-}Sep)} - ETA_{(Apr\text{-}Sep)} — S_{(Apr\text{-}Sep)} + AS_{(Apr\text{-}Sep)} \quad (1)$$

$$AS_{(Apr\text{-}Sep)} = AM\ snow_{(Apr\text{-}Sep)} — AG_{(Apr\text{-}Sep)} \quad (2)$$

$$AG_{(Apr\text{-}Sep)} = 0 \quad (3)$$

Where $SMBhydro_{(Apr\text{-}Sep)}$ is the simulated glacier-wide seasonal (ablation) summer mass balance from April- September for each simulated year, $Q_{in\text{-}situ\ (Apr\text{-}Sep)}$, $P_{tot\ (Apr\text{-}Sep)}$, $ETA_{(Apr\text{-}Sep)}$, $S_{(Apr\text{-}Sep)}$, is observed runoff, total precipitation, evapotranspiration, the sublimation of the overall ice and snow surfaces of the Naltar catchment and storage variation of catchment by end of melting season. $AS_{(Apr\text{-}Sep)}$ shows the storage variation of the catchment during ablation season, including the snow melt AM $snow_{(Apr\text{-}Sep)}$ contribution accumulated during (October-March) outside of the glacierized areas and the groundwater $AG_{(Apr\text{-}Sep)}$. The later is assumed to be equal to zero. The glacier storage variation is included in the glacier-wide seasonal surface mass-balance term. All quantities are in mm/day.

3.4 Visualizing Water Balance Change in Non-Dimensional Space

Non-dimensionless visualization tools are helpful to study water balance especially in complex and data scare catchments. The most prominent suggested by (Turc 1955) and (Budyko et al. 1974). In this study, the hydrological alternative of the Turc-Budyko plot was employed to analyze the observed precipitation data for reproducing a reasonable water-energy balance. In this method, the realistic closure of water-energy balance was examined using observed

precipitation data. Seasonal runoff coefficient or water yield (*Q/P*) was plotted as a function of seasonal long term aridity index (P/ET_p) (Coron et al. 2015).

$$Q/P = f\left(P/ET_p\right) \quad (1)$$

Here, ET_p, *Q and P* depicts evapotranspiration, specific runoff and precipitation in a given watershed respectively. The aridity index in equation 2 determines wettest and driest condition of catchment based on input precipitation (higher value of (P/ET_p) infers wetter catchment). There are generally three limits which illustrates this non-dimensionless hydrological interpretation: (1) $Q \geq 0$, (2) $Q \geq P - ET_p$,, (3) $Q \leq P$. All these assumptions are based on simple traditional water balance in a watertight (conservative) catchment:

$$P = Q + \alpha ET_p \quad (\text{where } \alpha < 1) \quad (2)$$

If a relationship for a specific year lies above the water limit i.e. (Q>P) limit, it is referred as glacier dominating catchment/ "Gaining zone" (Andréassian and Perrin 2012). If a glacierized catchment based on water energy balance lies within the Gaining zone (Q>P), it indicates that there are some additional water resources that contribute to net streamflow. This additional water is contributed by glacier melt. Alternatively, a catchment is considered as rainfall dominating catchment when a relationship for a simulated year is located below water and accumulated runoff is less than available energy, it means either the precipitation is overestimated or part of net runoff is unaccounted from water balance. The simple water balance equation in a glacierized catchment can be written as:

$$\frac{\Delta S}{\Delta t} = P - \langle Q + ET_a \rangle + MP \quad (3)$$

Here MB and ET_a depicts mass balance and evapotranspiration in the catchment. $\frac{\Delta S}{\Delta t}$is change in storage. If $\Delta S = 0$, the catchment is marked as "True" catchment. The true catchment can encompass indicate incoming and outgoing flow becoming zero by the end of simulated year which practically is not possible. Normally, it is observed that "Gaining"/glacier dominating catchment mostly have negative change in storage ($\Delta S < 0$) while "Leaky" rainfall dominant catchment has generally positive change in storage ($\Delta S > 0$).

4. Results and Discussion

In this section, PDSLIM optimization and simulated results at the Naltar catchment are presented and discussed. Performance of model mass balance are checked and presented in tabular form. Simulated snow cover area (SCA) at catchment level were compared with MODIS and Landsat SCA. Graphical flow composition and comparison between model and observed runoff have been shown and reasons for overestimation/underestimation reviewed.

4.1 Snow Cover Simulation

The ability of PDSLIM model to access snow cover simulation was accessed by comparing with LANDSAT and (M*D10A1GL06) derived snow and ice cover area at both temporal and spatial scale from 1st April to 30th September for each simulated year. The spatial and temporal

distribution of model SCA based on MODSCAG and SPRIES approaches is shown in (Fig.2.7, Table 2.7(a) and 2.7(b)). Despite the scale difference and lack of representations of in situ measurements, PDSLIM results are in agreement for simulating snow cover with (R^2 = 0.96, *NSE* = 0.95 and negative bias 1.8%) using SPIRES and (R^2 = 0.96, *NSE* = 0.94 and positive bias 6.12%) using MODSACG.

Based on this analysis, both approaches are simulating well to reproduce snow + ice melt progression. It also observed that simulated snow and ice cover showed underestimation patterns using (MODSCAG) and slightly overestimation (SPIRES) especially by the end of melting season. Such underestimation/overestimation is possibly related to misclassification or coarse resolution of MODIS pixels and low/high values of SWE products which ultimately are incorporated into simulated PDSLIM results. Moreover, sensitivity analysis was also applied are discussed in a later part of this study.

The mean maximum simulated snow cover area using (MODSCAG and SPIRES) was recorded (92.44% and 94.24%) (224.26 km^2 and 228.56 km^2) respectively which were closer to MODIS based snow cover 94.51% (229.31 km^2). Similarly, the results mean minimum simulated snow cover area using (MODSCAG and SPIRES) was measured (18.4% and 23.2%) (44.60 km^2 and 56.37 km^2) respectively and these results were also in agreement with mean minimum MODIS snow cover area 19.8% (48 km^2) by end of melting season.

Generally, snow melt progression starting higher by end of April with increase of solar radiation and air temperature follows MODIS SCA curve. The snow melt progression generally reached its peak by the end of July except in high altitude zone where snow persists throughout ablation period as shown in Fig.2.8. Afterwards, glacier melt starts, except in some high elevation zones due to low temperature. It is also observed that model and MODIS snow cover area also experienced a very short abrupt snowmelt or snow accumulation during the simulation period (2009 and 2010). Such changes are possibly due to the occurrence of precipitation as a snowfall event at high altitude zones where temperature is already below 0^oC as shown in Fig.2.7.

Further, the simulated SCA results were also crosschecked with high resolution LANDSAT based SCA to check reliability of model at higher spatial and temporal scale. A 20% threshold for cloud covers were applied while selecting LANDSAT tiles for specific area of interest. It is also concluded that model displays satisfactory results for snow and ice melt progression at high spatial resolution during the entire melting season except a moderate underestimation have been observed for 2016 year as shown in Fig S2.1. Such underestimation is primarily due to presence of cloud covers in the study catchment which are clearly visible in NIR bands as shown in Fig S2.1.

2006

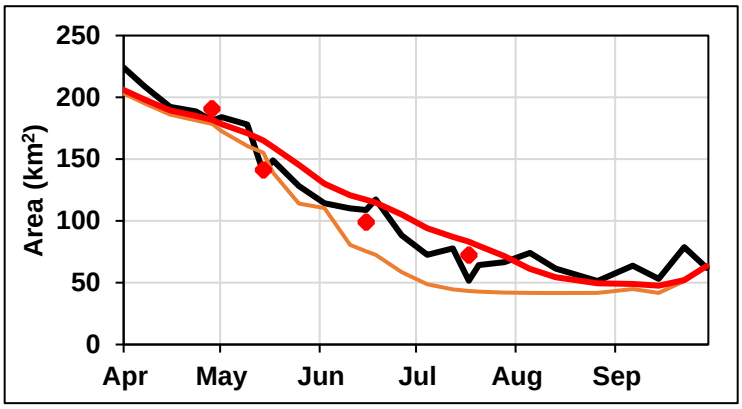

2006

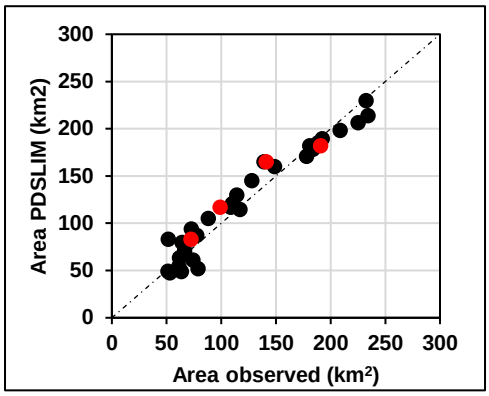

2008

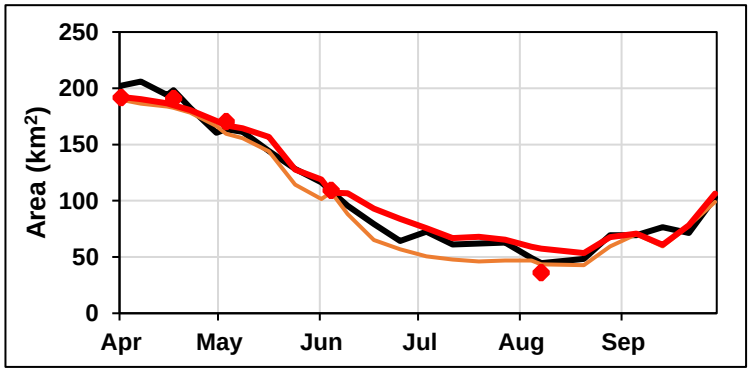

2008

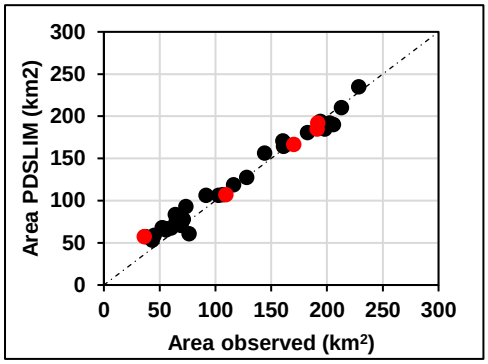

2009

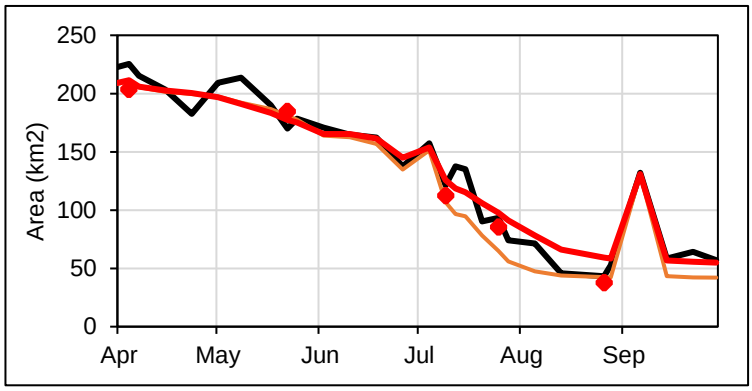

2009

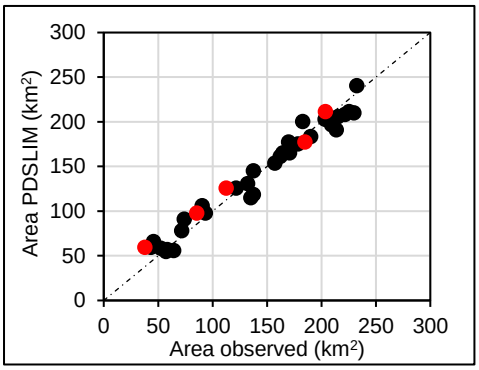

2010

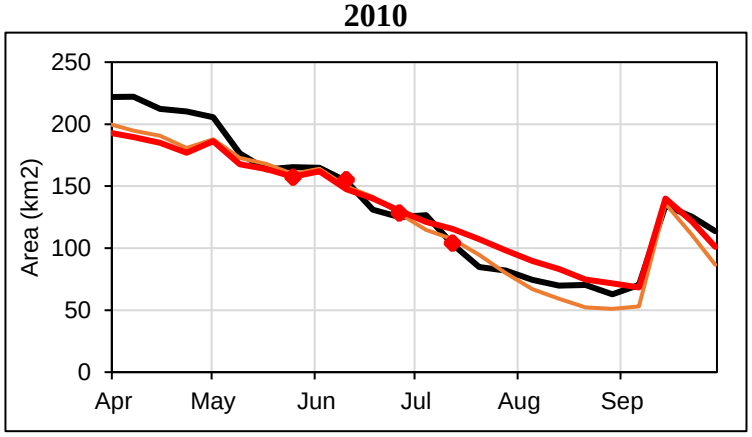

2010

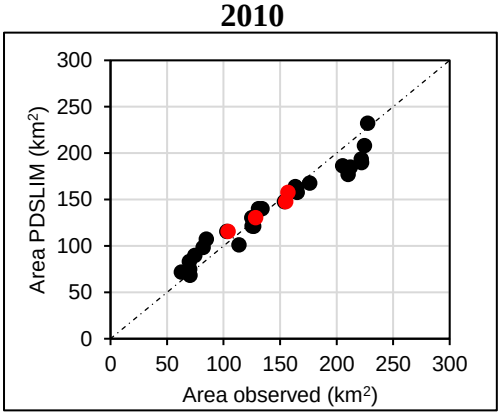

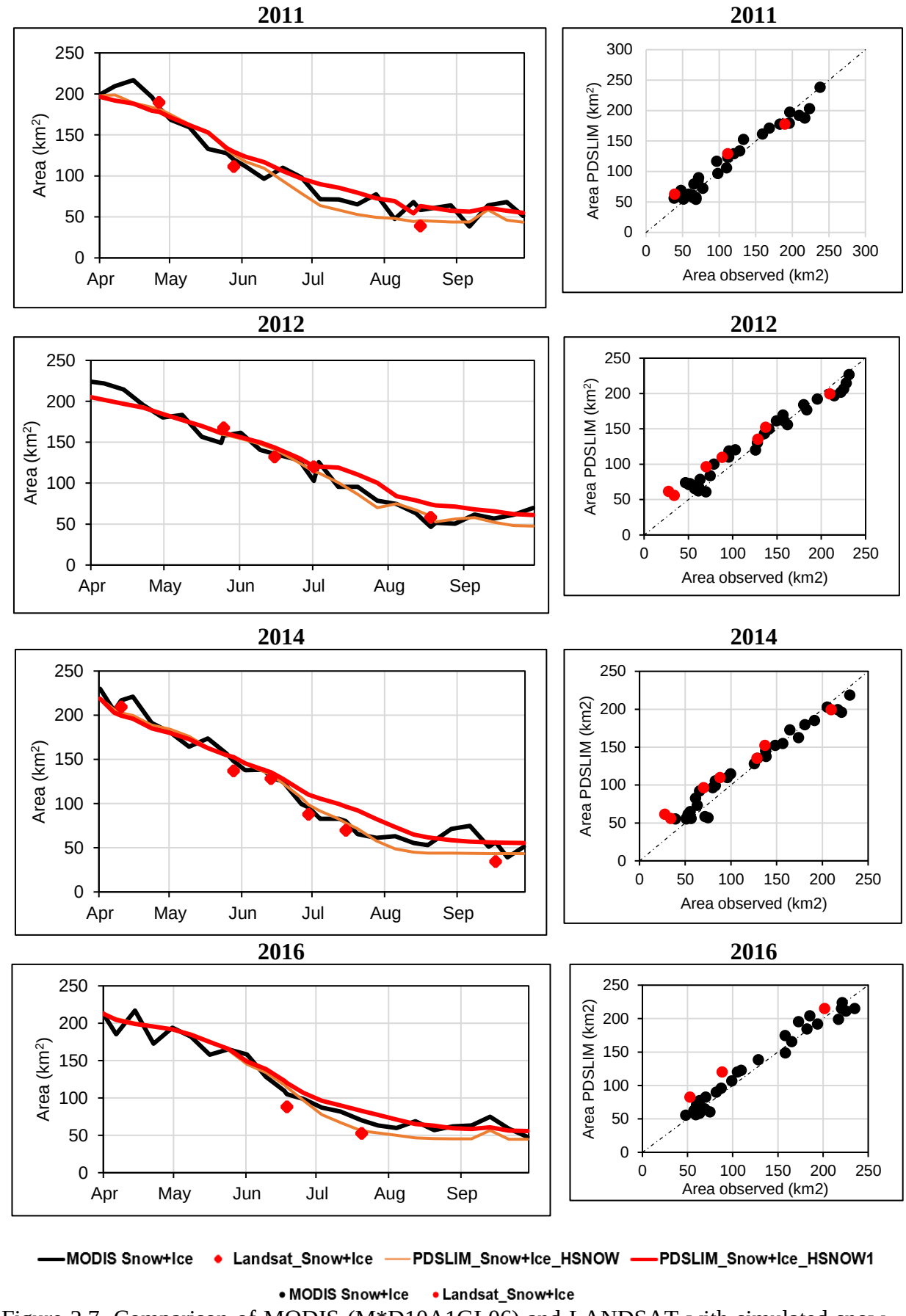

Figure 2.7. Comparison of MODIS (M*D10A1GL06) and LANDSAT with simulated snow cover area (2006-2016) for the same time with TLR (-0.0065 ^{o}C 100 m^{-1} and -0.0051 ^{o}C 100 m^{-1}) for clear sky and cloud cover. Here HSNOW refers to snow depth derived from

MODSCAG based SWE and HSNOW1 refers to snow depth derived SPIRES based SWE.

Table.2.7 (a) Statistics evaluation of snow cover simulation of Naltar catchment using MODSCAG based SWE for 2006-2016

Year	NSE	ME (km^2)	%Bias	MAPE (%)	RMSE (km^2)	R^2
2006	0.83	25.1	14.9	20.3	21.3	0.91
2008	0.96	7.7	6.7	10.0	11.1	0.98
2009	0.92	21.3	8.0	12.2	16.7	0.96
2010	0.92	17.5	6.7	9.8	14.7	0.95
2011	0.93	7.6	6.1	13.6	14.4	0.95
2012	0.97	10.3	2.1	8.3	10.4	0.97
2014	0.96	-1.4	3.5	9.3	10.9	0.97
2016	0.95	24.2	4.1	12.5	13.5	0.97
Average	0.94	14.0	6.1	11.5	13.6	0.96

Table.2.7 (b) Statistics evaluation of snow cover simulation of Naltar catchment using SPIRES based SWE for 2006-2016

Year	NSE	ME (km^2)	%Bias	MAPE (%)	RMSE (km^2)	R^2
2006	0.93	20.5	-2.3	13.0	14.1	0.93
2008	0.97	2.5	-2.1	8.3	9.0	0.98
2009	0.96	19.9	0.5	9.1	11.5	0.97
2010	0.91	16.8	2.4	9.8	15.9	0.96
2011	0.94	19.8	-2.0	12.9	13.2	0.95
2012	0.94	13.1	-4.8	14.0	14.1	0.97
2014	0.95	2.1	-3.0	12.5	12.9	0.96
2016	0.96	19.8	-3.3	13.0	11.4	0.97
Average	0.95	14.3	-1.8	11.6	12.8	0.96

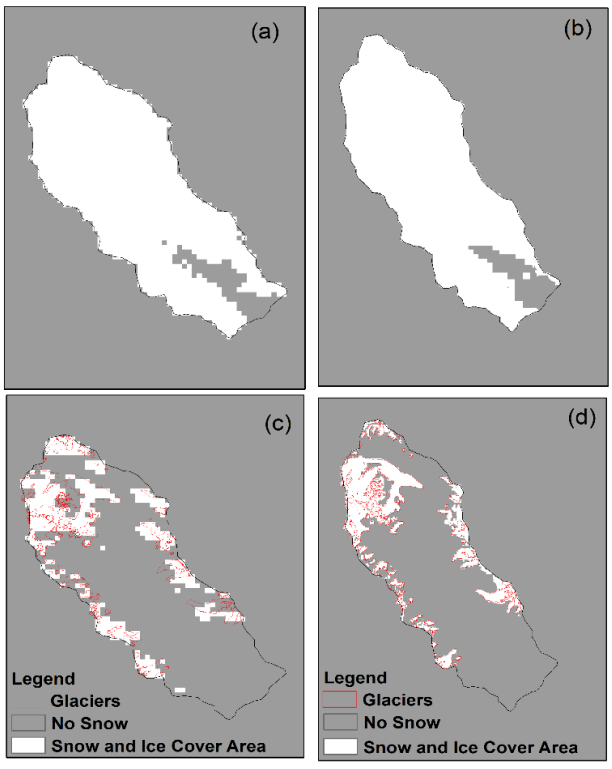

Figure 2.8 Comparison of maximum snow cover extent from 1st April based on (a) MODIS and (b) PDSLIM respectively. Minimum snow cover extent in August based on (c) MODIS and (d) PDSLIM.

4.2 Hydrological Simulations

The simple LRM model is setup in Naltar catchment to examine the hydrological regimes more specifically snow-glacier contribution to net streamflow. The simulated runoff computed by LRM model were compared with observed runoff at daily scale. A split sample method was applied for calibration and validation of simulated against observed runoff. The glacier boundaries derive from (Randolph Glacier Inventory V 6.0) are located between 3800 m to 5800 m elevation range and their spatial coverage is used as input in PDSLIM. The PDSLIM simulated glacier melt at hourly scale from Naltar catchment. Four years (2006, 2008, 2010 and 2016) marked as low, medium and high flow years were selected for calibration while the remaining four years (2009, 2011,2012 and 2014) were used for validation.

Fig.2.9 depicts the observed and simulated daily runoff relationship for both calibration and validation period with net precipitation along with bar plot. Table 2.8 shows statistical indicators exhibits relationship between observed and simulated runoff both for calibration and validation period. The graphical and statical comparison revealed that LRM model reasonably develop hydrological simulations with mean R^2 value of 0.92 and NSE 0.90 for calibration and mean R^2 value of 0.93 and NSE 0.89 for validation period based on outputs of PDSLIM as shown in Table.8. Overall, both the efficiency criteria and visual inspection showed that simulated runoff have reliable relationship with observed runoff especially (base flow+ runoff peaks) in both the calibration and validation period based on NSE, KGE and R^2 threshold suggested by Moriasi et al. (2007) for reliable working of any hydrological model
.
The mean maximum flow during the calibration was recorded across ablation period (observed 17.99 mm/day: simulated 13.62 mm /day). Similarly, mean maximum runoff during validation was correlated throughout ablation period (observed 11.35 mm/day: simulated 10.13 mm/day). Generally, simulated runoff exhibited twice peak in a year, first one occurred in late spring possibly due to snow melt and secondly in summer due to glacier melt and monsoon rainfall. Although rainfall have small contribution in net streamflow, it poses significant high flow peaks in some years (2010, 2014, 2016).

The discharge curve started rising from mid of April and reached its peak during mid of July to early August while, downward trends in runoff started from mid of August till end of September. The hydrological response of Naltar catchment primarily due to snow-glacier melt runoff followed by monsoon rainfall. The baseflow was fairly simulated during both the calibration and validation periods. Generally, the increasing and decreasing simulated runoff limbs were also correlated with observed runoff with slight overestimation and underestimation. Additionally, the model also captured the August 2010 extreme flood event as is evident from Fig.2.9. However, sub-optimal performance has been noted during glacier

melt dominated runoff period from (Aug-Sep) for 2010 and 2016. Such overestimation is possibly due to abnormal high wind speed which boosts the turbulent fluxes over snow surfaces. Turbulent fluxes directly impact energy balance and increase the heat flux that penetrates the snowpack causing overestimation of melt.

Additionally, uncertainty in observed data is also one of possible reason that cause overestimation of melt rate. Fig.S2.2 also illustrates scatter plot relationship between daily simulated and observed runoff values. The results also exhibited satisfactory performance on a daily scale.

Table. 2.8 Statical evaluation of observed and simulated runoff during calibration and in bold values with validation period.

Year	**Q_{obs} Mean (mm/d)**	**S.D. (mm/d)**	**NSE**	**KGE**	**PBIAS (%)**	**MAPE (%)**	**RMSE (mm/d)**	**R^2**
2006	4.83	2.08	0.89	0.90	4.79	18.49	0.72	0.91
2008	5.30	1.59	0.82	0.84	-8.19	9.38	0.76	0.89
2009	**5.08**	**1.96**	**0.91**	**0.89**	**-6.23**	**10.98**	**0.64**	**0.93**
2010	5.47	3.36	0.82	0.81	17.50	24.59	1.48	0.90
2011	**5.23**	**2.29**	**0.85**	**0.82**	**8.79**	**9.46**	**0.77**	**0.94**
2012	**5.24**	**2.14**	**0.83**	**0.87**	**5.13**	**12.54**	**0.90**	**0.85**
2014	**5.96**	**3.11**	**0.94**	**0.91**	**0.70**	**14.72**	**0.84**	**0.95**
2016	7.63	2.99	0.85	0.83	-14.10	13.83	1.34	0.96
Average	5.47	2.51	0.90	0.89	2.74	13.93	0.78	0.92

The average precise computation of snow-glacier melt contribution to net streamflow is one of important component of any hydrological model for a glacierized catchment. In this study, net streamflow is combination of glacier runoff, sub-surface runoff and surface runoff. Total runoff is composed of rainfall on land, glacier runoff consists of (snowmelt on ice+ runoff on ice and ice melt) and sub-surface encompass (snow melt over ice free areas and net rainfall over snow and ice free areas) runoff. The baseflow is low flow regime from October/ November to march of next year. Baseflow mainly derived from lakes within study area, groundwater and snowmelt from lower elevation zone in study region when temperatures rise melt threshold.

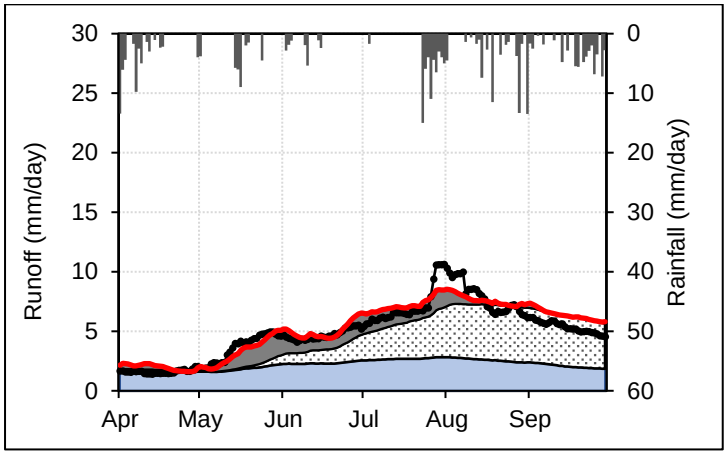
Runoff (mm/day)
Rainfall (mm/day)
Apr
May
Jun
Jul
Aug
Sep

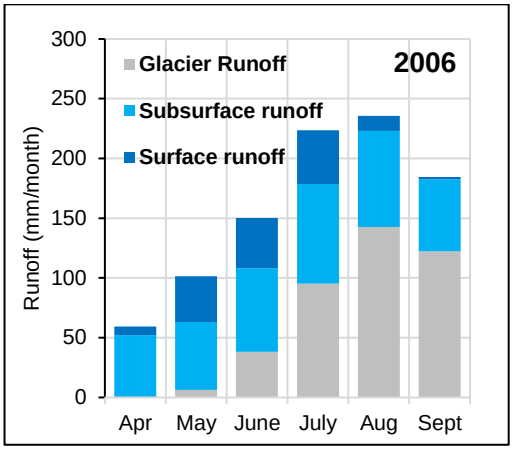
Glacier Runoff
Subsurface runoff
Surface runoff
2006
Runoff (mm/month)
Apr
May
June
July
Aug
Sept

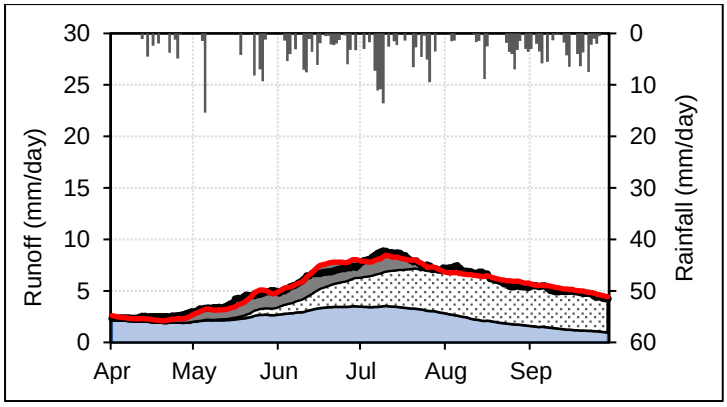
Runoff (mm/day)
Rainfall (mm/day)
Apr
May
Jun
Jul
Aug
Sep

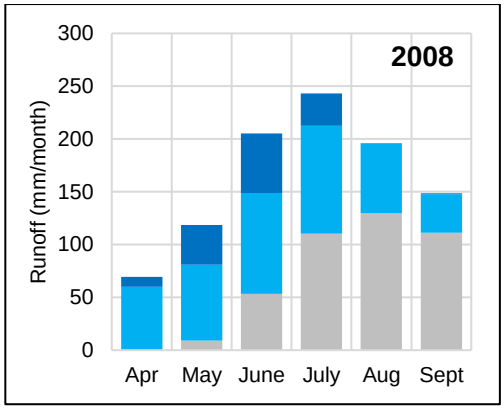
2008
Runoff (mm/month)
Apr
May
June
July
Aug
Sept

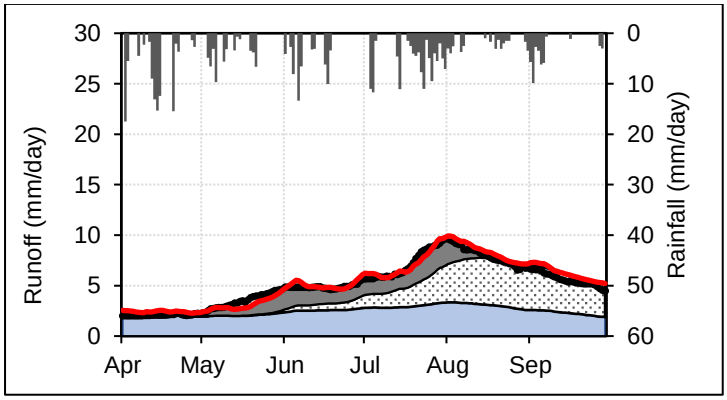
Runoff (mm/day)
Rainfall (mm/day)
Apr
May
Jun
Jul
Aug
Sep

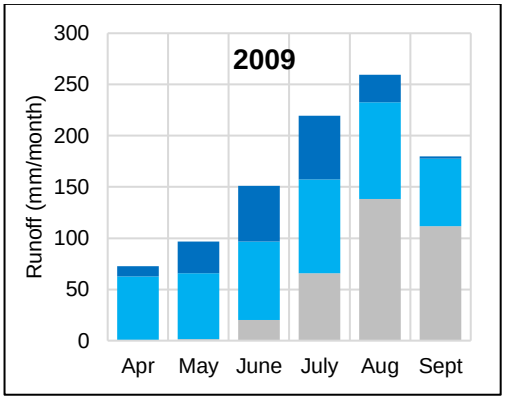
2009
Runoff (mm/month)
Apr
May
June
July
Aug
Sept

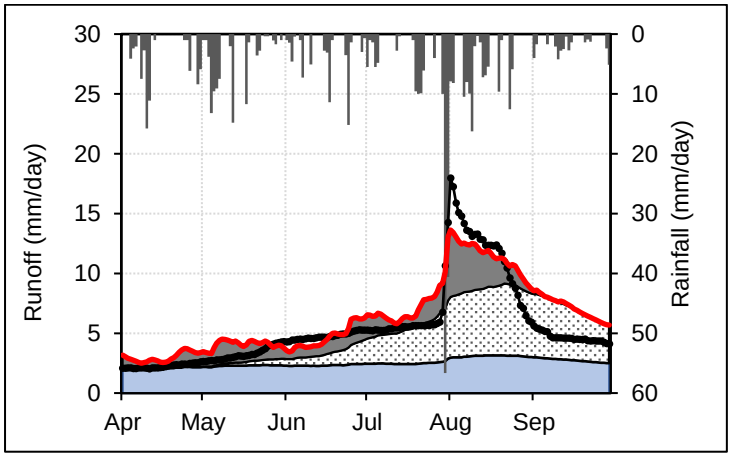
Runoff (mm/day)
Rainfall (mm/day)
Apr
May
Jun
Jul
Aug
Sep

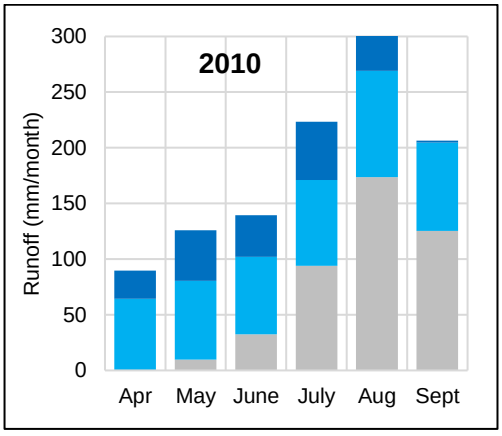
2010
Runoff (mm/month)
Apr
May
June
July
Aug
Sept

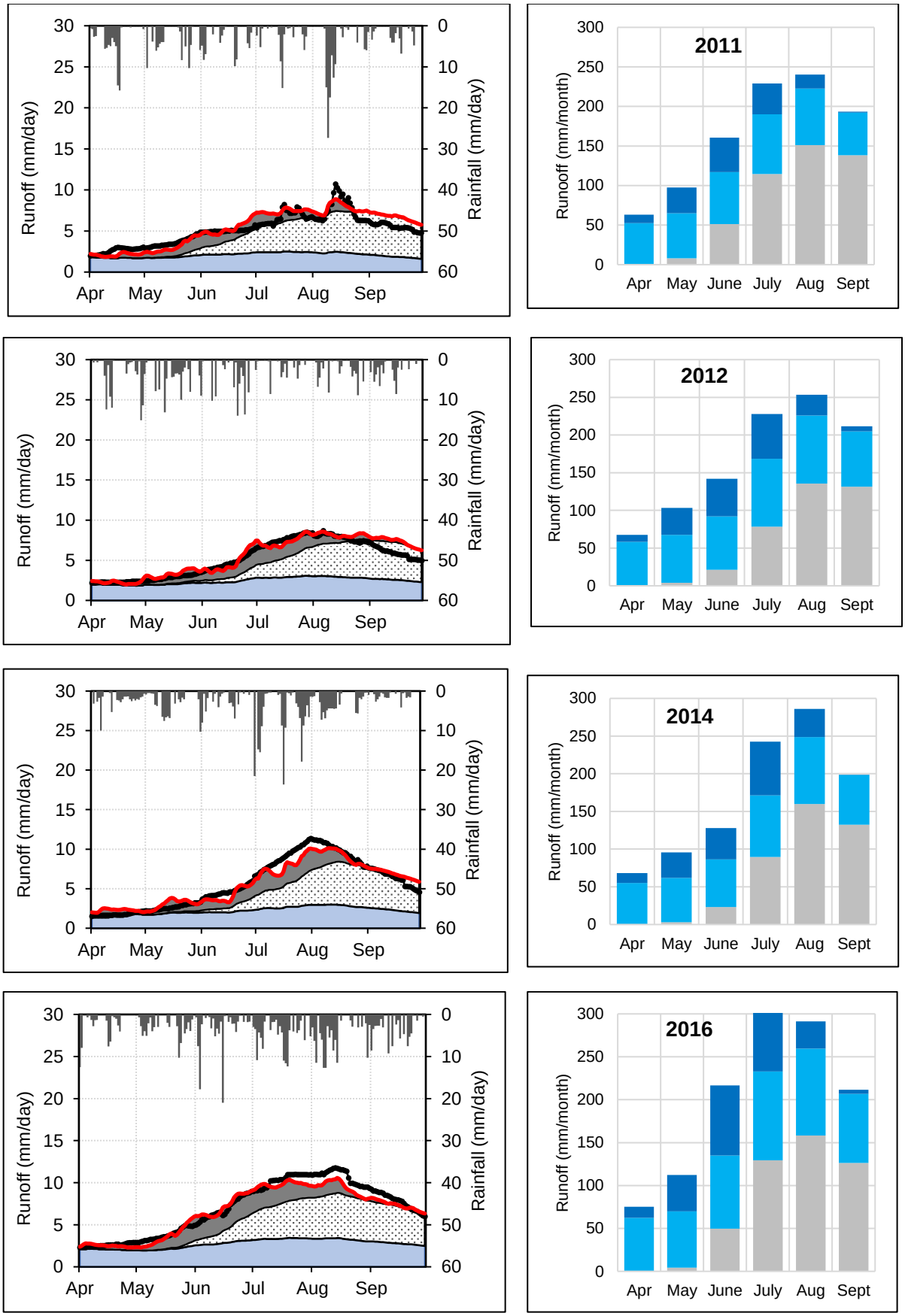

Figure.2.9 Comparison of observed and simulated runoff at Naltar Bala (Naltar Catchment outlet) during calibration (2006, 2008, 2009, 2010) and validation (2011, 2012, 2014, 2016)

with rainfall; seasonal distribution of mean monthly flow composition (Baseflow, Glacier runoff, Subsurface runoff, and Surface runoff).

The results in Fig.2.9 revealed that glacier and snow melt are in consistent agreement with the maximum flow peak of the runoff except some abnormal underestimations have been noted for 2014 and 2016. There can be two possibilities for such abnormal behavior: (1) precipitation occurs as snow during summer season at high elevation zones which is not contributing optimum to net streamflow (2) uncertainties in observed datasets especially in temperature, rainfall and windspeed which have significant impact on melt from snow and ice. The flow composition analysis shows that larger contribution is from sub-surface (42.07%) flow followed by glacier runoff (39.91%) and surface runoff (18.02%). The greater contribution of sub-surface is due to dominant presence of snowmelt in groundwater storage which returns to surface flow through baseflow. The results of current study about mix snow-glacier melt composition are also in agreement with Lutz et al. (2016) who also found similar mix melt composition for Hunza basin in western Karakorum. Similarly, results of (Shrestha et al. 2015) are also in line with current study who found significant contribution of snow and glacier melt (50% and 33%) into net Hunza river runoff followed by summer rainfall 17%.

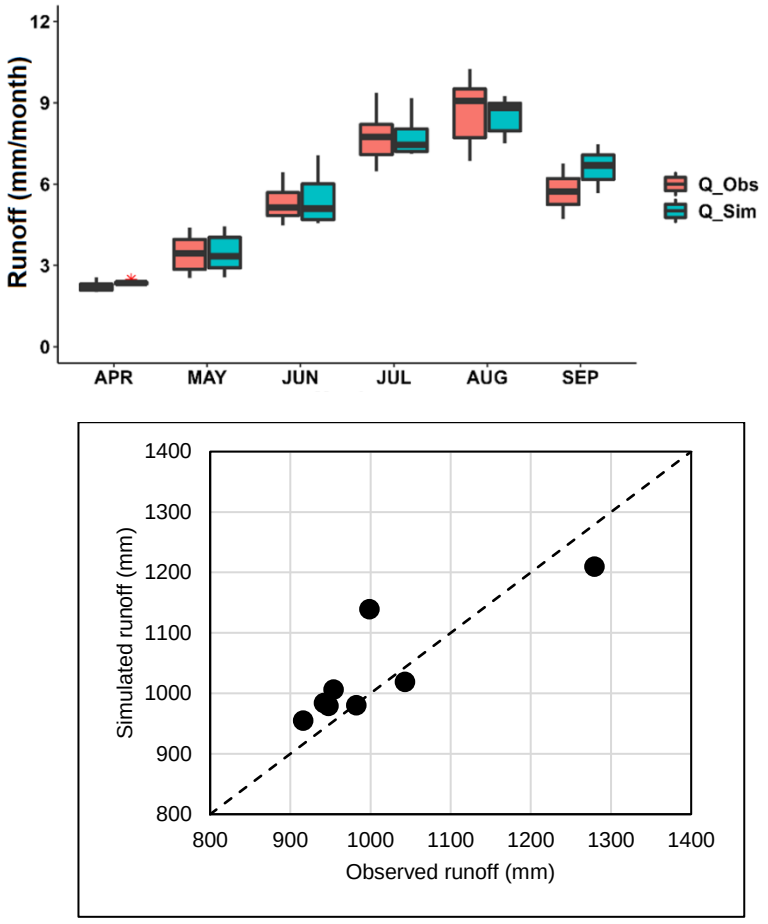

Figure.2.10 Observed and simulated runoff during the modeling period: (a) Boxplot of mean monthly observed and simulated runoff; (b) scattered plot of mean simulated and observed runoff.

The figure 2.10 (a) (b) depicts the average monthly observed and simulated runoff values and a scatter plot of the daily observed and simulated runoff values. Based on the graphical and statistical evaluation, it can be concluded that the PDSLIM model reproduces the hydrological dynamics reasonably well. Overall, it is concluded that seasonal summer hydrological cycle of Naltar catchment is dominated by snow-glacier melt contribution followed by glacier melt with small contribution from monsoon rainfall. Table.2.10 revealed mean monthly values of individual runoff components to net runoff. For all simulated, sub-surface contributions were higher until mid of June while snow-glacier contribution was higher from mid-July to end of September.

Table.2.10 Mean monthly snow glacier melt contribution to net runoff (2006-2016)

Month	**Glacier runoff (mm)**	**Surface runoff (mm)**	**Subsurface runoff (mm)**	**Total runoff (mm)**	**Q_{obs} (mm)**
Apr	0.1	12	58	71	66
May	6	37	64	106	107
Jun	36	51	75	162	159
July	97	54	88	239	239
Aug	149	30	86	265	270
Sep	125	2	64	192	167
Mean	413 (39.91%)	186 (18.02 %)	435 (42.07%)	1034	1008

Table.2.11 Comparison of mean observed and simulated hydrological runoff along with flow composition

Observed runoff (m^3)	Simulated runoff (m^3)	Glacier Runoff %	Sub-Surface Runoff %	Surface Runoff %
2.45×10^8	2.50×10^8	39.91	42.07	18.02

The results in Table.2.11 revealed that net simulated runoff volume computed by PDSLIM was in reasonable agreement and only 1.03 % higher than mean observed runoff volume with (NSE, R^2, MAPE) of (0.66, 0.72, 4.95%). Jain and Sharma (2014) suggested that performance of a model is "satisfactory" if percentage error fall between 15-23%. Hence, these results motivate the future usage of PDSLIM in Hindukush, Karakoram and Himalayans (HKH) mountain ranges and recommend that additional good results can be achieved if it is executed with better quality input data.

4.3 Water Balance

Water balance in a glacierized catchment can be represented as;

$$\mathbf{Q_{verfied} = (SWE_o - SWE_{end}) + P - ET + GM - (W_{surface.o} - W_{surface.end}) - (W_{sub\text{-}surface.o} - W_{sub\ surface.end}) - (W_{Glacier.o} - W_{Glacier.end})} \quad \mathbf{(1)}$$

Where, P is precipitation, GM is contribution from ice melt, ET is evapotranspiration, ($W_{surface.o} - W_{surface.end}$) represent change in surface storage change, ($W_{sub\text{-}surface.o} - W_{sub\text{-}surface.end}$) shows change in sub-surface storage change and ($W_{Glacier.o} - W_{Glacier.end}$) depicts glacier storage

change. Table.2.12 present a quantification of each component of water balance during summer season over eight years in Naltar catchment.

Table.2.12 Seasonal Water Balance change of Naltar Catchment

Year	2006	2008	2009	2010	2011	2012	2014	2016	Mean
	mm	mm	mm	mm	mm	mm	mm	mm	mm
$Q_{observe}$	916	982	947	999	942	954	1043	1279	1008
SWE_{start}	1362	1362	1278	1391	1311	1515	1365	1465	1381
SWE_{end}	25	46	42	109	83	121	69	99	74
Ice melt	193	245	148	101	192	147	174	140	167
Precipitation	296	324	411	535	406	397	441	530	417
Evaporation	575	682	645	551	597	631	640	565	611
$Q_{simulated}$	955	981	979	1139	984	1006	1019	1210	1034
$Q_{ice\ storage\ change}$	276	311	202	107	255	243	243	191	276
$Q_{surface\ storage\ change}$	0.87	0	0	0.36	0	0	0	0	0.87
$Q_{Sub\text{-}surface\ storage\ change}$	195	35	169	295	148	238	203	285	195
Baseflow	183	160	217	237	180	202	192	225	183
$Q_{verified}$	962	1016	994	1201	1007	1027	1017	1219	962

Looking at the evolution of the summer balance, it can be seen that runoff produced by simulated balance (including all its attributes) is similar in relation to observed runoff. Over the study period, the mean and individual contribution to the simulated outflow (Qsim) are in agreement in relation to outflow (Qverified) given by ($SWE_{start\text{-}end}$ + Ice melt + Precipitation+ Evaporation + Ice Storage Change+ Surface Storage + Sub-Surface Storage+ Baseflow).

4.3.1 Water Balance Analysis using Truc-Budyko

The water balance analysis in each simulated melt season (AMJJAS) was tested and plotted based on hydrological alternative of the Truc-Budyko plot as shown in Fig.2.12. The runoff coefficient (Q/P) and aridity index were computed (P/ETp) and plot on y-axis and x-axis, respectively. It is shown that almost all points were above water limit (Q/P = 1). These points marked the Naltar as a "Gaining" catchment. In gaining catchments, precipitation was not sufficient to complete the water balance cycle. In the "Gaining" catchments which break the water limit (Q>P) additional water is required to close the water balance. This additional water is fed by glacier melting in glacierized catchments. Such phenomena result in negative glacier storage change ($\Delta S < 0$). as shown in Table.2.12. The results show all years exhibited negative glacier storage which means significant glacier melt water contributed to net runoff. The modified form of Truck-Budko theory along with mass balance are useful to analyze the quantitative information about glacier storage change in simulate years. The storage change varies from 314 mm w.e. a^{-1} to -1354 mm w.e. a^{-1} for all simulated years with mean value -811 mm w.e. a^{-1}.

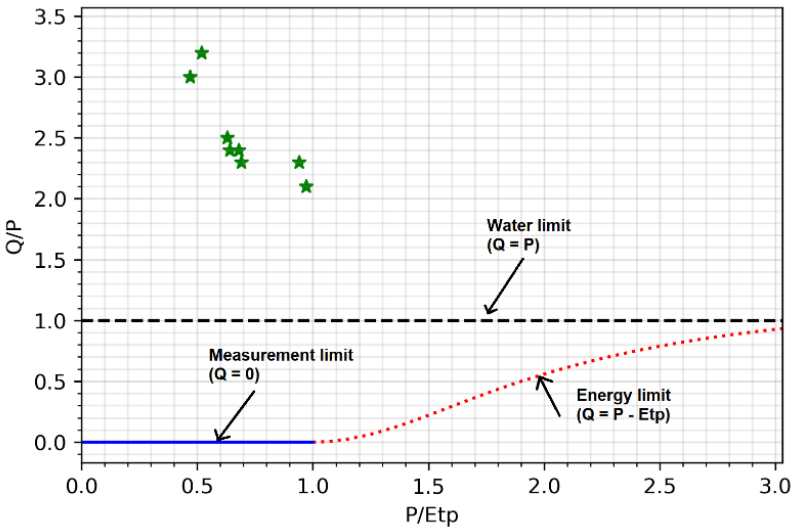

Figure.2.12 Truc-Budyko plot illustrating the water balance in Naltar catchment in AMJJAS

4.4 Net Glacier Mass Balance Simulations

The primary components of net glacier mass balance (NGMB): precipitation falls in the catchment, SWE, runoff and evapotranspiration. NGMB are difficult to simulate especially for large river basin. Therefore, it is convenient and informative to examine the NGMB and physical aspects of cryosphere of a catchment at smaller scale. Mean mass balance of all glaciers with positive and negative areas lies within Naltar catchment are computed and results are given in Table.2.13 and Fig.2.13.

Table.2.13 Simulated net glacier mass balance all simulated years

Year	**Positive Mass Balance**	**Negtive Mass Balance**	**Average Mass Balance**	**Positive Area**	**Negtive Area**
	(mm w.e. a^{-1})	(mm w.e. a^{-1})	(mm w.e. a^{-1})	km^2	km^2
2006	597	-1286	-1062	5.04	37.36
2008	777	-1665	-1354	5.4	36.99
2009	487	-1123	-831	7.68	34.72
2010	591	-1054	-334	18.55	23.85
2011	814	-1528	-912	11.15	31.25
2012	872	-1216	-600	12.5	29.9
2014	626	-1454	-837	12.57	29.82
2016	884	-1181	-560	12.76	29.64
Average	657	-1203	-811	8.93	33.47

NGMB was computed from 1st April to 30th September for each simulated year. NGMB in the catchment was estimated -334 mm w.e. a^{-1} to -1354mm w.e. a^{-1} and -600 mm w.e. a^{-1} to -837 mm w.e. a^{-1} during calibration and validation phase. Overall, catchment exhibited slightly negative mass balance -811 mm w.e. a^{-1}.

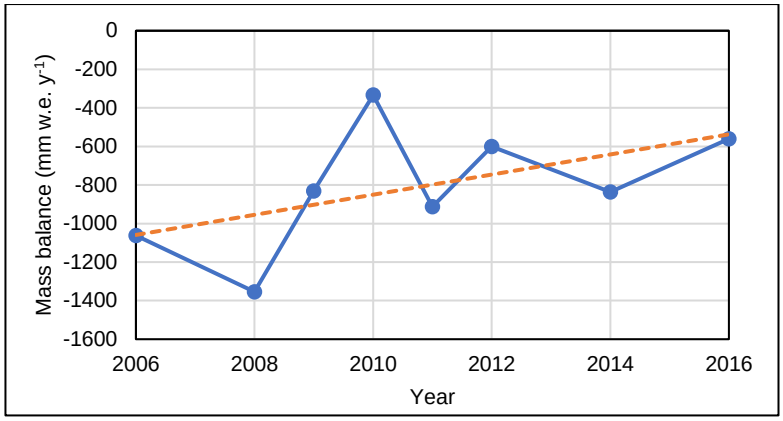

Figure.2.13 Simulated mass balance based on calibrated and validation PDSLIM model in Naltar catchment.

The results of our study are in good agreement with some previous studies based on remote sensing and geodetic mass balance which depicted that glacier mass balance in Karakoram are relatively stable or slightly decreasing (Berthier and Brun 2019; Kääb et al. 2012; Muhammad et al. 2019). Similarly, Shrestha et al. (2015) investigated the mass balance in different glaciers in Hunza basin. The results exhibited mixed response at small scale or glacier level. The results also support our NMB simulations which showed that glaciers near to Naltar catchment such as Mianpin, Batura, and Pasu also experienced negative or slightly positive mass balance.

4.5 Sensitivity Analysis.

Although, PDSLIM is well calibrated and validated as described in previous sections, it is necessary to investigate any potential uncertainties associated with model input (SWE) and parameters (TLR). Because major part of Naltar catchment is cover by snow/ice, rocks and bare soil, sensitivity to variations of LAI/FPAR were not considered. Snow and Ice melt progression, runoff regimes and net glacier mass simulations (NGMB) were investigated for each experiment. It was speculated that both low (MODSCAG) and high (SPIRES) derived SWE have substantial impact on snow and ice melt progression consequently on NGMB as shown in (Fig.2.7, Table 2.7 (a, b) and Table S1(a, b).

In first scenario, with standard temperature lapse rate (-0.0065 ^{o}C 100 m^{-1}) marked as TLR and usage of low MODSCAG based SWE values caused early melt of snow, which led to early exposure of glaciers. Consequently, glacier melt increased causing average net mass balance loss (-2114 mm a^{-1}, NSE 0.94, ME = 14.03, RMSE = 13.60) while SPIRES based SWE with TLR augmented the amount of snow depth, which ultimately reduced the negative NMB (-811 mm a^{-1}, NSE = 0.95, ME = 14.31, RMSE = 12.8); it had less effect on snow and ice area and runoff simulations.

In second scenario, by decreasing temperature lapse rate (-0.0085 ^{o}C 100 m^{-1}) marked as TLR1 using MODSCAG, and SPIRES shows the opposite situation as expected with less NMB (-1792 mm a^{-1} and -443 mm a^{-1}), both snow and ice melt rate decrease. Although, NMB decrease by changing lapse rate, but it reduced model efficiency and underestimation of runoff especially using SPIRES TLR1 as shown in Table S1(b). Based on these analyses, both SWE and TLR changes have significant impacts on net mass balance simulations and snowmelt

progression. Table 2.14 provide overall picture of net mass balance by incorporating two scenarios. Thus, sensitivity analysis showed that improvement of one efficiency criteria may reduce the other criteria as it can be seen in SPIRES TLR1 where NMB loss only (-443 mm a^{-1}) but we have to compromise on model efficiency in snow and ice melt progression and underestimation of runoff.

Table.2.14 Net glacier mass balance simulation. Here TLR refers temperature lapse rate (-0.0065 ^{o}C 100 m^{-1} and -0.0051 ^{o}C 100 m^{-1}) for clear sky and cloud cover and TLR1 refers temperature lapse rate (-0.0085 ^{o}C 100 m^{-1} and -0.0045 ^{o}C 100 m^{-1}) for clear sky and cloud cover

Year	**2006**	**2008**	**2009**	**2010**	**2011**	**2012**	**2014**	**2016**	**MB_{Avg}**
	mm	mm	mm	mm	mm	mm	mm	mm	mm
MODSCAG_TLR	-2636	-2547	-1860	-1447	-2406	-1956	-2264	-1797	-2114
SPIRES_TLR	-1062	1354	-831	-334	-912	-600	-837	-560	-811
MODSCAG_TLR1	-2358	-2253	-1759	-1089	-1967	-1607	-2102	-1200	-1792
SPIRES_TLR1	-800	-1124	-687	74	-363	-180	-746	281	-443

Thus, it is recommended to use SPIRES_TLR combination followed by MODSCAG_TLR1 for simulating future glacio-hydrological and mass balance studies in this region.

5. Discussion and Conclusion

The current study used the distributed energy balance PDSLIM model at hourly time scale and high resolution spatial scale to assess the hydro-glaciological behavior of Naltar catchment located in the Hunza basin (Pakistan) where snow and glacier melt runoff contribute in substantial amount to runoff. The overall objective was to test the model performance in view of its applicability in High Mountain Asia (HMA) to quantify snow-glacier melt, and the water and energy balance in mountain glacierized watershed, in the perspective of climate change impact assessment. The study has some limitations associated with input data. Firstly, observed data obtained from WAPDA have some inconsistencies and missing gaps at a specific date which were observed during consistency check. Although lot of efforts have already been given to remove these missing gaps, uncertainty in the data cannot be completely ignored. In order to examine the accuracy of snow cover simulation, we used improved MODIS snow cover product (M*D10A1GL06) developed by Muhammad and Thapa (2021). We used fixed number of classes (200,240, 242, 250 and 252) from this product as they are combination of snow and ice covered areas. However, pixels of these classes showed rise/drop in snow and ice cover simulation at specific time interval which is evident during years of 2006, 2009 and 2011. Such rise/drop of snow and ice cover area is due to coarse resolution or misclassification from original MODIS SCA data. Similarly, the observed runoff might also be affected by random and systematic measurement errors. For instance, abnormal rise/drop in runoff limbs were noted during 2006 and 2011. Such abnormal behavior in observed runoff series is probably due to water level measurement and its conversion using discharge rating curve. Finally, this study used fixed temperature lapse rate. It would be better to use varied temperature lapse rate in different elevation zones of a watershed which could further improve the model accuracy.

The following conclusions can be inferred from this study:

- The results of snow and ice cover simulation indicates that the model simulates the spatial and temporal distribution of Snow Cover Areas against MODIS and LANDSAT SCA with mean negative bias –1.8%, NSE=0.95, RMSE=12.8 km^2 and R^2=0.96. Some overestimation and underestimation were observed during the spatial and temporal analysis of SCA in the comparison with satellite data. Such biases might be due to misclassification or the coarse resolution of MODIS pixels or uncertainties in observed data. The snow and ice cover simulation facilitate to provide snow and glacier related parameters which are not only helpful for streamflow evaluation but also in water balance simulations.
- The streamflow dynamics revealed that PDSLIM and the Linear Runoff Model used to transform melt and net rainfall into runoff are able to develop reliable relationship between model and observed runoff with KGE, NSE and RMSE equal to 0.89, 0.90, 0.78 (mm/day) , respectively. Overall, both low and high simulated flow limbs were fairly in agreement with observed runoff. The results revealed that sub-surface runoff accounted for larger contribution to net streamflow (42.1%), glacier melts runoff contributed 39.9% while rainfall-induced surface runoff had the smallest contribution accounting for 18.0%. The larger share of sub-surface to net streamflow is probably due to dominant presence of snowmelt recharging groundwater storage which returns

to surface flow. Sub-optimal performance of the model has been observed in some years especially during glacier melt which is possibly due to uncertainties in spatialization of observed meteorological data. However the model was able to reproduce mean catchment runoff volume resulting only 1.03% times higher than observed runoff.

-

- The net glacier mass balance in Naltar catchment exhibited a slightly negative mass balance of –810 ± 311 mm w.e. a^{-1}. Similarly, Truc-Budkyo theory marked Naltar catchment as a "gaining" catchment indicating additional water from glacier melt is required to close the water balance. The results offer quantitative indications about snow and ice melt progression, streamflow, water balance and glacier mass balance and recommend further investigations in this region in order to compute the water fluxes.
- The results of this study indicate that PDSLIM model can be used to investigate the glacio-hydrological process at high altitude Hindukush, Karakoram and Himalayans (HKH) glacierized catchments. It is also important to mention that output performance of this energy balance can be improved by incorporating for optimization and simulations higher quality observed data with smaller errors. A careful selection of weather stations which depict accurate trends of weather in the study area plays a crucial role in model accuracy. The study also recommends using of physically based models as PDSLIM for possible future projections of energy and mass balance studies and to examine their potential application to assess climate change impact on the hydrological cycle. The study strongly recommends performing quality control check on observed hourly data obtained from meteorological stations due to the presence of uncertainties, gaps and outliers present in the data. In particular the existing stations are unable to capture snow water equivalent and measurement of solid precipitation is very uncertain. The study also suggests the need to install new or modify existing network of hydro- meteorological stations that are equipped with snow depth sensors and solid precipitation gauges that are capable to better monitor in the accumulation zones of glacierized catchments.

-

Future work is needed also to monitor the expansion/contraction of ice volumes and permafrost extent. Although high resolution satellite data become available on a daily basis, the need for ground-based values cannot be substituted. The so-called "Karakoram anomaly" could exist in some areas of the region but can be seriously put in doubt, especially in the future climate. Hence, long term monitoring should develop to ensure that hydrologists and other stakeholder agencies have adequate information to implement existing or new water management plans with a sound scientific basis.

Chapter III

Impact of climate change on Naltar Catchment Hydrology, Upper Indus Basin

Muhammad Usman Liaqat, Ana Casanueva[2,3], Givonna Grossi[1], Rubina Ansari[1] ,Roberto Ranzi

[1]Department of Civil, Environmental, Architectural Engineering and Mathematics, Università degli Studi di Brescia-DICATAM, Via Branze, 43, 25123 Brescia BS, Italy

[2]Dept. Matemática Aplicada y Ciencias de la Computación (MACC), Universidad de Cantabria, Santander (Spain)

[3]Grupo de Meteorología y Computación (Unidad Asociada al CSIC por el IFCA), Santander (Spain)

This chapter consists in a paper in preparation for Hydrology and Earth System Sciences:

Liaqat, M.U.,Ansari, R., Casanueva,G.,Ranzi, R. 2022. Energy balance modeling of snow and ice melt in the Naltar Catchment (UIB, Pakistan). Hydrology and Earth System Sciences (In preparation)

Summary

High Mountain Asia (HMA), including the Hindu Kush-Karakoram Himalayas (HKH) is one of the world's key "water towers", with the resources supporting hundreds of millions of people. Currently, this region is experiencing significant demographic and socio-economic growth. It is likely that this evolution will continue for the next few decades and will put even more pressure on resource management systems from inevitable climate change. Reliable hydrological projections of the future supply of water resources are essential, given the likelihood that water resources demand will continue to increase. In this study, CORDEX South Asia (CORDEX-WAS44) regional climate models (RCMs) and the Physical based Distributed Snow Land and Ice Model Grossi et al. (2013); Ranzi and Rosso (1991) are employed in the Naltar catchment (area of 236.17 km^2, with 36.12 km^2 glacierized), located in the Hunza river basin, Upper Indus Basin to project glacio-hydrological projections. The latter model was already calibrated and validated successfully using observed historical data from high altitude meteorological stations (Liaqat et al. 2021). For each of the CORDEX-WAS44 simulations, climate change signals for near future (2040-2059) and far future (2080-2099) under three Representative Concentration Pathways (RCPs) namely RCP2.6, RCP4.5, and RCP8.5 are presented with respect to corresponding present climate (1991-2010). Results show overall significant increases in mean temperature between (+0.87 to +6.02 ^oC) and total precipitation (29% (121 mm) from April to September between 1991-2010 and 2080-2099 for RCP 2.6, 4.5, and 8.5. The projected simulations of energy and mass balance indicate that snow + ice melt progression increases consistently in both future periods with an early shift in the timing of the maximum snowmelt (–51.3% –83%) as it appears in June during near future (2040-2059) and in May during far future (2080-2099) under the high emission scenario. The increase in temperature is also expected to have a substantial impact on the peak hydrological regime in the Naltar catchment, which is expected to occur one to two months earlier by 2090. Based on these results and the discussion above, we concluded that water availability in the Naltar catchment will be uncertain by the end of the century.

Keywords: Climate Change, Hydrological Modelling, Climate Projection, CORDEX South Asia, Regional, Climate Models

1. Introduction

The impact of climate change on the hydrological cycle is one of the key scientific interest both on global and local scale. These impacts vary from one region to another in magnitude, nature and intensity and they depend upon topography and morphological characteristics. However, there is common consensus that the probability of extreme events such as flood and droughts will likely increase in various parts of world. These impacts are more significant especially in cryosphere rich Hindu Kush Himalaya and Karakoram (HKH) (Fowler et al. 2003).

Snow and glaciers are the primary source of freshwater resources in HKH especially in Pakistan, where they release substantial amount of water supply during the whole year. Indus river, which is marked as lifeline in Pakistan water and energy sector, receive 70-80% of annual water at Tarbela outlet from snow-glacier melt in the Himalaya, Karakoram and the Hindu Kush (HKH) mountains. The hydrological setup of Pakistan is marked as a climate change "hotspot". In the last two-three decades, Pakistan has also become one of vulnerable region that confronted severe floods, droughts, and storm events (Hussain and Mumtaz 2014). The temperature rise due to global warming further enhances elevation-dependent warming and increases early snow melt rate during pre-monsoon which leads to significant impacts on magnitude, and timing of generated flows (Hasson and Böhner 2019). It is found that precipitation and streamflow also exhibit significant increasing observed trends especially during winter and pre-monsoon, while temperature decreases in summer season (Liaqat et al. 2022) . Moreover, the Government of Pakistan is also constructing multiple hydropower plants especially in Gilgit-Baltistan (GB) region of Karakoram to meet the growing demand of electricity. Hence, it is crucial to understand how glaciers are responding to climate change and its effect on the region's snow melt progression and hydrological systems.

Global climate models (GCMs) are the primary source of knowledge about future climate change. These models offer a simplified form of the physical processes that connect the atmosphere, ocean, sea ice, land surface, and biogeochemical system. GCMs have a typical horizontal resolution of approximately 100x100km resolution. Numerous studies have made use of hydrological models in combination with GCMs to assess future changes in the hydrological cycle in the HKH. Tahir et al. (2011) used the snowmelt runoff model (SRM) integrated with MODIS snow cover product to simulate daily runoff under climate change conditions in glacier covering Hunza basin (Upper Indus Basin). They found that a) increasing $1^{o}C$ temperature by keeping constant (precipitation and snow cover is anticipated to rise in summer runoff up to 33% b) under far future period 2-4 ^{o}C rise in mean temperature with 20% increase in snow cover area is expected to increase future streamflow by 100%. Laghari et al. (2012) examined current and future water availability in the Indus basin. They concluded that water availability will be increase in near future, while it will decrease in the long term.

Hasson et al. (2019) projected water availability in three important Himalayan watersheds (Kabul,

Indus and Jhelum). They found that if glaciers remain in current conditions, future water availability would increase by 34% and 43% on average under global warming levels of 1.5 °C and 2.0 °C, respectively. However, if the glacierized area in Himalayan watersheds is completely retreated by 100%, water availability will decline up to 25% under both warming levels. Similarly, some other studies also used different hydrological models to assess the possible impacts of climate change on the hydrological regime of the UIB with HKH ranges (Atif et al. 2019; Bocchiola et al. 2011a; Fowler et al. 2003; Ismail et al. 2020; Kiani et al. 2021; Lutz et al. 2016; Soncini et al. 2016). Despite the large availability of GCMs, their coarse resolution posed large limitations for simulating physical surface processes especially in HKH, where complex topography further introduced uncertainties in climate change projections and subsequently, in future water availability assessments (Hasson and Böhner 2019).

RCMs, with finer spatial resolution and better parameterized small-scale atmospheric processes, are considered more reliable to simulate the regional climate (Choudhary and Dimri 2018). RCMs are commonly developed on a 50x50 km or 25x25km grid and use boundary conditions of GCMs. Processes occurring at smaller scales than the grid spacing are introduced by means of physical parameterizations. The World Climate Research Programme (WCRP) started the Coordinated Regional Downscaling Experiment (CORDEX) that developed an ensemble of regional climate change projections for 14 continental domains, including South Asia (CORDEX-WAS44), developed on a 0.44ºx0.44º grid (approximately 50x50km) (Gutowski Jr et al. 2016). In the past years, different studies employed CORDEX-WAS44 simulations with integration of hydro-glaciological models to compute possible climate change and hydrological effects in HKH (Ahmad and Rasul 2018; Azmat et al. 2020; Fatima et al. 2020; Ismail et al. 2020; Khan et al. 2020). Each study developed specific criteria for model selection before their application in future projections and impact assessments. For instance, Fatima et al. (2020) selected four CORDEX-WAS44 RCMs based on the availability of all emission scenarios (RCPs, Representative Concentration Pathways) for consistency purposes. Azmat et al. (2020) other employed four CORDEX-WAS44 RCMs based on the temporal consistency of the historical simulations with observed data. Analyzing model performance before applying them in impact assessments can also be one way to reduce the overall uncertainties, but it is still questionable if a model exhibiting good agreement with the reference data in the historical period will have a more realistic behavior regarding its projected impacts.

Previous studies mainly focused on climate change impact assessment and hydro-glaciological projections at transboundary or large drainage basins (Bokhari et al. 2018; Kiani et al. 2021; Kraaijenbrink et al. 2017; Kraaijenbrink et al. 2021; Lutz et al. 2014b; Lutz et al. 2016; Rounce et al. 2020; Shah et al. 2020; Zheng et al. 2018). However, water resources management decisions, especially in complex topography, take place at smaller catchments/ sub-basins level (Shakoor and Ejaz 2019). Recently, the Government of Pakistan also approved construction of the Naltar hydropower project (Phase-III). Hence, it would be imperative to examine the evolution of future water availability in Naltar catchment which is not only important to compute water demand for

people living in downstream areas, but it is also helpful to fulfill energy demand for Naltar and surrounding areas.

Bearing all these issues in mind, this study examines the performance of the largest possible ensemble of fine resolution RCMs using a energy balance model Physical based Distributed Snow Land and Ice Model (PDSLIM), for the first time in Pakistan at the Naltar catchment located in the Hunza river basin. The study explores (i) the evolution of snow and ice melt progression using PDSLIM, (ii) future flow regimes generated by snow-glacier melt and precipitation by near future (2040-2059) and far future (2080-2099) under RCP 2.6, RCP 4.5 and RCP 8.5, (iii) how future changes in mass balance of glaciers reveal the Karakoram anomaly and if this anomaly applies to the Naltar basin. The outcomes of this study would provide substantial understanding about future snow and ice melt progression and water availability for efficient water resources management and for future power generation projects in the Naltar catchment. The findings will provide a basis for appropriate decision making and designing long-term plans, adaptation strategies to deal with future changes. The structure of this study is organized as follows. Section 2 summarizes the data and methodology used in this analysis. Section 3 describes results about snow and ice melt projections, runoff regimes and mass balance change, Section 4 summarizes the main conclusions and highlights further research directions.

2. Material and Methods

2.1 Study Area

Covering an area of 242.69 km^2, estimated by the ASTER Global Digital Elevation Model (ASTER GDEM) available at 90-m resolution, the Naltar catchment lies within high mountain ranges of Western Karakoram between 36.05º and 36.27º N and 74.08º and 74.28º E as shown in Fig 3.1. It is located in the Hunza basin about 42 km away from Gilgit city and 208 km from K2 (the second highest mountain in the world) in the Gilgit-Baltistan region of Pakistan (Gardezi et al. 2022). The largest part of the Naltar catchment is filled with snow-glacier cover due to the westerlies. According to Randolph Glacier Inventory (RGI 6.0), the glacier coverage in the Naltar catchment is 42 km^2 with a largest glacierized area of 19 km^2. The mean annual (2006-2016) snow coverage ranges between 93.5% of the basin area in March and 18.31% in September (Muhammad and Thapa 2021). The Naltar is characterized by complex topography and deep valleys. The elevation of the Naltar catchment ranges from 2270 m to 5869 m with a mean elevation of 4064 m.a.s.l. The mean annual accumulated precipitation and temperature recorded at the Naltar station (triangle in Fig.1) are 685 mm and 6.5ºC, respectively (Liaqat et al. 2022). There are three small operational hydropower plants in the Naltar river (Naltar-II, Naltar-IV, Naltar-V) with average capacity of 2.8 MW, 18 MW, 14.4. Recently, the Government of Pakistan also approved construction of another hydropower project (Naltar-III), which is not only helpful to control water coming from glacier melting but also fulfills energy demand of the Gilgit-Baltistan region.

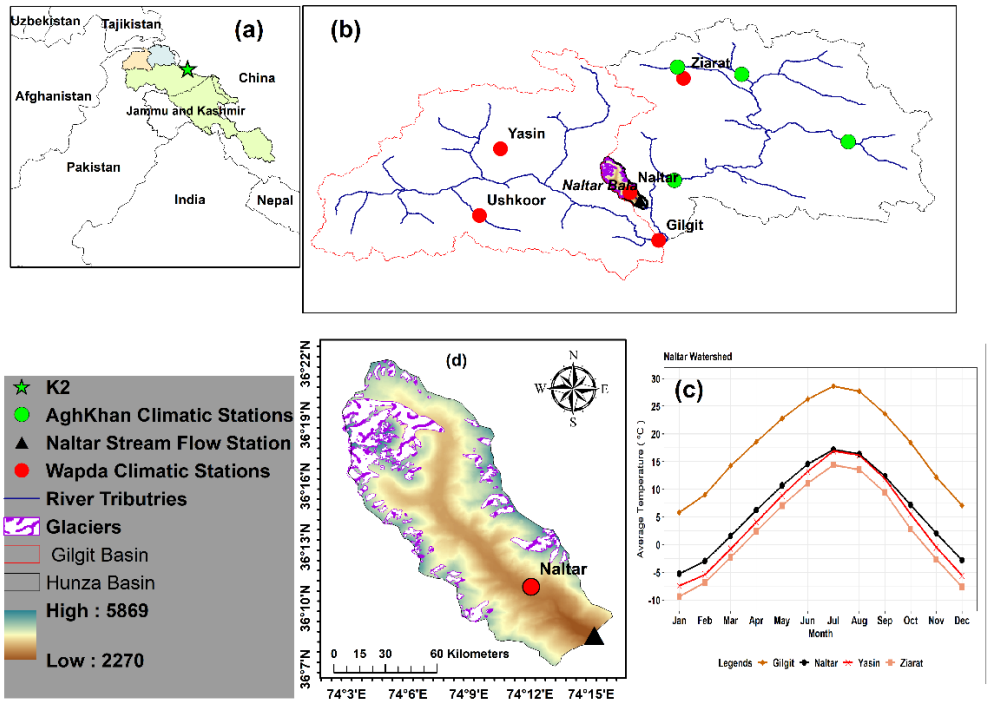

Figure.3.1 (a) The administrative and political boundary of the Upper Indus Basin (green), (b) Location of the Naltar catchment within the Hunza Basin (black border) and hydro-meteorological stations (circles), (c) Annual cycle of mean monthly temperature of several meteorological stations (d) a clear picture of Naltar catchment with glacier coverage.

2.2 Hydro- meteorological, satellite and snow cover measurements for the Naltar catchment

PDSLIM required both meteorological and satellite data to simulate snow and ice melt progression and runoff regimes. In this study, hourly meteorological data for eight years (2006-2016) were acquired from the Water and Power development Authority (WAPDA), Pakistan. A consistency check revealed that this dataset had some missing values for some variables at different dates and times. Initially, we selected 8 out of 11 years for which missing values amounted to less than 20%. The final set of years was 2006, 2008, 2009, 2010, 2011, 2012, 2014 and 2016 and simulations with PDSLIM cover from 1st April to 30th September each year. The remaining missing values were imputed through multiple linear regression as used by (Prabnakorn et al. 2019). The method involves developing a relationship between different sets of neighboring stations and choosing one (Naltar station) with the best coefficient of determination (R^2), but not less than 0.6 for precipitation, relative humidity, windspeed and solar radiation and 0.75 for temperature, respectively.

The input meteorological variables required to run the fully distributed PDSLIM model were precipitation, temperature, relative humidity, wind speed, solar radiation and air pressure. Air pressure values are not measured by WAPDA stations. These values were assessed from (Bair et

al. 2020). Similarly, streamflow data for Naltar river were also collected from WAPDA for same time period as metrological variables recorded. The detailed description of these hydro-meteorological stations are given in Table S3.1 and Fig.3.1. The Shuttle Radar Topographic Mission (SRTM) digital elevation model (DEM) at 90 m resolution was used to delineate the catchment boundary (STRM, 2013). For this study, present ice thickness and glacier coverage were derived from Kraaijenbrink et al. (2017) in order to compute projected ice thickness. A minimum number of pixels per elevation band is required for model simulations to be carried out, so glaciers with an area less than 0.4 km^2 were excluded from analysis. This resulted in a glacier coverage of 36.17 km^2 instead of 42 km^2. The landcover data based on ENVISAT's MERIS Level 1B with spatial resolution of 300 m was accessed from GlobCover landcover product developed by European Space Agency (ESA)-GlobCover for each simulated year. MODIS 8DAY composite leaf area index (LAI) product MYD15A2H.006 was obtained from Land Processes Distributed Active Archive Centre (LPDAAC) (https://lpdaacsvc.cr.usgs.gov/appeears/task/area) from the start of each simulated period.i.e. 1st April. MODIS snow cover products are a reliable source to examine spatial and temporal variability of snow cover areas. In this study, an improved version of MODIS snow cover product (M*D10A1GL06), developed by Muhammad and Thapa (2021) were used as reference data to check model accuracy to predict snow and ice progression during the melting period. More details about the dynamic data are available in Table S3.2.

2.3 Climate Projections

Climate projections given by regional climate models (RCMs) serve as an essential input for climate change studies and impact assessments (Giorgi et al. 2009). In this study, we employed sixteen CORDEX-WAS44 RCM simulations (3 RCMs unevenly driven by 10 GCMs) at 0.44^o (~50 km) spatial resolution for the period 1991-2099 (Table 3.1). In particular, we considered daily data from six meteorological variables (precipitation, temperature, solar radiation, wind speed, relative humidity and air pressure). Three representative concentration pathways (RCP 2.6, RCP 4.5 and RCP 8.5, from low to high emissions) were analyzed in this study in order to assess future snow and ice melt progression, mass balance change and runoff regimes. Note that the number of available simulations depends on the RCP (Table 3.1), and it is reduced from sixteen to five for RCP 2.6. The period 1991-2010 was selected as control period (CTL) due to the limited availability of observed hydro-climatic data to simulate the PDSLIM model. In order to build this control period we used data from the historical simulation (until 2005) and fill up the remaining 5 years with data of the corresponding RCP4.5 simulation for each model. Another reason was to maintain consistency and to extend previous work where PDSLIM setup (calibration + validation) was already verified by observed climatic data within this domain (Liaqat et al. 2021). Future projections are analyzed for two periods (SCE) as near (2040-2059) and far future (2080-2099), to take into account snow and ice melt changes and runoff regimes over the Naltar catchment.

Raw RCM data show systematic biases when compared with reference data. The use of raw RCM

outputs without any post-processing for future impact/modelling studies, might lead to adaptation decisions based on incomplete information (Christensen et al. 2008). These biases are mainly associated with temporal and spatial disaggregation Teutschbein and Seibert (2012), inaccurate and incomplete representations of basic physical processes Stevens and Bony (2013) and parametrizations of unresolved sub-grid-scale processes such as precipitation, temperature inversion, cloud formation and convection. Such biases need to be minimized in order to reduce their impact on the hydro-climatological conditions of the area of interest.

In this study, we used an improved form of the delta change method at daily scale, by using an additive delta for (temperature and air pressure Räisänen and Räty (2013) and multiplicative for (precipitation, relative humidity, wind speed and solar radiation) (Räty et al. 2014). In the typical delta change approach, a climate change signal ("delta") is computed by comparing raw climate model output for a future scenario period and a historical reference period. This delta is then used to scale observational time series in either an additive or a multiplicative manner, thus mean model biases are overlooked and the temporal structure of the new, projected time series follows the observed one. This method is a good alternative to bias correction when several variables are involved, since it preserves the inter-variable relationships in the reference data. However, one limitation of the method is the assumption of constant delta changes throughout the distribution. In order to account for varying deltas throughout the year, we use day-of-the-year (hereafter doy) dependent deltas. Initially, we computed the daily climatology (March-November) of each individual meteorological variable for CTL and SCE periods separately and for each RCM and used spectral smoothing (Bosshard et al. (2011), Eq.1) to reduce uncertainties and smooth the climate change signals by using a 31-day moving average.

In second stage, additive (temperature and air pressure) and multiplicative deltas (precipitation, relative humidity, solar radiation, wind speed) were calculated for both SCE periods (2040-2059 and 2080-2099), relative to the CTL period 1991-2010. These change signals were used to project the observed meteorological time series to future scenarios in order to build climate change meteorological forcings, which are required at hourly temporal resolution to assess the glacio-hydrological regimes. The general equations for the improved delta method using both additive and multiplicative deltas are given below:

$$X_{(h)}^{SCE,add} = \frac{X_{o(h)} - \acute{X}_{CTL(d)}}{\sigma_{CTL(d)}} \sigma_{SCE(d)} + \acute{X}_{SCE(d)} \quad (1)$$

$$X_{(h)}^{SCE,mult} = \frac{X_{o(h)}}{\acute{X}_{CTL(d)}} \acute{X}_{SCE(d)} \frac{\sigma_{SCE(d)}}{\sigma_{CTL(d)}} \quad (2)$$

where $X_{o\,(h)}$ indicates hourly meteorological observed series recorded at Naltar station, $\acute{X}_{SCE(d)}$ and $\acute{X}_{CTL(d)}$ denote the 20-year mean variable for the day d (March-November) for the control and scenario periods, respectively, and $\sigma_{SCE(d)}$ and $\sigma_{CTL(d)}$ stand for the 20-year standard deviation of the

variable for the day d (March-November) for the control and scenario periods, respectively.

2.4 Energy and mass balance of snow and ice: the physical based hydrological model

The snow and ice melt progression and summer specific mass balance of Naltar catchment from the 1st of April to the 30th of September for eight year was estimated in chapter #2 by simulation of the mass and energy balance with PDSLIM assuming similar type of modeling also adopted in current studies to project glacio-hydrological regimes. For a unit area, the melt rate for finite depth of layer of ice or snow superimposed over ice is computed using the energy balance equation:

$$H_m + H_c = S_{io} + L_{io} + H_l + H_s + H_p + H_g \quad , \qquad (3)$$

Here unit of all terms are W/m^2

H_m: energy available for melt,

H_c: Internal Energy of the snow or ice layer,

S_{io}: net shortwave radiation,

L_{io}: net longwave radiation,

H_l: latent heat,

H_s: sensible heat,

H_p: advective heat from precipitation,

H_g: Conductive heat at the bottom side of the snow or ice layer

For an snow or ice layer with finite depth Δz, mean Temperature T,specific heat C and density p changes over time

$$H_c = C\, p\, \Delta z\, dT/dt \qquad (4)$$

Here specific heat of ice is equal to $C = C_i = 2093.4$ J kg^{-1} K^{-1} and its density is assumed $p = p_i$ 830 kg m^{-3}. In case of snow, density changes over time according to snow pack simulation depicted by Cagnati et al. (2004); Ranzi and Rosso (1991). The detail description of the shortwave and longwave radiation terms of the energy balance equation, S_{io} and L_{io}, followed by global shortwave radiation measurements, R_m can be seen in (Ranzi and Rosso 1991; Ranzi and Rosso 1995). It is important to mention that shading is estimated using sun tracking algorithm and cloudiness index is computed by comparing measured global shortwave radiation on a horizontal surface R_m with clear-sky radiation. Direct radiation on each computational cell, measuring 90 x 90 m^2 and centered O is attained by projecting with scalar product estimated beam radiation R_b on the local vector normal to the surface V_n. Additionally, diffused radiation from the sky, R_d is weighted by sky view factor, $V_s = 1\text{-}V_t$ being V_t the terrain view factor which is function of the horizontal angle $h_o(\psi)$. in each azimuthal direction (ψ).

$$V_t = \frac{1}{\pi}\int_0^{2\pi h}\int_0^{h_0{}^{(\psi)}} \cos(h)\sin(h)\, dh d\psi = \frac{1}{\pi}\int_0^{2\pi}\frac{1}{2} sin^2[h(\psi)] d\psi \qquad (5)$$

Terrain covering each point depicts incoming measured radiation with a spatially-average albedo α_t

$$S_{in} = -R_b \,.\, V_n + V_s R_d + V_t\, \alpha_t R_m \qquad (6)$$

The results of net incoming shortwave radiation is written as $S_{io} = S_{in}\,(1-\alpha)$, being α marked as local albedo. Ice-albedo is derived from a map estimated from the radiation detected from the sensor ASTER satellite image dated 23 August 2003, when the glacier was almost snow-free. Future ice albedo is assumed to remain as in actual conditions. In case of snow cover area within the Naltar catchment, albedo is derived based on temperature-dependent snow ageing and diffused radiation Ranzi and Rosso (1991) and hence it values vary with the climate change scenario.
Net longwave radiation, L_{io} is calculated by assuming snow and ice as a black bodies and the Satterlund model for atmospheric emissivity (Satterlund 1979). Moreover, convective fluxes of latent heat, H_l and H_s are calculated based on mixing land theory (Ranzi et al. 2010).
In PDSLIM the ice is modelled as a 0.1 m thick surface layer with temperature Ti superimposed to a semi-infinite ice layer at constant 0^oC temperature, a reasonable assumption for a temperate glacier in the melt season. The surface layer can be covered by a debris layer, as occurred for instance in an earlier application of the model to simulate melt for the Belvedere glacier, in the Western Italian Alps (Ranzi et al. 2004; Taschner and Ranzi 2002). If this layer does not exist as for the Mandrone glacier, ice can be covered by a snowpack, modelled as a surface layer with 0.1 m thickness, superimposed to the bulk snowpack.

The snowpack model explained in Cagnati et al. (2004); Ranzi and Rosso (1991) computes liquid water content, snow depth, density and temperature. Conductive heat fluxes in snow and ice are derived based on the Fourier law and melt infiltration by supposing Colbeck's celerity (Colbeck 1976; Ranzi and Rosso 1991). It is important to mention that snow model does not take into account transformation from snow into ice and firn.

In order to predict the climate change impacts on streamflow of Naltar catchment for near future (2040-2059) and far future (2080-2099), the calibrated and validated LRM conceptual rainfall-runoff model used in chapter#2 is forced by meteorological data under RCP 2.6, RCP 4.5 and RCP 8.5 scenarios. It is important to mention that parameters of the model were kept the same as in the calibration/validation stage. Due to extreme topography and less human intervention in this catchment, land use/ land cover map of present simulated years is also used for future streamflow predictions.

Table.3.1 List of CORDEX South Asia (WAS-44) Regional Climate Model simulations, driving GCMs and available RCPs

RCM	RCM description	Contributing CORDEX modelling center	ID	Driving CMIP5 GCM	Contributing CMIP5 modeling center	RCP26	RCP45	RCP85
RegCM4	The Abdus Salam International Centre for Theoretical Physics (ICTP) Regional Climate Model version 4 (RegCM4; (Giorgi et al. 2012))	Centre for Climate Change Research (CCCR), Indian Institute of Tropical Meteorology (IITM), India	RCM1	CCCma-CanESM2	Canadian Center for Climate Modelling and Analysis (CCCma), Canada	×	✓	✓
			RCM2	CSIRO-QCCCE-CSIRO	Commonwealth Scientific and Industrial Research, Australia	×	✓	✓
			RCM3	IPSL-IPSL-CM5A-LR	Institut Pierre Simon Laplace, France	×	✓	✓
			RCM4	MPI-M-MPI-ESM	Max Plank Institute for Meteorology, Germany (MPI-M)	×	✓	✓
			RCM5	NOAA-GFDL-GFDL-ESM2M	National Oceanic and Atmospheric Administration, Geophysical Fluid Dynamics Laboratory (GFDL)	×	✓	✓
RCA4	Rossby Centre Regional Atmospheric Model version 4 (RCA4; (Samuelsson et al. 2011))	Rossby Centre, Swedish Meteorological and Hydrological Institute (SMHI), Sweden	RCM6	CCCma-CanESM2	Canadian Center for Climate Modelling and Analysis (CCCma), Canada	×	✓	✓
			RCM7	CNRM-CERFACS	National Centre for Meteorological Research, France	×	✓	✓
			RCM8	CSIRO-QCCCE-CSIRO	Commonwealth Scientific and Industrial Research, Australia	×	✓	✓
			RCM9	ICHEC-EC-EARTH	Irish Center for High-End Computing, European Consortium	✓	✓	✓
			RCM10	IPSL-IPSL-CM5A-MR	Institut Pierre Simon Laplace, France	×	✓	✓
			RCM11	MIROC-MIROC5	Model for Interdisciplinary Research on Climate (MIROC), Japan, Agency for Marine-Earth Science and Tech	✓	✓	✓
			RCM12	MOHC-HadGEM2-ES	Met Office Hadley Centre for Climate Science	✓	✓	✓
			RCM13	MPI-M-MPI-ESM	Max Plank Institute for Meteorology, Germany (MPI-M)	✓	✓	✓
			RCM14	NCC-NorESM1-M	Norwegian Climate Center (NCC), Norway	✓	✓	✓
			RCM15	NOAA-GFDL-GFDL-ESM2M	National Oceanic and Atmospheric Administration, Geophysical Fluid Dynamics Laboratory (GFDL)	×	✓	✓
REMO2009	MPI Regional model 2009 (REMO2009; (Teichmann et al. 2013)	Climate Service Center (CSC), Germany	RCM16	MPI-M-MPI-ESM	Max Plank Institute for Meteorology, Germany (MPI-M)	×	✓	✓

3. Results and discussions

3.1 Future Climate Forcings

The future climate forcings for precipitation, relative humidity, solar wind speed, solar radiation, temperature and air pressure are shown in Fig.3.2 and Fig.S3.1. Results show the change factor for the scenario period (2040-2059 and 2080-2099) relative to control period (1991-2010) using 16 CORDEX-WAS44 simulations for the gridbox over the Naltar catchment under three RCPs (2.6, 4.5 and 8.5) as representatives of future climate change over the Naltar catchment. We focus on the months from April to September in order to examine the melting season. The ranges of the mean projected changes and the projected changes in standard deviation were examined and served to detect outliers which might lead to undesired effects in the multi-model ensemble.

In case of precipitation, multiplicative delta changes vary largely across models during summer season, especially in RCM11, RCM12, RCM13, RCM14, RCM15, for both mean values and their standard deviation under RCP 4.5 and 8.5, as shown in Fig.3.2 and Fig.S3.1. For RCP 2.6, where data from only five simulations are available in both scenario periods, RCMs 11, 12,13 present larger departures. The change factors of the overall CORDEX-WAS44 ensemble from April to September ranges between 0.37 – 3.85 for mean precipitation and 0.33 – 6.24 for standard deviation. Such larger differences in change factors projected significant overestimation up to 52% under RCP 8.5 in precipitation values, which is not fully coherent in light of the present observed precipitation trends (Liaqat et al. 2022). Moreover, according to the IPCC Atlas Diez-Sierra et al. (2022) the projected increase in precipitation using CORDEX-WAS44 in this region is expected to lie between 25-35% by the end of the 21st century. If we exclude from the final ensemble the above mentioned five RCMs which exhibited significant deviation in the change factor and standard deviation projected increase in precipitation lie around 29 % by the end of this century under RCP 8.5. Hence, our rejection criterion of precipitation range suggested by IPCC atlas and several other studies Azmat et al. (2020); Jury et al. (2020) leads to exclusion of 5 RCMs from the subsequent analysis.

An increase in temperature was found for both future periods under RCP 4.5 and RCP 8.5, especially towards the end of the century (2080-2099) under RCP 8.5. It is also observed that a substantial rise in change factor and standard deviation for temperature is more accentuated during the pre-monsoon especially for 2080-2099 under RCP 8.5, which enhances the early snow melt rate followed by glacier retreat. Similarly, the rising delta change of temperature is also prominent in case of monsoon with temperature values ranging between +1.67 to +5.39 ^{o}C/day Overall, temperature increase by substituting projected delta changes into present temperature forcings vary largely across RCPs, spanning from 1.63 ± 0.95 to 6.02 ± 0.88 (^{o}C/day) in the far future period. The rise in temperature and precipitation changes of the current study are in line with previous field campaigns (Ali et al. 2015; Jury et al. 2020; Kraaijenbrink et al. 2017; Soncini et al. 2015).

For relative humidity, overall, small delta change was noted in both the mean and the standard deviation. It is also observed that a couple of outlier simulations leads to a larger increase in near future (RCM5) and decrease in the far future (RCM10). Overall, there is some indication of a decrease of RH with time and emission scenario. Change factors for the whole RCM

ensemble range between 0.58 – 1.38 for the mean relative humidity and 0.79 – 2.87 for standard deviation. For solar radiation, marginal change factors were found for RCP 2.6. However, signals get larger from near future to far future under RCPs 4.5 and 8.5 in April and May, which is also one evidence of global warming in this region. The range of the delta changes for the overall ensemble is 0.78 – 1.65 for mean radiation and 0.49 – 2.19 for its standard deviation, considering all RCPs. Wind speed is also an important component of energy balance and hydrological modelling studies. Overall, the climate change simulations revealed small changes in this variable, with some indication of future increase towards the end of the century. This increase is larger in the pre-monsoon season than in summer in terms of mean wind speed (Fig. 3.2). Such difference can be linked with early snow melt especially in glacierized catchments. Similarly, the increase in mean wind speed is larger for RCP 8.5 compared to RCP 4.5, while RCP 2.6 did not exhibit important changes, both in terms of mean and standard deviation. Overall, the change factors for the full ensemble range between 0.65 – 1.24 for mean wind speed and 0.54 – 1.39 for its standard deviation. For air pressure, an increasing delta change is projected both in terms of the mean and standard deviation, especially for RCP 8.5 for near future and RCP 4.5 and 8.5 for far future.

Overall, it is found that delta changes for temperature and precipitation exhibited large spread both in terms of the mean and standard deviation while other variables depict more robust and smaller changes. Temperature and precipitation have a critical role in hydrological and mass balance studies. With the exclusion of 5 RCMs (RCM11-RCM15) from the final model ensemble the unexpected and remarkable overestimation in terms of precipitation was reduced. Therefore, they were excluded from all meteorological variables for the subsequent hydrological simulations.

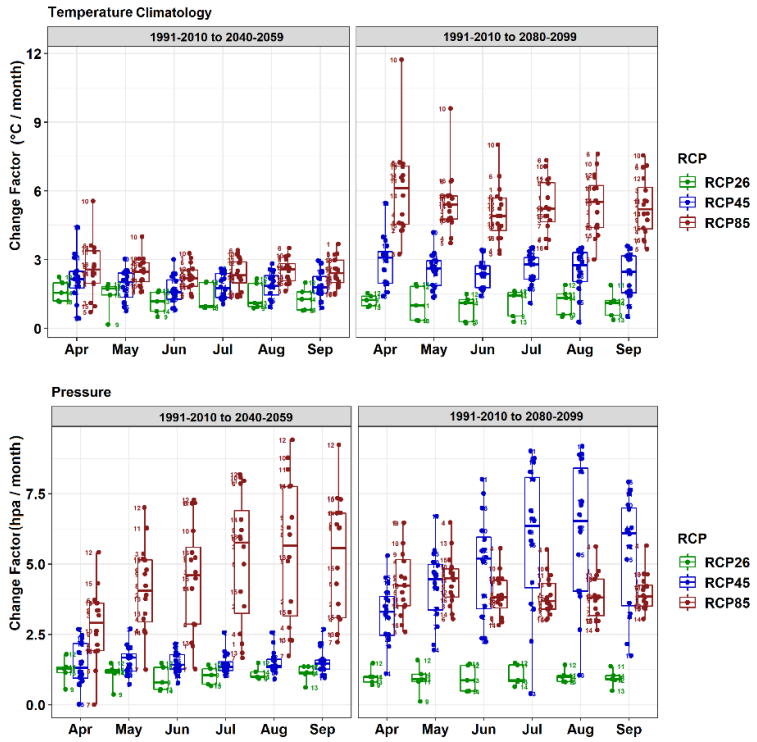

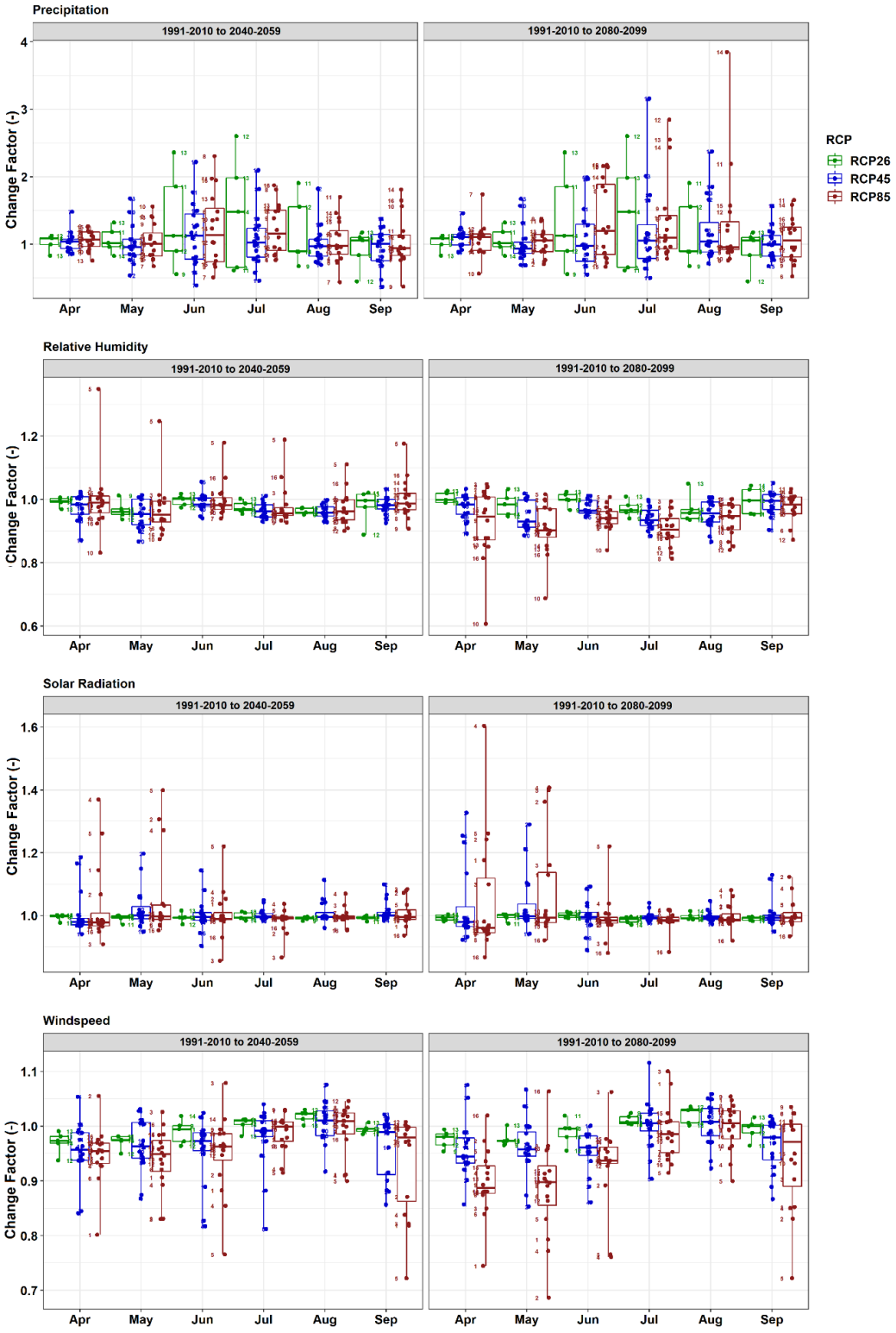

Figure 3.2 Annual cycle (April-September) of multiplicative (unitless) for precipitation, relative humidity, solar radiation, wind speed and additive change factors for temperature (°C) and air pressure (hpa) over the scenario periods (2040-2059 and 2080-2099) relative to the control period (1991-2010) for the 16 CORDEX-WAS44 simulations (individual numbered dots within the boxes) under 3 RCPs (colours). The change factors were obtained for each doy, from the daily annual cycle in the scenario and control periods (see Methodology) and here were averaged into monthly values.

3.2 Projected changes in snow water equivalent

The projected rise of temperature in Naltar catchment is predicted to have substantial implications on snow water equivalent (SWE), snow melt and runoff regimes. The projected changes of seasonal SWE at the beginning of April for both scenario periods and RCPs are provided in Table.3.2. The PDSLIM simulations indicated that at present (control period, average over the years 2006-2016), the average snow water equivalent in Naltar catchment is 1465 mm. The SWE proportion is predicted to decrease from 1465 mm at present to 1332 mm (~ 9.1%) and 1184 mm (~19.2%) with ensemble mean in near future (2040-2059) under RCP 4.5 and RCP 8.5. Additionally, by the far future (2080-2099), the proportion of SWE will reduce to ~6.1 % and ~37.4% under RCP4.5 and RCP8.5 scenarios. In case of RCP 2.6, projected SWE will show an increasing rate in SWE (21.2%) in near future and decreasing rate (-17.2%) in far future. Overall, the PDSLIM simulations predicted a significant decrease in SWE reference to control period in both scenario periods and under all RCPs.

Table.3.2 Projected changed in snow water equivalent proportion at the beginning of April in both future time segments relative to control period under RCP 2.6, RCP 4.5 and RCP 8.5

		1991-2010 to 2040-2059		**1991-2010 to 2080-2099**	
		mm	Change (%)	mm	Change (%)
RCP	Reference	1465		1465	
RCP26	*RCM9*	*1775*	*21.2*	*1213*	*-17.2*
RCP45	RCM1	1238	-15.5	1376	-6.1
	RCM2	1238	-15.5	1376	-6.1
	RCM3	1238	-15.5	1376	-6.1
	RCM4	1332	-9.1	1342	-8.4
	RCM5	1332	-9.1	1376	-6.1
	RCM6	1095	-25.3	1302	-11.1
	RCM7	1790	22.2	1775	21.2
	RCM8	1612	10.1	1494	2.0
	RCM9	*1553*	*6.0*	*1435*	*-2.0*
	RCM10	681	-53.5	1583	8.0
	RCM16	1332	-9.1	1376	-6.1
	Ensemble	**1332**	**-9.1**	**1376**	**-6.1**
RCP85	RCM1	1101	-24.9	918	-37.4
	RCM2	1101	-24.9	918	-37.4
	RCM3	1101	-24.9	918	-37.4
	RCM4	1184	-19.2	918	-37.4
	RCM5	1184	-19.2	918	-37.4
	RCM6	844	-42.4	696	-52.5
	RCM7	1627	11.1	1435	-2.0
	RCM8	932	-36.4	1036	-29.3
	RCM9	*1479*	*1.0*	*1154*	*-21.2*
	RCM10	932	-36.4	282	-80.8
	RCM16	1184	-19.2	918	-37.4
	Ensemble	**1184**	**-19.2**	**918**	**-37.4**

The reduced SWE during accumulation period and rapid melting of depleted snow also led to early exposure of the glacier surfaces consequently boosting up the melting of glaciers because of the reduced albedo. The results of current study are in line with previous studies Lutz et al. (2016); Romshoo and Marazi (2022) who found significant changes in form of precipitation and SWE in Indus and Jehlum basin.

3.3 Projected change in snow and ice melt progression and mass balance

The temporal pattern of the projected changes in seasonal RCMs and its ensemble mean snow and ice cover area based on CORDEX for the near future (2050s) and far future period (2090s) relative to control period (1991-2010) and individual years under RCP (2.6, 4.5 and 8.5) are shown in Fig.3.3. The primary reason to develop snow and ice melt progression is using individual models to examine spread in glacio-hydrological projections especially during flood occurrence years which some time neglected by making ensemble of all simulated models. For RCP 2.6, where projected simulation is available for only one experiment (RCM9), the obtained results indicate increasing magnitude in projected change of snow and ice melting shrinkage (–25.9%) in near future (2040-2059) and (–51.5%) in far future (2080-2099) relative to control period.

In case of RCP 4.5 and RCP 8.5, almost all RCMs and their ensemble means exhibited gradual increase in snow followed by ice melt. It is also noticed that relative change in snow and ice melt progression produced by each RCM in Naltar catchment is different from each other. Under RCP 4.5, snow and ice melt depletion ranges from (–5.4% to –56.3%) with ensemble mean –36.5 % in the near future (2040-2059) and depleted further up to (–30.4% to –67.9%) with ensemble mean (–47.7%) by end of century. The higher projected increase in snow and ice melt is mostly linked with higher temperature. Under RCP 8.5, rapid snow and ice melt depletion is observed with snow cover completely disappeared by mid of June followed by ice melt in early July. The projected change in SCA with respect to control period ranges from (0.2% to –78.2%) with ensemble mean –51.5% during near future (2040-2059) and depleted further up to (–67.4% to –87.6%) with ensemble mean (–83%) in far future (2080-2099).

The largest increase is noted for the transitional months (May and June) as shown in Fig.3 (a) where larger part of precipitation is projected to fall into liquid form in the future followed by early ice melt in July. Early seasonal snow and ice melt progression is likely caused by warming in elevated regions, resulting in not only earlier temperatures but also in a likely risk of increased flooding and landslides. As one example, a glacial surge occurred in the Upper Naltar valley on July 5, 2021. There were four fatalities, over 150 livestock killed, and 4km of pastureland was destroyed by the avalanche (DAWN 2021). The reduced snow precipitation during the accumulation period and rapid melting of the depleted snow also led to the early exposure of the glacier surfaces thus enhancing the melting of glaciers in the catchment.

Moreover, climate change scenarios using ensemble RCMs also translated into projected change in glacier extent and mass balance given in Table.3.3. Although, the moving average of climatology and standard deviation signals predict increases in precipitation, glacier extent and mass balance are expected to shrink by the end of 21st century in Naltar catchment, since precipitation increase cannot compensate for the substantial rise in temperature.

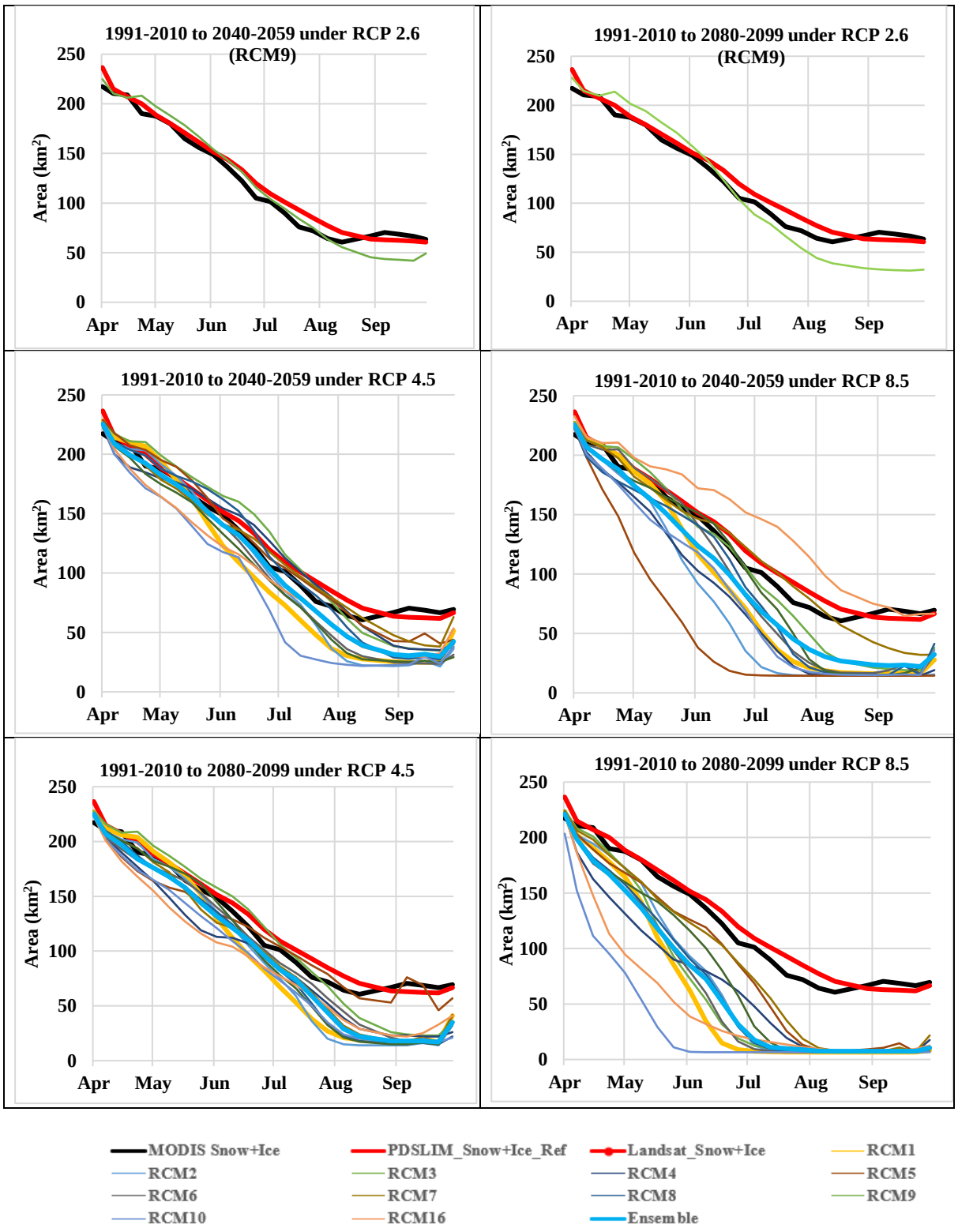

Figure.3.3 Temporal change of snow and ice melt progression from control period average for 8 years over Naltar catchment in different CORDEX experiments and their ensemble for near future (2040-2059) and far future (2080-2099) for RCPs (2.6, 4.5, 8.5).

Such projected changes will accelerate snow and ice melt and eventually reduction in ice volumes ranges from –27% to –80% and increment in glacier mass balance (–654 to – 2597) mm w.e. a^{-1}) under different scenario period as shown in Table.3.3. The result shows that

glacier extent in Naltar catchment is projected to lose (–27% to -41%) under RCP 2.6, (–41% to –60%) under the RCP 4.5, and (–58% to –80%) under the RCP 8.5. The spatial variability in glacier retreat relevant to the reference time is shown in Fig.3.4.

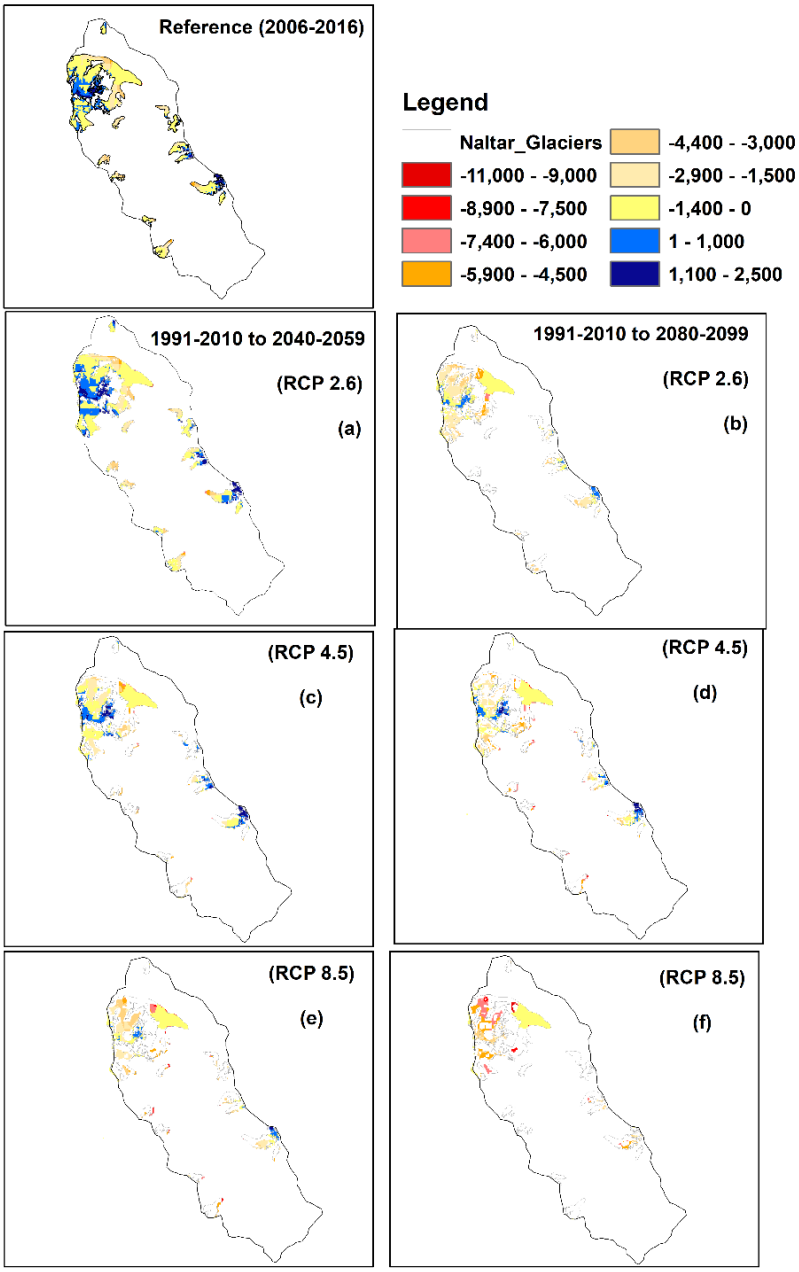

Figure.3.4. Projected changes in the glacier mass loss (mm w.e. a^{-1}) simulated by the integration of ensembles of 11 different CORDEX-SA RCM experiments with PDSLIM and LRM for 2040-2059 and 2080-2099 under RCP 2.6, RCP 4.5 and RCP 8.5 relative to control period 1991-2010.

Table.3.3 Projected change in mass balance and ice extent for 2050 and 2090 relative to reference period (2014) in Naltar catchment, when forced by ensemble members

Mass balance scenario	Avg (mm w.e. a^{-1})	Ice extent (km^2)	Change (%)
Reference Period (Average for 8 years)	–737	36.17	
1991-2010 to 2040-2059 under RCP 2.6 (RCM9)	–654	26.40	-27%
1991-2010 to 2040-2059 under RCP 4.5	–887	21.50	-41%
1991-2010 to 2040-2059 under RCP 8.5	–2018	15.10	-58%
1991-2010 to 2080-2099 under RCP 2.6 (RCM9)	–1621	20.60	-43%
1991-2010 to 2080-2099 under RCP 4.5	–1154	14.50	-60%
1991-2010 to 2080-2099 under RCP 8.5	–2597	7.40	-80%

The findings of this current study are also in agreement with Rounce et al. (2020) projected glacier mass change in High Mountain Asia using PyGEM model by employing data of 22 GCMs and four RCPs. Overall, their results exhibited retreat of glaciers in the Naltar catchment varies considering uncertainties (–35% to –71%). Unsurprisingly, the mass loss in Naltar catchment 5-10% higher under different RCPs in our study. Such differences in glacier projections are possibly due to usage of different climate forcings (GCM and RCP scenarios), model physics and calibration scheme, present day mass balance, projected changes in climate forcings and various glacier attributes (e.g., ice thickness and glacier hypsometry). Rounce et al. (2020) also mentioned that PyGEM presently designed for large scale applications and its model physics allows instant estimations over large catchments (e.g., use of mass distribution curves), care should be taken when applying this model application especially for small scale while, PDSLIM normally used for small scale applications (Grossi et al. 2013; Ranzi and Rosso 1991). Moreover, Kraaijenbrink et al. (2017) also found that regional variation in mass loss in HMA is quite high and there are several regions where mass loss drop below 10% under RCP 8.5. Hence, these arguments strengthened our results about higher mass loss and glacier retreat as compared to other part of HMA where the so-called Karakorum anomaly prevails. As a result of these projections, regional water management and mountain communities may experience serious consequences. The results of our study also show that the Karakorum anomaly has less impacts especially at small scale catchment in the southern region of Karakoram. Future work should seek to continue the use of physically models as PDSLIM for future mass balance and glacier retreat studies and to explore the Karakoram anomaly in the context of climate change in glacierized catchments as well as glacier outburst regions in Pakistan.

3.4 Glacier Mass Change Projections

To estimate the response of the Naltar glaciers in response to future climate forcings, we setup PDSLIM model as described in chapter#2 (section 3.3) to project seasonal summer mass balance for all individual glaciers with area larger than 0.4 km^2. Overall results as described in Fig.3.5 indicating that glaciers are out of balance in Naltar catchment.

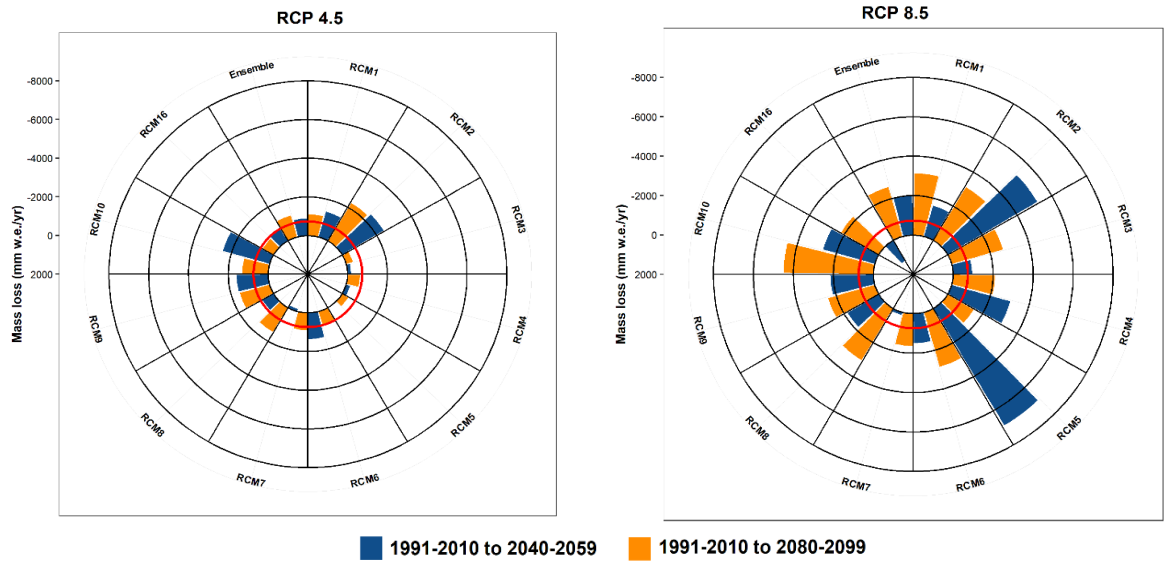

Figure.3.5. Projected changes in mass balance loss over Naltar catchment in 11 CORDEX experiments and their ensemble for near future (2040-2059) and far future (2080-2099) scenarios for RCPs (4.5, 8.5). Red marked as reference period with mass loss (-737 mm w.e. a^{-1}).

Projections estimate that from 2010 to 2100, glaciers in Naltar catchment varies the mass balance (–654 to –1621 mm w.e. a^{-1} by 2050 and 2090) in the two scenario periods under RCP 2.6 with RCM9, For RCP4.5 mass balance varies between (128 to –2436 mm w.e. a^{-1}) with ensemble mean (–887 mm w.e. a^{-1}) in near future (2040-2059) and (–352 to –2277 mm w.e. a^{-1}) with ensemble mean (–1154 mm w.e. a^{-1}) in far future scenario (2080-2099) with reference(-737 mm w.e. a^{-1}). For RCP8.5 mass balance varies between (1197 to –6913 mm w.e. a^{-1}) with ensemble mean (–2018 mm w.e. a^{-1}) in near future (2040-2059) and (–1508 to –4489 mm w.e. a^{-1}) with ensemble mean (–2597 mm w.e. a^{-1}) in far future scenario (2080-2099). The spatial variability in projected mass loss is dependent on the projected temperature, precipitation, present-day mass balance and several glacier attributes such as, e.g., ice thickness and glacier hypsometry. Overall, a rise in temperature varies between 1.63 ± 0.95 to 6.02 ± 0.88 (°C/day) during both scenario periods under all RCPs. Although precipitation is also projected to increase 28.7% under high emission scenario by the end of century, it cannot compensate the substantial increase in temperature.

3.5 Projected change in streamflow

In order to predict the impact of climate change on future streamflow, the linear reservoir model already calibrated and validated in the previous chapter was executed with future climate forcings. The model parameters were kept the same during future simulation, except initial baseflow. The predicted streamflow hydrographs for two future scenario periods (2040-2059) and (2080-2099) with reference to control period 1991-2010 under three RCPs 2.6, 4.5 and 8.5 are shown in Fig.3.6. The uncertainty in the future climate of Naltar catchment is also evident in projections of future hydrology. The result show different projected seasonal variability in streamflow in all selected climate models under three RCPs in Naltar catchment. Under RCP

2.6 with RCM9, the projected streamflow is found to be increasing in magnitude in near future followed by steady decline during far future period relative to control period. It is also seen in Fig.3.6. that peak stream flow is shifted from Aug-Sep to June-July by end of the century in both future periods.

Under RCP 4.5, projected streamflow exhibited increasing and decreasing rate in both future scenarios relevant to control period in different RCMs. Overall, the ensemble projected streamflow is expected to follow a slightly decreasing trend (-1.88%) in near future (2040-2059) following the steady increase (3.61%) in far future (2080-2099). The peak runoff curve is also shifted from Aug-Sep to July-Aug by the end of the century. Under RCP 8.5, the projected streamflow is expected to continuously decrease (-3.02%) in near future (2040-2059) and (-23.69%) in far future (2080-2099). Similarly peak streamflow duration in majority of RCMs as well as their ensemble mean also shifted significantly from Aug-Sep to mid of June to July in near future whereas mid of May to end of June in far future.

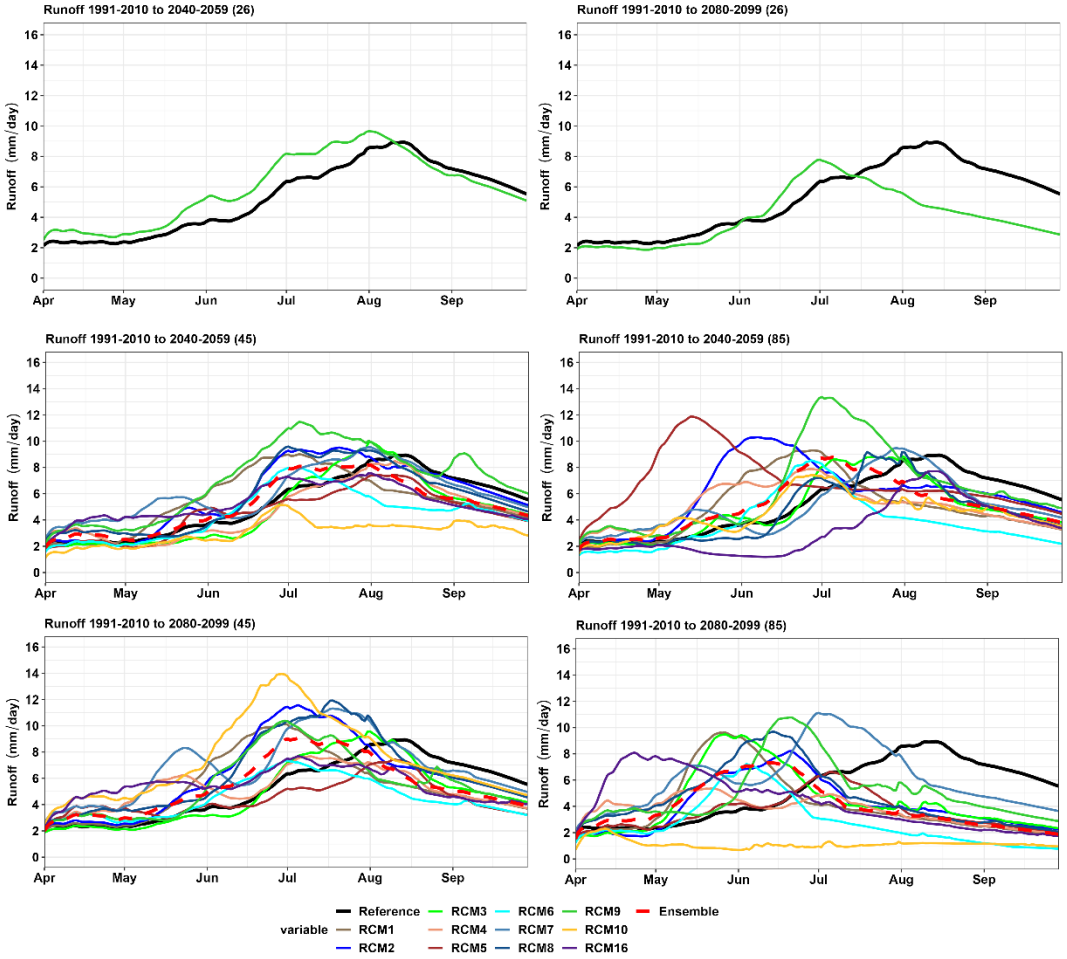

Figure.3.6. Comparison between daily runoff of control period (1991-2010) and projected runoff of scenario years (2040-2059) & (2080-2099) under RCP 2.6, RCP 4.5 and RCP 8.5 of Naltar catchment.

Table.3.4 illustrates the projected monthly variation in streamflow and its change under three RCPs (2.6, 4.5, 8.5) for each selected model and its ensembles. The change in future climate induced significant variation in seasonal runoff especially during pre-monsoon (April-June) and monsoon seasons (July-September). During the spring season, the streamflow is normally

generated due to snowmelt with small contributions from the rainfall whereas during monsoon periods, streamflow is dominated by glacier melt with monsoon precipitation. From Table.3.4 it can be seen that in the present climate scenario peak streamflow period normally lies from July-Sep while maximum increment in projected streamflow were noticed during the pre-monsoon season under RCP 4.5 and RCP 8.5 in all selected models and their ensembles. Under RCP 2.6, the streamflow shows substantial increase in magnitude during (pre-monsoon) (25.3 to 33.6%) while a downward trend (–7%) during the monsoon in near future and it is stronger decrease in far future scenario up to (–46.9%).

For RCP 4.5 simulations, streamflow evident ensemble increasing rate (13.8%) during pre-monsoon in both scenario period and it is more pronounced (34.1%) by end of century. Similarly in 8.5 simulations, projected streamflow also exhibited substantial mean rise in streamflow in both scenario periods (25.6% & 48.4%). It was also noticed that almost all RCM-simulations and their ensembles recorded substantial decline of streamflow during monsoon despite significant increases in streamflow was examined at control period. For RCP 4.5, the ensemble streamflow during monsoon decreased by –9.4% to –11.4% during near 2050s and far future 2090s periods respectively which was even stronger in case of RCP 8.5 simulations with –17.8% in 2050s and –57.2% in 2090s. It is mainly linked to the bilateral relationship between significant increase in temperature and early onset of snow and glacier melt during pre-monsoon (April-June: snow melt followed by extreme events in conjunction with glacier melt) consequently one month earlier peak flow pre-monsoon (July) was observed under RCP 4.5 in both scenario periods whereas peak streamflow shifted to late pre-monsoon (June) than the reference (August) under RCP 8.5 by end of century.

Several factors may have contributed to these substantial shifts in hydrological regime, including regional hydroclimatic factors and the physical characteristics (presence of snow and glaciers) of the study region. Naltar catchment is mainly characterized by snow fed- glacierized catchment with major influence of westerlies circulations. During the pre-monsoon period, there was a significant rise in temperature, and solid precipitation occurred in high altitude parts during the control period; this precipitation could occur in a liquid state during the scenario periods. It may result occurrence of earlier peak cryosphere melt with varied magnitude during pre-monsoon in both future scenarios under considered RCPs. Results from our PDSLIM and LRM models for intra-seasonal streamflow changes are consistent with projections developed by Lutz et al. (2016) using the Spatial Processes in Hydrology (SPHY) model, Azmat et al. (2020) using multiple models in Hunza and Mishra et al. (2020) in two sub-catchments of HMA (Naltar in Karakoram and Trishuli in Nepal. Due to varying scenarios and climate models, it is difficult to make a direct comparison with absolute results. As a result of the uncertainty surrounding the future climate change projections, climate models must be improved in order to make better predictions about the future. Overall, intra-annual potential change in streamflow show a substantial alteration in hydrological regime of the selected study basins attaining decline of peak flows one-two month early than the current natural conditions. Further, it should be important to know that the streamflow during early pre-monsoon season is mainly contributed by the seasonal snowmelt and partially by glacier-melt and this phenomena is vice versa in case of monsoon season.

Table.3.4. Naltar monthly streamflow changes by CORDEX climate models under RCP 2.6, RCP 4.5 and RCP 8.5 as compared to control period

RCM	RCP	Decade	April	May	June	July	August	September
RCM1	RCP45	2050s	1.2	45.7	66.9	16.6	-24.4	-23.2
		2090s	3.2	33.0	97.8	15.0	-35.5	-34.2
	RCP85	2050s	-1.6	54.3	78.6	-4.3	-39.9	-40.5
		2090s	-4.3	142.3	46.0	-47.6	-65.7	-66.6
RCM2	RCP45	2050s	6.3	23.0	33.0	31.1	-2.3	-2.4
		2090s	10.1	29.5	88.0	47.9	-17.4	-16.7
	RCP85	2050s	10.6	94.9	96.4	-0.2	-18.5	-13.8
		2090s	-20.4	63.3	64.0	-35.9	-57.3	-58.6
RCM3	RCP45	2050s	-3.0	-22.2	-30.3	21.1	-3.5	-20.2
		2090s	-5.8	-10.3	-5.7	18.0	-10.0	-26.0
	RCP85	2050s	0.2	11.0	-0.9	35.6	-20.2	-28.8
		2090s	-16.5	122.2	68.0	-40.9	-55.3	-57.6
RCM4	RCP45	2050s	19.6	-19.4	-17.6	-3.4	-9.2	-21.2
		2090s	38.0	86.0	13.5	4.2	-27.4	-33.9
	RCP85	2050s	34.0	83.4	59.2	-14.2	-39.3	-40.2
		2090s	60.4	68.9	-7.0	-40.9	-64.8	-65.6
RCM5	RCP45	2050s	-6.3	1.4	7.2	-14.2	-18.9	-29.0
		2090s	47.8	15.7	-8.0	-21.0	-21.8	-40.4
	RCP85	2050s	127.9	264.4	64.5	-10.5	-26.6	-20.0
		2090s	-1.4	12.6	3.0	-22.1	-61.9	-62.8
RCM6	RCP45	2050s	-7.5	-10.8	25.1	-0.5	-40.2	-28.4
		2090s	25.0	8.0	31.0	-6.2	-42.9	-41.4
	RCP85	2050s	-32.3	-7.8	48.0	-19.6	-55.9	-57.9
		2090s	-14.6	39.2	24.0	-63.7	-80.4	-85.5
RCM7	RCP45	2050s	58.4	77.4	9.7	19.7	-1.1	-9.6
		2090s	54.3	122.0	47.7	52.0	-4.5	-9.9
	RCP85	2050s	24.9	43.9	-17.1	10.2	-10.6	-26.6
		2090s	48.1	114.9	64.1	38.0	-31.7	-34.7
RCM8	RCP45	2050s	30.3	-0.5	35.5	29.4	-7.0	-14.1
		2090s	37.9	34.0	71.3	54.8	-9.2	-17.1
	RCP85	2050s	-4.5	-16.2	2.7	9.0	-21.1	-33.4
		2090s	38.3	91.6	96.2	-31.3	-61.4	-61.3
RCM9	RCP26	2050s	25.3	25.6	33.1	22.2	-0.4	-7.0
		2090s	-14.8	-16.0	21.4	-6.2	-44.7	-46.9
	RCP45	2050s	41.3	44.4	87.9	50.4	0.2	15.5
		2090s	27.1	10.5	79.9	24.1	-29.1	-25.0
	RCP85	2050s	31.5	21.1	65.8	60.5	-16.9	-14.2
		2090s	44.1	24.6	103.1	-12.4	-42.1	-47.2
RCM10	RCP45	2050s	-24.3	-22.2	-22.0	-46.8	-58.2	-46.0
		2090s	78.7	88.7	149.9	56.2	-12.9	-14.9
	RCP85	2050s	-0.1	24.3	26.8	-15.3	-39.7	-34.5
		2090s	-31.1	-69.0	-78.9	-85.0	-85.8	-83.3
RCM16	RCP45	2050s	57.0	46.3	28.8	-0.4	-24.2	-29.0
		2090s	82.1	89.1	32.1	1.0	-30.9	-33.8
	RCP85	2050s	-19.5	-44.2	-66.1	-41.0	-19.5	-34.7
		2090s	155.6	129.1	11.6	-49.4	-69.0	-69.3
Ensemble	RCP45	2050s	13.4	7.6	20.6	13.3	-19.7	-21.7
		2090s	25.6	30.3	46.2	22.6	-26.7	-30.0
	RCP85	2050s	1.6	27.6	47.5	12.6	-33.3	-32.7
		2090s	16.3	76.2	52.9	-43.0	-63.5	-65.2

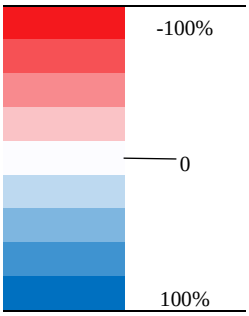

3.6 Projected change in hydrological components to net streamflow

The impact of climate change on hydrological components (glacier runoff, surface runoff and sub-surface runoff) to net streamflow is of highly important especially in snow-glacier dominated catchment. Table.3.5. depicts the relative change in individual hydrological contributions to net flow during for all RCMs and their ensemble during scenario periods relative to control period. Similarly, projected changes in hydrological components by integration of ensemble of 11 RCMs for both future scenario periods are given in Fig.3.7.

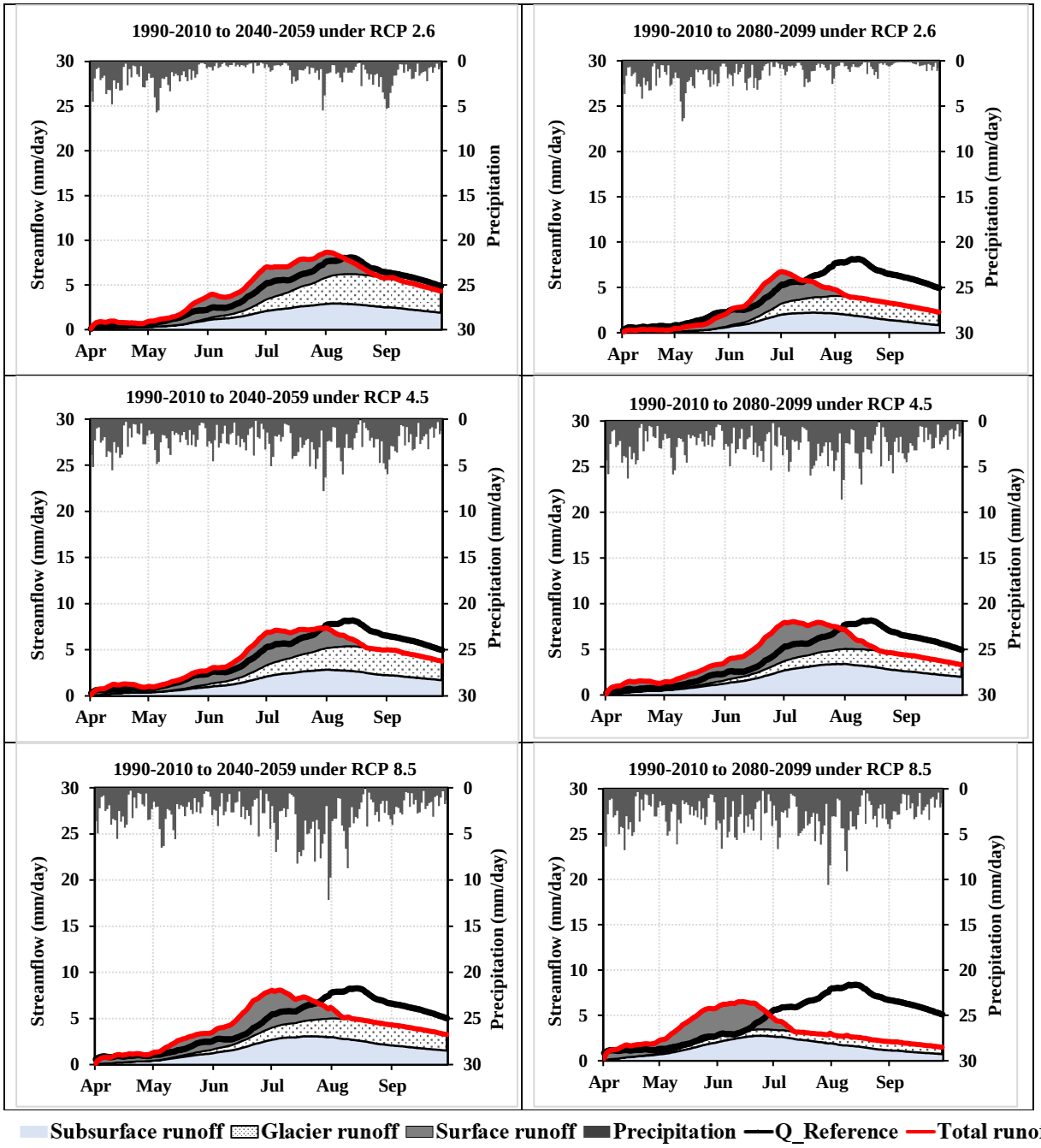

Figure.3.7 Projected changes in the contribution of individual components to total flow simulated by the integration of ensembles of 11 different CORDEX-SA RCM experiments with PDSLIM and LRM for 2040-2059 and 2080-2099 under RCP 2.6, RCP 4.5 and RCP 8.5 relative to control period 1991-2010

Table.3.5 Hydrological contributions to the Naltar streamflow considering RCP 2.6, RCP 4.5 and RCP 8.5 climate scenarios using PDSLIM and LRM

		1991-2010 to 2040-2059						**1991-2010 to 2080-2099**					
RCP		Glacier Runoff (mm)		Surface Runoff (mm)		Sub-surface Runoff (mm)		Glacier Runoff (mm)		Surface Runoff (mm)		Sub-surface Runoff (mm)	
	Reference	**368**		**177**		**416**		**368**		**177**		**416**	
	MODEL	Value	Change	Value	Change	Value	Change	Value	Change	Value	Change	Value	Change
		mm	%	mm	%	mm	%	mm	%	mm	%	mm	%
RCP26	*RCM9*	*259*	*-29.6*	*248*	*40.1*	*563*	*35.3*	*177*	*-51.9*	*169*	*-4.5*	*402*	*-3.4*
RCP45	RCM1	266	-27.7	239	35.2	507	21.8	177	-51.9	270	52.7	555	33.3
	RCM2	323	-12.2	246	38.7	500	20.2	225	-38.8	317	78.9	600	44.2
	RCM3	183	-50.2	236	33.2	457	9.8	136	-63.2	266	50.4	502	20.7
	RCM4	181	-50.7	227	28.1	454	9.0	155	-58.0	261	47.5	543	30.6
	RCM5	175	-52.4	212	19.9	445	7.0	114	-68.9	230	29.9	476	14.3
	RCM6	223	-39.3	195	10.2	403	-3.2	141	-61.8	216	22.2	468	12.6
	RCM7	215	-41.7	282	59.2	611	46.9	199	-45.9	349	97.0	710	70.7
	RCM8	239	-35.0	257	44.9	553	33.0	202	-45.2	337	90.4	640	53.8
	RCM9	*314*	*-14.7*	*333*	*88.0*	*642*	*54.2*	*193*	*-47.6*	*280*	*58.4*	*555*	*33.3*
	RCM10	243	-34.0	102	-42.3	210	-49.6	217	-41.0	395	123.1	749	80.0
	RCM16	229	-37.7	233	31.7	501	20.5	160	-56.4	289	63.5	552	32.7
	Ensemble	**230**	**-37.6**	**231**	**30.5**	**481**	**15.7**	**168**	**-54.3**	**275**	**55.4**	**550**	**32.2**
RCP85	RCM1	198	-46.3	240	35.6	487	17.1	127	-65.4	215	21.2	409	-1.7
	RCM2	345	-6.2	250	41.5	509	22.3	126	-65.8	212	19.5	417	0.2
	RCM3	158	-57.2	242	36.6	493	18.5	121	-67.2	237	33.7	455	9.3
	RCM4	253	-31.3	207	17.1	472	13.5	100	-72.9	182	2.6	396	-4.9
	RCM5	446	21.2	257	45.1	547	31.4	87	-76.4	185	4.5	378	-9.2
	RCM6	157	-57.4	191	7.8	353	-15.3	102	-72.2	156	-12.1	254	-39.0
	RCM7	149	-59.4	255	44.3	535	28.7	117	-68.3	342	93.0	664	59.6
	RCM8	188	-48.9	240	35.5	421	1.1	128	-65.1	260	46.8	471	13.1
	RCM9	*242*	*-34.3*	*313*	*76.7*	*598*	*43.9*	*123*	*-66.5*	*272*	*53.9*	*533*	*28.0*
	RCM10	221	-40.0	198	12.0	399	-4.1	125	-66.0	33	-81.5	48	-88.4
	RCM16	59	-83.9	198	12.1	354	-14.8	109	-70.3	222	25.4	456	9.6
	Ensemble	**209**	**-43.3**	**244**	**38.0**	**478**	**15.0**	**114**	**-69.0**	**208**	**17.6**	**410**	**-1.3**

It can be seen that relative change in each hydrological component produced by RCMs is significantly different from each other. The results indicate that direct surface runoff is found to contribute less to net streamflow in Naltar catchment while it is significantly influenced by both subsurface and glacier runoff. Under RCP 2.6, the results show a continuous decrease in surface and glacier runoff in both scenario periods. Further an abrupt increase in sub-surface runoff (13.7%) and subsequent decline (–42.1%) even below control period is projected for far future scenario.

In RCP 4.5 simulations, the glacier runoff is projected to decrease in all RCMs and their associated ensembles –37.6% and –54.3% in both future scenarios by end of century. Infact, the decrease is strongest under RCP 8.5 in all RCMs and their ensembles decline up to –43.3% during 2040-2059 and –69% during 2080-2099. Similarly, projected surface runoff in all considered scenarios is found to be higher than control period. In RCP 4.5, the projected surface runoff contribution to net streamflow is expected to peak (56.2%) by end of century which was steady declined (42.6% to 17.6%) under the RCP 8.5 but still higher than control period.

In Naltar catchment, sub-surface runoff contributes more to net streamflow through most of the year. The largest contribution of sub-surface runoff is due to dominant present of snowmelt in groundwater storage which returns to surface flow through baseflow. The contribution of sub-surface runoff in net streamflow pattern is continue in future and maximum contribution (56.2%) is reached during far-future scenario (2080-2099) under RCP 4.5 subsequently steady decline (–1.3%) until 2099 with RCP 8.5. Another reason for higher contribution of sub-surface runoff in Naltar catchment, glacier area is gradually reduced in both future scenarios under three considered RCPs, the contribution of store snow melt in favor of glacier melt. Hence, seasonal snow provides considerable amount of melt water.

Lutz et al. (2016) found significant increase in winter precipitation in Karakoram, but rapid increase in temperature especially at high altitude zones lead to shift precipitation pattern to fall as rain instead of snow. Thus, reduced snow precipitation during accumulation period and rapid melting of snowpack from subsurface layers also result in early exposure of glacier surfaces, which enhances the melting of glaciers in the basin. It is also observed that glaciers initially contribute a significant amount to net streamflow in near future under RCP4.5 and RCP8.5 until glacier mass depletion reaches tipping points in the far future scenario under RCP8.5 consequently a sharp decline in streamflow 733 mm (–23.69%) as shown in Table.3.6. The findings from our glacier and hydrology modeling components, indicating an increasing glacier melt driving an increase in river runoff from glaciers and a subsequent decline in river flow, are a characteristic of "peak water" conditions. The dynamics of our results are in an agreement with previous studies with earlier shift in snow melt followed by significant increasing trend in ice melt/glacier shrinkage and peak shift in streamflow at large scale (Kraaijenbrink et al. 2017); Rounce et al. (2020) and regional/catchment level (Ali et al. 2018; Azmat et al. 2020; Mishra et al. 2020; Soncini et al. 2015).

3.7 Projected change in water balance

The projected water balance analysis in all RCMs and their ensemble was estimated and plotted based on hydrological alternative of the Truc-Budyko plot as shown in Fig.3.8. Further, projected values of individual component of water balance were computed and displayed in Table.3.6. The runoff coefficient (Q/P) and aridity index were computed (P/ETp) and plot on y-axis and x-axis, respectively.

Under RCP 2.6, 4.5 & 8.5, most of RCMs and their ensemble broke the water limit and were located within the “Gaining” domain as shown in Fig 3.8(a-f) in both future scenarios. In gaining catchments, precipitation was not sufficient (underestimated) to close the water balance cycle. In the “Gaining” catchments which break the water limit (Q>P) additional water is required to close the water balance. This additional water is fed by glacier melting in glacierized catchments. Such phenomena result in negative glacier mass balance. as shown in Fig.3.5. It is also noticed that one of RCM10 under RCP 8.5 in far future scenario not only below water limit but also out of the energy limit i.e., simulated streamflow was highly underestimated. Such underestimation is due to lower projected values of snow depth ratio as shown in Table S3.3 which ultimately put impact on all glaciological and hydrological simulations as shown in Fig.3.3 and Fig.3.5.

Given the importance of glacier melt contribution to streamflow in Naltar catchment, it is also found that projected mass balance loss significantly increases in both future scenario under all RCPs due to increase in temperature (6.15%) and evapotranspiration (23.72%), consequently less ice melt is available in the future. Additionally, RCMs and their ensemble also projected increase in precipitation in both future scenarios (+5.39% to +27.95%). Based on such arguments, it can be seen in Fig 3.8, RCMs and their ensemble are moving towards water limit line in both future scenarios especially under RCP 8.5 and there is possibility that state of hydrological regime of Naltar can convert from snow & glacier melt dominance to rainfall dominance.

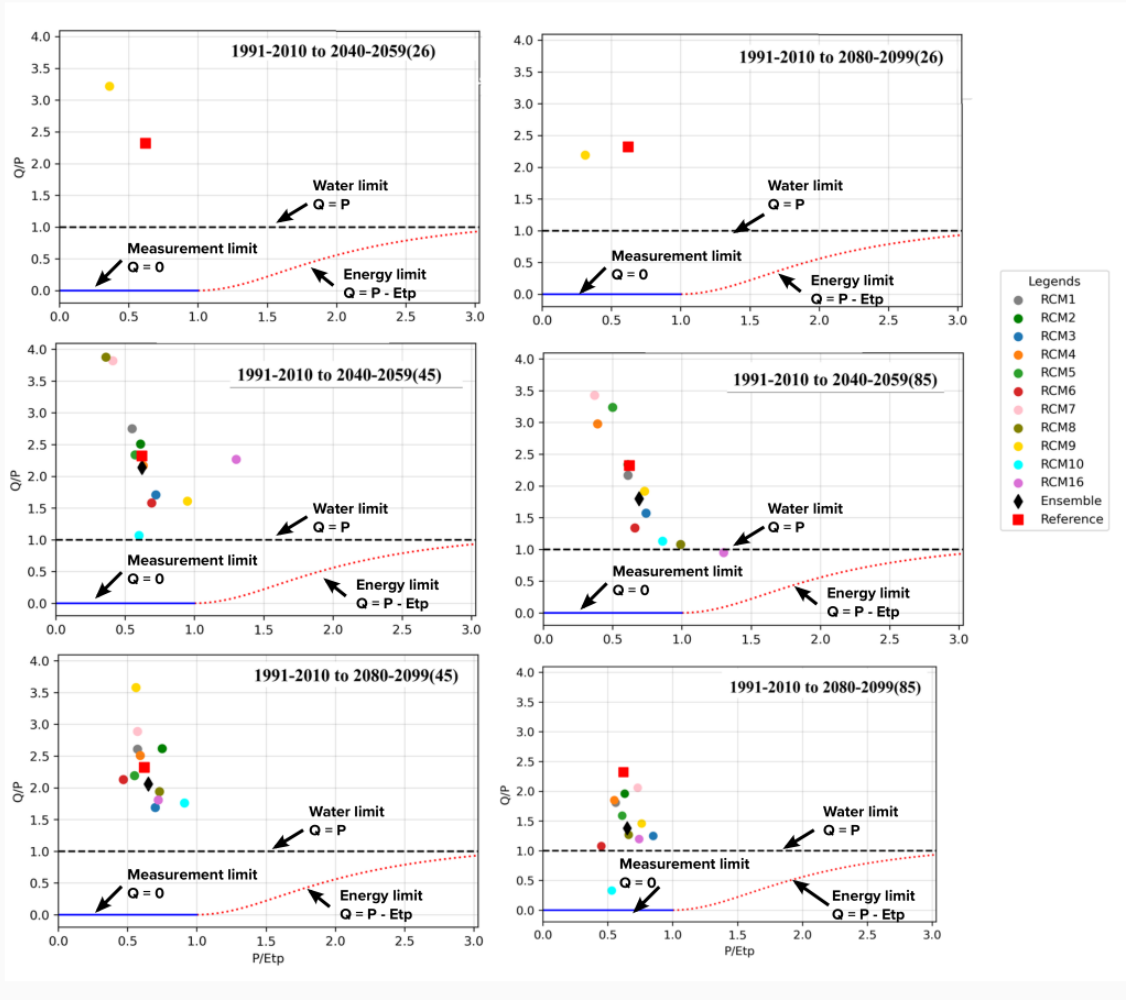

Figure.3.8. The hydrological alternative of the Turc-Budyko plot for 11 RCMs and their ensemble in future scenarios (2040-2059) & (2080-2099) relative to control period (1991-2010). Reference point marked relationship during present condition .

Table.3.6 Projected changed in water balance components from 2010-2099 under RCP 2.6, RCP 4.5 and RCP 8.5.

		1991-2010 to 2040-2059					**1991-2010 to 2080-2099**				
RCP		SWE	Ice melt	Precipitation	ET	Q simulated	SWE	Ice melt	Precipitation	ET	Q simulated
		mm	mm	mm	mm	mm	mm	mm	mm	mm	mm
	Reference	**1294**	**133**	**414**	**664**	**960**	**1294**	**133**	**414**	**664**	**960**
	MODEL										
RCP26	RCM9	*1671*	*48*	*262*	*720*	*1080*	*1161*	*61*	*227*	*718*	*748*
RCP45	RCM1	1311	129	363	659	1012	1362	72	384	676	1002
	RCM2	1330	214	419	683	1069	1376	136	434	578	1142
	RCM3	1267	42	509	710	876	1338	38	533	764	904
	RCM4	1261	48	396	627	862	1341	53	383	648	959
	RCM5	1237	39	355	621	833	1241	17	375	676	820
	RCM6	1083	125	515	750	821	1284	54	387	830	825
	RCM7	1680	38	289	706	1107	1761	60	435	762	1258
	RCM8	1582	71	269	743	1049	1486	91	607	828	1178
	RCM9	*1532*	*139*	*765*	*801*	*1288*	*1431*	*95*	*431*	*790*	*1028*
	RCM10	679	214	503	792	555	1567	86	772	852	1360
	RCM16	1290	89	421	699	964	1338	54	554	769	1002
	Ensemble	**1302**	**91**	**437**	**704**	**942**	**1360**	**64**	**481**	**742**	**993**
RCP85	RCM1	1176	105	418	682	925	918	92	415	735	751
	RCM2	1184	324	451	733	1104	918	93	384	613	754
	RCM3	1169	66	563	763	892	918	78	652	771	812
	RCM4	1184	188	303	778	932	917	62	367	663	677
	RCM5	1184	429	364	727	1250	917	44	409	674	649
	RCM6	839	94	513	771	700	696	85	473	1048	511
	RCM7	1546	34	272	744	940	1435	48	545	745	1122
	RCM8	930	113	773	777	849	1036	90	677	1019	859
	RCM9	*1478*	*133*	*617*	*850*	*1153*	*1154*	*71*	*634*	*833*	*928*
	RCM10	931	167	702	817	818	282	132	622	1180	206
	RCM16	669	3	644	496	612	917	65	654	883	787
	Ensemble	**1182**	**126**	**511**	**738**	**931**	**918**	**77**	**536**	**821**	**733**

4. Conclusions

As global climate change progresses, interacting processes in physical systems and economic activities become highly complicated and uncertain (Abbasi et al. 2017). In the High Mountain Asia (HMA), assessing future hydro-glaciological changes is complicated by uncertainties associated with the historical and projected climate data, glacier extent, glacier mass balance, and model processes and parameters. In this study, the energy balance model named Physically based Distributed Snow Land and Ice Model (PDSLIM) was used in Pakistan to explore its applicability and assess the relative impacts of projected climatic changes in glaciological and hydrological regimes of Naltar catchment, located in Hunza, one of largest glacierized region in High Mountain Asia (HMA).

To select the most appropriate set of RCMs for climate change assessments on glacio-hydrology, a multi-perspective approach based on improved delta change method and 31-days moving window was proposed and applied in Naltar catchment as a case study. Using this approach, eleven RCMs were shortlisted out an initial pool of 17 from CORDEX- SA domain with two future scenarios (2040-2059 and 2080-2099) under three RCPs representing the full spectrum of projected changes in mean and extreme climate conditions. By using the proposed approach, 37 simulations of RCMs and their ensemble from the CORDEX-SA were selected to produce a full range of climate change ensembles, which ultimately results in a reduction of the glacio hydrological simulation task.

The climate projection exhibited significant increase in warming between +0.87 to +6.02 ^{o}C and precipitation up to +29% (121 mm) from April-September between 1991-2010 and 2080-2099 for RCP 2.6, 4.5 and 8.5. A maximum increase in precipitation and temperature was observed during the 2090s under RCP8.5, whereas seasonal changes were observed during pre-monsoon for temperature and early monsoon for precipitation. A similar increase in solar radiation was also evident in both future scenarios under RCP 4.5 and 8.5, which is also indicative of the presence of global warming in this region. Additionally, relative humidity, wind speed, and pressure are showing increasing trends both in the near term and in the long term, but the variability of these variables is not as high as that of temperature and precipitation.

The projected simulations of energy and mass balance indicate that snow and ice melt progression consistently increases in both future scenarios with early shift in the timing of the maximum snowmelt (65% -80%) as it appears in June during near future (2040-2059) and in May for far future (2080-2099) under high emission scenario. Further, projections of glacier mass balance show glaciers in Naltar catchment are expected to retreat (–39% to –40%) for 2.6, (–46% to –62%) for 4.5 and (–65% to –80%) for 8.5 ensemble scenarios. The glacier extent is expected to change sharply after the 2050s for most glaciers, indicating that glaciers are retreating more rapidly and that some glaciers may be disappeared by the end of century. Such earlier seasonal snowmelt followed by glacier retreat is likely to be a result of warming over elevated regions, which drives not only temperatures to melt earlier in the season but also may lead to more severe floods and landslide events in future. An example of such a catastrophic event occurred on July 5, 2021, when a glacial surge caused extensive damage to infrastructure and the death of four people in the Upper Naltar valley.

Water availability in the Naltar catchment is highly uncertain based on PDSLIM and LRM simulations that exhibited variable time distribution at monthly scale. Projected changes of water availability for RCP 4.5 (–2.7% to +3.38%) and (–4% to –23.69%) for RCP 8.5 under ensemble scenarios with respect to 2010 are highly variable. Separating the flow into primary

sources of glacier runoff, sub-surface runoff and surface runoff depicts decreasing contribution of glacier runoff up to (-69%) by the end of the century under RCP 8.5. Additionally, the rise in temperature is expected to have a substantial impact on the hydrological regime at seasonal scale. Based on the monthly projections, it is apparent that the streamflow in the Naltar will significantly increase in the pre-monsoon season and then decrease in the monsoon season in both future scenarios. The effects of these changes are likely to result in a shift of peak hydrological regime from one to two months earlier by 2090s over Naltar catchment. Using Turc-Budyko approach, the water energy and mass balance indicate that Naltar's hydrological regime can shift from snow and glacier melt dominance to rainfall dominance.

In light of the above results and discussion, we concluded that water availability in the Naltar catchment will be highly uncertain by the end of century in comparison with the current situation. Pakistan is investing in hydropower development in Northern areas to meet energy demand. It is estimated that a combined hydropower capacity of 51.2 MW will be operational by 2030 on the Naltar river, which not only helps to control water from glacier melt but also meets energy demands in Gilgit-Baltistan. The results of this study will help the government and other stakeholders to take informed decisions and assess financial risks for further development of reservoir operation and agriculture on farm water management in downstream areas by considering change in hydrological patterns driven by a projected climatic variable.

Bibliography

Abbasi S, Ahmad B, Ali M, Anwar M, Dahri Z, Habib N, Hussain A, Iqbal B, Ishaq S, Mustafa NJH-AWP (2017) The Indus Basin: A glacier-fed lifeline for Pakistan 11

Adnan M, Nabi G, Kang S, Zhang G, Adnan RM, Anjum MN, Iqbal M, Ali AF (2017) Snowmelt Runoff Modelling under Projected Climate Change Patterns in the Gilgit River Basin of Northern Pakistan J Polish Journal of Environmental Studies 26

Ahmad B, Rasul G (2018) Statistically downscaled projections of CORDEX South Asia using quantile mapping approach over Pakistan region International Journal of Global Warming 16:435-460

Ahmad I, Zhang F, Tayyab M, Anjum MN, Zaman M, Liu J, Farid HU, Saddique Q (2018) Spatiotemporal analysis of precipitation variability in annual, seasonal and extreme values over upper Indus River basin Atmospheric Research 213:346-360

Ahmad Z, Hafeez M, Ahmad I (2012) Hydrology of mountainous areas in the upper Indus Basin, Northern Pakistan with the perspective of climate change Environmental monitoring and assessment 184:5255-5274

Akhtar M, Ahmad N, Booij MJ (2008) The impact of climate change on the water resources of Hindukush–Karakorum–Himalaya region under different glacier coverage scenarios Journal of hydrology 355:148-163

Ali AF, Xiao C-d, Zhang X-p, Adnan M, Iqbal M, Khan G (2018) Projection of future streamflow of the Hunza River Basin, Karakoram Range (Pakistan) using HBV hydrological model Journal of Mountain Science 15:2218-2235

Ali S, Li D, Congbin F, Khan F (2015) Twenty first century climatic and hydrological changes over Upper Indus Basin of Himalayan region of Pakistan Environmental Research Letters 10:014007

Andermann C, Bonnet S, Gloaguen R (2011) Evaluation of precipitation data sets along the Himalayan front Geochemistry, Geophysics, Geosystems 12

Andréassian V, Perrin C (2012) On the ambiguous interpretation of the Turc-Budyko nondimensional graph Water Resources Research 48

Anjum MN, Ding Y, Shangguan D, Ahmad I, Ijaz MW, Farid HU, Yagoub YE, Zaman M, Adnan M (2018) Performance evaluation of latest integrated multi-satellite retrievals for Global Precipitation Measurement (IMERG) over the northern highlands of Pakistan Atmospheric Research 205:134-146

Archer DR, Fowler HJ (2004) Spatial and temporal variations in precipitation in the Upper Indus Basin, global teleconnections and hydrological implications Hydrology and Earth System Sciences Discussions 8:47-61

Arfan M, Lund J, Hassan D, Saleem M, Ahmad A (2019) Assessment of spatial and temporal flow variability of the Indus river Resources 8:103

Ashouri H, Hsu K-L, Sorooshian S, Braithwaite DK, Knapp KR, Cecil LD, Nelson BR, Prat OP (2015) PERSIANN-CDR: Daily precipitation climate data record from multisatellite observations for hydrological and climate studies Bulletin of the American Meteorological Society 96:69-83

Atif I, Iqbal J, Su L-j (2019) Modeling hydrological response to climate change in a data-scarce glacierized high mountain Astore Basin using a fully distributed TOPKAPI model Climate 7:127

Ayub S, Akhter G, Ashraf A, Iqbal M (2020) Snow and glacier melt runoff simulation under variable altitudes and climate scenarios in Gilgit River Basin, Karakoram region Modeling Earth Systems Environment 6:1607-1618

Azmat M, Wahab A, Huggel C, Qamar MU, Hussain E, Ahmad S, Waheed A (2020) Climatic and hydrological projections to changing climate under CORDEX-South Asia experiments over the Karakoram-Hindukush-Himalayan water towers Science of the Total Environment 703:135010

Bair EH, Abreu Calfa A, Rittger K, Dozier J (2018) Using machine learning for real-time estimates of snow water equivalent in the watersheds of Afghanistan The Cryosphere 12:1579-1594
Bair EH, Rittger K, Ahmad JA, Chabot D (2020) Comparison of modeled snow properties in Afghanistan, Pakistan, and Tajikistan The Cryosphere 14:331-347
Bair EH, Rittger K, Davis RE, Painter TH, Dozier J (2016) Validating reconstruction of snow water equivalent in C alifornia's S ierra N evada using measurements from the NASA A irborne S now O bservatory Water Resources Research 52:8437-8460
Bair EH, Rittger K, Skiles SM, Dozier J (2019) An examination of snow albedo estimates from MODIS and their impact on snow water equivalent reconstruction Water Resources Research 55:7826-7842
Baudouin J-P, Herzog M, Petrie CA (2020) Contribution of cross-barrier moisture transport to precipitation in the upper Indus River Basin Monthly Weather Review 148:2801-2818
Benn D, Bolch T, Hands K, Gulley J, Luckman A, Nicholson L, Quincey D, Thompson S, Toumi R, Wiseman S (2012) Response of debris-covered glaciers in the Mount Everest region to recent warming, and implications for outburst flood hazards Earth-Science Reviews 114:156-174
Bergström S (1976) Development and application of a conceptual runoff model for Scandinavian catchments.
Berthier É, Brun F (2019) Karakoram geodetic glacier mass balances between 2008 and 2016: persistence of the anomaly and influence of a large rock avalanche on Siachen Glacier Journal of Glaciology 65:494-507
Biemans H, Siderius C, Lutz A, Nepal S, Ahmad B, Hassan T, von Bloh W, Wijngaard R, Wester P, Shrestha A (2019) Importance of snow and glacier meltwater for agriculture on the Indo-Gangetic Plain Nature Sustainability 2:594-601
Blöschl G, Bierkens MF, Chambel A, Cudennec C, Destouni G, Fiori A, Kirchner JW, McDonnell JJ, Savenije HH, Sivapalan M (2019) Twenty-three unsolved problems in hydrology (UPH)–a community perspective Hydrological sciences journal 64:1141-1158
Bocchiola D, Diolaiuti G (2013) Recent (1980–2009) evidence of climate change in the upper Karakoram, Pakistan Theoretical and applied climatology 113:611-641
Bocchiola D, Diolaiuti G, Soncini A, Mihalcea C, D'agata C, Mayer C, Lambrecht A, Rosso R, Smiraglia C (2011a) Prediction of future hydrological regimes in poorly gauged high altitude basins: the case study of the upper Indus, Pakistan
Bocchiola D, Diolaiuti G, Soncini A, Mihalcea C, D'agata C, Mayer C, Lambrecht A, Rosso R, Smiraglia C (2011b) Prediction of future hydrological regimes in poorly gauged high altitude basins: the case study of the upper Indus, Pakistan Hydrology and Earth System Sciences 15:2059-2075
Bokhari SAA, Ahmad B, Ali J, Ahmad S, Mushtaq H, Rasul G (2018) Future climate change projections of the Kabul River Basin using a multi-model ensemble of high-resolution statistically downscaled data Earth Systems Environment 2:477-497
Bolch T, Kulkarni A, Kääb A, Huggel C, Paul F, Cogley JG, Frey H, Kargel JS, Fujita K, Scheel M (2012) The state and fate of Himalayan glaciers Science 336:310-314
Bolch T, Pieczonka T, Mukherjee K, Shea J (2017) Brief communication: Glaciers in the Hunza catchment (Karakoram) have been nearly in balance since the 1970s The Cryosphere 11:531-539
Bosshard T, Kotlarski S, Ewen T, Schär C (2011) Spectral representation of the annual cycle in the climate change signal Hydrology Earth System Sciences 15:2777-2788
Brun F, Berthier E, Wagnon P, Kääb A, Treichler D (2017) A spatially resolved estimate of High Mountain Asia glacier mass balances from 2000 to 2016 Nature geoscience 10:668-673
Brunetti M, Lentini G, Maugeri M, Nanni T, Simolo C, Spinoni J (2012) Projecting North Eastern Italy temperature and precipitation secular records onto a high-resolution grid Physics and Chemistry of the Earth, Parts A/B/C 40:9-22
Budyko MI, Miller DH, Miller DH (1974) Climate and life vol 508. Academic press New York,

Cagnati A, Crepaz A, Macelloni G, Pampaloni P, Ranzi R, Tedesco M, Tomirotti M, Valt MJJoG (2004) Study of the snow melt–freeze cycle using multi-sensor data and snow modeling 50:419-426
Cannon F, Carvalho LM, Jones C, Bookhagen B (2015) Multi-annual variations in winter westerly disturbance activity affecting the Himalaya Climate dynamics 44:441-455
Carturan L, Baroni C, Brunetti M, Carton A, Dalla Fontana G, Salvatore MC, Zanoner T, Zuecco G (2016) Analysis of the mass balance time series of glaciers in the Italian Alps The Cryosphere 10:695-712
Cheema MJM, Bastiaanssen WG (2012) Local calibration of remotely sensed rainfall from the TRMM satellite for different periods and spatial scales in the Indus Basin International Journal of Remote Sensing 33:2603-2627
Choudhary A, Dimri A (2018) Assessment of CORDEX-South Asia experiments for monsoonal precipitation over Himalayan region for future climate Climate dynamics 50:3009-3030
Christensen JH, Boberg F, Christensen OB, Lucas-Picher P (2008) On the need for bias correction of regional climate change projections of temperature and precipitation Geophysical research letters 35
Colbeck SCJWRR (1976) An analysis of water flow in dry snow 12:523-527
Coron L, Andréassian V, Perrin C, Le Moine N (2015) Graphical tools based on Turc-Budyko plots to detect changes in catchment behaviour Hydrological Sciences Journal 60:1394-1407
Crespi A, Brunetti M, Lentini G, Maugeri M (2018) 1961–1990 high-resolution monthly precipitation climatologies for Italy International Journal of Climatology 38:878-895
Crespi A, Brunetti M, Ranzi R, Tomirotti M, Maugeri M (2021) A multi-century meteo-hydrological analysis for the Adda river basin (Central Alps). Part I: Gridded monthly precipitation (1800–2016) records International Journal of Climatology 41:162-180
Dahri ZH, Ludwig F, Moors E, Ahmad B, Khan A, Kabat P (2016) An appraisal of precipitation distribution in the high-altitude catchments of the Indus basin Science of the Total Environment 548:289-306
DAWN (2021) 4 people missing as glacial surge blocks nullah in Naltar DAWN News Paper doi:https://www.dawn.com/news/1633418
Diez-Sierra J, Iturbide M, Gutiérrez JM, Fernández J, Milovac J, Cofiño AS, Cimadevilla E, Nikulin G, Levavasseur G, Kjellström E (2022) The worldwide C3S CORDEX grand ensemble: A major contribution to assess regional climate change in the IPCC AR6 Atlas Bulletin of the American Meteorological Society
Dile YT, Srinivasan R (2014) Evaluation of CFSR climate data for hydrologic prediction in data-scarce watersheds: an application in the Blue Nile River Basin JAWRA Journal of the American Water Resources Association 50:1226-1241
Dolk M, Penton DJ, Ahmad MD (2020) Amplification of hydrological model uncertainties in projected climate simulations of the Upper Indus Basin: Does it matter where the water is coming from? Hydrological Processes 34:2200-2218
Eccel E, Cau P, Ranzi R (2012) Data reconstruction and homogenization for reducing uncertainties in high-resolution climate analysis in Alpine regions Theoretical and Applied Climatology 110:345-358
Faiz MA, Liu D, Tahir AA, Li H, Fu Q, Adnan M, Zhang L, Naz F (2020) Comprehensive evaluation of 0.25° precipitation datasets combined with MOD10A2 snow cover data in the ice-dominated river basins of Pakistan Atmospheric Research 231:104653
Fallah A, Rakhshandehroo GR, Berg P, O S, Orth R (2019) Evaluation of precipitation datasets against local observations in Southwestern Iran International Journal of Climatology
Farhan SB, Zhang Y, Aziz A, Gao H, Ma Y, Kazmi J, Shahzad A, Hussain I, Mansha M, Umar M (2020) Assessing the impacts of climate change on the high altitude snow-and glacier-fed hydrological regimes of Astore and Hunza, the sub-catchments of Upper Indus Basin Journal of Water Climate Change 11:479-490

Farhan SB, Zhang Y, Ma Y, Guo Y, Ma N (2015) Hydrological regimes under the conjunction of westerly and monsoon climates: a case investigation in the Astore Basin, Northwestern Himalaya Climate Dynamics 44:3015-3032
Farinotti D, Immerzeel WW, de Kok RJ, Quincey DJ, Dehecq A (2020) Manifestations and mechanisms of the Karakoram glacier Anomaly Nature Geoscience 13:8-16
Farinotti D, Magnusson J, Huss M, Bauder A (2010) Snow accumulation distribution inferred from time-lapse photography and simple modelling Hydrological Processes 24:2087-2097
Fatima E, Hassan M, Hasson Su, Ahmad B, Ali SSF (2020) Future water availability from the western Karakoram under representative concentration pathways as simulated by CORDEX South Asia Theoretical and Applied Climatology 141:1093-1108
Fowler H, Archer D (2006) Conflicting signals of climatic change in the Upper Indus Basin Journal of Climate 19:4276-4293
Fowler H, Kilsby C, O'Connell P (2003) Modeling the impacts of climatic change and variability on the reliability, resilience, and vulnerability of a water resource system Water Resources Research 39
Funk C, Peterson P, Landsfeld M, Pedreros D, Verdin J, Shukla S (2015) The climate hazards infrared precipitation with stations—a new environmental record for monitoring extremes. Sci Data. 2015; 2: 150066. Epub 2015/12/10. https://doi. org/10.1038/sdata. 2015.66 PMID: 26646728,
Gao Y, Liu M (2013) Evaluation of high-resolution satellite precipitation products using rain gauge observations over the Tibetan Plateau Hydrology and Earth system sciences 17:837
Gardezi H, Xing A, Bilal M, Zhuang Y, Muhammad S, Janjua S (2022) Preliminary investigation and dynamic analysis of a multiphase ice-rock avalanche on July 5, 2021, in the upper Naltar valley, Gilgit, Pakistan Landslides 19:451-463
Garee K, Chen X, Bao A, Wang Y, Meng F (2017) Hydrological modeling of the upper indus basin: A case study from a high-altitude glacierized catchment Hunza Water 9:17
Giorgi F, Coppola E, Solmon F, Mariotti L, Sylla M, Bi X, Elguindi N, Diro G, Nair V, Giuliani G (2012) RegCM4: model description and preliminary tests over multiple CORDEX domains Climate Research 52:7-29
Giorgi F, Jones C, Asrar GR (2009) Addressing climate information needs at the regional level: the CORDEX framework World Meteorological Organization Bulletin 58:175
Godwin-Austen HH (1864) On the glaciers of the Mustakh Range The Journal of the Royal Geographical Society of London 34:19-56
Grossi G, Caronna P, Ranzi R (2013) Hydrologic vulnerability to climate change of the Mandrone glacier (Adamello-Presanella group, Italian Alps) Advances in water resources 55:190-203
Grossi G, Falappi L (2003) Comparison of energy fluxes at the land surface-atmosphere interface in an Alpine valley as simulated with different models Hydrology Earth System Sciences
Gupta HV, Kling H, Yilmaz KK, Martinez GF (2009) Decomposition of the mean squared error and NSE performance criteria: Implications for improving hydrological modelling Journal of hydrology 377:80-91
Gutowski Jr WJ, Giorgi F, Timbal B, Frigon A, Jacob D, Kang H-S, Raghavan K, Lee B, Lennard C, Nikulin G (2016) WCRP coordinated regional downscaling experiment (CORDEX): a diagnostic MIP for CMIP6 Geoscientific Model Development 9:4087-4095
Hasson S (2016) Future water availability from Hindukush-Karakoram-Himalaya Upper Indus Basin under conflicting climate change scenarios. Climate 2016: 40.
Hasson S, Böhner J, Lucarini V (2017) Prevailing climatic trends and runoff response from Hindukush–Karakoram–Himalaya, upper Indus Basin Earth System Dynamics 8:337-355
Hasson S, Lucarini V, Khan MR, Petitta M, Bolch T, Gioli G (2014) Early 21st century snow cover state over the western river basins of the Indus River system Hydrology and Earth System Sciences 18:4077-4100

Hasson S, Lucarini V, Pascale S (2013) Hydrological cycle over South and Southeast Asian river basins as simulated by PCMDI/CMIP3 experiments Earth System Dynamics 4:199-217
Hasson S, Saeed F, Böhner J, Schleussner C-F (2019) Water availability in Pakistan from Hindukush–Karakoram–Himalayan watersheds at 1.5 C and 2 C Paris Agreement targets J Advances in Water Resources 131:103365
Hasson Su, Böhner J (2019) Hydrological Cycle Over the Indus Basin at Monsoon Margins: Present and Future. In: Indus River Basin. Elsevier, pp 245-264
Hayat H, Akbar TA, Tahir AA, Hassan QK, Dewan A, Irshad M (2019) Simulating current and future river-flows in the Karakoram and Himalayan regions of Pakistan using Snowmelt-Runoff model and RCP scenarios Water 11:761
Hayden H (1907) Notes on certain glaciers in Northwest Kashmir Rec. Geol. Surv. India 35:127-137
Hewitt K (2005) The Karakoram anomaly? Glacier expansion and the 'elevation effect,'Karakoram Himalaya Mountain Research Development 25:332-340
Hewitt K (2011) Glacier change, concentration, and elevation effects in the Karakoram Himalaya, Upper Indus Basin Mountain Research and Development 31:188-200
Hock R (1998) Modelling of glacier melt and discharge. ETH Zurich
Hock R, Holmgren B (2005) A distributed surface energy-balance model for complex topography and its application to Storglaciären, Sweden Journal of Glaciology 51:25-36
Huffman GJ, Bolvin DT (2013) TRMM and other data precipitation data set documentation NASA, Greenbelt, USA 28:1
Hussain M, Mumtaz S (2014) Climate change and managing water crisis: Pakistan's perspective J Reviews on environmental health 29:71-77
Hussain S, Song X, Ren G, Hussain I, Han D, Zaman M (2017) Evaluation of gridded precipitation data in the Hindu Kush–Karakoram–Himalaya mountainous area Hydrological sciences journal 62:2393-2405
Immerzeel W, Bierkens M (2010) Seasonal prediction of monsoon rainfall in three Asian river basins: the importance of snow cover on the Tibetan Plateau International Journal of Climatology 30:1835-1842
Immerzeel W, Bierkens M (2012) Asia's water balance Nature Geoscience 5:841
Immerzeel W, Wanders N, Lutz A, Shea J, Bierkens M (2015) Reconciling high-altitude precipitation in the upper Indus basin with glacier mass balances and runoff Hydrology and Earth System Sciences 19:4673-4687
Immerzeel WW, Droogers P, De Jong S, Bierkens M (2009) Large-scale monitoring of snow cover and runoff simulation in Himalayan river basins using remote sensing Remote sensing of Environment 113:40-49
Immerzeel WW, Van Beek LP, Bierkens MF (2010) Climate change will affect the Asian water towers Science 328:1382-1385
Iqbal Z, Shahid S, Ahmed K, Ismail T, Nawaz N (2019) Spatial distribution of the trends in precipitation and precipitation extremes in the sub-Himalayan region of Pakistan Theoretical and Applied Climatology 137:2755-2769
Ismail MF, Naz BS, Wortmann M, Disse M, Bowling LC, Bogacki W (2020) Comparison of two model calibration approaches and their influence on future projections under climate change in the Upper Indus Basin Climatic Change 163:1227-1246
Jain M, Sharma S Hydrological Modeling of Vam Sadhara River Basin, India, Using SWAT. In: International Conference on Emerging Trends in Computer and Image Processing (ICETCIP-2014). Pattaya, Thailand.:[sn], 2014.
Jain SK, Agarwal PK, Singh VP (2007) Hydrology and water resources of India vol 57. Springer Science & Business Media,
Janes TJ, Bush AB (2012) The role of atmospheric dynamics and climate change on the possible fate of glaciers in the Karakoram Journal of Climate 25:8308-8327

Javed A, Kumar P, Hodges KI, Sein DV, Dubey AK, Tiwari G (2022) Does the recent revival of Western Disturbances govern the Karakoram Anomaly? Journal of Climate:1-57
Jury MW, Mendlik T, Tani S, Truhetz H, Maraun D, Immerzeel WW, Lutz AF (2020) Climate projections for glacier change modelling over the Himalayas International Journal of Climatology 40:1738-1754
Kääb A, Berthier E, Nuth C, Gardelle J, Arnaud Y (2012) Contrasting patterns of early twenty-first-century glacier mass change in the Himalayas Nature 488:495-498
Kääb A, Treichler D, Nuth C, Berthier E (2015) Brief Communication: Contending estimates of 2003–2008 glacier mass balance over the Pamir–Karakoram–Himalaya Cryosphere 9
Kendall MG (1948) Rank correlation methods
Khan AJ, Koch M (2018) Correction and informed regionalization of precipitation data in a high mountainous region (Upper Indus Basin) and its effect on SWAT-modelled discharge Water 10:1557
Khan AJ, Koch M, Tahir AAJS (2020) Impacts of climate change on the water availability, seasonality and extremes in the Upper Indus Basin (UIB) 12:1283
Khattak MS, Babel M, Sharif M (2011) Hydro-meteorological trends in the upper Indus River basin in Pakistan Climate research 46:103-119
Kiani RS, Ali S, Ashfaq M, Khan F, Muhammad S, Reboita MS, Farooqi A (2021) Hydrological projections over the Upper Indus Basin at 1.5° C and 2.0° C temperature increase Science of The Total Environment 788:147759
Kraaijenbrink PD, Bierkens M, Lutz A, Immerzeel W (2017) Impact of a global temperature rise of 1.5 degrees Celsius on Asia's glaciers Nature 549:257-260
Kraaijenbrink PD, Stigter EE, Yao T, Immerzeel WW (2021) Climate change decisive for Asia's snow meltwater supply Nature Climate Change 11:591-597
Krakauer NY, Lakhankar T, Dars GH (2019) Precipitation Trends over the Indus Basin Climate 7:116
Kult J, Choi W, Keuser A (2012) Snowmelt runoff modeling: Limitations and potential for mitigating water disputes Journal of Hydrology 430:179-181
Laghari AN, Vanham D, Rauch W (2012) The Indus basin in the framework of current and future water resources management Hydrology Earth System Sciences 16:1063-1083
Latif Y, Yaoming M, Yaseen M (2018) Spatial analysis of precipitation time series over the Upper Indus Basin Theoretical and applied climatology 131:761-775
Li D, Yang K, Tang W, Li X, Zhou X, Guo D (2020) Characterizing precipitation in high altitudes of the western Tibetan plateau with a focus on major glacier areas International Journal of Climatology
Liaqat MU, Grossi G, Ansari R, Ranzi R Modeling Hydrological Vulnerability to Climate Change in the Glacierized Naltar Catchment (Pakistan) Using a Distributed Energy Balance Model. In: AGU Fall Meeting 2021, 2021. AGU,
Liaqat MU, Grossi G, Ranzi R (2022) Characterization of interannual and seasonal variability of hydro-climatic trends in the Upper Indus Basin Theoretical Applied Climatology 147:1163-1184 doi:https://doi.org/10.1007/s00704-021-03850-3
Lutz A, Immerzeel W, Kraaijenbrink P (2014a) Gridded meteorological datasets and hydrological modelling in the Upper Indus Basin Final Report, for International Centre for Integrated Mountain Development (ICIMOD), FutureWater, Costerweg 1:6702
Lutz A, Immerzeel W, Shrestha A, Bierkens M (2014b) Consistent increase in High Asia's runoff due to increasing glacier melt and precipitation Nature Climate Change 4:587-592
Lutz AF, Immerzeel W, Kraaijenbrink P, Shrestha AB, Bierkens MF (2016) Climate change impacts on the upper Indus hydrology: Sources, shifts and extremes PloS one 11:e0165630
Madhura R, Krishnan R, Revadekar J, Mujumdar M, Goswami B (2015) Changes in western disturbances over the Western Himalayas in a warming environment Climate dynamics 44:1157-1168

Mann HB (1945) Nonparametric tests against trend Econometrica: Journal of the Econometric Society:245-259
Masood M, Shakir AS, Azhar AH, Nabi G (2019) Assessment of Real Time, Multi-Satellite Precipitation Products under Diverse Climatic and Topographic Conditions Asia-Pacific Journal of Atmospheric Sciences:1-15
Minallah S, Ivanov VY (2019) Interannual variability and seasonality of precipitation in the Indus River basin Journal of Hydrometeorology 20:379-395
Minora U, Bocchiola D, D'Agata C, Maragno D, Mayer C, Lambrecht A, Mosconi B, Vuillermoz E, Senese A, Compostella C (2013) 2001–2010 glacier changes in the Central Karakoram National Park: a contribution to evaluate the magnitude and rate of the" Karakoram anomaly" The Cryosphere Discussions 7:2891-2941
Minora U, Bocchiola D, D'Agata C, Maragno D, Mayer C, Lambrecht A, Vuillermoz E, Senese A, Compostella C, Smiraglia C (2016) Glacier area stability in the Central Karakoram National Park (Pakistan) in 2001–2010: the "Karakoram Anomaly" in the spotlight Progress in Physical Geography 40:629-660
Mishra SK, Veselka TD, Prusevich AA, Grogan DS, Lammers RB, Rounce DR, Ali SH, Christian MH (2020) Differential impact of climate change on the hydropower economics of two river basins in high mountain Asia Frontiers in Environmental Science 8:26
Monteith JJQJotRMS (1981) Evaporation and surface temperature Quarterly Journal of the Royal Meteorological Society 107:1-27
Moriasi DN, Arnold JG, Van Liew MW, Bingner RL, Harmel RD, Veith TL (2007) Model evaluation guidelines for systematic quantification of accuracy in watershed simulations Transactions of the ASABE 50:885-900
Muhammad S, Thapa A (2021) Daily Terra–Aqua MODIS cloud-free snow and Randolph Glacier Inventory 6.0 combined product (M* D10A1GL06) for high-mountain Asia between 2002 and 2019 Earth System Science Data 13:767-776
Muhammad S, Tian L, Khan A (2019) Early twenty-first century glacier mass losses in the Indus Basin constrained by density assumptions Journal of Hydrology 574:467-475
Mukhopadhyay B, Khan A (2015) A reevaluation of the snowmelt and glacial melt in river flows within Upper Indus Basin and its significance in a changing climate Journal of Hydrology 527:119-132
Naeem UA, Hashmi HN, Shamim MA, Ejaz N (2016) Flow variation in astore river under assumed glaciated extents due to climate change Pakistan Journal of Engineering Applied Sciences
Palaniswami S, Muthiah K (2018) Change Point Detection and Trend Analysis of Rainfall and Temperature Series over the Vellar River Basin Polish Journal of Environmental Studies 27
Pang H, Hou S, Kaspari S, Mayewski P (2014) Influence of regional precipitation patterns on stable isotopes in ice cores from the central Himalayas The Cryosphere 8:289-301
Paul F, Arnaud Y, Ranzi R, Rott H (2014) European Alps. In: Kargel JS, Leonard GJ, Bishop MP, Kääb A, Raup BH (eds) Global Land Ice Measurements from Space. Springer Berlin Heidelberg, Berlin, Heidelberg, pp 439-463. doi:10.1007/978-3-540-79818-7_20
Pellicciotti F, Buergi C, Immerzeel WW, Konz M, Shrestha AB (2012) Challenges and uncertainties in hydrological modeling of remote Hindu Kush–Karakoram–Himalayan (HKH) basins: suggestions for calibration strategies Mountain Research Development 32:39-50
Petäjä T, O'Connor EJ, Moisseev D, Sinclair VA, Manninen AJ, Väänänen R, von Lerber A, Thornton JA, Nicoll K, Petersen W (2016) BAECC: A field campaign to elucidate the impact of biogenic aerosols on clouds and climate Bulletin of the American Meteorological Society 97:1909-1928
Plüss C, Mazzoni R (1994) The Role of Turbulent Heat Fluxes in the Energy Balance of High Alpine Snow Cover: Paper presented at EGS XVIII General Assembly (Wiesbaden, Germany–May 1993) Hydrology Research 25:25-38

Poloczanska E, Mintenbeck K, Portner HO, Roberts D, Levin LA The IPCC special report on the ocean and cryosphere in a changing climate. In: 2018 Ocean Sciences Meeting, 2018. AGU,
Prabnakorn S, Suryadi F, Chongwilaikasem J, De Fraiture C (2019) Development of an integrated flood hazard assessment model for a complex river system: a case study of the Mun River Basin, Thailand Modeling Earth Systems Environment 5:1265-1281
Ragettli S, Pellicciotti F, Bordoy R, Immerzeel W (2013) Sources of uncertainty in modeling the glaciohydrological response of a Karakoram watershed to climate change Water Resources Research 49:6048-6066
Rahman K, Shang S, Shahid M, Li J (2018) Developing an ensemble precipitation algorithm from satellite products and its topographical and seasonal evaluations over Pakistan Remote Sensing 10:1835
Räisänen J, Räty O (2013) Projections of daily mean temperature variability in the future: cross-validation tests with ENSEMBLES regional climate simulations Climate dynamics 41:1553-1568
Ranzi R, Grossi G, Gitti A, Taschner S (2010) Energy and mass balance of the mandrone glacier (Adamello, Central Alps) Geografia Fisica e Dinamica Quaternaria 33:45-60
Ranzi R, Grossi G, Iacovelli L, Taschner S Use of multispectral ASTER images for mapping debris-covered glaciers within the GLIMS project. In: IGARSS 2004. 2004 IEEE International Geoscience and Remote Sensing Symposium, 2004. IEEE, pp 1144-1147
Ranzi R, Michailidi EM, Tomirotti M, Crespi A, Brunetti M, Maugeri M (2021) A multi-century meteo-hydrological analysis for the Adda river basin (Central Alps). Part II: Daily runoff (1845–2016) at different scales International Journal of Climatology 41:181-199
Ranzi R, Rosso R (1991) Physically based approach to modelling distributed snowmelt in a small alpine catchment IAHS PUBL, IAHS, WALLINGFORD,(ENGL):141-150
Ranzi R, Rosso R (1995) Distributed estimation of incoming direct solar radiation over a drainage basin Journal of Hydrology 166:461-478
Rasul G, Chaudhry Q, Mahmood A, Hyder K, Dahe Q (2011) Glaciers and glacial lakes under changing climate in Pakistan Pakistan Journal of Meteorology 8
Räty O, Räisänen J, Ylhäisi JS (2014) Evaluation of delta change and bias correction methods for future daily precipitation: intermodel cross-validation using ENSEMBLES simulations Climate dynamics 42:2287-2303
Reggiani P, Rientjes T (2015) A reflection on the long-term water balance of the Upper Indus Basin Hydrology research 46:446-462
Ridley J, Wiltshire A, Mathison C (2013) More frequent occurrence of westerly disturbances in Karakoram up to 2100 Science of the Total Environment 468:S31-S35
Rieu-Clarke AJIJoWG (2015) Transboundary hydropower projects seen through the lens of three international legal regimes: Foreign investment, environmental protection and human rights 3:27-48
Ringler C, Anwar A (2013) Water for food security: challenges for Pakistan Water International 38:505-514
Rittger K, Bair EH, Kahl A, Dozier J (2016) Spatial estimates of snow water equivalent from reconstruction Advances in water resources 94:345-363
Rizwan M, Li X, Jamal K, Chen Y, Chauhdary JN, Zheng D, Anjum L, Ran Y, Pan X (2019) Precipitation Variations under a Changing Climate from 1961–2015 in the Source Region of the Indus River Water 11:1366
Romshoo SA, Marazi A (2022) Impact of climate change on snow precipitation and streamflow in the Upper Indus Basin ending twenty-first century Climatic Change 170:1-20
Rounce DR, Hock R, Shean DE (2020) Glacier mass change in High Mountain Asia through 2100 using the open-source python glacier evolution model (PyGEM) Frontiers in Earth Science 7:331

Saha S, Moorthi S, Pan H-L, Wu X, Wang J, Nadiga S, Tripp P, Kistler R, Woollen J, Behringer D (2010) The NCEP climate forecast system reanalysis Bulletin of the American Meteorological Society 91:1015-1058
Saifullah M, Liu S, Adnan M, Ashraf M, Zaman M, Hashim S, Muhammad S (2020) Risks of Glaciers Lakes Outburst Flood along China Pakistan Economic Corridor. In: Glaciers and Polar Environment. IntechOpen,
Saleem J, Butt A, Shafiq A, Ahmad SS (2020) Cryosphere dynamic study of Hunza Basin using remote sensing, GIS and runoff modeling Journal of King Saud University-Science 32:2462-2467
Samuelsson P, Jones CG, Will´ En U, Ullerstig A, Gollvik S, Hansson U, Jansson E, Kjellstro¨ M C, Nikulin G, Wyser K (2011) The Rossby Centre Regional Climate model RCA3: model description and performance Tellus A: Dynamic Meteorology Oceanography 63:4-23
Satterlund DR (1979) An improved equation for estimating long-wave radiation from the atmosphere Water Resources Research 15:1649-1650
Sen P (1968) E stim ates of the R egression C oefficient based on K en d all's T au. J. A m er Statist. Assoc 63:1379-1389
Shafeeque M, Luo Y, Wang X, Sun L (2019) Revealing Vertical Distribution of Precipitation in the Glacierized Upper Indus Basin Based on Multiple Datasets Journal of Hydrometeorology 20:2291-2314
Shah MI, Khan A, Akbar TA, Hassan QK, Khan AJ, Dewan A (2020) Predicting hydrologic responses to climate changes in highly glacierized and mountainous region Upper Indus Basin Royal Society open science 7:191957
Shakoor A, Ejaz N (2019) Flow Analysis at the Snow Covered High Altitude Catchment via Distributed Energy Balance Modeling Scientific reports 9:1-14
Sharif M, Archer D, Fowler H, Forsythe N (2013) Trends in timing and magnitude of flow in the Upper Indus Basin Hydrology and Earth System Sciences 17:1503-1516
Shrestha M, Koike T, Hirabayashi Y, Xue Y, Wang L, Rasul G, Ahmad B (2015) Integrated simulation of snow and glacier melt in water and energy balance-based, distributed hydrological modeling framework at Hunza River Basin of Pakistan Karakoram region Journal of Geophysical Research: Atmospheres 120:4889-4919
Shrestha S, Nepal SJW (2019) Water balance assessment under different glacier coverage scenarios in the Hunza Basin Water 11:1124
Siddique M, Hashmi D (2012) Recent trends in high altitude temperatures and river flows in the Upper Indus Basin Centenary Celebration 714:149-166
Smiraglia C, Mayer C, Mihalcea C, Diolaiuti G, Belò M, Vassena G (2007) 26 Ongoing variations of Himalayan and Karakoram glaciers as witnesses of global changes: recent studies on selected glaciers Developments in Earth Surface Processes 10:235-247
Soncini A, Bocchiola D, Confortola G, Bianchi A, Rosso R, Mayer C, Lambrecht A, Palazzi E, Smiraglia C, Diolaiuti G (2015) Future hydrological regimes in the upper indus basin: A case study from a high-altitude glacierized catchment Journal of Hydrometeorology 16:306-326
Soncini A, Bocchiola D, Confortola G, Minora U, Vuillermoz E, Salerno F, Viviano G, Shrestha D, Senese A, Smiraglia C (2016) Future hydrological regimes and glacier cover in the Everest region: The case study of the upper Dudh Koshi basin Science of the Total Environment 565:1084-1101
Stevens B, Bony S (2013) What are climate models missing? Science 340:1053-1054
Sun Q, Miao C, Duan Q, Ashouri H, Sorooshian S, Hsu KL (2018) A review of global precipitation data sets: Data sources, estimation, and intercomparisons Reviews of Geophysics 56:79-107
Syed F, Giorgi F, Pal J, King M (2006) Effect of remote forcings on the winter precipitation of central southwest Asia part 1: observations Theoretical and Applied Climatology 86:147-160
Tabari H, Talaee PH (2011) Recent trends of mean maximum and minimum air temperatures in the western half of Iran Meteorology and atmospheric physics 111:121-131

Tahir AA, Chevallier P, Arnaud Y, Neppel L, Ahmad B (2011) Modeling snowmelt-runoff under climate scenarios in the Hunza River basin, Karakoram Range, Northern Pakistan Journal of hydrology 409:104-117
Tarek M, Brissette FP, Arsenault R (2019) Evaluation of the ERA5 reanalysis as a potential reference dataset for hydrological modeling over North-America Hydrology and Earth System Sciences Discussions:1-35
Taschner S, Ranzi R Comparing the opportunities of Landsat-TM and Aster data for monitoring a debris covered glacier in the Italian Alps within the GLIMS project. In: IEEE International Geoscience and Remote Sensing Symposium, 2002. IEEE, pp 1044-1046
Teichmann C, Eggert B, Elizalde A, Haensler A, Jacob D, Kumar P, Moseley C, Pfeifer S, Rechid D, Remedio AR (2013) How does a regional climate model modify the projected climate change signal of the driving GCM: a study over different CORDEX regions using REMO Atmosphere 4:214-236
Teutschbein C, Seibert J (2012) Bias correction of regional climate model simulations for hydrological climate-change impact studies: Review and evaluation of different methods Journal of hydrology 456:12-29
Theil H A rank-invariant method of linear and polynominal regression analysis (parts 1-3). In: Ned. Akad. Wetensch. Proc. Ser. A, 1950. pp 1397-1412
Turc L (1955) Le bilan d'eau des sols: relations entre les précipitations, l'évaporation et l'écoulement Journées de l'hydraulique 3:36-44
Ullah S, You Q, Ullah W, Ali A (2018) Observed changes in precipitation in China-Pakistan economic corridor during 1980–2016 Atmospheric Research 210:1-14
Wigmosta MS, Vail LW, Lettenmaier DP (1994) A distributed hydrology-vegetation model for complex terrain Water resources research 30:1665-1679
Winiger M, Gumpert M, Yamout H (2005) Karakorum–Hindukush–western Himalaya: assessing high-altitude water resources Hydrological Processes: An International Journal 19:2329-2338
Wortmann M, Bolch T, Menz C, Tong J, Krysanova V (2018) Comparison and correction of high-mountain precipitation data based on glacio-hydrological modeling in the Tarim River headwaters (High Asia) Journal of Hydrometeorology 19:777-801
Yaseen M, Ahmad I, Guo J, Azam MI, Latif Y (2020) Spatiotemporal Variability in the Hydrometeorological Time-Series over Upper Indus River Basin of Pakistan Advances in Meteorology 2020
Yatagai A, Kamiguchi K, Arakawa O, Hamada A, Yasutomi N, Kitoh A (2012) APHRODITE: Constructing a long-term daily gridded precipitation dataset for Asia based on a dense network of rain gauges Bulletin of the American Meteorological Society 93:1401-1415
You Q-L, Ren G-Y, Zhang Y-Q, Ren Y-Y, Sun X-B, Zhan Y-J, Shrestha AB, Krishnan R (2017) An overview of studies of observed climate change in the Hindu Kush Himalayan (HKH) region Advances in Climate Change Research 8:141-147
Zaman M, Ahmad I, Usman M, Saifullah M, Anjum MN, Khan MI, Uzair Qamar M (2020) Event-Based Time Distribution Patterns, Return Levels, and Their Trends of Extreme Precipitation across Indus Basin Water 12:3373
Zaman M, Fang G, Mehmood K, Saifullah M (2015) Trend change study of climate variables in Xin'anjiang-Fuchunjiang Watershed, China Advances in Meteorology 2015
Zaman M, Fang G, Saifullah M, Javed Q (2016) Seasonal and Annual Precipitation Trend Prediction in Xin'Anjiang China Fresen Environ Bull 25:89-102
Zhang A, Zheng C, Wang S, Yao Y (2015) Analysis of streamflow variations in the Heihe River Basin, northwest China: Trends, abrupt changes, driving factors and ecological influences Journal of Hydrology: Regional Studies 3:106-124
Zheng H, Chiew FH, Charles S, Podger G (2018) Future climate and runoff projections across South Asia from CMIP5 global climate models and hydrological modelling Journal of Hydrology: Regional Studies 18:92-109

Conclusion and perspectives of the PhD thesis

1 Conclusion

In the data scarce region of High Mountain Asia, it is imperative to understand the sensitivity of the hydrological regime, snow melt water runoff, and glaciers' evolution to climate variability. A change in hydro-glaciological regime in upstream affects the availability of water for hundreds of millions of people living downstream and poses new management challenges. The studies of the interaction between glaciers, climate and hydrology are not so many because of the few observed hydro- meteorological time series long enough for climatological studies available in this region.

The study is focused on the Naltar catchment covering an area of 242.62 km^2 in Hunza basin, High Mountain Asia with glacierized area 42 km^2. The objectives are: 1) Characterization of Interannual and Seasonal Variability of Hydro-Climatic Trends in the Upper Indus Basin; (2) Energy balance modeling of snow and ice melt in the Naltar Catchment (UIB, Pakistan (3) Impact of climate change on Naltar Catchment Hydrology, Upper Indus Basin.

The specific conclusions of each chapter are reported as follows:

1. The performance of four gridded datasets shows that CHIRPS produces the lowest BIAS, MAPE, and RMSE at the annual and seasonal scales, followed by ERA5. The mean annual corrected precipitation was calculated as 536 mm a^{-1} in the UIB gauged at Besham Qila. Based on the mean seasonal precipitation over the entire study basin, precipitation in the winter is 96 mm, in the spring 150 mm, in the summer 220 mm, and in the autumn 70 mm (SON). Both the annual and seasonal precipitation climatology showed that the lower part of the basin experienced a higher amount of precipitation. In glacierized basins, rainfall runoff coefficients are higher, suggesting that glacier retreat and snowmelt are significant contributors in net stream flow with under catch precipitation. It is also recommended that gridded precipitation be corrected before it is used in hydrological model studies, particularly those that include glacierized catchments. A novel running trend analysis and spectral analysis based on a moving window approach revealed significant seasonal variation in precipitation rather than annual variability. Summer is drying while winter is wetting. A significant increase in temperature was observed for the winter, spring, and annual scale, while a significant cooling was observed for the summer season. In terms of streamflow, variabilities are more pronounced seasonally than annually. The results indicate that runoff increased significantly or slightly in winter and spring in all sub-basins, while in summer it decreased. A possible explanation for the increased flow during the winter and spring may be due to warming over elevated regions, which causes temperatures to rise earlier in the spring season, leading to earlier melt of the snow. The impact of these issues on glacier and snow melt on total flow from each subbasin requires further investigation.

2. Energy budget based distributed modeling at high-altitude glacerized catchments is indispensable to examine the glacio-hydrological processes and quantify flow rate. In this study, the energy balance Physical Based Distributed Snow Land and Ice Model (PDSLIM) are employed for the first time in Pakistan at Naltar catchment located in Hunza river basin to simulate snow ice melt progression, summer glacier mass balance as well as seasonal runoff. The results exhibited satisfactory performance with coefficient of determination (R^2) = 0.96 and Nash-Sutcliffe Efficiency *(NSE) = 0.95* of model against satellite-based snow +ice cover area for all simulated years. In terms of streamflow dynamics, PDSLIM and LRM have been found to be capable of developing reliable relationships between the model and observed runoff based on *KGE, NSE, and RMSE (0.89, 0.90, 0.78)*. Both low and high simulated flow limbs were fairly correlated with observed runoff. Flow composition analysis reveals the simulated lake flow is comprised of glacier runoff, sub-surface runoff, and surface runoff. Sub-surface runoff accounted for a large proportion of Naltar catchment runoff (42.07%); whereas glacier runoff contributed 39.91% and surface runoff had the smallest contribution (18.02%). During the 8-year simulations, the average value of the net glacier summer mass balance is slightly negative (–810 ± 311 mm w.e. a-1) which shows that the Karakoram anomaly is varying especially at the catchment scale. Based on these findings, possible future projections of energy and mass balance studies should be conducted and their impact on climate change should be considered. Overall, PDSLIM perform well for snow-glacier retreat dynamics and put a strong foundation for the potential usage of highly accurate distributed energy balance in the glacierized catchments of HMA to understand snow-glacier melt runoff dynamics in highly complex terrain with glacier rich mountains.

3. In Natar catchment, hydro-glaciological projections were developed from an ensemble of 37 simulations in two future scenarios (2040-2059) and (2080-2099) under RCP 2.6, RCP 4.5 and RCP 8.5. It appears from the overall analysis that the Naltar catchment faces an uncertain future in terms of the availability of water. Based on the projected climate, there will be an increase in both warming (+0.87 to +6.02 ^{o}C) and precipitation up to +29% (121 mm) from April to September in a far future scenario (2080-2099) relative to the reference period 2010. Projections of glacier mass balance indicate that glaciers in the Naltar catchment will retreat (–27% to –43%) for 2.6, (–41% to –60%) for 4.5 and (–58% to –80%) for 8.5 under ensemble scenarios. According to the projected simulations of energy and mass balance, snow and ice melt progression by integration ensemble of RCMs is consistently increasing in both future scenarios (–47.7% to –83%), with an earlier shift in the timing of the maximum snowmelt. Further, projected changes of water availability by integration ensemble of RCMs in far future varies from (+3.41% to –23.69%) relevant to reference 2010. Turc-Budyko's approach suggests that Naltar's hydrological regime will possibly shift from (snow and glacier melt dominance) to (rainfall dominance). The intra-seasonal shift in water availability across catchment-wide patterns is changing across both future scenarios, despite large uncertainties about climate and water availability. The effects of these changes are likely to result in a shift of peak hydrological regime from one to two months earlier by 2090s over Naltar catchment. This finding underlines the relationship between the runoff and glacier changes in highly glacierized catchments.

Overall, this study highlighted the importance of the evaluation of all available static and dynamic datasets (hydro- meteorological, gridded datasets, snow cover area), the associated uncertainties before performing an energy mass balance and hydrological modelling. This finding underlines the relationship between the runoff and glacier changes in highly glacierized catchments. It provides a better understanding of the physical processes taking place within a catchment. Additionally, this study can provide further insight for temporal and spatial changes in the projected snow and ice melt seasonal cycle under climate change scenarios. Moreover, the suitability of a PDSLIM in simulating the hydrological regime is an important result, since four operational and one under construction hydropower plants a're strongly dependent on glacier runoff generated by Naltar glaciers. Finally, the limitations and potential for further improvement have been identified, providing new research challenges.

2 Outlook for further research

1) This study used precipitation data for a period of 23 years (1995-2017) to develop a high resolution precipitation climatology and examined seasonal and annual trends. World Metrological Organization (WMO) recommends a 30-year reference period for monitoring global and regional climate anomalies. Moreover, the relationship between station elevation and measured precipitation is represented in (Chapter#1: Fig.1.2), which shows that no significant altitudinal trend can be observed, although doubts arise about the reliability of precipitation data when snowfall occurs. The development of an altitude trend at sub-basin levels is recommended. It would be beneficial to consider these points in future work.
2) The study also has some limitations associated with input data. Firstly, observed data obtained from WAPDA have some inconsistencies and missing gaps at a specific date which were observed during consistency check. Although, lot of efforts have already been made to remove these missing gaps, uncertainty in the data cannot be completely ignored. There is a need to strengthen the existing network of hydro-meteorological monitoring and to increase the length of record.
3) Currently, the majority of glacio-hydrological studies, including this study, rely on remote sensing data for calibration and validation of snow cover extent and mass balance. Remote sensing datasets have their own limitations as discussed in chapter#2. A short-term specific monitoring program in the HMA Alps could provide a useful substitute for long-term observations by quantifying water budgets and actual cryosphere status.
4) The potential of PDSLIM to simulate glacio-hydrological processes in HMA Alps is highly recommended especially in the context of climate change. Furthermore, the study encourages the use of PDSLIM for future studies of energy and mass balance as well as exploring its potential application for glacier lakes outburst in Pakistan.

Supplementary Material Chapter # 1

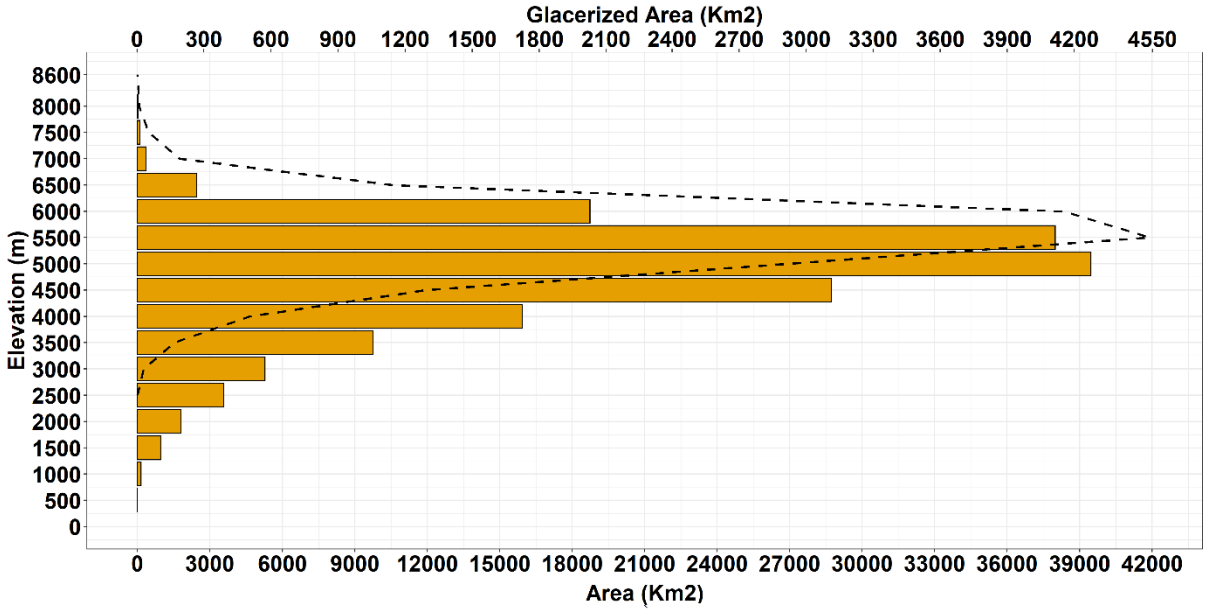

Figure.S1.1 The hypsometric curve of Upper Indus Basin (UIB), Pakistan

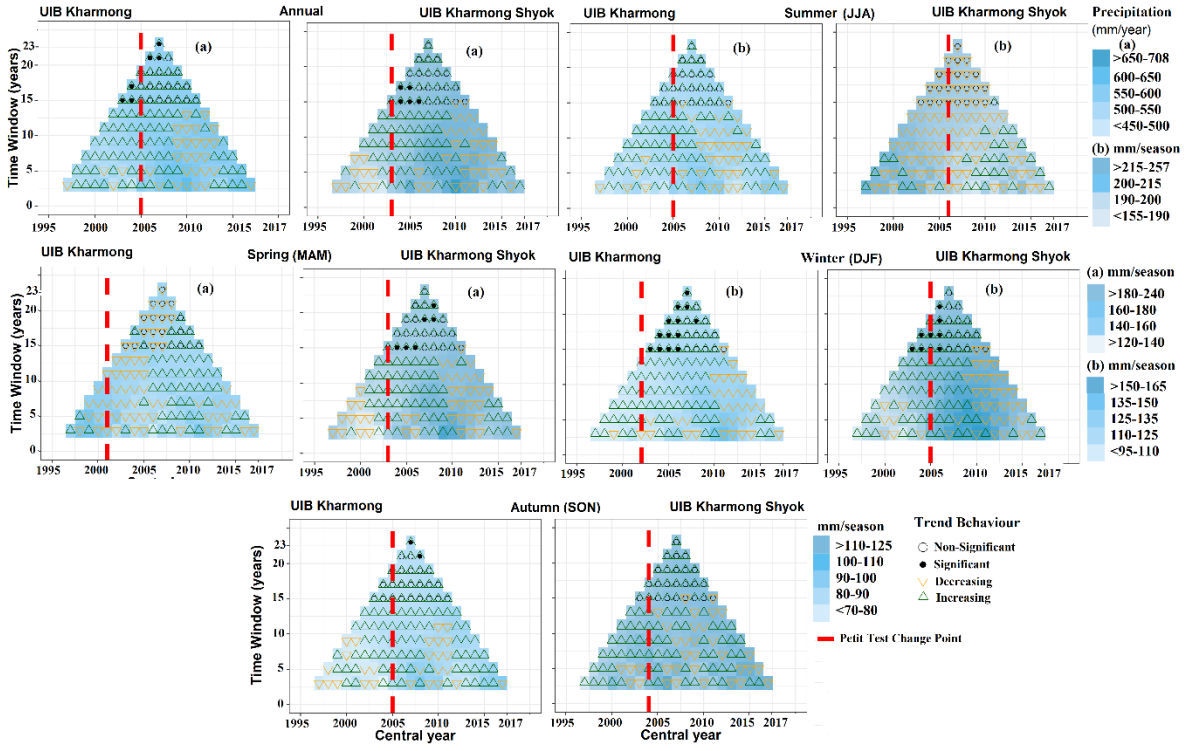

Figure.S1.2 Running trend of annual and seasonal precipitation series. Average Precipitation values are divided into various classes (white to dark blue). Trend values are showed by upward (green) and downward triangles (black) while trend significance is described by hollow (nonsignificant) and filled circles (significant) with Mann-Kendall p-values < 0.05). Red vertical line expressed change point (Petit Test) in whole time series. The x axis is the starting year (central year), while the y axis is the moving window (a minimum assessment duration of 5 year is selected).

Table.S1.1 Streamflow Pettit Test (<0.05 Significance Level) at Annual and Seasonal scale

Stream Flow Pettit Test (<0.05 Significance Level)					
Basins	DJF	MAM	JJA	SON	ANN
Indus_BQ	**0.01**	**0.05**	0.82	0.43	0.91
Indus_Kachura	**0.01**	0.1	**0.02**	0.03	**0.00**
Indus_Shyok	**0.002**	0.11	0.07	0.15	**0.04**
Indus_Kharmong	0.63	0.51	0.08	0.63	0.09
Indus_Bunji	**0.01**	**0.01**	0.20	**0.04**	**0.03**
Astore	**0.01**	**0.05**	0.32	**0.00**	**0.03**
Shigar	0.11	0.43	**0.06**	0.43	0.24
BQ-Kharmong	0.36	0.04	0.91	0.11	0.80
BQ-Kharmong-Shyok	0.41	0.06	0.84	0.06	0.54

Table S.1.2 Precipitation Pettit Test (<0.05 Significance Level) at Annual and Seasonal scale

Precipitation Pettit Test (<0.05 Significance Level)					
Basins	DJF	MAM	JJA	SON	ANN
Shingo	0.27	**0.01**	0.13	0.81	0.2
Shyok	**0.00**	0.50	**0.01**	**0.00**	**0.00**
Shigar	0.09	0.36	0.80	**0.01**	0.07
Astore	1.00	0.50	0.67	0.78	0.87
Hunza	**0.03**	0.67	0.40	**0.03**	**0.05**
Gilgit	**0.05**	0.55	0.22	**0.01**	0.17
BQ	0.55	0.50	0.80	0.67	0.1

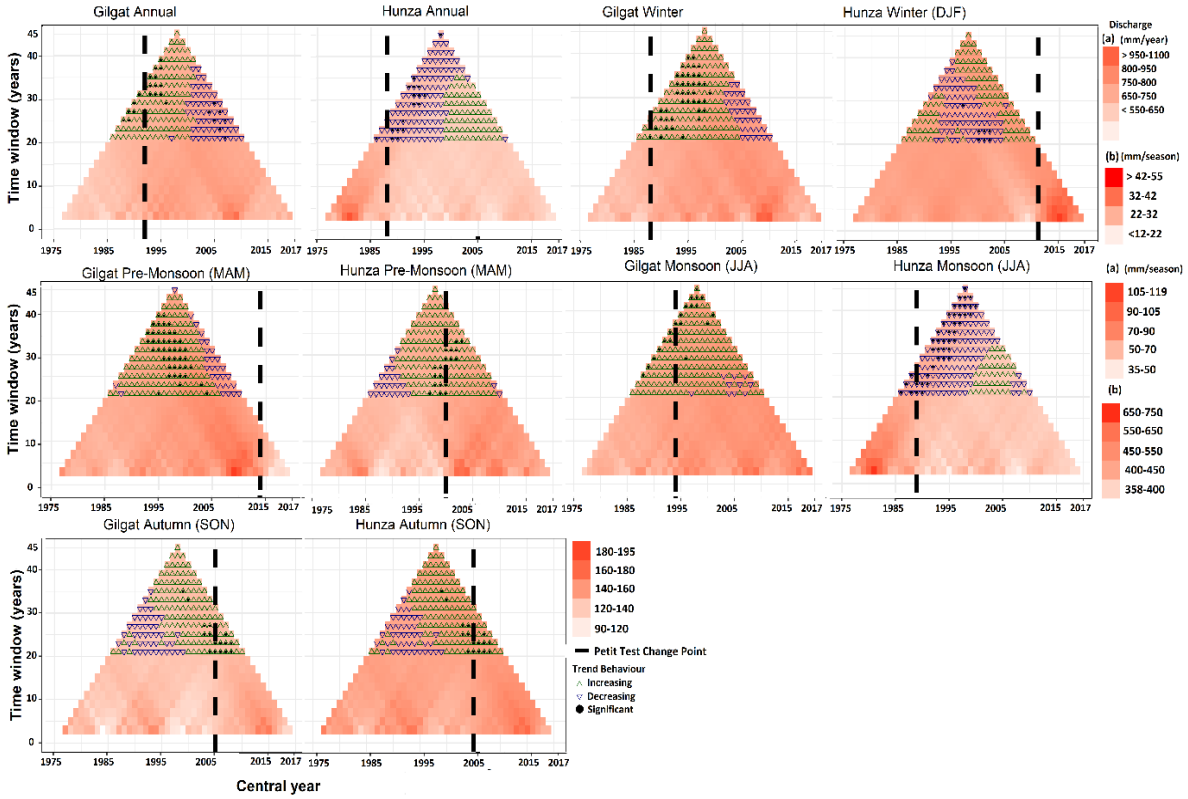

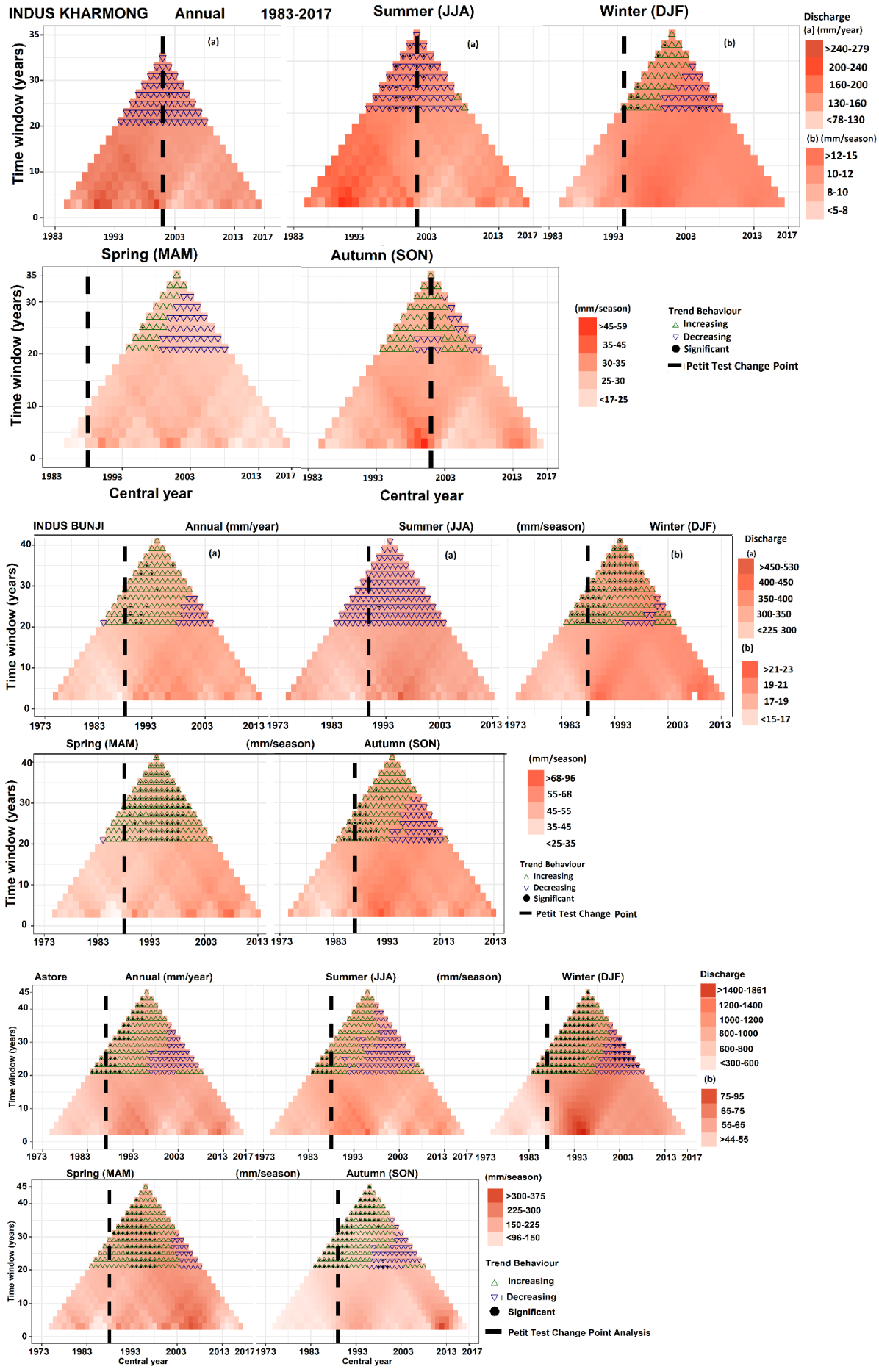
INDUS KHARMONG
Annual
1983-2017
Summer (JJA)
Winter (DJF)
Spring (MAM)
Autumn (SON)
Time window (years)
Central year
Discharge
(a) (mm/year)
>240-279
200-240
160-200
130-160
<78-130
(b) (mm/season)
>12-15
10-12
8-10
<5-8
(mm/season)
>45-59
35-45
30-35
25-30
<17-25
Trend Behaviour
Increasing
Decreasing
Significant
Petit Test Change Point
INDUS BUNJI
Annual (mm/year)
(mm/season)
>450-530
400-450
350-400
300-350
<225-300
>21-23
19-21
17-19
<15-17
>68-96
55-68
45-55
35-45
<25-35
Petit Test Change Point
Astore
>1400-1861
1200-1400
1000-1200
800-1000
600-800
<300-600
75-95
65-75
55-65
>44-55
>300-375
225-300
150-225
<96-150
Petit Test Change Point Analysis

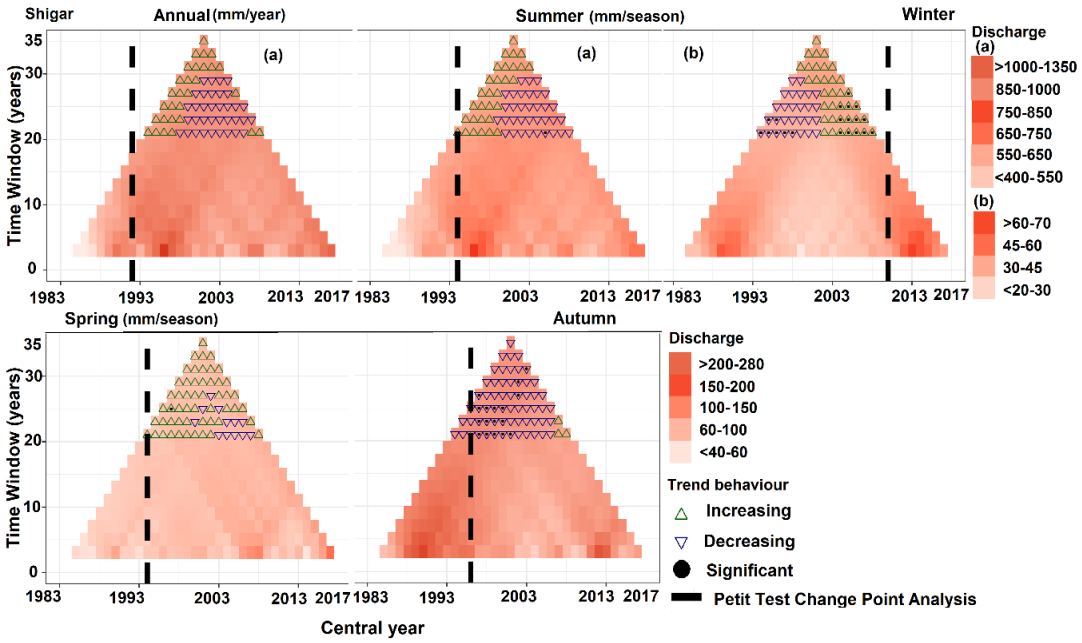

Figure.S1.3 Running trend of annual and seasonal runoff series. Average runoff values are divided into various classes (white to red). Trend values are showed by upward (green) and downward triangles (blue) while trend significance is described by filled circles (significant) with Mann-Kendall p-values < 0.05). Black vertical line expressed change point (Petit Test) in whole time series. The x axis is the starting year (central year), while the y axis is the moving window (a minimum assessment duration of 10 year is selected).

Rainfall Runoff Relationship in Upper Indus Basin

The rainfall runoff relationship and runoff coefficients are first order representation of under or overestimation of precipitation in the watershed. The annual and monthly runoff coefficients at sub-basins scale were developed as shown in Table.5 and Fig.9.

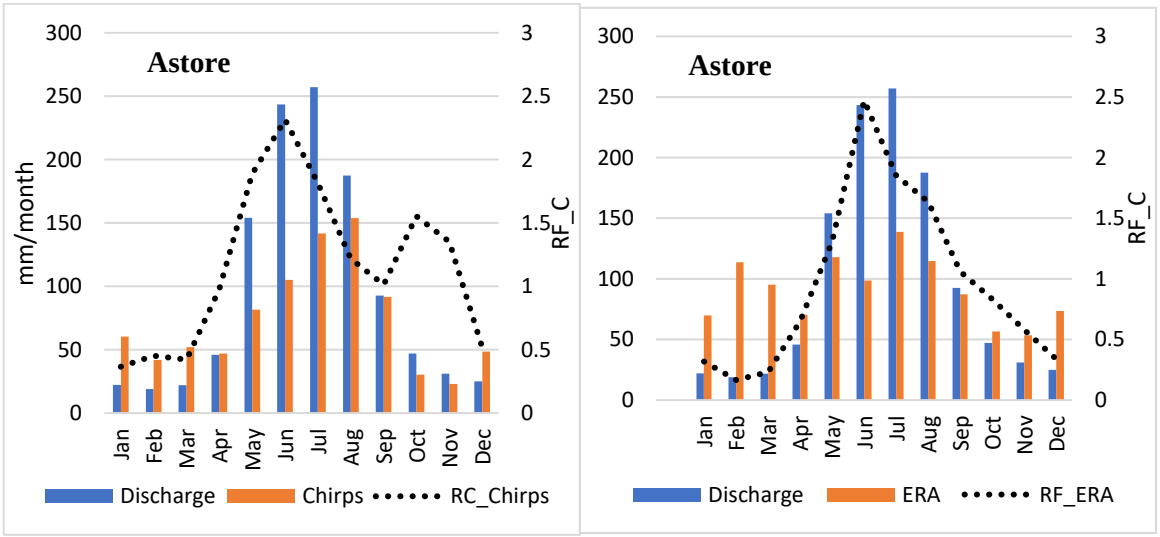

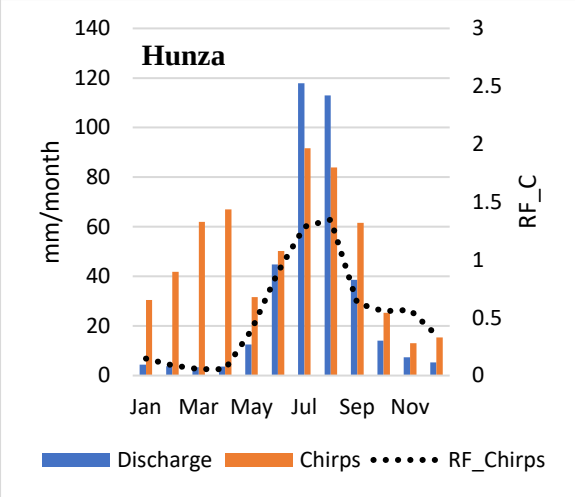
Hunza
mm/month
RF_C
Jan Mar May Jul Sep Nov
Discharge
Chirps
RF_Chirps

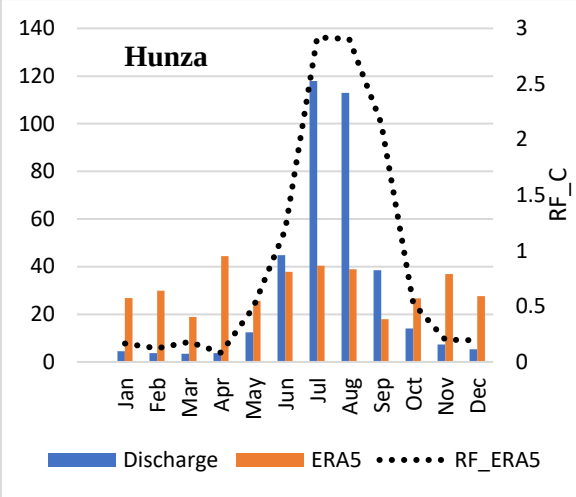
Hunza
RF_C
Jan Feb Mar Apr May Jun Jul Aug Sep Oct Nov Dec
Discharge
ERA5
RF_ERA5

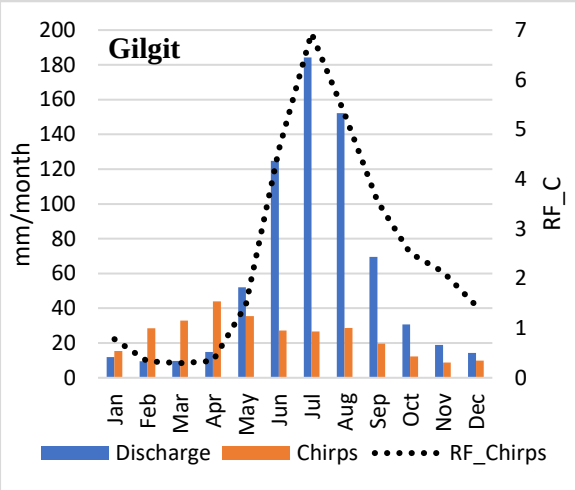
Gilgit
mm/month
RF_C
Jan Feb Mar Apr May Jun Jul Aug Sep Oct Nov Dec
Discharge
Chirps
RF_Chirps

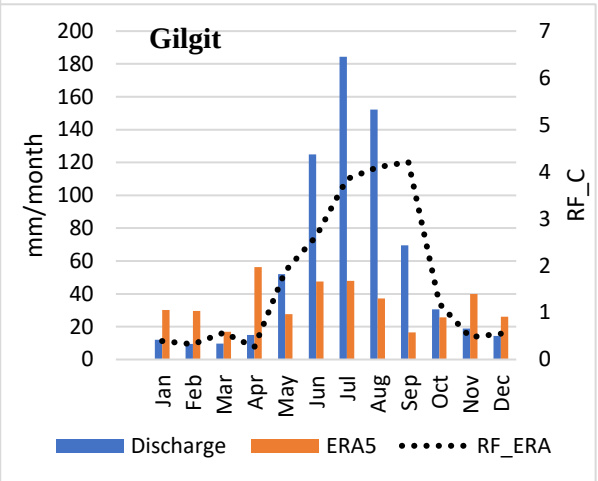
Gilgit
mm/month
RF_C
Jan Feb Mar Apr May Jun Jul Aug Sep Oct Nov Dec
Discharge
ERA5
RF_ERA

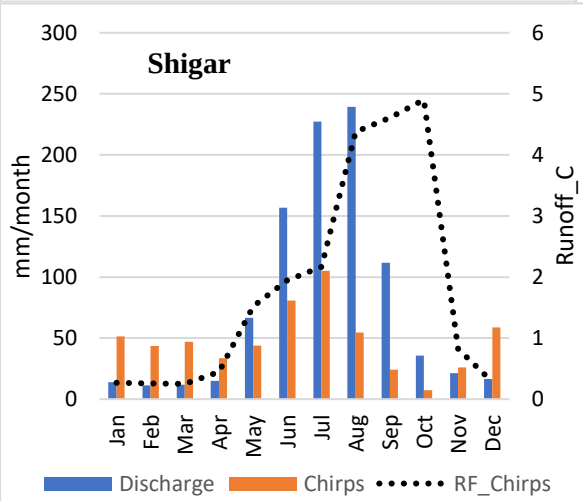
Shigar
mm/month
Runoff_C
Jan Feb Mar Apr May Jun Jul Aug Sep Oct Nov Dec
Discharge
Chirps
RF_Chirps

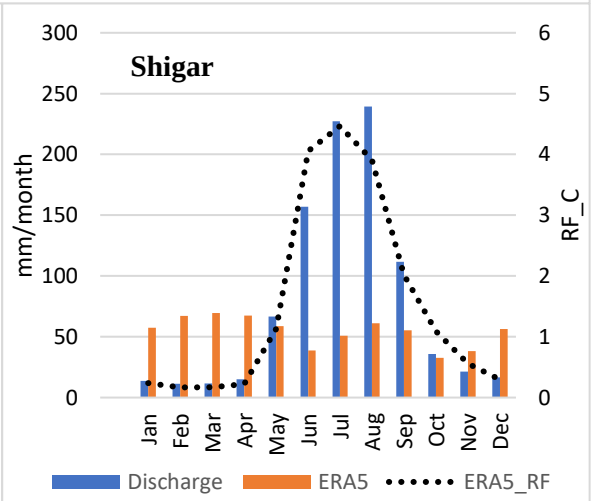
Shigar
mm/month
RF_C
Jan Feb Mar Apr May Jun Jul Aug Sep Oct Nov Dec
Discharge
ERA5
ERA5_RF

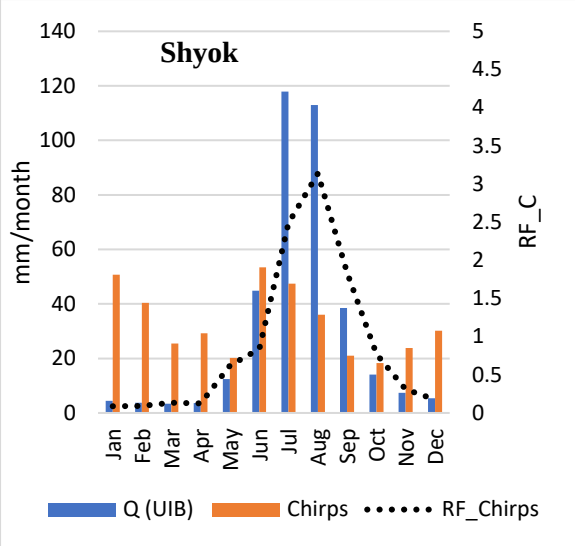
Shyok
mm/month
RF_C
Jan Feb Mar Apr May Jun Jul Aug Sep Oct Nov Dec
Q (UIB)
Chirps
RF_Chirps

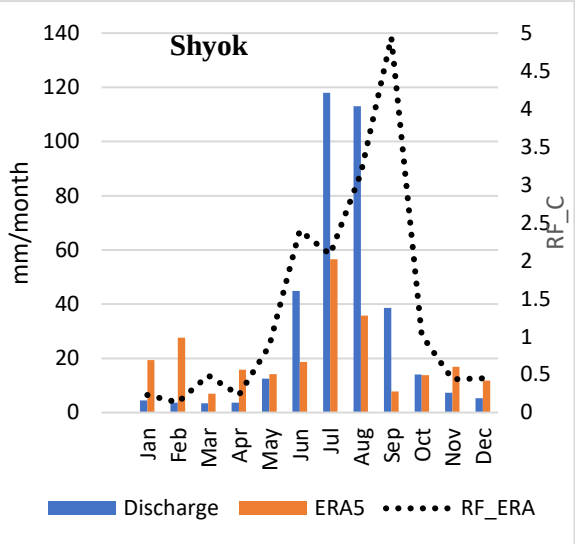
Shyok
mm/month
RF_C
Jan Feb Mar Apr May Jun Jul Aug Sep Oct Nov Dec
Discharge
ERA5
RF_ERA

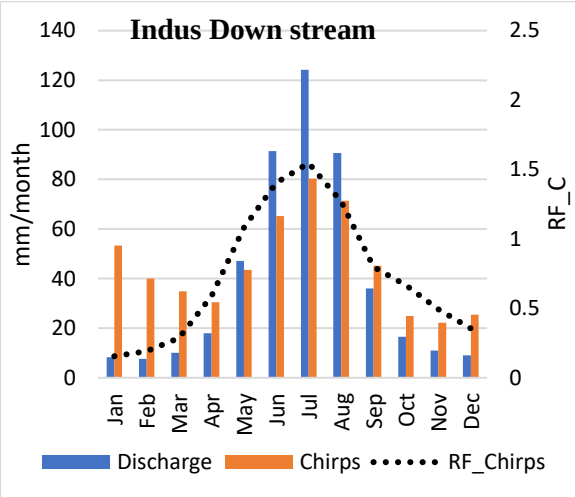
Indus Down stream
mm/month
RF_C
Jan Feb Mar Apr May Jun Jul Aug Sep Oct Nov Dec
Discharge
Chirps
RF_Chirps

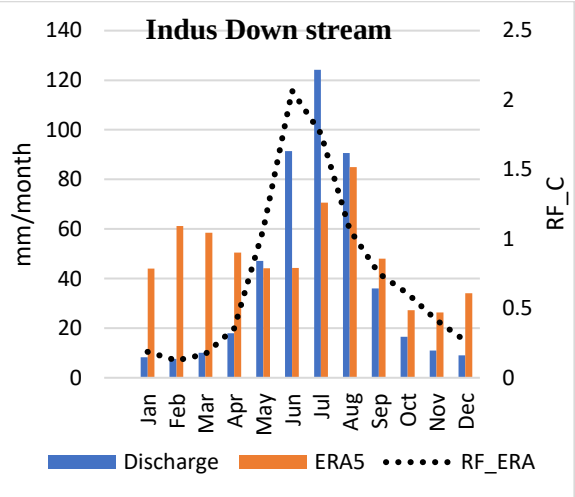
Indus Down stream
mm/month
RF_C
Jan Feb Mar Apr May Jun Jul Aug Sep Oct Nov Dec
Discharge
ERA5
RF_ERA

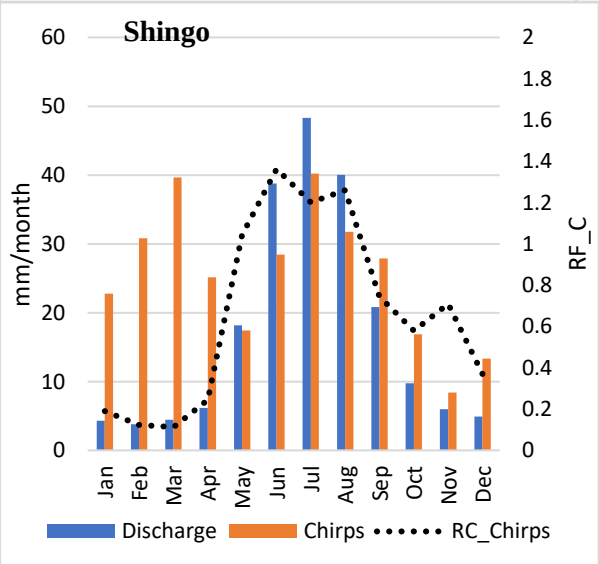
Shingo
mm/month
RF_C
Jan Feb Mar Apr May Jun Jul Aug Sep Oct Nov Dec
Discharge
Chirps
RC_Chirps

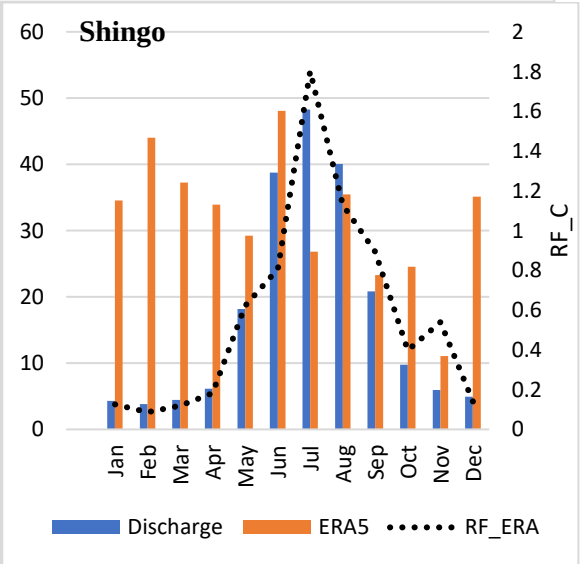
Shingo
mm/month
RF_C
Jan Feb Mar Apr May Jun Jul Aug Sep Oct Nov Dec
Discharge
ERA5
RF_ERA

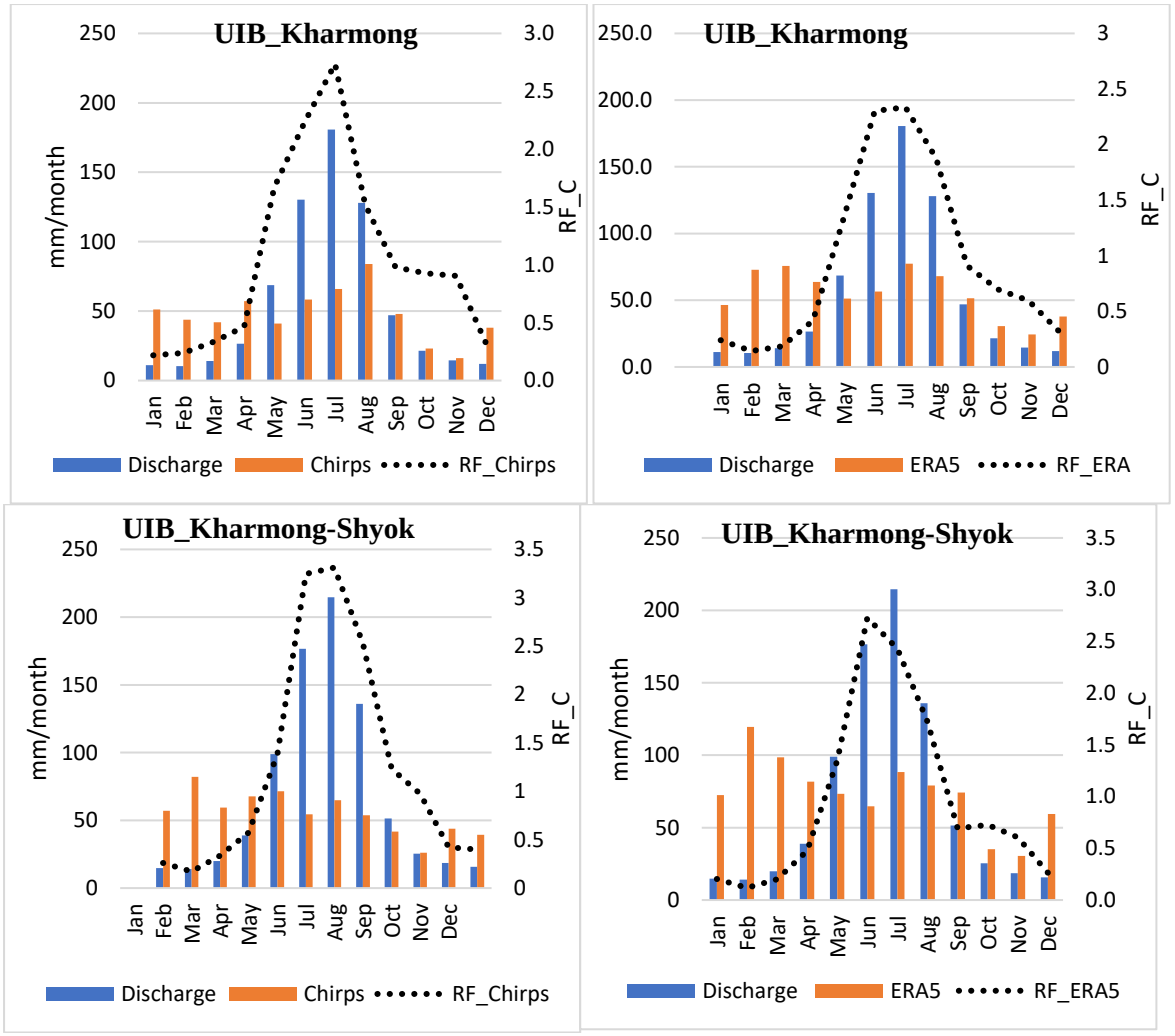

Figure S1.4. Rainfall runoff relationship among bias corrected ERA5, Chirps precipitation and runoff at sub-basins level.

Supplementary Material Chapter # 2

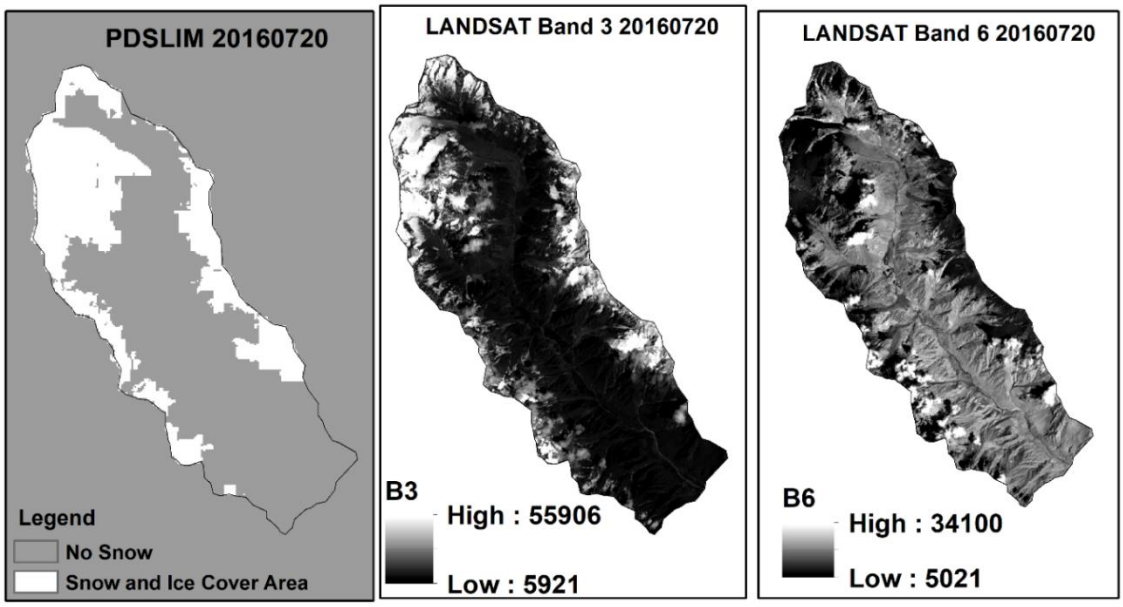

Fig S1. LANDSAT based snow cover area with B3(Green Band) and B6(NIR Band) for 20/07/2016

Table.S1 (a) Statistics Evaluation of Snow Cover Simulation of Naltar Catchment using MODSCAG based SWE for 2006-2016 (TLR for clear sky (-0.0085) and cloud cover (-0.0045))

Year	NSE	ME (Km^2)	%Bias	MAPE (%)	RMSE (Km^2)	R^2
2006	0.92	20.14	6.79	14.00	14.82	0.96
2008	0.95	12.65	6.57	9.82	11.78	0.97
2009	0.96	13.14	0.91	9.41	11.80	0.96
2010	0.91	14.22	4.35	9.97	16.13	0.92
2011	0.93	13.67	-1.53	13.97	14.21	0.94
2012	0.94	10.03	-2.02	12.54	11.02	0.96
2014	0.95	-3.16	-1.72	12.06	12.60	0.96
2016	0.95	14.15	-1.94	9.95	12.50	0.96
Average	0.94	11.85	1.43	11.46	13.11	0.95

Table.S1 (b) Statistics Evaluation of Snow Cover Simulation of Naltar Catchment using SPIRES based SWE for 2006-2016 (TLR for clear sky (-0.0085) and cloud cover (-0.0045))

Year	NSE	ME (Km^2)	%Bias	MAPE (%)	RMSE (Km^2)	R^2
2006	0.90	19.59	-4.94	14.90	16.21	0.92
2008	0.90	-0.50	-7.84	17.57	17.18	0.94
2009	0.95	18.68	0.23	11.43	13.58	0.96
2010	0.85	15.41	1.00	15.13	20.63	0.89
2011	0.92	19.00	-6.38	15.77	15.58	0.95
2012	0.92	12.16	-7.97	16.48	16.22	0.96
2014	0.94	3.46	-5.48	14.78	14.65	0.96
2016	0.90	19.43	-11.17	18.55	18.70	0.96
Average	0.91	13.40	-5.32	15.58	16.59	0.94

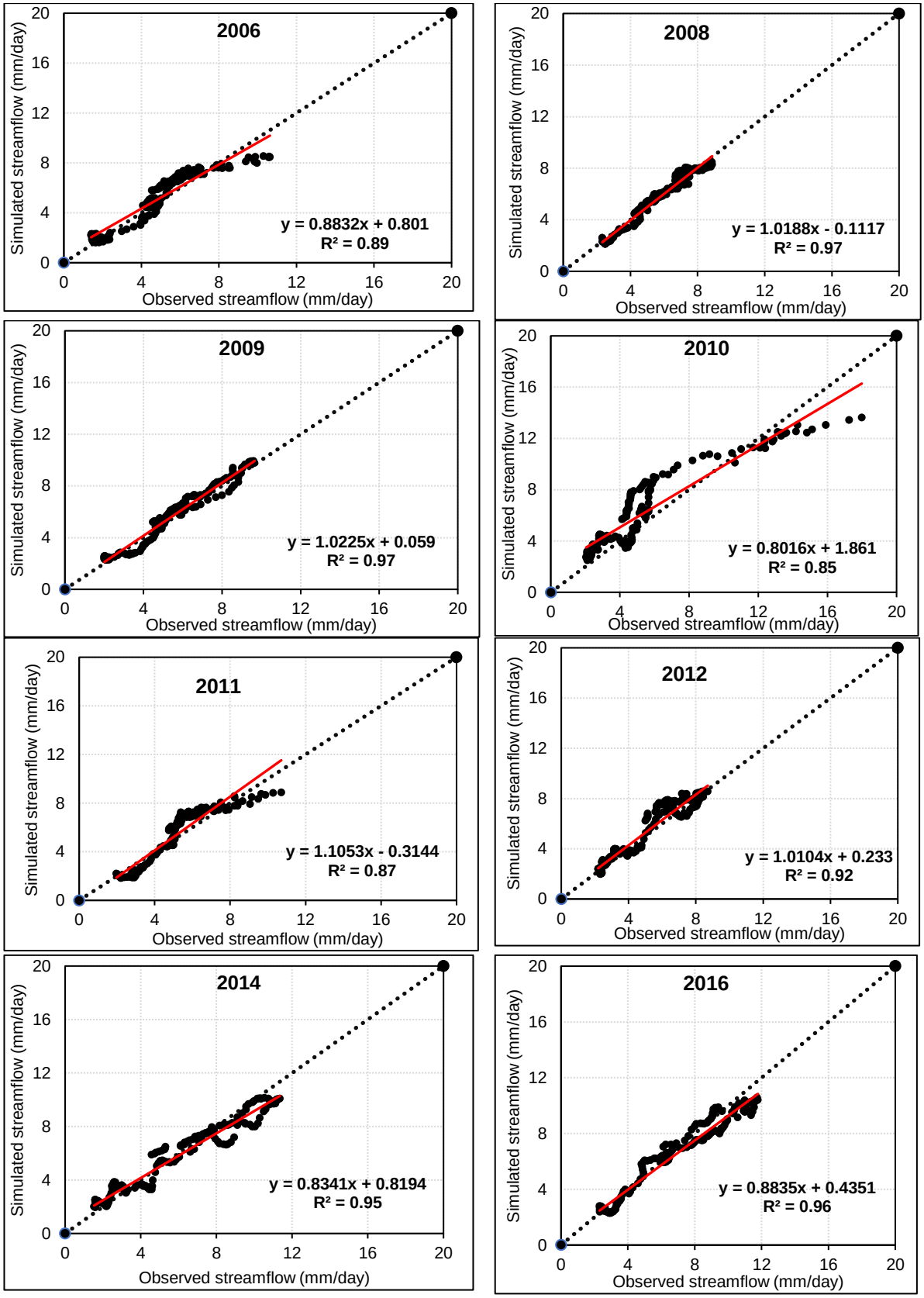

Figure S.2.2 Scattered plot between observed and simulated streamflow

Table S2: Calibrated Parameters for PDSLIM and LRM model in Naltar Catchment

Parameter	Description	Initial Range	Calibrated
$Surface_{RF}$	Surface runoff fraction	0.25-0.31	0.28
$T_{threshold}$	Threshold temperature (ºC)	0- 3.0	0
T_{LR}	Temperature lapse rate (°C m^{-1})	-0.0085-0.0045	-0.0065
k_{ice}	Time constant for ice layer	815-2160	1480
$k_{surface}$	Time constant for surface layer	168-240	217
$k_{sub\text{-}surface}$	Time constant for sub-surface layer	2400-4800	3840

Supplementary Material for Chapter # 3

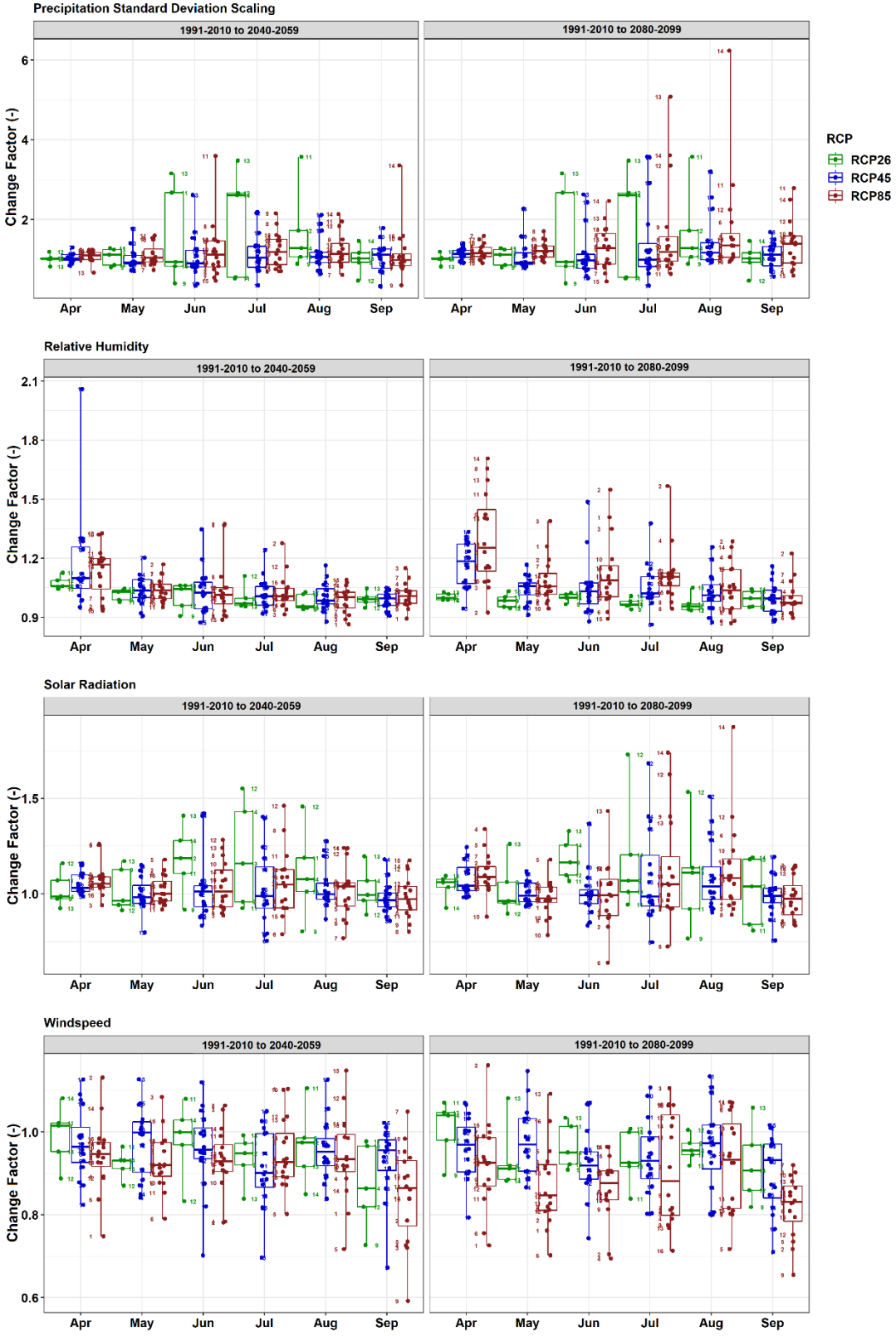

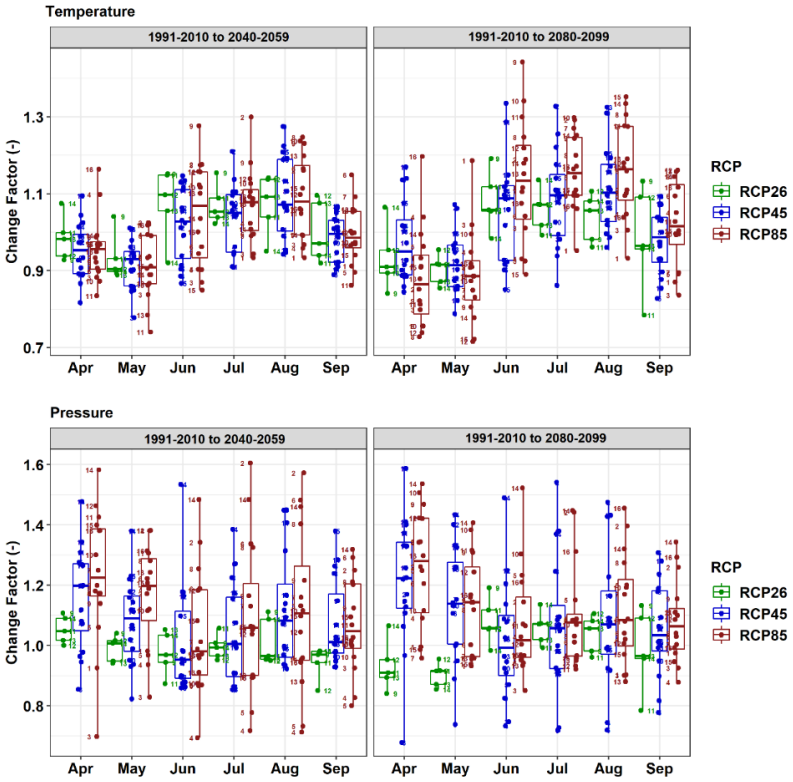

Figure.S3.1 Same as Fig.2, but for the change factors of the 20-year standard deviation for the six variables.

Table.S3.1 Details of meteorological data used in the study and their sources.

Basin	Stations	Period from	Period to	Agency	Latitude (^{0})	Longitude (^{0})	Elevation (m asl)
Gligat	Gilgit	2006	2016	WAPDA	35.92	74.33	1460
	Yasin	2006	2016	WAPDA	36.4	73.5	3280
Hunza	Ziarat	2006	2016	WAPDA	36.77	74.46	3629
	Naltar	2006	2016	WAPDA	36.17	74.18	2898

Table. S3.2 Sources, description and type of data used in this study.

Data Type	Data Source	Scale	Description
Digital Elevation Model	NASA-SRTM (90m)	grid cell (90 x 90 m)	NASA Shuttle Radar Topographic Mission (SRTM)
Landuse / Land Cover	GlobCover land cover	300 m	European Space Agency (ESA) GlobCover land cover product
LAI	MODIS	500 m	MODIS 8-day composite LAI product MYD15A2H.006
ALBEDO	MODIS	500 m	MOD10A.006 Daily Snow Albedo
Meteorological Data	WAPDA (Bair et al. 2020)	Hourly	Temperature, Wind Speed Relative Humidity, Solar Radiation, Rainfall Pressure
Discharge Data	WAPDA	Daily	Mean Daily Discharge at Naltar Bala Station (m^3/sec)
Snow Water equivalent (SWE)	(Bair et al. 2020)	Daily	Reconstructed MODIS SWE product

Table. S3.3 Projected Snow Depth Raito with respect to the reference snow depth from (control run period:1991-2010 to scenario period (2050;2090) under RCP 2.6, RCP 4.5 and RCP 8.5

		1991-2010 to 2040-2059	**1991-2010 to 2080-2099**
	Reference (SPCK)	1	1
RCP26	RCM9	1.21	0.83
RCP45	RCM1	0.91	0.94
	RCM2	0.91	0.94
	RCM3	0.91	0.94
	RCM4	0.91	0.94
	RCM5	0.91	0.94
	RCM6	0.75	0.89
	RCM7	1.22	1.21
	RCM8	1.1	1.02
	RCM9	1.06	0.98
	RCM10	0.47	1.08
	RCM16	0.91	0.94
	Ensemble	0.91	0.94
RCP85	RCM1	0.81	0.63
	RCM2	0.81	0.63
	RCM3	0.81	0.63
	RCM4	0.81	0.63
	RCM5	0.81	0.63
	RCM6	0.58	0.48
	RCM7	1.11	0.96
	RCM8	0.68	0.71
	RCM9	1.01	0.79
	RCM10	0.64	0.2
	RCM16	0.81	0.63
	Ensemble	0.81	0.63

Table S3.4. Projected change in summer glacier mass balance for both scenario period relative to control period under RCP 2.6, RCP 4.5 and RCP 8.5

		1991-2010 to 2040-2059		**1991-2010 to 2080-2099**	
		(mm w.e. a^{-1})	Change (%)	(mm w.e. a^{-1})	Change (%)
RCP	**Reference**	-737		-737	
RCP2.6	*RCM9*	*-1150*	*56.0*	*-1287*	*74.6*
RCP4.5	RCM1	-1342	82.1	-1257	70.6
	RCM2	-2373	222.0	-2377	222.5
	RCM3	-185	-74.9	-493	-33.1
	RCM4	-223	-69.7	-797	8.1
	RCM5	-30.65	-95.8	-235	-68.1
	RCM6	-1328	80.2	-903	22.5
	RCM7	-101	-86.3	-1022	38.7
	RCM8	-650	-11.8	-1618	119.5
	RCM9	*-1553*	*110.7*	*-463*	*-37.2*
	RCM10	-2380	222.9	-1483	101.2
	RCM16	-804	9.1	-803	9.0
	Ensemble	**-881**	**19.6**	**-1103**	**49.7**
RCP8.5	RCM1	-1636	122.0	-3133	325.1
	RCM2	-4918	567.3	-3156	328.2
	RCM3	-988	34.1	-2663	261.3
	RCM4	-2918	295.9	-2091	183.7
	RCM5	-6480	779.2	-1508	104.6
	RCM6	-1490	102.2	-2870	289.4
	RCM7	-265	-64.0	-1630	121.2
	RCM8	-1784	142.1	-3056	314.7
	RCM9	*-1999*	*171.2*	*-2420*	*228.4*
	RCM10	-2611	254.3	-4489	509.1
	RCM16	1196	-262.3	-2197	198.1
	Ensemble	**-1982**	**168.9**	**-2597**	**252.4**

Details of scientific activities performed during Ph.D.

1. International mobility

Erasmus plus traineeship at Meteorology Group of the Dept. Applied Mathematics and Computer Science, University of Cantabria, Spain from October 2021 to December 2021 (three months).

2. Conference Publications

1) **Liaqat MU**, Ranzi R (2022) Simulating the Hydrological Regimes of the Snow fed and Glacierized Naltar Catchment (Pakistan) Using a Distributed Energy Balance Model, International Association for Hydro- Environment Engineering and Research,(19-24 June, 2022) Spain
2) **Liaqat, M.U**., Casanueva, A., Grossi, G. and Ranzi, R., 2022. Future climate and runoff projections in the Naltar Catchment, Upper Indus Basin from CORDEX-South Asia regional climate models and hydrological modelling (No. EGU22-6030). Copernicus Meetings.
3) **Liaqat, M.U**., Casanueva, A., Grossi, G. and Ranzi, R., 2022.Hydrological Response to Climate change under CORDEX-South Asia Experiments in Western Karakoram, Upper Indus Basin, International Conference on Water Resources Management and Sustainability: Solutions for Arid Regions, Dubai, UAE, March 22-24, 2022.
4) **Liaqat, M.U**., Grossi, G., Ansari, R. and Ranzi, R., 2021, December. Modeling Hydrological Vulnerability to Climate Change in the Glacierized Naltar Catchment (Pakistan) Using a Distributed Energy Balance Model. In AGU Fall Meeting 2021. USA.
5) **Liaqat, M.U**., Grossi, G. and Ranzi, R., 2021. Evaluation of Snow Melt Progression in Karakorum Using Distributed Energy Balance Modeling for flood prediction, Le giornate dell'Idrologia 2021, Naples, Italy.
6) **Liaqat, M.U**., Ranzi, R., Grossi, G., and Mahmood, T., "Characterization of Interannual and Seasonal Variability of Hydro-Climatic Trends in the Upper Indus Basin", 2020. doi:10.5194/egusphere-egu2020-5867.
7) Pini, M., Scalvini, A., **Liaqat, M.U**., Ranzi, R., Serina, I. and Mehmood, T., 2020. Evaluation of Machine Learning Techniques for Inflow Prediction in Lake Como, Italy. Procedia Computer Science, 176, pp.918-927.

3. Journal Publications

1) **Liaqat MU**, Grossi G, Hasson Su, Ranzi R (2022) Characterization of interannual and seasonal variability of hydro-climatic trends in the Upper Indus Basin Theoretical and Applied Climatology doi:10.1007/ s00704-021-03850-3. (ISI/Scopus)
2) Ansari, R., **Liaqat, M.U**. and Grossi, G., 2022. Evaluation of gridded datasets for terrestrial water budget assessment in the Upper Jhelum River Basin-South Asia. Journal of Hydrology, p.128294. (ISI/Scopus)

3) **Liaqat MU**, Ranzi R (2022) Energy balance modeling of snow and ice melt in the Naltar Catchment (UIB, Pakistan), Journal of Hydrology (Under Submission)
4) **Liaqat MU**, Grossi G, Casanueva A, Ranzi R (2022) Hydrological Response to Climate change under CORDEXSouth Asia Experiments in Western Karakoram, Upper Indus Basin, Hydrology and Earth System Sciences (HESS) (Under submission)

4. Courses

I hugely benefited from attending following valuable courses

1) GEOframe Winter School GWS2021, 7 - 16 January 2021.
2) IS-ENES3 virtual Spring School on Climate data use for impact assessments, (March 2nd to April 16th, 2021).
3) 12th Annual Catchment Science Summer School University, Aug 29-Sept 3, 2021, University of Birmingham, UK
4) Big Data Analysis for Water-related Applications

5. Seminars and workshops

1) "From the Myths of Hercules to the reality of climate change" on 26-27 November 2020, organized by 1) UNESCO Category II Centre on Integrated and Multidisciplinary Water Resources Management, Thessaloniki, Greece, and 2) IAHR
2) Large Scale Variations in Hydrological Characteristics, 6- April 2022
3) WCRP Southern Asia Climate Research Forum, Nov 30, 2021.
4) Le giornate dell'Idrologia 2021, Naples, Italy.
5) American Geophysical Union, Fall Meeting, 17-21 December 2021 (on line)
6) Skill Hub: PhD Talent Day, 01-April 2022
7) From the Alps to Karakorum: Climate Variability and Water Resources for Agriculture, DICATAM, Brescia, 11 July 2022.
8) Doctorate @Futura (Fiera di Brescia) - Tuesday 4 October 2022, UNIBS
9) Un suono in estinzione – Preserving the Sound of Alpine Glaciers, 13 dicembre 2022, UNIBS